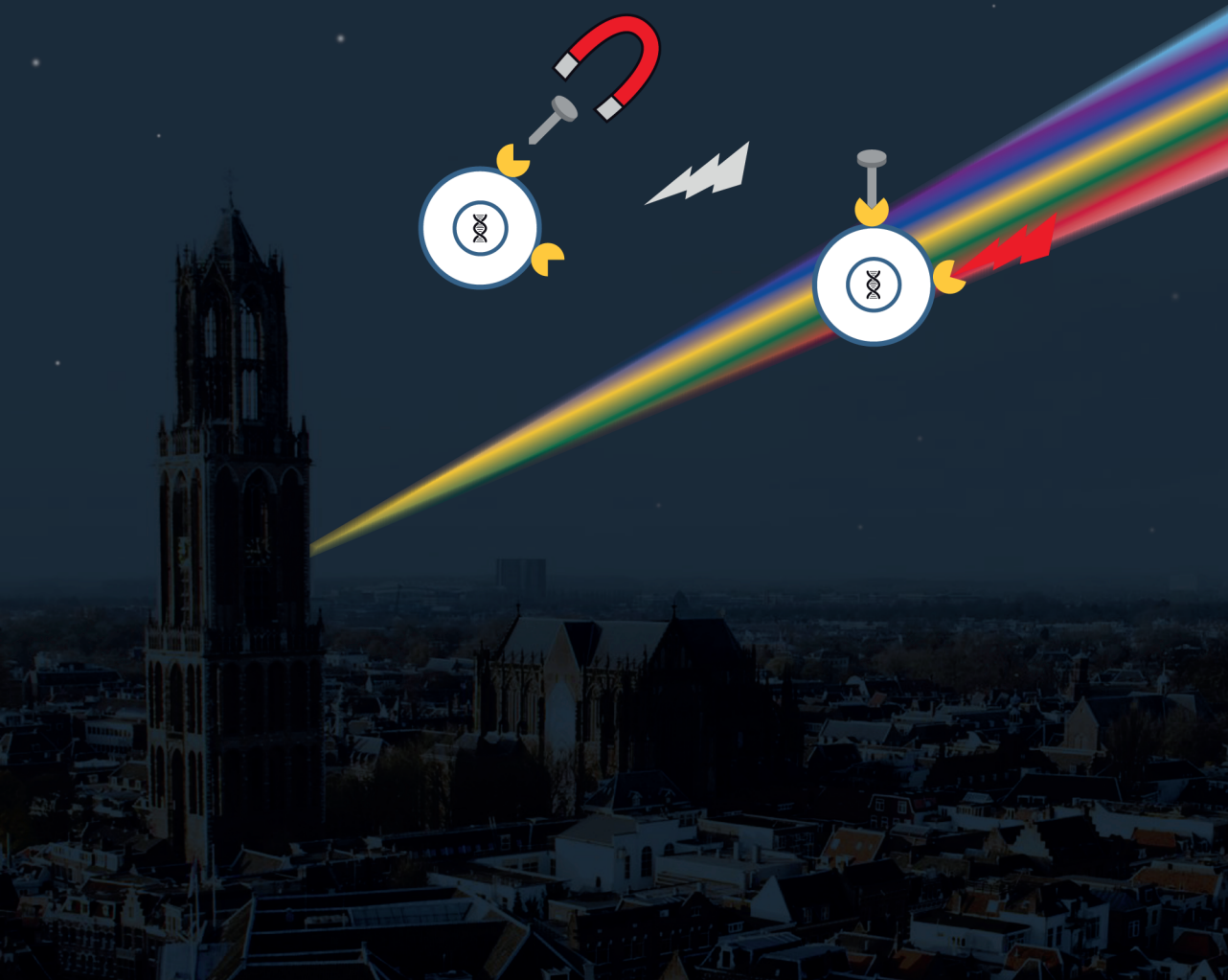


# Clinical pharmacology of anticancer agents with focus on neuro-oncology and biomarker assessment

Mark T.J. van Bussel





# **Clinical pharmacology of anticancer agents with focus on neuro-oncology and biomarker assessment**

Mark T.J. van Bussel

ISBN/EAN: 978-94-6323-767-3

© Mark T.J. van Bussel, 2019

Cover design: Everdina Meilink & Mark van Bussel

Book design & layout: Everdina Meilink, XML 2 PUBLISH

Printed by: Gildeprint, Enschede

# **Clinical pharmacology of anticancer agents with focus on neuro-oncology and biomarker assessment**

## **Klinische farmacologie van anti-kanker middelen met focus op neuro-oncologie en biomarker onderzoek**

(met een samenvatting in het Nederlands)

### **Proefschrift**

ter verkrijging van de graad van doctor aan de Universiteit Utrecht op gezag van de rector magnificus, prof. dr. H.R.B.M. Kummeling ingevolge van het besluit van het college van promoties, in het openbaar te verdedigen op woensdag 11 september 2019 des middags te 2.30 uur  
door

**Mark Theodorus Johannes van Bussel**  
geboren op 15 april 1987  
te Helmond

**Promotor:** Prof. dr. J.H. Beijnen

**Copromotor:** Dr. D. Brandsma

The research described in this thesis was performed at the Division of Pharmacology and the Department of Clinical Pharmacology, Division of Medical Oncology of The Netherlands Cancer Institute, Amsterdam, the Netherlands.

Printing of this thesis was financially supported by:  
Utrecht Institute of Pharmaceutical Sciences (UIPS)  
The Netherlands Cancer Institute

# Contents

	Preface	9
<b>Part I</b>	<b>Biomarker development and assessment</b>	<b>13</b>
Chapter 1	EpCAM-based assays for epithelial tumor cell detection in cerebrospinal fluid <i>Journal of Neuro-Oncology 2017;137(1):1-10.</i>	15
Chapter 2	Circulating epithelial tumor cell analysis in cerebrospinal fluid in patients with leptomeningeal metastases <i>Accepted for publication in Neurology</i>	33
Chapter 3	Circulating melanoma cell detection and driver mutation analysis in cerebrospinal fluid in melanoma patients with suspected leptomeningeal metastases <i>Submitted</i>	49
<b>Part II</b>	<b>Clinical pharmacology of anticancer agents</b>	<b>73</b>
Chapter 4	Intracranial antitumor responses of nivolumab and ipilimumab: a pharmacodynamic and pharmacokinetic perspective, a scoping systematic review <i>BMC Cancer. 2019;19(1):519.</i>	75
Chapter 5	Enzyme linked immunosorbent assay for the quantification of nivolumab and pembrolizumab in human serum and cerebrospinal fluid <i>Journal of Pharmaceutical and Biomedical Analysis 2019;164:128-134.</i>	91
Chapter 6	Liquid chromatography-tandem mass spectrometric assay for the T790M mutant EGFR inhibitor osimertinib (AZD9291) in human plasma <i>Journal of Chromatography B. 2016;1031:80-85.</i>	113
Chapter 7	A phase Ib/II multi-center, open label, dose escalation study of WNT974, LGX818 and cetuximab in patients with BRAFV600-mutant KRAS wild-type metastatic colorectal cancer harboring Wnt pathway mutations <i>To be submitted</i>	129
Chapter 8	Observations of severe bone toxicity in a phase 1 dose escalation combination trial of anticancer agents to inhibit EGFR, BRAF and WNT pathways in colon carcinoma <i>To be submitted</i>	149
Chapter 9	A first-in-man phase I study of the DNA-dependent protein kinase inhibitor M3814 in patients with advanced solid tumors <i>Submitted</i>	165



<b>Conclusions and perspectives</b>	187
<b>Appendix</b>	195
Author affiliations	197
Summary	199
Nederlandse samenvatting	203
Dankwoord	209
Curriculum vitae	211
Overview of publications	213
Molecular structures	217



## Preface

### Part I Biomarker development and assessment

Leptomeningeal metastases (LM), also known as leptomeningeal carcinomatosis or neoplastic meningitis, is a diffuse dissemination of tumor cells into the cerebrospinal fluid (CSF) and leptomeninges.<sup>1</sup> Approximately ten percent of patients with cancer ultimately develop LM.<sup>2</sup> Survival of patients with LM varies from several weeks to more than a year, depending on the tumor type, performance status and treatment of LM, consisting of radiotherapy of symptomatic sites and/or systemic therapy.<sup>3,4</sup> The median survival is 6-8 weeks without treatment. Gadolinium enhanced magnetic resonance imaging (MRI) of the symptomatic sites of the nervous system is the radiological method of choice as diagnostic technique when LM is clinically suspected.<sup>2</sup> The sensitivity of MRI with gadolinium for the diagnosis of LM is approximately 75% and the specificity approximately 77%.<sup>5</sup> When MRI does not show equivocal abnormalities, CSF cytology needs to be performed. Sensitivity of CSF cytology is also low: 44-67% at first LP, increasing to 84-91% upon second sampling.<sup>6-14</sup> Therefore, improved CSF diagnostics for LM are needed to either rule out the diagnosis or expedite treatment without further delay. In part I of this thesis the isolation, molecular characterization and quantification of circulating tumor cells (CTC) in CSF using flow cytometry is described in patients with a clinical suspicion on LM from epithelial tumors such as breast cancer, lung cancer and ovarian cancer. **Chapter 1** provides an overview of several CTC assays for epithelial tumor cell detection in CSF. The diagnostic performance of an immunoflow cytometry CTC assay for epithelial tumor cell quantification in CSF is investigated in **Chapter 2**. In addition the presence of circulating tumor DNA fragments and the driver mutation distribution is explored. The development of an immunoflow cytometry assay and the molecular characterization of circulating melanoma tumor cells is described in **Chapter 3**.

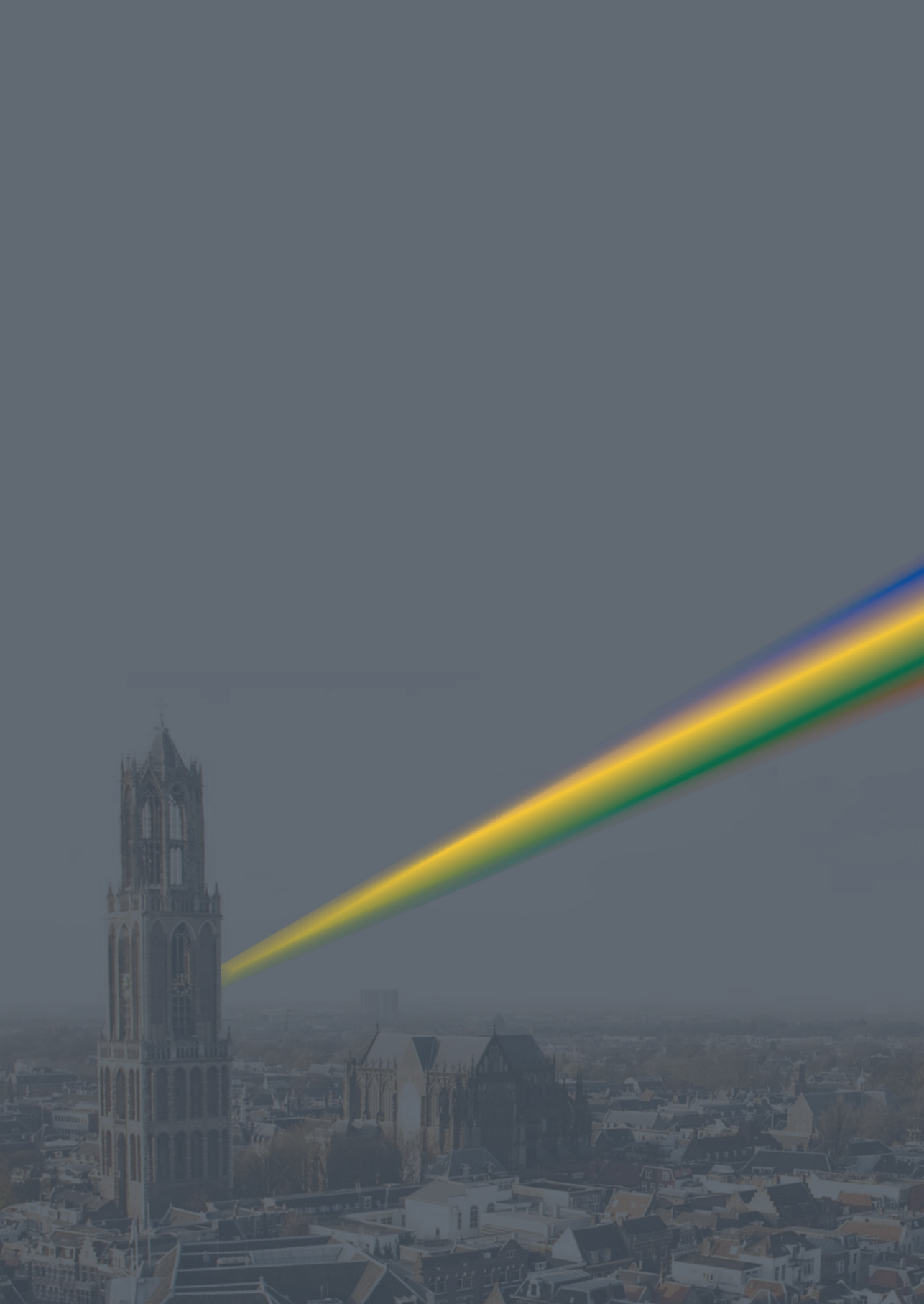
### Part II Clinical pharmacology of anticancer agents

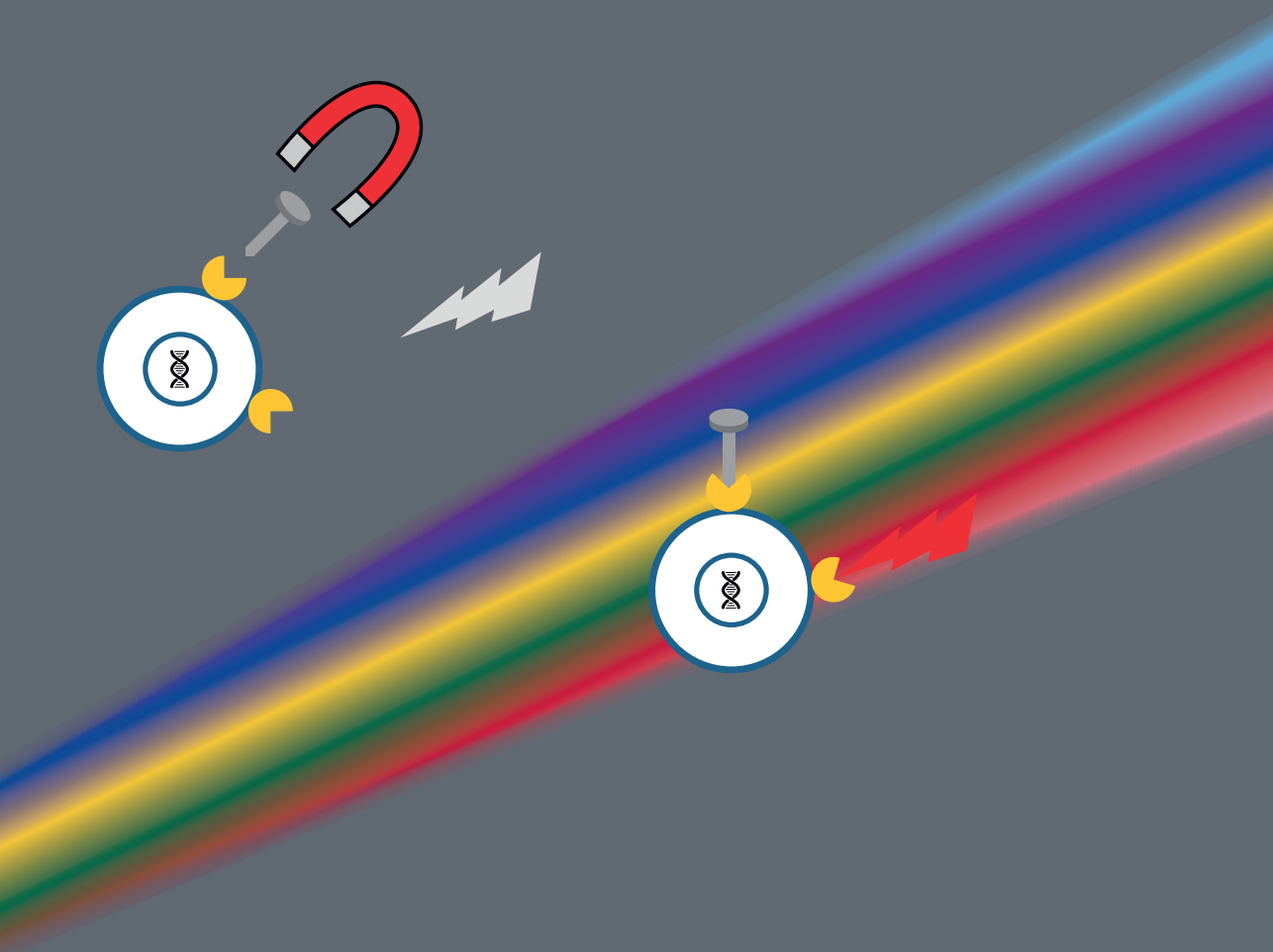
Part II of this thesis focus on several anticancer agents in relation to their clinical pharmacokinetics and pharmacodynamics. Several laboratory techniques are described to quantify monoclonal antibodies and small molecules. **Chapter 4** provides a systematic review about the intracranial antitumor activity of immunotherapy with the monoclonal antibodies nivolumab and ipilimumab and a pharmacodynamic and pharmacokinetic perspective. **Chapter 5** describes the development of an enzyme linked immunosorbent assay for the quantification of the monoclonal antibodies nivolumab and pembrolizumab in human serum and CSF. A liquid chromatography-tandem mass spectrometric assay for the epidermal growth factor receptor inhibitor osimertinib in human plasma is presented in **Chapter 6**. The clinical pharmacology of

a novel combination of anticancer agents has been explored in the phase Ib/II multi-center, open label, dose escalation study of the safety of WNT974, encorafenib and cetuximab in patients with *BRAFV600*-mutant *KRAS* wild-type metastatic colorectal cancer harboring Wnt pathway mutations in **Chapter 7**. A case report of two patients who experienced severe bone toxicity in the trial of WNT974, encorafenib and cetuximab is described in **Chapter 8**. The results of a first-in-man phase I study of the DNA-dependent protein kinase inhibitor M3814 in patients with advanced solid tumors are presented in **Chapter 9**.

## References

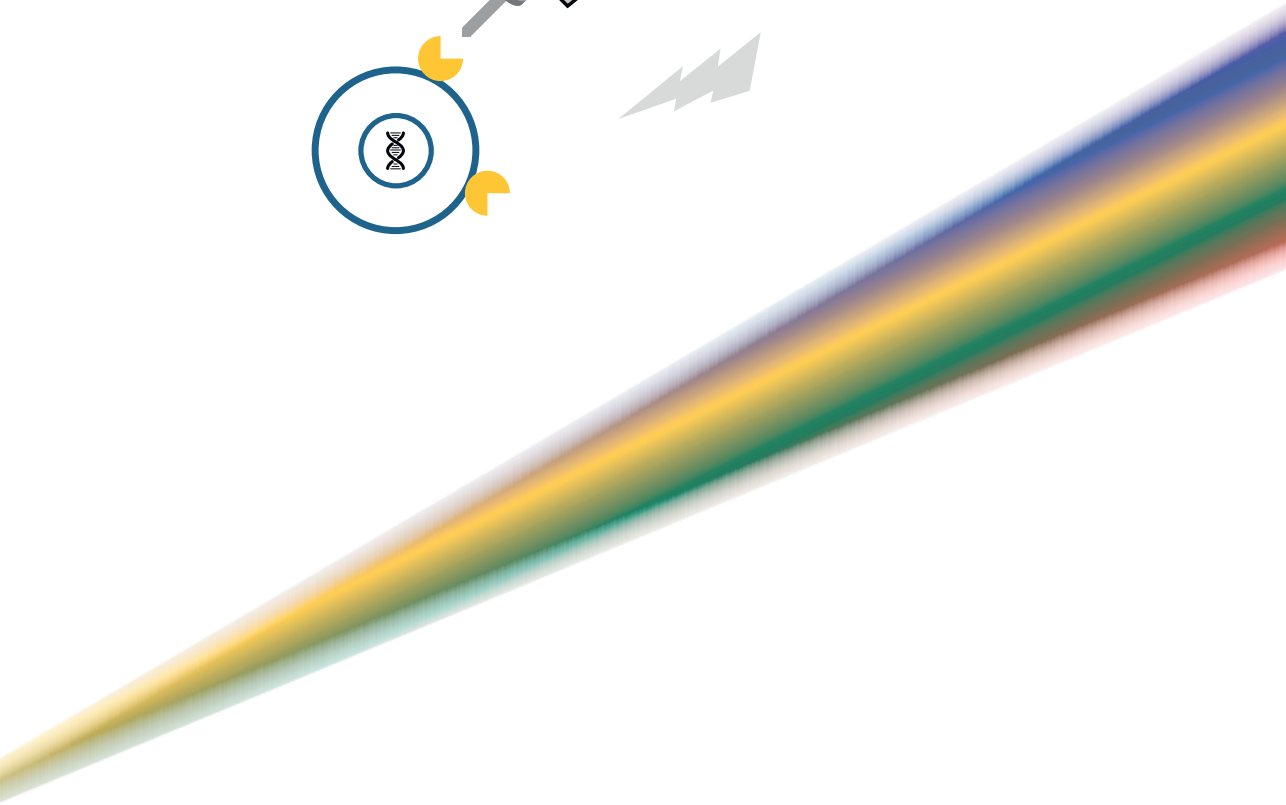
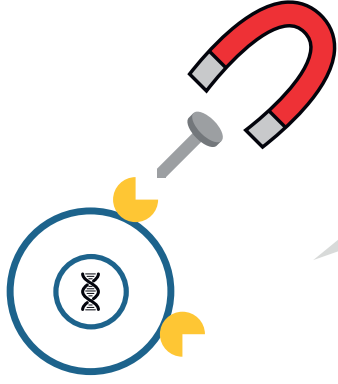
1. Chamberlain M, Soffietti R, Raizer J, et al. Leptomeningeal metastasis: a Response Assessment in Neuro-Oncology critical review of endpoints and response criteria of published randomized clinical trials. *Neuro Oncol.* 2014;16(9):1176-1185.
2. Le Rhun E, Weller M, Brandsma D, et al. EANO-ESMO Clinical Practice Guidelines for diagnosis, treatment and follow-up of patients with leptomeningeal metastasis from solid tumours. *Ann Oncol Off J Eur Soc Med Oncol.* 2017;28(suppl\_4):iv84-iv99.
3. Harstad L, Hess KR, Groves MD. Prognostic factors and outcomes in patients with leptomeningeal melanomatosis. *Neuro Oncol.* 2008;10(6):1010-1018.
4. Brower J V, Saha S, Rosenberg SA, Hullett CR, Ian Robins H. Management of leptomeningeal metastases: Prognostic factors and associated outcomes. *J Clin Neurosci.* 2016;27:130-137.
5. Straathof CS, de Bruin HG, Dippel DW, Vecht CJ. The diagnostic accuracy of magnetic resonance imaging and cerebrospinal fluid cytology in leptomeningeal metastasis. *J Neurol.* 1999;246(9):810-814.
6. Wasserstrom WR, Glass JP, Posner JB. Diagnosis and treatment of leptomeningeal metastases from solid tumors: experience with 90 patients. *Cancer.* 1982;49(4):759-772.
7. van Oostenbrugge RJ, Twijnstra A. Presenting features and value of diagnostic procedures in leptomeningeal metastases. *Neurology.* 1999;53(2):382-385.
8. Tu Q, Wu X, Le Rhun E, et al. CellSearch technology applied to the detection and quantification of tumor cells in CSF of patients with lung cancer leptomeningeal metastasis. *Lung Cancer.* 2015;90(2):352-357.
9. Lee JS, Melisko ME, Magbanua MJ, et al. Detection of cerebrospinal fluid tumor cells and its clinical relevance in leptomeningeal metastasis of breast cancer. *Breast Cancer Res Treat.* 2015;154(2):339-349.
10. Nayak L, Fleisher M, Gonzalez-Espinoza R, et al. Rare cell capture technology for the diagnosis of leptomeningeal metastasis in solid tumors. *Neurology.* 2013;80(17):1598-605; discussion 1603.
11. Jiang B-Y, Li Y-S, Guo W-B, et al. Detection of Driver and Resistance Mutations in Leptomeningeal Metastases of NSCLC by Next-Generation Sequencing of Cerebrospinal Fluid Circulating Tumor Cells. *Clin Cancer Res.* 2017;23(18):5480-5488.
12. Milojkovic Kerklaan B, Pluim D, Bol M, et al. EpCAM-based flow cytometry in cerebrospinal fluid greatly improves diagnostic accuracy of leptomeningeal metastases from epithelial tumors. *Neuro Oncol.* 2016;18(6):855-862.
13. Subira D, Serrano C, Castanon S, et al. Role of flow cytometry immunophenotyping in the diagnosis of leptomeningeal carcinomatosis. *Neuro Oncol.* 2012;14(1):43-52.
14. Subira D, Simo M, Illan J, et al. Diagnostic and prognostic significance of flow cytometry immunophenotyping in patients with leptomeningeal carcinomatosis. *Clin Exp Metastasis.* 2015;32(4):383-391.



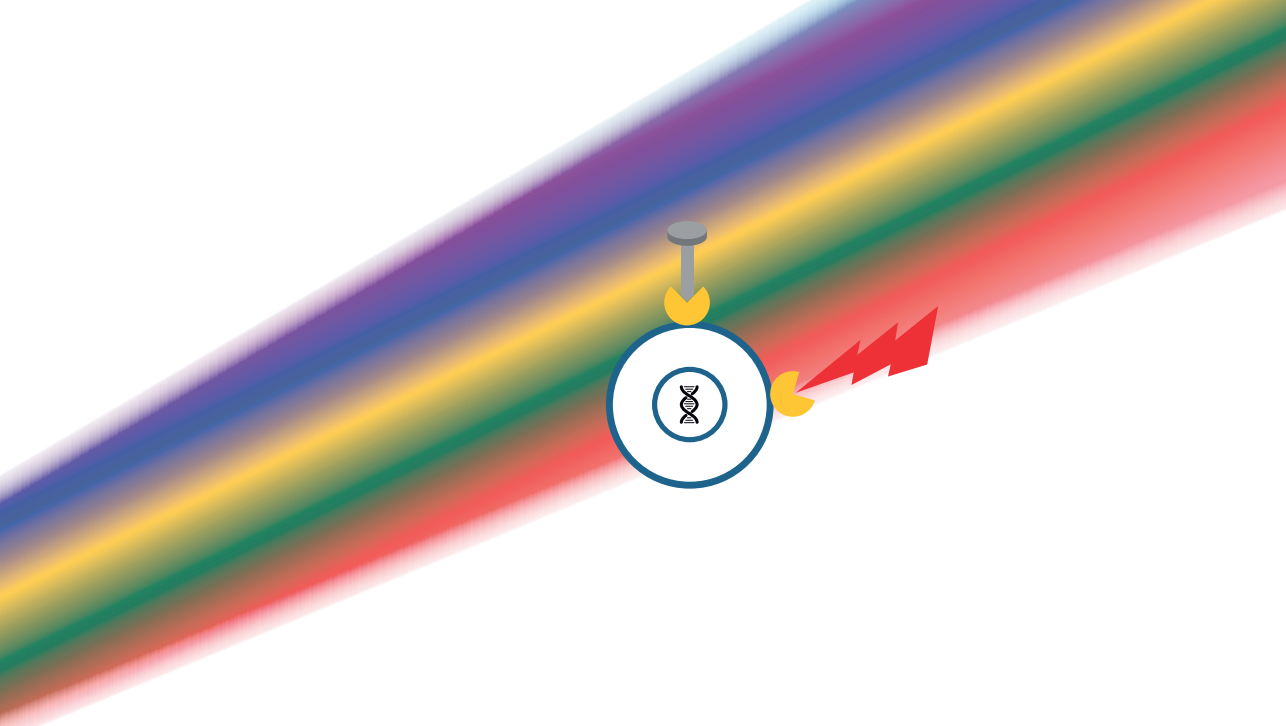


# Part I

Biomarker development and assessment







# Chapter 1

## EpCAM-based assays for epithelial tumor cell detection in cerebrospinal fluid

Mark T.J. van Bussel  
Dick Pluim  
Mijke Bol  
Jos H. Beijnen  
Jan H. M. Schellens  
Dieta Brandsma

*Journal of Neuro-Oncology* 2017;137(1):1-10.

## Summary

The diagnosis of leptomeningeal metastases (LM) of solid tumors is complicated due to low sensitivities of both magnetic resonance imaging (MRI) and cytology. MRI has a sensitivity of 76% for the diagnosis of LM and cerebrospinal fluid (CSF) cytology has a sensitivity of 44-67% at first lumbar puncture (LP) which increases to 84-91% upon second CSF sampling. Epithelial cell adhesion molecule (EpCAM) is expressed by solid tumors of epithelial origin like non-small-cell lung cancer, breast cancer or ovarium cancer. Recently, a CELLSEARCH® assay and flow cytometry laboratory techniques have been developed to detect circulating tumor cells (CTCs) of epithelial origin in CSF. These laboratory techniques are based on capture antibodies labelled with different fluorescent tags against EpCAM. In this review, we provide an overview of the available laboratory techniques and diagnostic accuracy for tumor cell detection in CSF. The reported sensitivities of the EpCAM-based CTC assays for the diagnosis of LM across the different studies are highly promising and vary between 76-100%. An overview of the different EpCAM-based techniques for the enumeration of CTCs in the CSF is given and a comparison is made with CSF cytology for the diagnoses of LM from epithelial tumors.

## Introduction

Two to eight percent of patients with solid tumors develop LM. Diagnosis of LM is currently based on clinical symptoms and typical contrast enhancement of the leptomeninges on MRI of brain and/or spine. However, MRI has a low sensitivity (76%) and specificity (77%) for the diagnosis of LM.<sup>1</sup> When MRI results are inconclusive, a LP is performed to obtain CSF. Sensitivity of CSF cytology, however, is also low: 44-67% at first LP, increasing to 84-91% upon second sampling.<sup>2-11</sup> EpCAM is a cell-cell adhesion molecule and a mitogenic signal transducer after regulated intramembrane proteolysis.<sup>11,12</sup> Solid tumors of epithelial origin like non-small-cell lung cancer, breast cancer or ovarium cancer express transmembrane glycoprotein EpCAM (also known as CD326).<sup>13</sup> In blood donors with nonmalignant diseases the background of EpCAM+ cells is extremely low with only 0.3% having  $\geq 2$  CTC per 7.5 mL.<sup>14</sup> EpCAM+ CTCs in blood have been detected in patients with metastasized epithelial tumors, like ovarian cancer, breast cancer and colorectal cancer and prostate and have prognostic value when CTC numbers are higher than 0.3-5 CTC/mL.<sup>15-18</sup> Therefore, multiple research groups started to investigate assays to detect and count EpCAM+ CTCs in CSF in patients with already diagnosed LM or clinically suspected LM. To improve CSF diagnostics, the enumeration of CTCs by flow cytometry and Veridex CELLSEARCH® has been introduced.<sup>4-6,19,20</sup> The CELLSEARCH® assay is an FDA-approved assay to detect and count CTC from solid tumors in blood.<sup>21,22</sup> Currently, two major EpCAM-based techniques have been studied: the CELLSEARCH® technology to detect CTCs in blood which has been adapted to detect CTCs in CSF and flow cytometry assays. In this review, an overview is given of the different assays and their performance in CSF for the enumeration of EpCAM+ CTCs. The EpCAM-based techniques are compared with CSF cytology for the diagnosis of LM from epithelial tumors.

## Methods

In June 2017, PubMed was searched for studies with the following terms “Cerebrospinal Fluid”[Mesh] and “Neoplastic Cells, Circulating”[Mesh], CELLSEARCH and cerebrospinal fluid or EpCAM and cerebrospinal fluid. The references of the selected articles were also reviewed for inclusion in this review. Articles in which non-EpCAM based assays were used for other tumor types such as melanoma or lymphoma were excluded. Reported CTC numbers in the various articles were standardized to cells/mL, if possible.

## Results

The initial article search resulted in twenty-one, six, and twenty-five hits, respectively. Eight articles were included for data extraction after reviewing of the abstracts. One additional article was included after reviewing the references of the selected articles.

### CELLSEARCH technique

The CELLSEARCH® assay is an FDA-approved assay to detect CTC in blood.<sup>21,22</sup> The CELLSEARCH® system consists of the CellTracks Autoprep, CellTracks Magnest and the CellTracks Analyzer II.<sup>23</sup> First, blood is drawn in the CellSave collection tube which preserves the sample up to 96 hours. Then, the blood is gently mixed with a dedicated dilution buffer provided in the CELLSEARCH® kit and centrifuged at 800 x g at room temperature for 10 minutes.<sup>24</sup> Subsequently, the sample is transferred to the CellTracks Autoprep part of the CELLSEARCH® System. In the CellTracks Autoprep, the EpCAM+ CTCs are immunomagnetically enriched and the fluorescently labeled antibodies are added. Anti-EpCAM ferrofluid is added to the aspirated plasma/dilution buffer layer to select for cells of epithelial origin by immunomagnetically enrichment.<sup>25</sup> Captured cells are fixed and permeabilized with the CELLSEARCH® proprietary permeabilization reagents and subsequently stained with 4'6-diamidino-2-phenylindole, dihydrochloride (DAPI) for nuclear staining. Anti-CD45-allophycocyan (CD45-APC) was added to label leukocytes and distinguish them from tumor cells. Anti-cytokeratin (CK) 8, 18-Phycoerythrin (PE), and anti-cytokeratin 19 Phycoerythrin (CK-PE) were added to stain the epithelial tumor cells. Next, cells are deposited in the cartridge that is positioned in the CellTracks Magnest. Thereafter, the CellTracks Analyzer II generates images of the cells using filters for DAPI, PE, and APC. Cells that are stained with both DAPI and PE are automatically identified as CTCs and placed in an image gallery. (see for overview of the CellTracks Analyzer II Figure 1A). Finally, a reviewer observes the images and makes the final decision on the identification of CTCs, which are defined as nucleated DAPI+ cells, lacking CD45 and expressing CK-PE. An example of gallery images of tumor cells detected by CELLSEARCH® in CSF (B1) and peripheral blood (B2) is given in Figure 1B.

In the CELLSEARCH® assay plasma is aspirated based on the optical differences between plasma, buffy coat and erythrocytes. To use the CELLSEARCH® assay in CSF instead of blood, it is necessary to make some modifications to the original method. An overview of the CELLSEARCH® studies using CSF is given in Table 1. To calibrate the CELLSEARCH® system, the control mode is normally used.<sup>5</sup> In the control mode, a clear suspension of prestained fixed breast cancer cells is used and no separation line to aspirate the right fluid fraction is needed. Therefore, this mode can be used

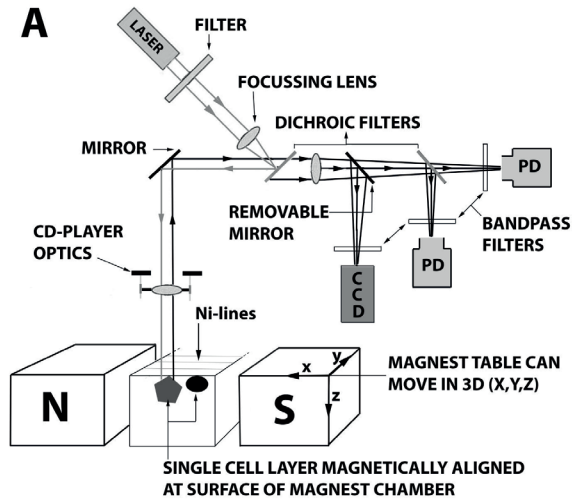
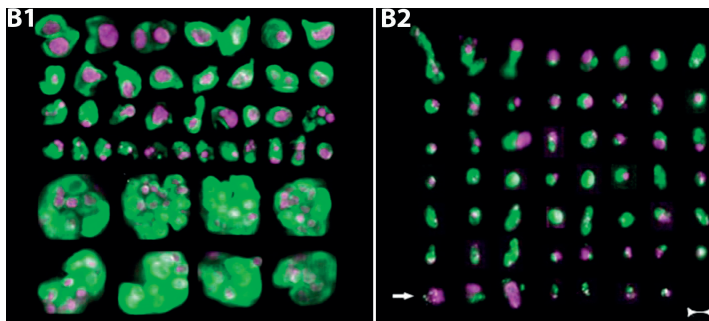


Figure 1.

**A.** Schematic representation of the CellTracks Analyzer II, used in the CellSearch® system.<sup>26</sup> Cells that have been enriched immunomagnetically and fluorescently labelled in the CellTracks Autoprep machine are magnetically (N, S = magnet North and South) aligned to nickel (Ni) lines at the inner surface of the Magnet chamber. The light from a laser diode is focused onto these cells via a normal CD-player objective. The fluorescent light is collected via the same objective and separated through a combination of filters onto the photodiode detectors (PD). Fluorescent images of the events of interest can be acquired by inserting a removable mirror and band pass filter. The fluorescent light captured by the CD objective is then focused onto the camera (CCD). The magnets and chamber (Magnet cartridge) are positioned on a computer-controlled stage and the cells cross the laser focus one after another when the stage is moved in the Y-direction. While scanning, a feedback system uses the Ni-lines to keep the laser focused on the aligned cells.



**B.** Gallery of images of tumor cells in CSF and peripheral blood using CELLSEARCH® technology.<sup>27</sup> Gallery of images of tumor cells in CSF (B1) and peripheral blood (B2) detected by CELLSEARCH® technology.<sup>4</sup> CTC are defined as  $\geq 4 \mu\text{m}$  in diameter, nucleated DAPI+ (purple), CD45-, and CK-PE+ (green). In the CSF sample, CTCs were either found as isolated cells or in clusters. Their morphology was similar to the CTCs found in the peripheral blood but without any apoptotic features, which were present in some of the CTCs in blood samples (arrow, shrunken cell containing CK inclusion). Scale bar is  $10 \mu\text{m}$ . *Abbreviations:* CSF=cerebrospinal fluid, CTC=circulating tumor cell, CK=cytokeratin.

Table 1. Overview CELLSEARCH® and flow cytometry studies

Study	Assay	N	Patient population	Median CTCs/mL in CSF	CTC range CTC/mL in CSF	Modification technique for CSF analysis CELLSEARCH® only target of capture antibody / fluorescent antibody flow cytometry only	Results control group
Tu et al. 2015 <sup>4</sup>	C	18	MRI confirmed LM in lung cancer (main histological subtype: NSCLC)	157	0.2 - >4000	Darkening the outside of the tube with a black felt-tip up to the fluid level to mimic the level of sediment erythrocytes <sup>a</sup>	Not reported
Le Rhun et al. 2012 <sup>19</sup>	C	8	Confirmed LM/ breast cancer treated patients	106	0.2-2100	Darkening of the outside of the tube with a black felt-tip up to the fluid level to mimic the level of sediment erythrocytes <sup>a</sup>	Not reported
Lee et al. 2015 <sup>5</sup>	C	38	Confirmed or suspected LM / breast cancer	14.9	0 - 9323	Elimination of the centrifugation step prior to enrichment and the use of the control mode <sup>b</sup>	n=14 <sup>c</sup> mean 0.3 CTC/mL median 0 CTC/mL
Nayak et al. 2013 <sup>6</sup>	C	51	Clinical suspicion of LM/ solid tumors (mainly NSCLC and breast cancer)	20.7	0.13 > -150	Elimination of the centrifugation step prior to enrichment and the use of the control mode <sup>b</sup>	n=9 <sup>d</sup> 0 CTC/mL
Patel et al. 2011 <sup>20</sup>	C	5	Metastatic breast cancer involving CNS	NA	NA	CSF suspension spiked into reconstituted blood <sup>e</sup>	Not reported
Jiang et al. 2017 <sup>7</sup>	C	21	NSCLC patients with suspected LM	129.3	3.6-1985	CELLSEARCH® standard procedure	Not reported
Acosta et al. 2016 <sup>26</sup>	FC	6 <sup>a</sup>	Clinical suspicion of LM, previously diagnosed carcinoma	not reported	not reported	EpCAM (clone Ber-EP4)	Not reported
Milojkovic Kerklaan et al. 2016 <sup>8</sup>	FC	29	Clinical suspicion of LM but a negative or inconclusive MRI (primary tumor mainly breast (n=13) and lung cancer (n=8))	316.5 (in LM patients)	160-4503 (in LM patients)	EpCAM magnetic beads/ EpCAM-PE (HEA-125 (isotype: mouse IgG1))	Not reported

Table 1. (continued)

Study	Assay	N	Patient population	Median CTCs/mL in CSF	CTC range CTC/mL in CSF	Modification technique for CSF analysis CELLSEARCH® only target of capture antibody / fluorescent antibody flow cytometry only	Results control group
Lee et al. 2015 <sup>5</sup>	FC	32 <sup>f</sup>	Confirmed LM suspected / breast cancer	3.5	0-11.634.4	EpCAM magnetic beads/ EpCAM-PE (clones MJ37/EBA-1)	Not reported
Subirá et al. <sup>8</sup> 2015 <sup>10</sup>	FC	144	Confirmed LM or clinically suspected LM (primary tumor, mainly breast (n=38) and lung (n=24))	260	10-2210 (interquartile range)	EpCAM (clones BerEP4; and EBA-1)/ 2-color (fluorescein isothiocyanate, FITC/PE)	Not reported
Subirá et al. <sup>8</sup> 2012 <sup>9</sup>	FC	78	Clinically suspected LM and previous diagnosis of epithelial-cell neoplasia mainly breast	Not reported	Not reported	EpCAM (clones BerEP4;and EBA-1)/ 2-color (fluorescein isothiocyanate, FITC/PE)	Not reported

<sup>a</sup> fluid level = Le Rhun et al. and Tu et al. darkened the outside of the tube with a black felt-tip up to the fluid level to mimic the level of sedimented erythrocytes to allow for the selection of clear CSF.<sup>4,19</sup>

<sup>b</sup> Control mode: a clear suspension of prestained, fixed cancer cells is used and no interface to aspirate the right fluid fraction is needed. Therefore, this mode can be used to aspirate the clear CSF automatically.

<sup>c</sup> Lee et al. included control patients who had a hematologic malignancy but no solid tumor and no clinical findings consistent with LM.<sup>5</sup>

<sup>d</sup> Nayak et al. included control patients with CSF pleocytosis but without solid tumors.<sup>6</sup>

<sup>e</sup> reconstituted blood = Patel et al. spiked the CSF in blood for calibration of the CELLSEARCH® system.<sup>20</sup>

<sup>f</sup> number of samples instead of number of patients.

<sup>g</sup> study cohorts are overlapping. *Abbreviations:* C=CELLSEARCH®, FC=flow cytometry, EpCAM-PE=epithelial cell adhesion molecule phycoerythrin, LM=leptomeningeal metastases.

to aspirate the clear CSF automatically. Lee et al. used the control mode and Patel et al. spiked the CSF in blood for calibration of the CELLSEARCH® system.<sup>5,20</sup> Le Rhun et al. and Tu et al. darkened the outside of the tube with a black felt-tip up to the fluid level to mimic the level of sedimented erythrocytes to allow for the selection of the clear CSF.<sup>4,19</sup> The reported sensitivity and specificity for the diagnosis of LM of both types of modified CELLSEARCH® assays for CSF are shown in Table 2.

### **Flow cytometry**

In fluorescence activated cell sorting systems (FACS) for CTCs enumeration of epithelial origin, different fluorescently labelled EpCAM antibodies are used to stain and count the cells. An overview of the FACS technology is depicted in Figure 2a. Milojkovic Kerklaan et al. and Lee et al. used immunomagnetic enrichment with anti-EpCAM MicroBeads prior to FACS analysis.<sup>5,8</sup> To distinguish between CTCs and leukocytes, anti-CD45-fluorescein isothiocyanate (FITC) for leucocyte labeling was added. FACS plots of CSF obtained by this method are shown in Figure 2b. In addition to these markers, Acosta et al. used anti-CD33 to improve differentiation between monocyte/macrophages/granulocytes (CD45- CD33+ CD326+) and epithelial cells (CD45- CD33- CD326+).<sup>28</sup> Milojkovic Kerklaan et al. and Subirá et al. used Hoechst33258 and DRAQ5, respectively, for nuclear DNA-staining whereas Lee et al. did not use a DNA-dye.<sup>9,10</sup> An overview of flow cytometry studies is given in Table 1. The reported sensitivity and specificity of these assays for the diagnosis of LM are shown in Table 2.

### **Discussion**

The diagnosis of LM is hampered by the low sensitivities of its diagnostic tools: MRI of brain and /or spine and CSF cytology. Although CSF cytology still is the gold standard for LM with a reported sensitivity of 44-67% at the first CSF examination, LM can also be diagnosed by the combination of neurological symptoms compatible with LM and leptomeningeal contrast enhancement in patients with known (metastasized) tumors.<sup>2</sup> The low sensitivity of cytology could be attributed partially to the spill of tumor cells at cytopsin preparation. Furthermore, limited sample volume, delayed sample processing and sample collection at a suboptimal site (LP when there are mainly intracranial LM).<sup>29</sup> Leptomeningeal contrast enhancement on MRI has a sensitivity of 76% for LM.<sup>1</sup> Currently, multiple techniques are used to detect and count EpCAM+ CTCs in CSF to improve the CSF diagnostics for LM in patients with epithelial tumors. The reported results of the EpCAM-based techniques in CSF are highly promising with a detection limit of 0.4 CTC/mL. However, these techniques are not yet fully ready for clinical implementation due to lack of assay standardization and proper multicenter



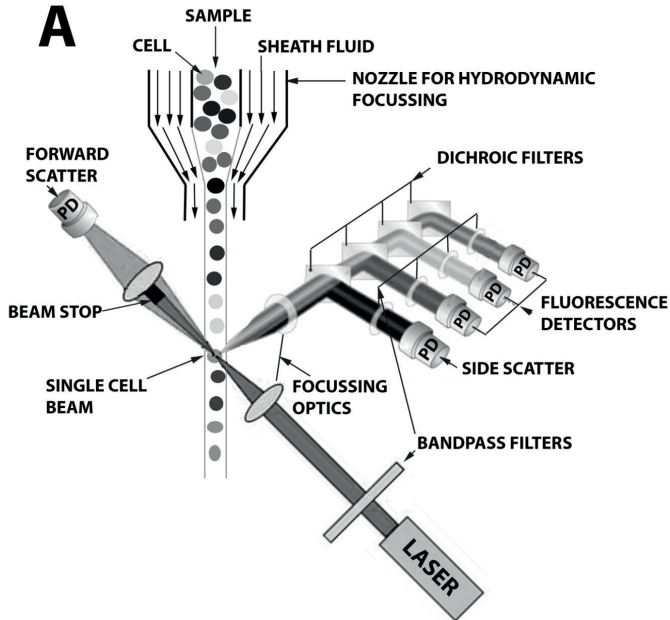
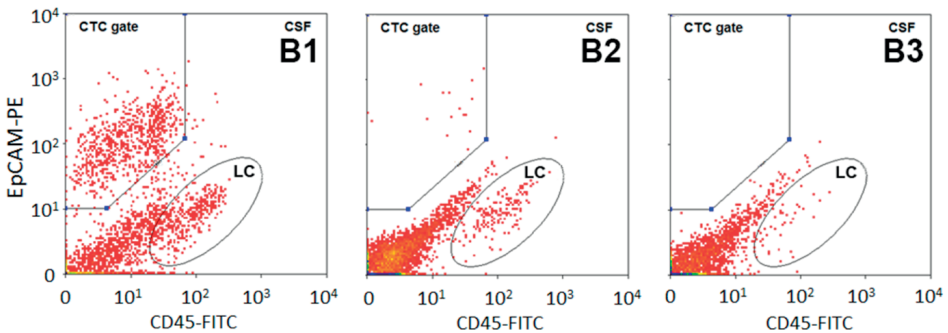


Figure 2.

A. Schematic representation of fluorescence activated cell sorting (FACS). Cells in the sample are focused into a stream of single cells by hydrodynamic focusing with sheath fluid. A laser is focused on the middle of this stream. Forward scatter is measured in a straight line opposite the laser beam and is used to distinguish cells on the basis of size. Sideward scatter and fluorescence is measured perpendicular to the laser beam and provide, respectively, information about internal complexity and amount of cell-bound fluorescently labelled antibody or dye. The signals from the photodiode detectors (PD) are processed by a computer using flow cytometry software.



B. Representative examples of epithelial cell adhesion molecule (EpCAM)-based flow cytometry plots of cerebrospinal fluid (CSF) from three individual patients. Circulating tumor cells (CTC) are defined as EpCAM<sup>+</sup> and CD45<sup>-</sup> and will therefore be sorted to the CTC gate.

**b1:** non-small cell lung cancer patient with LM with EpCAM-positive CTCs (162 CTCs/mL); CSF cytology was positive (not shown). **b2:** breast cancer patient with LM with EpCAM-positive CTCs (3 CTCs/mL). CSF cytology in this patient was negative (not shown). **b3:** breast cancer patient without LM. No EpCAM-positive CTCs in CSF. CSF cytology in this patient was also negative (not shown). *Abbreviations:* FACS=fluorescence activated cell sorting systems, CTC=circulating tumor cell, EpCAM=epithelial cell adhesion molecule, LC=leucocytes.

Table 2. Overview CELLSEARCH® and flow cytometry studies in CSF with reported sensitivity and specificity versus cytology

Study	Assay N	Patient population	Sensitivity (95% CI)	Specificity (95% CI)	Sensitivity (95% CI) cytology	Specificity (95% CI) cytology
Tu et al. 2015 <sup>4</sup>	C	18 MRI confirmed LM / lung cancer	77.8 (52.4-93.6)	100 (47.8-100)	44.4 (21.5-69.2)	Not reported
Lee et al. 2015 <sup>5</sup>	C	38 Confirmed LM/ suspected LM / breast cancer	80.95 (58.1-94.4)	84.62 (54.5-97.6)	66.67 (43.04-85.35)	Used as gold standard 100%
Nayak et al. 2013 <sup>6</sup>	C	51 Clinical suspicion of LM/ solid tumors (mainly NSCLC and breast cancer)	100 (78.1-100)	97.2 (85.4-99.9)	66.7 (38.3-88.1)	Used as gold standard
Jiang et al. 2017 <sup>7</sup>	C	21 NSCLC patients with suspected LM	95.2 (NA)	100 (NA)	57.1 (NA)	Not reported
Acosta et al. 2016 <sup>26</sup>	FC	6 <sup>a</sup> Clinical suspicion of LM previous diagnosed carcinoma	100% (NA)	100% (NA)	Not reported	Not reported
Miljkovic Kerklaan 2016 <sup>8</sup>	FC	29 Clinical suspicion of LM but a negative or inconclusive MRI, previously diagnosed carcinoma	100 (75-100)	100 (79-100)	61.5 (32-86)	100 (79-100)
Subirá et al. <sup>b</sup> 2015 <sup>10</sup>	FC	144 Confirmed LM or clinically suspected LM	79.8 (NA)	84 (NA)	50 (NA)	100 (NA)
Subirá et al. <sup>b</sup> 2012 <sup>9</sup>	FC	78 Clinically suspected LM and previous diagnosis of epithelial-cell neoplasia	75.5 (63.5-87.6)	96.1 (88.8-100)	65.3 (52.0-78.6)	100 (100-100)

Abbreviations: C=CELLSEARCH®, FC=flow cytometry, 95CI=95% confidence interval, MRI=magnetic resonance imaging, LM=leptomeningeal metastases, NA=not available, <sup>a</sup> number of samples instead of number of patients, <sup>b</sup> study cohorts are overlapping.

validation studies with adequate control groups. These studies are required for each individual CTC assay before clinical implementation. Furthermore, patients groups that have been investigated so far were rather small ranging from 6 to 144 patients. Sensitivity of the EpCAM based techniques may be lower in larger patients studies suspected for LM as it is known that tumor cells of epithelial origin can lose EpCAM expression due to epithelial to mesenchymal cell transition.<sup>30</sup> This may explain that patients with LM can have positive CSF cytology but no detectable CTCs.<sup>19</sup>

The FDA-approved CELLSEARCH®-assay was initially validated in blood in a prospective, double-blind, multicenter clinical trial involving 177 metastatic breast cancer patients at 20 clinical centers.<sup>31</sup> The reported sensitivities of the EpCAM-based CTC assays for the diagnosis of LM across the different studies are highly promising and vary between 76-100%. However, none of the studied EpCAM assays for the enumeration of CTCs in CSF have yet been shown to be statistically significant better than CSF cytology.<sup>4-10,19,20,28</sup> This can be attributed to the insufficient number of patients ultimately diagnosed with LM in the study cohorts. Furthermore, in order to establish the real value of the new techniques in CSF, standardization of the patient selection process is critical to ensure selection of patients with true diagnostic uncertainty of LM. A patient population with a true diagnostic uncertainty with clinical suspicion of LM was investigated in only two studies.<sup>6,8</sup> All other studies that reported sensitivity for tumor cell detection in CSF also included patients with already proven LM based on MRI and/or CSF cytolog.<sup>4,5,9,10</sup> Future validation studies should be performed in properly defined study populations with a clinical suspicion on LM in prospective, multicenter triple blind (clinician, lab technician and patient) studies. A possible risk in CSF analysis is the detection of CTCs in the CSF due to contamination with blood in a traumatic LP. When high numbers of CTCs per mL blood are present, contamination of 5 mL CSF with just a few  $\mu$ L of blood may raise CTC levels above the detection limit, which can possibly effect the specificity of the assay.<sup>14</sup> Therefore, it is recommended to determine CTC-numbers in blood simultaneously with CSF, which up till now only has been done in one study.<sup>8</sup>

The question which technique, CELLSEARCH® or flow cytometry, is optimal to detect epithelial tumor cells in CSF is unresolved as comparable sensitivity and specificity rates can be gained with both methods (Table 2). No direct comparison with adequate power between both methods in patients with a clinical suspicion on LM has been done hitherto.<sup>5</sup> The CELLSEARCH® method requires specific reviewer training to minimize inter-reviewer discordant results.<sup>32</sup> Besides, a major limitation of the CELLSEARCH® analysis is the requirement of CELLSEARCH® reagents, CELLSEARCH® laboratory equipment and central laboratories equipped with CellTracks Autoprep, the CellTracks Analyzer II and trained operators. These prerequisites may limit wide-

spread application.<sup>23</sup> Flow cytometry assays for CTCs utilize standard flow cytometry equipment, which makes these assays more widely applicable and can potentially shorten the time to LM diagnosis compared to the CELLSEARCH® analysis. Another important merit of flow cytometry is their reliance on a predefined tumor cell gate, which allows fully automatic identification and enumeration of CTCs in CSF. From an analytical perspective it makes sense to perform a pre-enrichment step using magnetic cell sorting with ferrolabelled antibodies against EpCAM to lower the amount of cellular background events. This has been applied in the CELLSEARCH® assay and in some flow cytometry assays.<sup>5,8</sup> An overview of the benefits and drawbacks of flow cytometry and CELLSEARCH assays is given in Table 3.

**Table 3. Benefits and drawbacks of different flow cytometry and CELLSEARCH assays**

	<b>Benefit</b>	<b>Drawback</b>
CELLSEARCH®	<ul style="list-style-type: none"> <li>- FDA approved in blood<sup>21</sup></li> <li>- Interlaboratory validated</li> </ul>	<ul style="list-style-type: none"> <li>- Subjective identification of CTCs results in inter reviewer discordant results in 4-31% of 6 samples assessed by 14 institutes despite specific reviewer training<sup>a,30</sup></li> <li>- Less specific anti-cytokeratin-8, 18 and 19- PE staining</li> </ul>
	96 hours sample stability <sup>a,21</sup>	High between-laboratory coefficient of 45-64% <sup>a,30</sup>
Flow cytometry	Commercially available	Dedicated CELLSEARCH® equipment needed
	<ul style="list-style-type: none"> <li>-Fully automatic cell counting eliminates interobserver variability</li> <li>-Standard flow cytometry equipment can be used</li> <li>-More specific EpCAM-PE staining</li> </ul>	<ul style="list-style-type: none"> <li>-Not standardized between laboratories</li> <li>-Subirá et al. no immunomagnetic sample enrichment<sup>24,25</sup></li> </ul>

<sup>a</sup> Determined in blood. *Abbreviations:* EpCAM=epithelial cell adhesion molecule, PE=phycoerythrin.

A critical review of the randomized trials in LM using intra-CSF therapy, of which five of them enrolled patients with solid tumors, revealed that all these studies have methodological limitations with a lack of standardization for the evaluation of treatment response and long time-periods needed for accrual.<sup>33</sup> Also phase one clinical trials in patients with LM with targeted agents failed due to slow patient accrual.<sup>34,35</sup> To improve the accrual rate of (early) LM patients and the reliability of response evaluation in clinical trials, CTC assays in CSF are promising tools as tumor cells can be quantified at very low levels. As LM often has a devastating course with median reported survival between 2-5 months,<sup>36</sup> it is important to include patients with a low CSF tumor burden. A validated and sensitive CTC assay in CSF that can diagnose patients at an early LM stage when CSF cytology is still negative, is crucial. This was demonstrated by Milojkovic-Kerklaan et al., who reported that the EpCAM-

based flow cytometry assay in CSF brings higher sensitivity than CSF cytology for the diagnosis of LM, especially when CTC numbers in the CSF drop below 50 cells/mL.<sup>8</sup> The specificity of the different EpCAM assays varies between 84-100%. Future large scale study cohorts need to reveal the true sensitivity and specificity of CTC assays in CSF. It is of particular interest to determine the optimal cut-off value for the number of CTCs per mL with an optimal sensitivity and specificity by using Receiver Operating Curves.

CSF cytology is a non-quantitative method with a low sensitivity, which renders the technique insufficient for monitoring of treatment response. A sensitive quantitative technique enables patient treatment response monitoring. A decrease in the CTC number would be indicative for a response to treatment. In several articles described in our review, sequential CSF samples from patients have been obtained for treatment monitoring using CTC enumeration.<sup>4,5,19,20</sup> Lee et al. showed that in three of seven patients who had been treated for LM, no CTCs were detectable after treatment. CSF clearance of CTCs was associated with the longest survival with an average of 2 years.<sup>5</sup> Although the number of studies performed so far are limited, CTC enumeration in CSF has the potential to be a sensitive, specific, and quantitative biomarker for evaluating treatment response in LM. The new CTC assays do not only have the potential to be more sensitive, specific and quantitative in the diagnosis and treatment of LM, they also provide the possibility of expanding our knowledge on the pathophysiology of LM. Single cell analysis and the use of other molecular markers in the identification of the cells in the CSF may help to understand why this highly malignant cells metastasize to the CSF. Recently, Cordone et al. (2017) showed the presence of syndecan-1 and MUC-1 overexpression and the putative stem cell markers CD15, CD24, CD44 and CD133 on CTCs in the CSF of breast cancer patients with LM.<sup>37</sup>

In conclusion, we have shown in our review that the EpCAM-based assays are promising new techniques for epithelial tumor cell detection in CSF, although assay standardization and proper multicenter validation studies are needed before clinical implementation. Furthermore, the possibility of detecting (and isolating) low numbers of tumor cells in the CSF using flow cytometry assays opens new ways to further understand why these malignant cells metastasize to the central nervous system.

### **Conflict of interest**

The authors declare that they have no conflict of interest.

## References

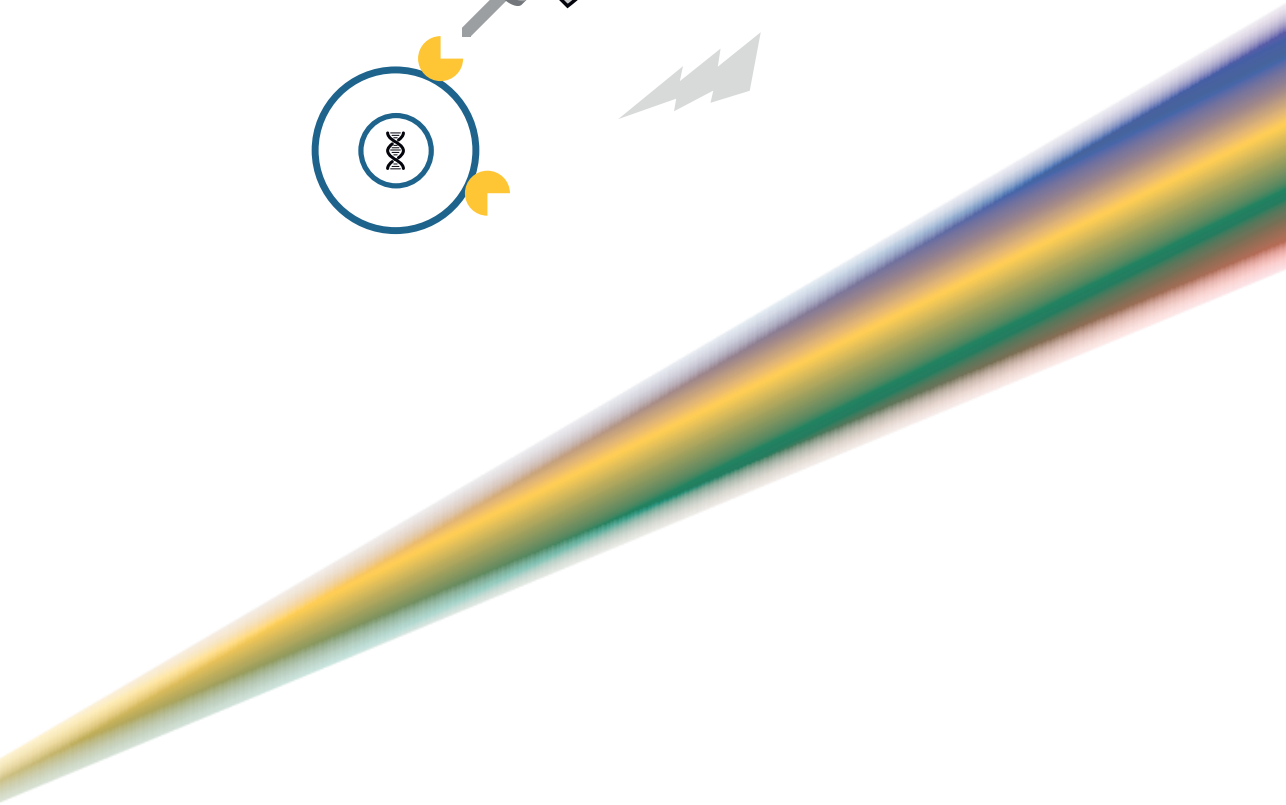
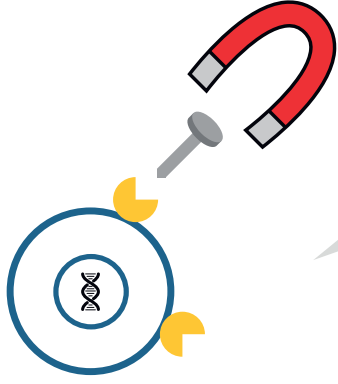
1. Straathof CS, de Bruin HG, Dippel DW, Vecht CJ. The diagnostic accuracy of magnetic resonance imaging and cerebrospinal fluid cytology in leptomeningeal metastasis. *J Neurol*. 1999;246(9):810-814.
2. Wasserstrom WR, Glass JP, Posner JB. Diagnosis and treatment of leptomeningeal metastases from solid tumors: experience with 90 patients. *Cancer*. 1982;49(4):759-772.
3. van Oostenbrugge RJ, Twijnstra A. Presenting features and value of diagnostic procedures in leptomeningeal metastases. *Neurology*. 1999;53(2):382-385.
4. Tu Q, Wu X, Le Rhun E, et al. CellSearch technology applied to the detection and quantification of tumor cells in CSF of patients with lung cancer leptomeningeal metastasis. *Lung Cancer*. 2015;90(2):352-357.
5. Lee JS, Melisko ME, Magbanua MJ, et al. Detection of cerebrospinal fluid tumor cells and its clinical relevance in leptomeningeal metastasis of breast cancer. *Breast Cancer Res Treat*. 2015;154(2):339-349.
6. Nayak L, Fleisher M, Gonzalez-Espinoza R, et al. Rare cell capture technology for the diagnosis of leptomeningeal metastasis in solid tumors. *Neurology*. 2013;80(17):1598-605; discussion 1603.
7. Jiang BY, Li YS, Guo WB, et al. Detection of Driver and Resistance Mutations in Leptomeningeal Metastases of NSCLC by Next-Generation Sequencing of Cerebrospinal Fluid Circulating Tumor Cells. *Clin Cancer Res*. 2017.
8. Milojkovic Kerklaan B, Pluim D, Bol M, et al. EpCAM-based flow cytometry in cerebrospinal fluid greatly improves diagnostic accuracy of leptomeningeal metastases from epithelial tumors. *Neuro Oncol*. 2016;18(6):855-862.
9. Subira D, Serrano C, Castanon S, et al. Role of flow cytometry immunophenotyping in the diagnosis of leptomeningeal carcinomatosis. *Neuro Oncol*. 2012;14(1):43-52.
10. Subira D, Simo M, Illan J, et al. Diagnostic and prognostic significance of flow cytometry immunophenotyping in patients with leptomeningeal carcinomatosis. *Clin Exp Metastasis*. 2015;32(4):383-391.
11. Maetzel D, Denzel S, Mack B, et al. Nuclear signalling by tumour-associated antigen EpCAM. *Nat Cell Biol*. 2009;11(2):162-171.
12. Litvinov S V, Velders MP, Bakker HA, Fleuren GJ, Warnaar SO. Ep-CAM: a human epithelial antigen is a homophilic cell-cell adhesion molecule. *J Cell Biol*. 1994;125(2):437-446.
13. Went PT, Lugli A, Meier S, et al. Frequent EpCam protein expression in human carcinomas. *Hum Pathol*. 2004;35(1):122-128.
14. Allard WJ, Matera J, Miller MC, et al. Tumor cells circulate in the peripheral blood of all major carcinomas but not in healthy subjects or patients with nonmalignant diseases. *Clin Cancer Res*. 2004;10(20):6897-6904.
15. Zhou Y, Bian B, Yuan X, Xie G, Ma Y, Shen L. Prognostic Value of Circulating Tumor Cells in Ovarian Cancer: A Meta-Analysis. *PLoS One*. 2015;10(6):e0130873.
16. Lv Q, Gong L, Zhang T, et al. Prognostic value of circulating tumor cells in metastatic breast cancer: a systemic review and meta-analysis. *Clin Transl Oncol*. 2016;18(3):322-330.
17. Huang X, Gao P, Song Y, et al. Meta-analysis of the prognostic value of circulating tumor cells detected with the CellSearch System in colorectal cancer. *BMC Cancer*. 2015;15:202.

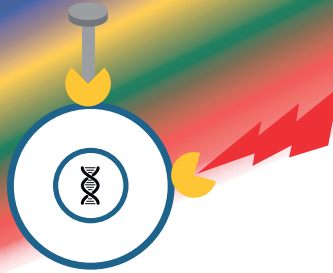
18. Ma X, Xiao Z, Li X, et al. Prognostic role of circulating tumor cells and disseminated tumor cells in patients with prostate cancer: a systematic review and meta-analysis. *Tumour Biol.* 2014;35(6):5551-5560.
19. Le Rhun E, Massin F, Tu Q, Bonnetterre J, Bittencourt Mde C, Faure GC. Development of a new method for identification and quantification in cerebrospinal fluid of malignant cells from breast carcinoma leptomeningeal metastasis. *BMC Clin Pathol.* 2012;12:21.
20. Patel AS, Allen JE, Dicker DT, et al. Identification and enumeration of circulating tumor cells in the cerebrospinal fluid of breast cancer patients with central nervous system metastases. *Oncotarget.* 2011;2(10):752-760.
21. Andree KC, van Dalum G, Terstappen LW. Challenges in circulating tumor cell detection by the CellSearch system. *Mol Oncol.* 2016;10(3):395-407.
22. CellSearch™ Circulating Tumor Cell Kit Premarket Notification- Expanded Indications for Use- Colorectal. Available at [https://www.accessdata.fda.gov/cdrh\\_docs/pdf7/k071729.pdf](https://www.accessdata.fda.gov/cdrh_docs/pdf7/k071729.pdf) Accessed 21 Mar 2017.
23. de Wit S, van Dalum G, Terstappen LW. Detection of circulating tumor cells. *Sci.* 2014;2014:819362.
24. Cellsearch® Circulating Tumor Cell Kit (Epithelial). Available at [http://documents.cellsearchctc.com/pdf/e631600004/e631600004\\_EN.pdf](http://documents.cellsearchctc.com/pdf/e631600004/e631600004_EN.pdf) Accessed 22 Mar 2017.
25. Riethdorf S, Fritsche H, Muller V, et al. Detection of circulating tumor cells in peripheral blood of patients with metastatic breast cancer: a validation study of the CellSearch system. *Clin Cancer Res.* 2007;13(3):920-928.
26. Tibbe AG, de Grooth BG, Greve J, Dolan GJ, Terstappen LW. Imaging technique implemented in CellTracks system. *Cytometry.* 2002;47(4):248-255.
27. Reprinted from Lung Cancer: vol. 90 number 2, Tu Q, Wu X, Le Rhun E, Blonski M, Wittwer B, Taillandier L, De Carvalho Bittencourt M, Faure GC. CellSearch technology applied to the detection and quantification of tumor cells in CSF of patients with lung cancer leptomeningeal metastasis, Pages No. 352-7 Copyright (2015), with permission from Elsevier.
28. Acosta M, Pereira J, Arroz M. Screening of carcinoma metastasis by flow cytometry: A study of 238 cases. *Cytom B Clin Cytom.* 2016;90(3):289-294.
29. Glantz MJ, Cole BF, Glantz LK, et al. Cerebrospinal fluid cytology in patients with cancer: minimizing false-negative results. *Cancer.* 1998;82(4):733-739.
30. Hyun KA, Koo GB, Han H, et al. Epithelial-to-mesenchymal transition leads to loss of EpCAM and different physical properties in circulating tumor cells from metastatic breast cancer. *Oncotarget.* 2016;7(17):24677-24687.
31. Hayes DF, Cristofanilli M, Budd GT, et al. Circulating tumor cells at each follow-up time point during therapy of metastatic breast cancer patients predict progression-free and overall survival. *Clin Cancer Res.* 2006;12(14 Pt 1):4218-4224.
32. Kraan J, Sleijfer S, Srijbos MH, et al. External quality assurance of circulating tumor cell enumeration using the CellSearch((R)) system: a feasibility study. *Cytom B Clin Cytom.* 2011;80(2):112-118.
33. Chamberlain M, Soffietti R, Raizer J, et al. Leptomeningeal metastasis: a Response Assessment in Neuro-Oncology critical review of endpoints and response criteria of published randomized clinical trials. *Neuro Oncol.* 2014;16(9):1176-1185.

34. Jackman DM, Cioffredi LA, Jacobs L, et al. A phase I trial of high dose gefitinib for patients with leptomeningeal metastases from non-small cell lung cancer. *Oncotarget*. 2015;6(6):4527-4536.
35. Wu PF, Lin CH, Kuo CH, et al. A pilot study of bevacizumab combined with etoposide and cisplatin in breast cancer patients with leptomeningeal carcinomatosis. *BMC Cancer*. 2015;15:299.
36. Brower J V, Saha S, Rosenberg SA, Hullett CR, Ian Robins H. Management of leptomeningeal metastases: Prognostic factors and associated outcomes. *J Clin Neurosci*. 2016;27:130-137.
37. Cordone I, Masi S, Summa V, et al. Overexpression of syndecan-1, MUC-1, and putative stem cell markers in breast cancer leptomeningeal metastasis: a cerebrospinal fluid flow cytometry study. *Breast Cancer Res*. 2017;19(1):46.









# Chapter 2

## Circulating epithelial tumor cell analysis in cerebrospinal fluid in patients with leptomeningeal metastases

Mark T.J. van Bussel  
Dick Pluim  
Bojana Milojkovic Kerklaan  
Mijke Bol  
Karolina Sikorska  
Dorothe Linders  
Daan van den Broek  
Jos H. Beijnen  
Jan H. M. Schellens  
Dieta Brandsma

*Accepted for publication in Neurology*

## Summary

### Objective

The primary objective was to determine the sensitivity and specificity of epithelial cell adhesion molecule (EpCAM) immunoflow cytometry circulating tumor cells (CTC) analysis in cerebrospinal fluid (CSF) in patients with suspected leptomeningeal metastases (LM). The secondary objective was to explore the distribution of driver mutations in the primary tumor, plasma, cell free (cf)CSF and isolated CTC from CSF in non-small cell lung cancer (NSCLC).

### Methods

We tested the performance of the CTC assay versus CSF cytology in a prospective study in 81 patients with a clinical suspicion of LM but a non-confirmatory MRI. In a NSCLC subcohort we analyzed circulating tumor (ct)DNA of the selected driver mutations by digital droplet (dd)PCR.

### Results

The sensitivity of the CTC assay was 94% (95% CI 80-99) and the specificity was 100% (95% CI 91-100) at the optimal cut-off of 0.9 CTC/mL. The sensitivity of cytology was 76% (95% CI 58-89). Twelve of the 23 NSCLC patients were epidermal growth factor receptor (EGFR) mutated. All 5 tested patients with LM demonstrated the primary EGFR driver mutation in cfCSF. The driver mutation could also be detected in CTC isolated from CSF.

### Conclusion

CTC in CSF are detected with a high sensitivity for the diagnosis of LM. ddPCR can determine EGFR mutations in both cfCSF and isolated CTC from CSF of EGFR mutated NSCLC patients with LM.

### Classification of evidence

This study provides Class III evidence that in patients clinically suspected for LM, EpCAM-based flow cytometry analysis of CSF is recommended as part of routine diagnostic workup.

## Introduction

Approximately 10% of patients with solid tumors develop leptomeningeal metastases (LM).<sup>1</sup> The diagnosis of LM can be based on clinical symptoms compatible with LM and typical contrast enhancement of the leptomeninges on MRI brain and/or spine. However, MRI has a low sensitivity (76%) and specificity (77%) for the diagnosis of LM.<sup>2</sup> When MRI is normal or results are inconclusive, a lumbar puncture (LP) is performed to obtain cerebrospinal fluid (CSF). Sensitivity of CSF cytology is also low: 44-67% at first LP, increasing to 84-91% upon second sampling.<sup>3-11</sup> To improve CSF diagnostics in patients with solid tumors, epithelial cell adhesion molecule (EpCAM) assays have been developed to detect CTC in CSF with reported sensitivities of 76-100%.<sup>5-11</sup> Here we describe the results of an EpCAM immunoflow cytometry assay in CSF compared to CSF cytology in 81 patients for the diagnosis of LM.

Tumor cell detection in CSF is pivotal for the diagnosis of LM, but ctDNA analysis of CSF can be of additive value for driver mutation detection. Driver mutation determination by circulating tumor DNA (ctDNA) analysis in plasma has clinical utility in epidermal growth factor receptor mutated (EGFR) non-small-cell lung cancer (NSCLC).<sup>12</sup> Furthermore, EGFR mutant DNA copy number in CSF can be used for response evaluation.<sup>13</sup> In 6 out of 7 patients with brain metastases from various tumor types, including two EGFR mutated NSCLC patients, ctDNA fragments were detected in the CSF.<sup>14</sup> It is unknown whether the presence of ctDNA in CSF can currently be used to diagnose LM, as ctDNA fragments may also be present in patients with brain metastases only. In the current study, both cell-free ctDNA analysis in CSF and DNA mutation analysis of isolated CTC from CSF is performed to determine the known driver tumor mutations of the primary tumor.

## Methods

### Patients

The institutional review board of the Netherlands Cancer Institute - Antoni van Leeuwenhoek and the Medical Center Slotervaart approved the study. Written informed consent was obtained from all participants. Patients were consecutively included in the prospective study between October 2012 and Augustus 2018. Patients  $\geq 18$  years with a (metastasized) epithelial tumor and clinical suspicion of LM but a normal or inconclusive MRI who had to undergo a diagnostic LP were asked to participate. CSF pressure was measured. Next 20 mL CSF was collected: 1x5 mL CSF for cytology, 1x5mL for leukocyte count and biochemical parameters, 1x5 mL for

CTC analysis and 1x5mL for CTC isolation. Cytology and CTC analysis were performed by independent operators. Diagnosis of LM was defined as follows: a positive CSF cytology at the initial LP or repeated LP performed within 6 weeks after the initial LP, or a follow-up MRI of the brain or spine performed after the diagnostic LP within 2 months following the first MRI, showing unequivocal evidence of LM and/or progressive neurological symptoms compatible with LM and exclusion of other causes (e.g. infectious meningitis, treatment side effects). Patients with possible or probable LM were classified according to the European Association of Neuro-Oncology - European Society of Medical Oncology (EANO-ESMO) clinical practice guidelines for LM.<sup>1</sup> The final diagnoses were made by one neurologist (D.B.) who had access to index test results and the reference standard. Non-oncological patients with a clinical indication for a diagnostic LP due to a suspicion on an infectious or auto-immune meningitis or subarachnoid hemorrhage were included for the control group. Exclusion criteria for a LP in both groups were: intracranial or intraspinal tumor with mass effect heralding the risk of herniation during LP and uncorrected thrombocytopenia or coagulation disorders. Patients were interviewed via a follow-up telephone call for evaluation of post-punctional headache at day 3 of the study. The primary objective of the study was to determine the sensitivity and specificity of detection of CTC in patients with epithelial tumors compared to cytology in the CSF, in patients clinically suspected of LM (Class III level of evidence). The secondary objective was to explore the distribution of driver mutations in the primary tumor, plasma, cell free (cf)CSF and isolated CTC from CSF in non-small cell lung cancer (NSCLC). This trial was registered at [www.clinicaltrials.gov](http://www.clinicaltrials.gov) (NCT01713699).

### **CTC and ctDNA assays**

We used the same EpCAM immunoflow cytometry assay for CTC detection as the one employed in a previous study.<sup>15,16</sup> In case the CSF-CTC sample (5 mL) appeared to be positive, the extra collected CSF-CTC sample (5 mL) was used to isolate the CTC fraction via fluorescence-activated cell sorting (FACS) for determination of the selected driver mutation of the CTC. Selective driver mutation analysis was performed as a secondary exploratory endpoint. Blood samples were collected in K2EDTA (ethylene diamine tetra acetic acid) tubes (BD Vacutainer, Franklin Lakes, NJ, USA) and plasma was separated by centrifugation. The cfDNA was extracted using the QIA Symphony DSP circulating DNA Kit. (Qiagen, Hilden, Germany). cfDNA of plasma and CSF samples was analysed by the QX200TM Droplet DigitalTM PCR (ddPCR) system (Bio-Rad).<sup>17</sup>

## Statistical analysis

### Sample size calculation

The aim of the study was to include 100 patients. The power calculation was performed for sensitivity of the CTC-assay in CSF. A sensitivity of the CSF-CTC assay higher than the reported sensitivity of cytology of 67% would be of clinical interest.<sup>7</sup> We expected to achieve a sensitivity of 95% for the CTC-CSF assay.<sup>15</sup> At the start of the trial the prevalence of LM was unknown, but it was set to 20%-50%. A sample size of 100 patients has around 92% power to test the sample sensitivity at the two-sided alpha level of 0.05. Confidence intervals for the sensitivities and specificities were calculated using Clopper and Pearson method. The best cut-off for the CTC was optimized by maximizing sensitivity and specificity using the R package OptimalCutpoints. The Standards for Reporting Diagnostic accuracy studies (STARD) were used as a guideline for preparation of the final report.<sup>18</sup>

### Data Availability Statement

Data can be requested from the corresponding author.

## Results

In total, 98 patients were potentially eligible for the study as shown in Figure 1, of whom 81 patients with a clinical suspicion of LM were eligible for the assessment of

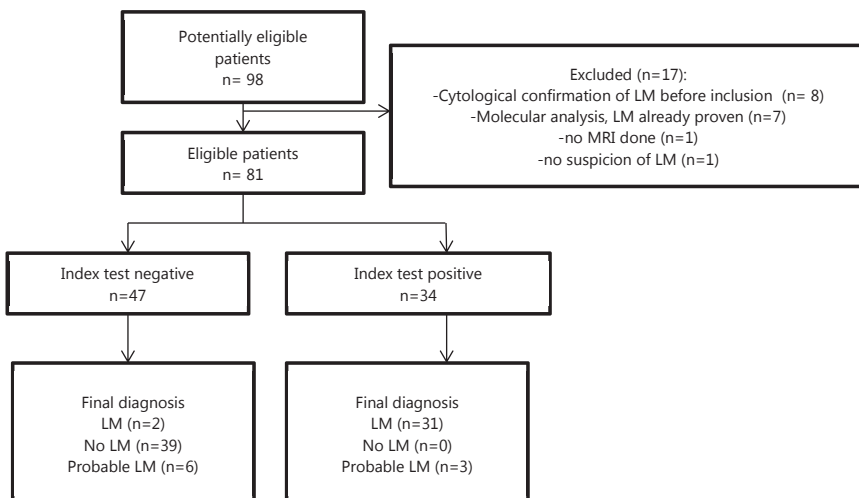


**Figure 1.** STARD diagram to report flow of participants through the study  
*Abbreviations:* LM=leptomeningeal metastases.

the index test. In 9 patients the LM diagnosis was not definitive but these patients were scored as possible or probable LM or lack of evidence for LM according to the EANO-ESMO guidelines. The test characteristics are therefore calculated based on the remaining 72 patients. The baseline characteristics of the remaining 72 patients are shown in Table 1. The presenting neurological symptoms are depicted in Table 2.

**Table 1. Baseline patient characteristics (n=72)**

Mean age in years [range]	58 [32-82]
Female, number (%)	53 (74)
Primary tumor type	Number (%)
Breast cancer	28 (39)
-Ductal	16
-Lobular	10
Lung cancer	26 (36)
-NSCLC	23
-SCLC	3
Gastrointestinal tract	5 (7)
-Colorectal	2
-Oesophageal	2
-Gastric	1
Ovarian	2 (3)
Urothelial carcinoma	4 (6)
Other <sup>a</sup>	7 (10)

<sup>a</sup>These patients had the following diagnosis: nasopharynx carcinoma, or 2 primary tumors: ductal breast cancer and NSCLC, neuro endocrine tumor and esophageal tumor, ductal breast cancer and colon carcinoma, basal cell carcinoma and breast cancer, melanoma and breast cancer, melanoma and thyroid cancer. *Abbreviations:* NSCLC=non-small-cell lung cancer, SCLC= small-cell lung cancer.

The prevalence of LM in the eligible cohort was 41% (n=33). The final diagnosis of definitive LM was based on CSF cytology or MRI and/or progressive neurological symptoms compatible with LM as shown in Figure 2. 25 (76%) patients had positive CSF cytology, 7 (21%) patients were diagnosed with LM based on both MRI and progressive neurological symptoms and 1 (3%) patient was diagnosed with LM based on progressive neurological symptoms only.



**Table 2. Presenting neurological symptoms (n=72)**

Clinically affected domain	N (%)
Cognitive function	7 (10)
Speech / language	5 (7)
Cranial nerves	24 (34)
Strength	13 (18)
Coordination of arms and legs	12 (17)
Sensibility of arms and legs	14 (20)
Walking pattern	17 (26)

Presenting neurological symptoms in 72 included patients with a clinical suspicion of leptomeningeal metastases but a normal or inconclusive MRI. Patients could have more than one presenting symptom.

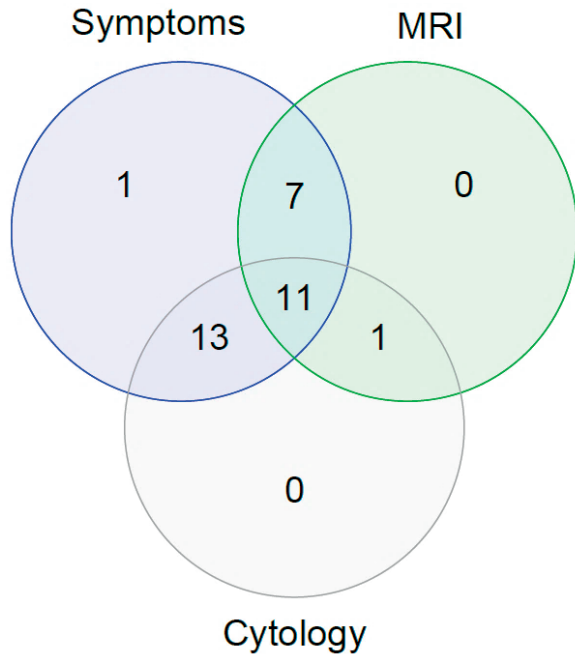


**Figure 2. Venn diagram of the diagnosis of definitive leptomeningeal metastases based on CSF cytology, MRI and progressive neurological symptoms**

In 9 of the 81 patients LM diagnosis was not proven/definitive, but according to the EANO-ESMO LM clinical practice guidelines for LM they were diagnosed with possible or probable LM as shown in Table 3.<sup>1</sup> 12 patients with a non-oncological disease were included as a control group. These patients had the following diagnoses: a neurological infectious disease (neuroborreliosis, neurolues, viral myelitis), multiple sclerosis, dementia, neuropathy or a non-neurological disease.

Table 3. Patients with probable and possible leptomeningeal metastases

Patient	Tumor type	Symptoms	MRI	CSF Cytology in CSF	CTC /mL	EANO LM classification
17	NSCLC - EGFR mutation	No typical LM symptoms	Leptomeningeal contrast enhancing lesions	Negative 0		Possible LM IIC
26	Breast cancer	Epilepsy	Focal leptomeningeal contrast enhancing lesion	Negative 3		Possible LM IIA
71	Breast cancer	Headache, increased ICP	Dural contrast enhancement; no leptomeningeal contrast enhancement	Negative 0.6		Lack of evidence for LM - IID
86	NSCLC - EGFR mutation	Encephalopathy	No leptomeningeal contrast enhancement	Negative 49.6		Possible LM IID
87	NSCLC - EGFR mutation	No typical LM symptoms	Nodular leptomeningeal lesions	Negative 3.2		Possible LM IIB
88	NSCLC - no EGFR mutation	Hearing loss, headache	Single nodular leptomeningeal lesion	Negative 0		Possible LM IIB
111	NSCLC - EGFR mutation	No neurological symptoms	Linear and nodular leptomeningeal lesions	Negative 0.2		Possible LM IIC
129	NSCLC - ALK translocated	Apathy, dysphasia, right-sided hemiparesis	Linear leptomeningeal lesions	Negative 0		Possible LM IIA
144	NSCLC - EGFR mutation	Cerebellar syndrome, cranial nerve dysfunction (N V and N II right-sided)	Linear and nodular leptomeningeal enhancement	Negative 0		Probable LM IIC

Patients with probable and possible LM according to EANO-ESMO guidelines.<sup>1</sup> Abbreviations: LM=leptomeningeal metastases, EANO=European Association of Neuro-Oncology, ICP=intracranial pressure, NSCLC=non-small-cell lung cancer, SCLC=small-cell lung cancer, CTC=circulating tumor cells, EGFR=epidermal growth factor receptor, ALK=Anaplastic lymphoma kinase.

### CSF pressure, cell count and biochemical parameters

CSF pressure was increased (>20 cm H<sub>2</sub>O) in 52% of patients with definitive LM. Increased total protein CSF levels (>0.45 g/L) were present in 85% of patients with LM. Leucocyte CSF counts were increased (>3/mm<sup>3</sup>) in 61% of patients with LM. LDH CSF levels were increased (>40 U/L) in 48% and glucose CSF/serum ratio was decreased (<0.66) in 94% of patients with LM. 10% of the patients experienced post lumbar puncture headache.

### Diagnostic accuracy of CSF cytology versus EpCAM-based immunoflow cytometry

CSF cytology had a sensitivity of 76% (95% CI 58-89) for the diagnosis of LM. The specificity of CSF cytology is 100% as it is accepted as the gold standard for the diagnosis of LM in this patient population.<sup>6</sup>

For the EpCAM-based immunoflow cytometry assay in CSF a receiver operating characteristic (ROC) analysis was done to define the optimal cut-off value of the CTC number per mL CSF for the definitive diagnosis of LM. The optimal cut-off value for the flow cytometry assay was 0.86 CTC/mL. This cut-off value provides a sensitivity of 94% (95% CI 80 - 99) and a specificity of 100% (95% CI 91 - 100). The positive predictive value was 100% (95% CI 89 - 100) and the negative predictive value was 95% (95% CI 83 - 99). The receiver operating characteristic (ROC) Area Under the Curve was 0.98 (95% CI 0.94-1). All control patients with non-oncological diseases had a CSF-CTC number equal or less than 0.2 CTC/mL.

### Driver mutation analysis in NSCLC patients

NSCLC was the primary tumor in 23 of 72 (32%) included patients. In 12 of these patients (52%) an EGFR mutation was present in their primary tumor or metastases. In 10 patients the EGFR driver or resistance mutation was determined in cfDNA CSF samples. In 3 patients without LM the EGFR mutation in cfCSF was not detected. In 5 out of 5 patients with LM the primary EGFR driver mutation was detected in cfCSF. In four of these patients the primary EGFR mutation was detected in CTC from CSF, isolated by immunoflow cytometry. Three of them were positive for the L858R mutation of exon 21 and one had an exon 19 deletion. In two LM patients with a T790M mutation in recurrent tumor or metastasis after 1<sup>st</sup> line EGFR inhibitor treatment, T790M was assessed in cfCSF. One patient was T790M positive and the other one was negative. In the patient with negative cfCSF for T790M, isolated CTC from CSF were also negative. In 6 out of 8 assessed plasma samples from individual EGFR mutated NSCLC patients we detected the primary EGFR driver mutation in cfDNA. The EGFR driver mutation distribution in primary tumor, plasma and CSF is depicted in Table 4.

Table 4. EGFR driver mutation distribution

Diagnosis	EGFR Mutation				Flow cytometry CTC/mL CSF
	Primary tumor or metastases	Plasma	cfCSF	Isolated CTC from CSF	
LM	Exon 19 del	Not done	Exon 19 del	Not done	42
LM	Exon 19 del	Exon 19 del	Exon 19 del	Not done	69
LM	L858R T790M	Not done Not done	Not done Negative	Not done Negative	2.2
LM	L858R	L858R	L858R	L858R	166
LM	L858R T790M	Negative Not done	Not done T790M	L858R Not done	30
LM	Exon 19 del	Exon 19 del	Exon 19 del	Exon 19 del	0.86
LM	L858R	L858R	L858R	L858R	13
No LM	Exon 19 del	Negative	Negative	-	0
No LM	L858R	L858R	Negative	-	0.20
No LM	Exon 19 del Negative	Exon 19 del T790M	Inconclusive due to low DNA content in CSF sample	-	0

*Abbreviations:* LM=leptomeningeal metastases, EGFR=epidermal growth factor receptor, cf=cell free, CSF=cerebrospinal fluid, NSCLC=non-small-cell lung cancer, CTC=circulating tumor cells.

## Discussion

This prospective clinical diagnostic study shows a high sensitivity of 94% and specificity of 100% for the detection of CTC with our EpCAM-based flow cytometry assay in CSF of patients with epithelial tumors and LM. It showed similar results with regard to the sensitivity and specificity in diagnosing LM as previously published for the CELLSEARCH® CTC assay.<sup>19</sup> EpCAM is expressed by tumors of epithelial origin like NSCLC, breast cancer or ovarian cancer.<sup>20</sup> The CELLSEARCH® assay is a FDA-approved assay to detect EpCAM positive CTC in blood and is adapted for use in CSF.<sup>16,21</sup> This method was recommended for use as part of routine LM work-up. However, in the CELLSEARCH® assay CTC are identified by an operator which coincides with inter-reviewer discordant results.<sup>22</sup> To avoid operator bias, immunoflow cytometry CTC assays of the CSF can be used. Our data indicate that the EpCAM-based CTC immunoflow cytometry analysis of CSF is an adequate, alternative method to detect CTC of epithelial tumors in CSF for the diagnosis of LM. Both the CELLSEARCH® CTC assay and our immunoflow cytometry EpCAM assay do not show a 100% diagnostic accuracy for LM. In studies using the CELLSEARCH® technique 2 out of 8 patients and 2 out of 81 samples respectively were found with a positive CSF cytology but negative CTC.<sup>6,23</sup> Our series showed two patients with LM who were negative for CTC and CSF cytology. This could be due to

loss of EpCAM expression of malignant cells during the metastatic cascade of cells to the CSF.<sup>24</sup> The false-negative findings of EpCAM CTC analysis in patients with positive CSF cytology support the choice for cytology as an additional, non-EpCAM dependent dual diagnostic CSF method for LM. In the past, questions have been raised whether circulating epithelial cells in the blood detected by CELLSEARCH® are indeed CTC.<sup>25</sup> Based on the driver mutation analysis of the EpCAM-positive CTC in CSF and the absence of CTC in CSF both in patients without LM and the non-oncology control patients, we conclude that the EpCAM positive CTC found in CSF are indeed epithelial tumor cells. All diagnostic studies for LM are hampered by the lack of a golden standard for LM in case of negative CSF cytology. When CSF cytology is negative, LM diagnosis is based on an interpretation of progressive neurological symptoms and subsequent MRIs, in our study this was performed by one neurologist (D.B.) experienced in LM. A group of 9 patients was scored initially with an uncertain LM diagnosis. We ultimately scored these patients according the EANO/ESMO guidelines as probable LM, possible LM or lack of evidence of LM.<sup>1</sup> In only 3 of 9 patients with possible or probable LM, CSF-CTC were  $\geq 0.9/\text{mL}$  confirming the diagnosis of LM.

EpCAM CTC analysis in CSF is not only a sensitive way to diagnose LM, but is also a quantitative assay and therefore enables patient treatment response monitoring. Thus far, LM-response is based on change of neurological symptoms and MRI and CSF cytological results. Response measurement in LM is hampered by of the lack of sensitivity of CSF cytology and validation problems in response measurement of both neurological symptoms and MRI abnormalities in LM, despite ongoing efforts of the Response Assessment in Neuro-Oncology (RANO) LM group.<sup>1,26</sup> In this respect, it will be important to include CTC analysis methods in CSF in future LM studies and determine whether CTC numbers in CSF reflect treatment response and predict survival/prognosis in an accurate way.

In our study we included 23 NSCLC patients of whom 12 having an EGFR mutation in the primary tumor and/or metastases. In NSCLC the prevalence of EGFR driver mutations in the primary tumor is 10-20% in the Caucasian population.<sup>27</sup> About 90% of the EGFR mutations are deletions in exon 19 or a L858R substitution mutation in exon 21. EGFR mutated NSCLC can be treated with ATP competitive EGFR tyrosine kinase inhibitors (TKI) of the first generation (erlotinib and gefitinib) or the irreversibly binding second generation TKI (afatinib). The T790M exon 20 substitution is in 50-60% of the cases the cause of resistance to first- and second-generation EGFR TKIs. The irreversibly binding third generation TKI osimertinib was initially registered for T790M NSCLC only. Recently, osimertinib has become first-line treatment in EGFR mutated NSCLC in case of an exon 19 deletion or L858R mutation.<sup>27</sup> In our study we found the

primary EGFR mutation in cfCSF and isolated CTC from CSF in patients with LM. The presence of the driver mutation in the EGFR gene of the CTC isolated from CSF with FACS confirms that we indeed detect cancer cells in the CTC gate of the immunoflow cytometry assay.

Molecular analysis of tumor tissue biopsies, CTC and ctDNA derived from blood of 120 patients with EGFR mutated NSCLC showed an agreement of 95%.<sup>28</sup> The isolation of tumor cells from CSF using immunoflow cytometry sorting opens the way for more extensive mutation analysis (both driver mutations and resistance mutations) of tumor cells that have metastasized to the CSF. These mutation analyses of CTC in CSF may be used to guide future treatment, in particular in those patients with progressive CNS metastases and stable systemic metastases. Furthermore, Next Generation Sequencing of isolated tumor cells from CSF compared to tumor cells isolated from the primary tumor and the systemic metastases may reveal the genetic mechanisms that support cells to metastasize to the CSF.

Further research with larger cohorts of patients with MRI brain (for brain metastases detection), concomitant CTC analysis of CSF (for LM detection) and paired plasma-CSF ctDNA sampling is essential in order to draw conclusions on the clinical utility of the presence of ctDNA in CSF for the diagnosis of LM. In particular patients with brain metastases near the CSF compartment may shed DNA into the CSF suggesting LM, which is not the case according to CTC-CSF analysis (false positive results). ctDNA analysis has an average sensitivity of 66% (95% CI 63-69) and a specificity of 96% (95% CI 83-99) in blood in patients with NSCLC.<sup>12</sup> The sensitivity of ctDNA detection in CSF in NSCLC for the diagnosis of LM is unknown but based on the results in plasma, we would expect a higher false negative rate of ctDNA detection in CSF than for CTC for the diagnosis of LM. Moreover, ctDNA mutation analysis in the CSF cannot be used currently to diagnose LM as ctDNA in CSF has also been detected in patients with brain metastases only.

In conclusion, we recommend including an EpCAM-based CTC method, either our EpCAM immunoflow cytometry assay or the FDA-approved CELLSEARCH® CTC assay, in the diagnostic work-up for patients with a clinical suspicion of LM next to CSF cytology. Driver mutation analysis of cfCSF and isolated CTC from CSF can further be used to guide future therapy of CNS metastases and unravel the pathophysiological and /genetic mechanisms of tumor cells metastasizing to the CSF.

### **Conflict of interest**

The trial has been sponsored by the Netherlands Cancer Institute-Antoni van Leeuwenhoek.

### **Acknowledgements**

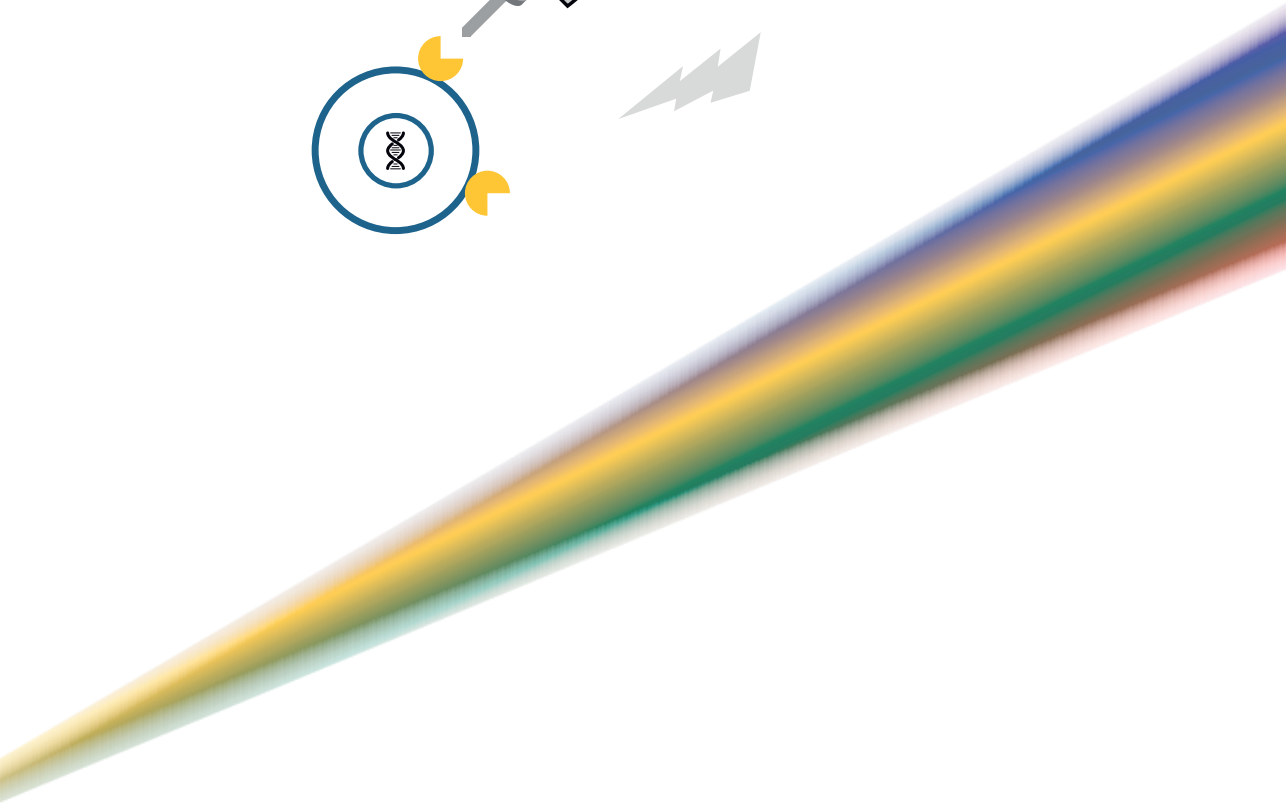
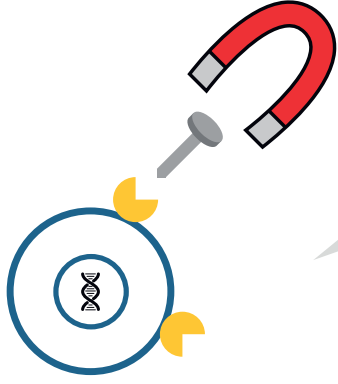
We would like to acknowledge NKI-AVL Core Facility Molecular Pathology & Biobanking (CFMPB) for supplying NKI-AVL Biobank material and/or laboratory support.

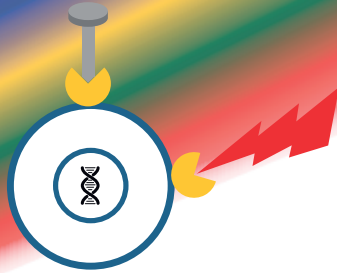
## References

1. Le Rhun E, Weller M, Brandsma D, et al. EANO-ESMO Clinical Practice Guidelines for diagnosis, treatment and follow-up of patients with leptomeningeal metastasis from solid tumours. *Ann Oncol*. 2017;28(suppl\_4):iv84-iv99.
2. Straathof CS, de Bruin HG, Dippel DW, Vecht CJ. The diagnostic accuracy of magnetic resonance imaging and cerebrospinal fluid cytology in leptomeningeal metastasis. *J Neurol*. 1999;246(9):810-814.
3. Wasserstrom WR, Glass JP, Posner JB. Diagnosis and treatment of leptomeningeal metastases from solid tumors: experience with 90 patients. *Cancer*. 1982;49(4):759-772.
4. van Oostenbrugge RJ, Twijnstra A. Presenting features and value of diagnostic procedures in leptomeningeal metastases. *Neurology*. 1999;53(2):382-385.
5. Tu Q, Wu X, Le Rhun E, et al. CellSearch technology applied to the detection and quantification of tumor cells in CSF of patients with lung cancer leptomeningeal metastasis. *Lung Cancer*. 2015;90(2):352-357.
6. Lee JS, Melisko ME, Magbanua MJ, et al. Detection of cerebrospinal fluid tumor cells and its clinical relevance in leptomeningeal metastasis of breast cancer. *Breast Cancer Res Treat*. 2015;154(2):339-349.
7. Nayak L, Fleisher M, Gonzalez-Espinoza R, et al. Rare cell capture technology for the diagnosis of leptomeningeal metastasis in solid tumors. *Neurology*. 2013;80(17):1598-605; discussion 1603.
8. Jiang B-Y, Li Y-S, Guo W-B, et al. Detection of Driver and Resistance Mutations in Leptomeningeal Metastases of NSCLC by Next-Generation Sequencing of Cerebrospinal Fluid Circulating Tumor Cells. *Clin Cancer Res*. 2017;23(18):5480-5488.
9. Milojkovic Kerklaan B, Pluim D, Bol M, et al. EpCAM-based flow cytometry in cerebrospinal fluid greatly improves diagnostic accuracy of leptomeningeal metastases from epithelial tumors. *Neuro Oncol*. 2016;18(6):855-862.
10. Subira D, Serrano C, Castanon S, et al. Role of flow cytometry immunophenotyping in the diagnosis of leptomeningeal carcinomatosis. *Neuro Oncol*. 2012;14(1):43-52.
11. Subira D, Simo M, Illan J, et al. Diagnostic and prognostic significance of flow cytometry immunophenotyping in patients with leptomeningeal carcinomatosis. *Clin Exp Metastasis*. 2015;32(4):383-391.
12. Merker JD, Oxnard GR, Compton C, et al. Circulating Tumor DNA Analysis in Patients With Cancer: American Society of Clinical Oncology and College of American Pathologists Joint Review. *J Clin Oncol*. 2018;36(16):1631-1641.
13. Ahn MJ, Kim DW, Cho BC, et al. Activity and safety of AZD3759 in EGFR-mutant non-small-cell lung cancer with CNS metastases (BLOOM): a phase 1, open-label, dose-escalation and dose-expansion study. *Lancet Respir Med*. 2017;5(11):891-902.
14. Pan W, Gu W, Nagpal S, Gephart MH, Quake SR. Brain tumor mutations detected in cerebral spinal fluid. *Clin Chem*. 2015;61(3):514-522.
15. Pluim D, Devriese LA, Beijnen JH, Schellens JHM. Validation of a multiparameter flow cytometry method for the determination of phosphorylated extracellular-signal-regulated kinase and DNA in circulating tumor cells. *Cytometry A*. 2012;81(8):664-671.
16. van Bussel MTJ, Pluim D, Bol M, Beijnen JH, Schellens JHM, Brandsma D. EpCAM-based assays for epithelial tumor cell detection in cerebrospinal fluid. *J Neurooncol*. 2018;137(1):1-10.



17. van Ginkel JH, van den Broek DA, van Kuik J, et al. Preanalytical blood sample workup for cell-free DNA analysis using Droplet Digital PCR for future molecular cancer diagnostics. *Cancer Med.* 2017;6(10):2297-2307.
18. Bossuyt PM, Reitsma JB, Bruns DE, et al. STARD 2015: an updated list of essential items for reporting diagnostic accuracy studies. *BMJ.* 2015;351(12):h5527.
19. Lin X, Fleisher M, Rosenblum M, et al. Cerebrospinal fluid circulating tumor cells: a novel tool to diagnose leptomeningeal metastases from epithelial tumors. *Neuro Oncol.* 2017;19(9):1248-1254.
20. Went PT, Lugli A, Meier S, et al. Frequent EpCam protein expression in human carcinomas. *Hum Pathol.* 2004;35(1):122-128.
21. Hayes DF, Cristofanilli M, Budd GT, et al. Circulating tumor cells at each follow-up time point during therapy of metastatic breast cancer patients predict progression-free and overall survival. *Clin Cancer Res.* 2006;12(14 Pt 1):4218-4224.
22. Kraan J, Sleijfer S, Srijbos MH, et al. External quality assurance of circulating tumor cell enumeration using the CellSearch(®) system: a feasibility study. *Cytometry B Clin Cytom.* 2011;80(2):112-118.
23. Le Rhun E, Massin F, Tu Q, Bonnetterre J, Bittencourt Mde C, Faure GC. Development of a new method for identification and quantification in cerebrospinal fluid of malignant cells from breast carcinoma leptomeningeal metastasis. *BMC Clin Pathol.* 2012;12:21.
24. Königsberg R, Obermayr E, Bises G, et al. Detection of EpCAM positive and negative circulating tumor cells in metastatic breast cancer patients. *Acta Oncol.* 2011;50(5):700-710.
25. Fiegl M, Denz H. Circulating epithelial cells in breast cancer. *N Engl J Med.* 2004;351(23):2452-4; author reply 2452-4.
26. Chamberlain M, Junck L, Brandsma D, et al. Leptomeningeal metastases: A RANO proposal for response criteria. *Neuro Oncol.* 2017;19(4):484-492.
27. Planchard D, Popat S, Kerr K, et al. Metastatic non-small cell lung cancer: ESMO Clinical Practice Guidelines for diagnosis, treatment and follow-up. *Ann Oncol.* 2018;29(Supplement\_4):iv192-iv237.
28. He J, Tan W, Ma J. Circulating tumor cells and DNA for real-time EGFR detection and monitoring of non-small-cell lung cancer. *Future Oncol.* 2017;13(9):787-797.





# Chapter 3

## **Circulating melanoma cell detection and driver mutation analysis in cerebrospinal fluid in melanoma patients with suspected leptomeningeal metastases**

Mark T.J. van Bussel  
Dick Pluim  
Bojana Milojkovic Kerklaan  
Emilie Le Rhun  
Mijke Bol  
Dorothe Linders  
Daan van den Broek  
Karolina Sikorska  
Annette Compter  
Jos H. Beijnen  
Jan H. M. Schellens  
Dieta Brandsma

*Submitted*

## Summary

### Background

MRI has a low sensitivity of 76% for the diagnosis of leptomeningeal metastases (LM). Cerebrospinal fluid (CSF) cytology sensitivity varies from 44-67% at first lumbar puncture (LP). To improve CSF diagnostics for LM in melanoma patients, a melanoma-associated chondroitin sulphate proteoglycan (MCSP) and CD146-based circulating melanoma cell (CMC) immunoflow cytometry assay has been developed.

### Methods

In this multicentre, prospective clinical study we evaluate the CMC enumeration in CSF of 42 patients with a clinical suspicion for LM. Thirty-six of them had a negative or equivocal MRI and 6 showed typical leptomeningeal contrast enhancement on MRI. Furthermore, CMC in CSF were enumerated in 10 non-oncological control patients. EANO-ESMO clinical practice guidelines were used to classify LM diagnosis. Driver mutation analysis of *BRAFV600E* was performed on paired cell free CSF, isolated CMC from CSF and plasma samples in 15 patients with *BRAFV600E* mutated melanoma.

### Results

As determined by the EANO-ESMO LM criteria, 13 patients had confirmed LM by CSF cytology, 1 probable LM, 8 possible LM and 20 no LM. CMC were detected in CSF in 11 of 12 patients with confirmed LM in whom CSF was available (1.9 - 5587 CMC/mL). In one of 12 patients no CMC were found. One patient with probable LM had 180 CMC/mL and 2 out of 8 patients with possible LM had 9.8 CMC/mL and 3.5 CMC/mL, respectively. Control patients and non-LM patients had  $\leq 0.3$  CMC/mL. Cell-free CSF samples of all four patients with *BRAFV600E* mutated melanoma and cytology confirmed LM were positive for the *BRAFV600E* driver mutation. CMC isolated from CSF in 2 of these patients with confirmed LM were *BRAFV600E* positive.

### Conclusion

The newly developed MCSP/CD146 immunoflow cytometry assay is a promising tool to detect melanoma cells in CSF and diagnose LM. Driver mutation analysis can be used to detect *BRAFV600E* mutations in both cell-free CSF and CMC isolated from CSF. Both assays need further validation for diagnostic accuracy in a larger patient cohort.

## Introduction

Patients with leptomeningeal metastases (LM) of melanoma usually have a poor prognosis with a survival of 1.7-2.5 months.<sup>1-3</sup> Melanoma is the primary tumor type in 5-25% of the patients with LM from solid tumors.<sup>4</sup> In a cohort of 355 patients with stage IV metastasized melanoma with brain metastases, LM was diagnosed on MRI in 11% of patients.<sup>5</sup> Diagnosis of LM is 'definitive' when CSF cytology is positive and 'probable' at combination of typical clinical symptoms and contrast enhancing (nodular or linear) leptomeningeal lesions on MRI of brain and/or spine in a patient with known (metastatic) cancer. However, clinical assessment may be challenging in the context of concomitant brain metastases and MRI has a low sensitivity (76%) and specificity (77%) for the diagnosis of LM in patients with solid tumors.<sup>6</sup> Sensitivity of cerebrospinal fluid (CSF) cytology is also low: 44-67% at first LP, increasing to 84-91% upon second sampling.<sup>7-15</sup> Circulating epithelial tumor cells can be quantified by assays which use antibodies against epithelial cell adhesion molecule (EpCAM). These assays show 76-100% sensitivity for epithelial tumor cell detection in CSF.<sup>9-15</sup> Circulating tumor cell (CTC) analysis in CSF can enable more accurate diagnostics of LM and may also enable monitoring of the treatment response in LM. Only one case series of two patients with LM from melanoma has been published in which circulating melanoma cells (CMC) in CSF were analyzed with an adapted CELLSEARCH® method.<sup>16</sup> Melanoma cell adhesion molecule (MCAM) or CD146 was used as a marker in the CELLSEARCH® assay for immuno-magnetical enrichment of CMC.<sup>17</sup> However, the CD146 capture antigen is not completely specific for CMC as endothelial cells and lymphocytes also express CD146.<sup>18,19</sup> Melanoma chondroitin sulfate proteoglycan (MCSP), also known as high molecular weight melanoma associated antigen (HMW-MAA) or neuron glia antigen-2 (NG2), is expressed by 75-100% of malignant lesions of melanocyte origin.<sup>20-22</sup> MCSP is involved in cell migration and cell proliferation<sup>23,24</sup> and is expressed in fetal skin, abdominal and perineal skin and occasionally in hair follicles and squamous and basal cell carcinomas.<sup>20</sup> It is also expressed in the developing and adult CNS.<sup>25</sup> To improve CSF diagnostics in melanoma patients, we developed a MCSP/CD146-based immunoflow cytometry assay for CMC detection in CSF. We tested the performance of this assay in CSF of 36 patients with a clinical suspicion on LM but negative or equivocal MRI and in 6 patients with clinical suspicion for LM and typical leptomeningeal contrast enhancement on MRI. Moreover, *BRAFV600E* mutation analysis was done using digital droplet PCR (ddPCR) in paired plasma and cell-free CSF and CMC isolated from CSF samples in 15 *BRAFV600E* mutated melanoma patients.

### **Methods and study design CMC immunoflow cytometry assay**

The CMC immunoflow cytometry assay development and validation is described in the supplement of this paper. CSF for CMC flow cytometry was collected in a conical 50 mL tube. After fixation with 4% formaldehyde samples were washed with 50 mL physiological saline and centrifuged at 1000 g for 7 minutes at 4°C. Pellets were resuspended in 50% methanol/phosphate buffered saline and stored at -80°C for a maximum of 12 months. CMC measurements were performed in batches. After defrosting on ice, the supernatant was removed and cell pellets were washed twice with ice-cold beads buffer (BB). After centrifugation, pellets were resuspended in the remaining 100 µL BB. Next, 40 µL of Fc-receptor block was added and samples were incubated for 1 h at room temperature (RT). Subsequently, a volume of 2.5 µL of anti-MCSP-Micro-Beads was added, and samples were incubated for an additional 1 h at RT. Next, samples were washed twice with 1 mL of BB, followed by centrifugation. After discarding the supernatant, cell pellets were resuspended in 500 µL of BB. Subsequently, labeled cells were separated using a magnetic antibody cell sorting (MACS) column. After removal of the column from the magnetic field, the retained MCSP-positive cells were eluted into 2 mL eppendorf tubes using two volumes of 1 mL BB. Next, the CMC enriched samples were stained in 100 µL Perm/Wash™ (P/W) containing 10 µM Hoechst33258, 0.25 µL CD146-allophycocyanin (APC), 5 µL anti-MCSP-phycoerythrin (PE), and 5 µL anti-human CD45 fluorescein isothiocyanate (FITC) for 1 h at RT. After extensive washing with BB, tumor cells were quantified by fluorescent activated cell sorting (FACS).

### **CMC morphology**

Stained and processed CSF samples from two melanoma patients were sorted using a FACSAria™ cell sorter with gates set for leucocytes and CMC as shown in Figure 1A. After centrifugation the cell pellet was resuspended in 100 µL of BB and stained with 5 µL of anti-CD45-APC for 1 h at RT. After washing twice with 1 mL of MQ, samples were resuspended in 10 µL of MQ and transferred to a microscope slide. The slide was dried for 5 min at 30°C by vacuum concentration in a SpeedVac (Savant, Rarimindale, USA). After applying 3 µL of Vectashield H-1000 (Vector, Burlingame, USA) a round object glass of 1 cm in diameter was put on top and sealed with nail polish. Stained DNA, MCSP, and CD45 were visualized as blue (Hoechst 33258), green (anti-MCSP-PE), and red (anti-CD45-APC) colours, respectively. CMC were identified and photographed using a SP5 confocal fluorescence microscope (Leica, Rijswijk, The Netherlands). A picture of the morphological analysis of CMC in CSF of the two patients is depicted in Figure 1B.

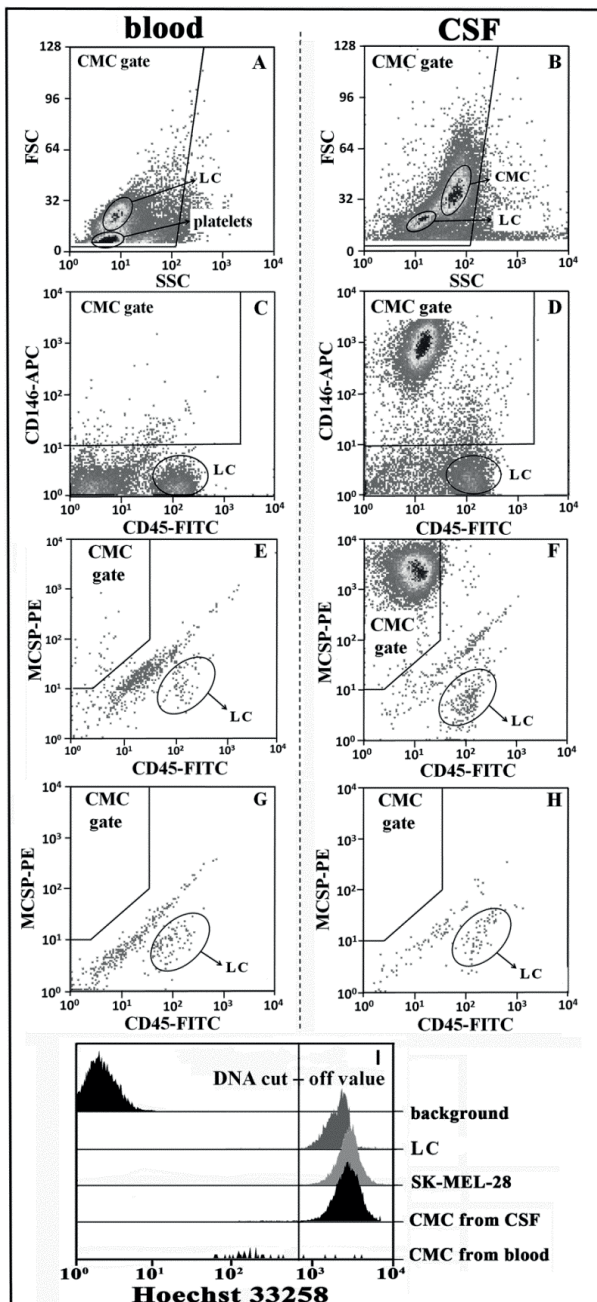


**Figure 1A. Fluorescence activated cell sorting plots of CMC in blood and CSF**

Representative fluorescence activated cell sorting (FACS) plots with indicated gate settings used for circulating melanoma cells (CMC) enumeration and DNA content determination. In step 1 (A and B), CMC are gated by forward and sideward scatter characteristics for size and cell complexity to eliminate debris. The background DNA, leucocytes (LC), platelets, and CMC isolated from blood and cerebrospinal fluid (CSF) are shown. In step 2 (C and D), CMC are gated for CD146-APC positivity. In step 3 (E and F) CMC are gated for MCSP-PE and CD45-FITC positivity to eliminate platelets and LC (patient with LM). G and H are FACS plots of blood and CSF from a patient without LM. The DNA cut-off value (I) was used to differentiate between CMC with low and normal to high DNA content.

*Abbreviations: CMC=circulating melanoma cells, LC=leucocytes, FSC=forward scatter, SSC=side scatter, CD146-APC=Cluster of Differentiation 146-AlloPhyCocyanin, CD45-FITC=Cluster of Differentiation 45-Fluorescein IsoThioCyanate, MCSP-PE=Melanoma Chondroitin Sulfate Proteoglycan-Phycoerythrin.*

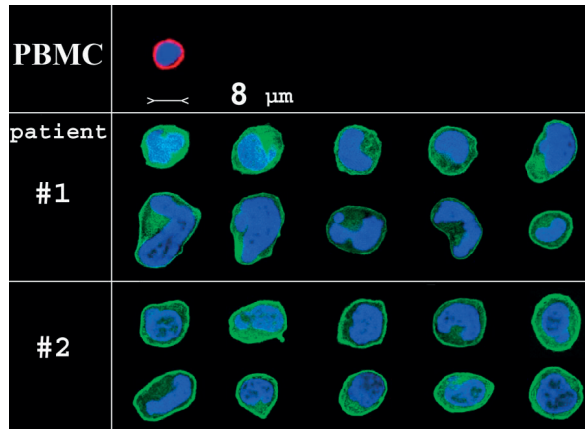


**Figure 1B. Morphology of circulating melanoma cells in CSF in two patients**

Morphology of representative circulating melanoma cells (CMC), isolated from 5 mL of cerebrospinal fluid (CSF) from two metastatic melanoma patients with LM (patient #1 and #2), sorted by fluorescence-activated cell sorting (FACS) using the CMC gate setting (Figure 1A-F). CD45, Hoechst33258, and MCSP are visible as red, blue, and green colors, respectively. An example of a typical leucocyte sorted by FACS using the leucocytes gate setting (Figure 1AE) is included. Imaging was performed at 100 times magnification. *Abbreviations:* CD45=Cluster of Differentiation 45, MCSP=Melanoma Chondroitin Sulfate Proteoglycan, PBMC=peripheral blood mononuclear cell.

### Driver mutation analysis

CMC from CSF were isolated with a FACSaria™ cell sorter. Selective driver mutation analysis of cell free CSF (cfCSF), plasma and CMC isolated from CSF was performed using a QX200™ Droplet Digital™ PCR (ddPCR) (Biorad Laboratories Inc, California, USA). CSF was collected in a Sterilin™ universal polystyrene container and cfCSF was obtained via centrifugation at 1700g for 10 min. Blood samples were collected in K2EDTA (di-potassium ethylene diamine tetra acetic acid) tubes (Becton Dickinson, Franklin Lakes, USA). Plasma was separated from the blood by centrifugation at 380g during 20 min. Cell free plasma was obtained by centrifugation at 20.000g during 10 min. CfDNA (cell-free DNA) was extracted using the QIAasymphony DSP circulating DNA Kit. (Qiagen, Hilden, Germany). CfDNA isolated from plasma and CSF was analysed by ddPCR.<sup>26</sup>

### Multicenter prospective clinical study

The institutional review boards of the Netherlands Cancer Institute - Antoni van Leeuwenhoek (Amsterdam, The Netherlands) Medical Center Slotervaart (Amsterdam, The Netherlands) and Oscar Lambret Center (Lille, France) approved the study. Patients  $\geq 18$  years with melanoma and a clinical suspicion of LM but a for LM negative or equivocal MRI, who had to undergo a diagnostic LP were asked to participate. Six patients were included with neurological symptoms suspicious for LM and typical



leptomeningeal (nodular or linear) contrast enhancing lesions on MRI. Written informed consent was obtained from all participants. The diagnosis of LM was defined according to the EANO-ESMO diagnostic criteria for LM.<sup>1</sup> Diagnostic categories were defined as follows: 1. *confirmed LM* by positive CSF cytology, 2. *probable LM* based on typical clinical findings and typical (linear or nodular) leptomeningeal contrast-enhancement of leptomeninges on MRI but negative CSF cytology 3. *possible LM* based on typical clinical signs, a normal MRI and negative CSF cytology or no typical clinical signs, typical (linear or nodular) contrast-enhancement on MRI and negative CSF cytology and 4. *no LM* (lack of evidence) defined as no typical clinical signs, normal MRI and negative CSF cytology. Exclusion criteria were contra-indications for a LP, including intracranial or intraspinal tumor with mass effect heralding the risk of herniation during LP and uncorrected thrombocytopenia or coagulation disorders. Patients were included between October 2012 and August 2018. This study is registered with ClinicalTrials.gov, number NCT01713699. The primary objective of the study was to determine the sensitivity and specificity of the detection of CMC for the diagnosis of LM in patients with melanoma compared to CSF cytology. In this paper the results of an interim analysis are being presented.

## Results

### Melanoma cell detection with MCSP/CD146 immunoflow cytometry

Representative FACS plots for CMC detection in blood and CSF with the MCSP/CD146 immunoflow cytometry assay are depicted in Figure 1A.

### CMC morphology in CSF

For determining morphology of CMC in CSF, CMC isolated from 5 mL of CSF from two melanoma patients with confirmed LM were processed and sorted by FACS. A picture of the morphological analysis of CMC in CSF of these two patients is shown in Figure 1B. The diameter of CMC varied between 12 and 22  $\mu\text{m}$ . Most CMC had an oval or irregular shape, with lobular nuclei and a fluorescent green membrane due to specific anti-MCSP-PE staining. CMC were easily distinguished from leucocytes, which were smaller with a mean diameter of  $8.0 \pm 1.5 \mu\text{m}$ , had a rounder shape and condensed nucleus, and a bright red cell membrane due to specific anti-CD45-APC staining. No leucocytes were detected in the CMC gate and vice versa no CMC were detected in the leucocyte gate.

### Multicenter prospective clinical study

In this multicenter, prospective clinical study 36 patients with a clinical suspicion on LM and a negative or equivocal MRI were included and 6 patients with a clinical suspicion on LM and typical leptomeningeal contrast-enhancing on MRI. The baseline patient characteristics and presenting neurological symptoms of these 42 patients are shown in Table 1. Ten patients with a non-oncological medical history and suspicion on a neurological disease (e.g. infectious or auto-immune meningitis, subarachnoid hemorrhage) were included.

**Table 1. Baseline characteristics and presenting neurological symptoms**

Patients suspected for LM with a negative or for LM inconclusive MRI (n=36) or already proven LM (n=6). Patients could have more than one presenting neurological symptom.

<b>Mean age in years, [range]</b>	<b>54 [20-83]</b>
<b>Gender, women n (%)</b>	<b>21 (49)</b>
<b>Type of mutation n (%)</b>	
- BRAF	29 (69)
- NRAS	6 (14)
- other mutation	2 (5)
- no mutation	3 (7)
- mutation not determined	2 (5)
<b>Brain metastases n (%)</b>	<b>19 (45)</b>
<b>Other metastases n (%)</b>	
- lymph node	29 (69)
- lung	17 (41)
- liver	7 (17)
- bone	10 (24)
- skin	14 (33)
<b>Systemic treatment before inclusion</b>	
- BRAF/MEK inhibition	11 (26)
- immunotherapy	16 (38)
<b>WHO performance state at inclusion study n (%)</b>	
-WHO 0-1	23 (55)
<b>Presenting neurological symptoms - clinically affected domain</b>	<b>n (%)</b>
- cognitive function	7 (17)
- speech/language	4 (10)
- cranial nerves	12 (29)
- strength	11 (29)
- coordination of arms and legs	12 (31)
- sensibility of arms and legs	12 (33)
- walking pattern	16 (43)

*Abbreviations:* BRAF=v-Raf murine sarcoma viral oncogene homolog B, NRAS=neuroblastoma RAS viral (v-ras) oncogene homolog protein, MEK=mitogen-activated protein kinase kinase, WHO=World Health Organization.

**LM diagnosis and CSF characteristics**

In Figure 2 the inclusion of patients and final diagnoses are depicted. LM diagnosis was confirmed by CSF cytology in 13 of 42 patients. 84% of these patients had concomitant brain metastases. In 100% of patients with confirmed LM, leucocytes in CSF were increased (> 3/mm<sup>3</sup>). Total protein CSF concentration was increased (>0.45 g/L) in 54% of patients and glucose CSF/serum ratio was decreased in 83% (glucose CSF/serum ratio <0.66). In 9 patients the diagnosis probable/possible LM (1 probable LM; 8 possible LM) was made. 33% of patients had concomitant brain metastases. Leucocytes in CSF were increased in 57%, total protein CSF concentration was increased in 75% and glucose CSF/serum ratio was decreased in 100% of patients. In the remaining 20 patients without LM, 20% of patients had concomitant brain metastases. Leucocytes were increased in CSF in 37%, total CSF protein concentration was increased in 58% and glucose CSF/serum ratio was decreased in 53% of patients.

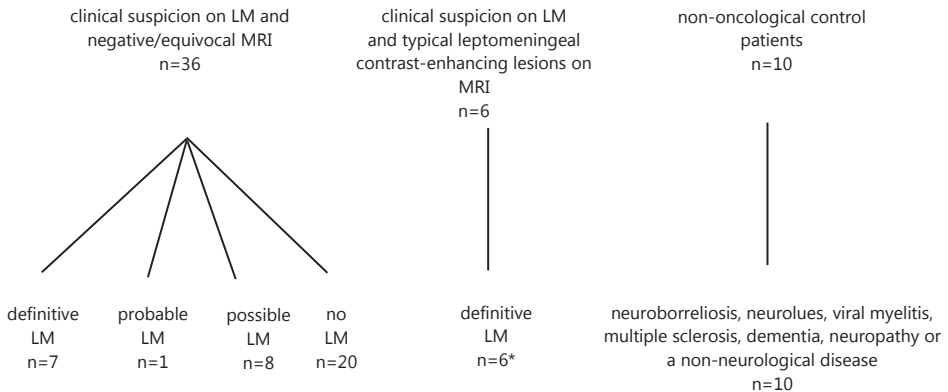


**Figure 2.**

Inclusion of patients in clinical study and final diagnoses. LM was classified according to the EANO-ESMO criteria as definitive LM (CSF cytology proven), probable LM (typical clinical symptoms and typical MRI abnormalities, CSF cytology negative) or possible LM (typical clinical symptoms, no typical MRI abnormalities, CSF cytology negative) and no LM.<sup>1</sup> LM=leptomeningeal metastases. \*No CSF for immunoflow cytometry available in one patient. *Abbreviations:* LM=leptomeningeal metastases, MRI= magnetic resonance imaging, CMC=Circulating Melanoma Cells, CSF=cerebrospinal fluid.

**CMC immunoflow cytometry results**

Results of CMC detection in the patient groups classified according to the EANO-ESMO LM criteria are shown in Table 2. Six patients had a clinical suspicion on LM and typical leptomeningeal contrast-enhancement on MRI before the LP was performed. In all 6 patients positive CSF cytology confirmed the diagnosis of LM. In 1 of these patients no CSF was available for CMC enumeration. In the other 5 patients 1.9 - 3592 CMC/mL CSF were detected. In 36 patients a LP was performed because of neurological

symptoms suspicious for LM with a negative or equivocal MRI. In 7 of these patients LM was confirmed based on positive CSF cytology: in 6 because of positive CSF cytology at first LP and in 1 patient based on positive CSF cytology at second LP (equivocal results of CSF cytology at first LP). In one of 7 patients with confirmed LM, CMC were negative. In the other 6 patients, CMC numbers in CSF varied from 4.3- 5587 CMC/mL. In the patient with equivocal CSF cytology at first LP and positive CSF cytology at second LP, 42 CMC/mL were found at first LP and 48 CMC/mL at second LP. One patient was diagnosed with probable LM according to the EANO-ESMO criteria. In this patient, 180 CMC/mL in CSF were found. The patient showed stable disease with BRAF- and MEK-inhibition, followed by anti-PD1 treatment during more than 3 years; he finally died 3.5 years after study inclusion, due to progressive metastatic disease, including progressive LM confirmed by MRI. Eight patients were diagnosed with possible LM. Six of these patients showed 0-0.2 CMC/mL. In two possible LM patients 9.8 CMC/mL and 3.5 CMC/mL CSF were found, respectively. The first patient died 9 months later, but it is unknown whether this was due to progressive LM; the other patient died from progression of concomitant brain metastases. Twenty patients with a clinical suspicion on LM but negative or equivocal MRI ultimately did not have LM. All these 20 patients had  $\leq 0.3$  CMC/mL. Furthermore, 10 patients with a non-oncological medical history with suspicion on a neurological disease and a clinical indication for a LP were included in the study. Final diagnoses were neuroborreliosis, neurolues, viral myelitis, multiple sclerosis, dementia, neuropathy or a non-neurological disease. CMC numbers in the CSF in these 10 control patients were also  $\leq 0.3$  CMC/mL.

**Table 2. Immunoflow cytometry results of CMC enumeration in CSF**

EANO-ESMO LM diagnosis	Mean (range) CMC/mL in CSF
Confirmed LM (n=12)	1076 (0-5587)
Probable LM (n=1)	180 (NA)
Possible LM (n=8)	1.7 (0-9.8)
No LM (n=20)	0.11 (0-0.3)

Immunoflow cytometry results of CMC enumeration in CSF of patients with the diagnosis of leptomeningeal metastases according to EANO-ESMO clinical practice guidelines.<sup>1</sup> *Abbreviations:* LM=leptomeningeal metastases, CMC=Circulating Melanoma Cells, CSF=cerebrospinal fluid, NA=not applicable. For one patient with confirmed LM no CSF sample was available for CMC analysis.

### **BRAFV600 driver mutation analysis**

In total 29 of the included 42 melanoma patients (67%) had a BRAFV600E mutation detected in either the primary tumor or metastasis. In a subset of 15 BRAFV600E positive patients in whom plasma and CSF samples were available, BRAFV600E mutation analysis of plasma, cfCSF and CMC isolated from CSF was performed. Results of BRAFV600E mutation analysis are depicted in Table 3. Two out of 6 metastatic

melanoma patients tested showed a *BRAFV600E* mutation in the plasma circulating tumor (ct)DNA. All four patients with confirmed LM showed a *BRAFV600E* mutation in cfCSF; in three patients with possible LM no *BRAFV600E* mutation was found in cfCSF (2 of 3 patients had 0 CMC/mL CSF and 1 patient had 9.8 CMC/mL CSF). *BRAFV600E* mutation was measured and detected in CMC isolated from CSF of 2 patients with confirmed LM and 1834 CMC/mL and 1622 CMC/mL CSF, respectively. In one patient with possible LM (9.8 CMC/mL) no *BRAFV600E* mutation was found in the isolated CMC from CSF; also cfCSF of this patient was negative. Two other patients with possible LM and 0 CMC/mL CSF also showed no *BRAFV600E* mutation in cfCSF. 1 out of 17 tested patients without LM was positive for *BRAFV600E* in cfCSF. This patient (no=128, see Table 3) had cervical intramedullary metastases.

**Table 3. Patients with *BRAFV600E* mutations in the primary tumor and driver mutation distribution in plasma, cfCSF and CMC isolated from CSF**

Diagnosis EANO-ESMO LM criteria (patient number)	Plasma <i>BRAFV600E</i>	cfCSF <i>BRAFV600E</i>	Isolated CMC in CSF <i>BRAFV600E</i>	CMC/mL CSF
Confirmed LM (6)	Not done	Positive	Not done	42
Confirmed LM (19)	Not done	Positive	Positive	1834
Confirmed LM (43)	Not done	Positive	Not done	15
Confirmed LM (72)	Not done	Positive	Positive	1622
Possible LM (12)	Not done	Negative	-	0
Possible LM (33)	Not done	Negative	Negative	9.8
Possible LM (140)	Negative	Negative	-	0
No LM (1)	Not done	Negative	-	0
No LM (5)	Not done	Negative	-	0
No LM (63)	Not done	Negative	-	0
No LM (113)	Negative	Negative	-	0.2
No LM (124)	Positive	Negative	-	0.2
No LM (128)	Positive	Positive	-	0.2
No LM (135)	Negative	Negative	-	0.2
No LM (137)	Negative	Negative	-	0.2

Patients with *BRAFV600E* mutations in the primary tumor and driver mutation distribution in plasma, cfCSF and CMC isolated from CSF. LM was diagnosed according to the EANO-ESMO clinical practice guidelines for LM. 3 patients with LM are excluded because of unknown *BRAFV600E* results in plasma and CSF and CMC. 6 patients without LM are excluded from this table because of unknown *BRAFV600E* results in plasma and CSF. *Abbreviations:* NA=not available, ND=not done, cfCSF=cell-free cerebrospinal fluid, CMC=circulating melanoma cells, *BRAFV600E*=v-Raf murine sarcoma viral oncogene homolog B, LM=leptomeningeal metastases, ND=not done.

## Discussion

Our study shows that we can enumerate melanoma cells in CSF by using our MCSP/CD146-based immunoflow cytometry assay. We detected melanoma cells in the CSF in 91% of patients with confirmed LM with CMC numbers varying from 1.9-5587 CMC/mL. In one of these patients, CMC detection outperformed CSF cytology as at first LP, CSF cytology was equivocal and CMC showed 42 CMC/mL. We consider that CMC are indeed melanoma cells, based on cytomorphological analysis of CMC isolated from CSF, which identified all the FACS events in the CMC gate as melanoma cells (Figure 1b). This is further supported by *BRAFV600E* mutation detection in isolated CMC from CSF of patients with LM. Moreover, patients with metastatic melanoma without LM and control non-oncological patients showed  $\leq 0.3$  CMC/mL CSF. Our data suggest that the MCSP/CD146 immunoflow cytometry is a promising CSF tool to diagnose LM in melanoma patients. The dataset is however too small to compare the sensitivity and specificity of immunoflow cytometry with CSF cytology for diagnosing LM. A larger patient cohort is needed to determine the accuracy of our test and to determine the optimal cut-off value of the CMC number in CSF for LM diagnosis. Based on the current small dataset we expect this to be  $\geq 1$  CMC/mL. The group of 9 patients with possible or probable LM in whom CMC were detected in 3 of them (1.7 - 180 CMC/mL) is interesting as this could indicate that although the diagnosis LM was not confirmed on the current EANO-ESMO LM criteria, this subgroup of patients may indeed have had LM. A further important advantage of the presented CMC immunoflow cytometry method is the fact that it is a quantitative assay with possible use for future treatment response monitoring. Moreover, it can be used for driver mutation analysis (e.g. *BRAFV600E*) of isolated CMC from CSF and opens way for broader mutational analysis of these cells. Based on the current dataset, the accuracies of MCSP/CD146 immunoflow cytometry and CSF cytology cannot be compared. It is also not yet known whether our assay outperforms the CELLSEARCH® method in melanoma cell detection in CSF, as there is only one study in two patients showing CMC in CSF with the adapted CELLSEARCH® method.<sup>4</sup> The MCSP/CD146 immunoflow cytometry method uses fixed gate settings and fully automatic CMC identification, which prevents the operator bias of the CELLSEARCH® method.<sup>4,27</sup> Furthermore, our method is based on MCSP to immunomagnetically enrich CMC, which is relatively more specific for melanoma than CD146 and eliminates the use of CD34 to discriminate between endothelial cells and CMC.<sup>18,19</sup> In our exploratory driver mutation analysis of cfCSF and isolated CMCs in CSF and plasma, *BRAFV600E* was detected in cfCSF of all four tested patients with cytology confirmed LM and in isolated CMC from CSF of 2 tested patients with 1622 and 1834 CMC/mL CSF. In a patient with possible LM and only 9.8 CMC/mL CSF, the *BRAFV600E* mutation could not be detected in isolated CMC. In an earlier

published study of 7 melanoma patients treated for LM there was a strong correlation between driver mutation status *BRAFV600E* detection by ddPCR, CSF cytology and abnormalities on MRI.<sup>28</sup> In another study, ctDNA fragments were detected in the CSF in 6 out of 7 patients with brain metastases from various tumor types, including two melanoma patients.<sup>29</sup> Tumor-derived ctDNA has also been detected in CSF of two patients who had brain melanoma metastases without radiographic evidence of leptomeningeal disease.<sup>30</sup> This indicates that it is currently unknown if *BRAFV600E* mutation detection in CSF is a useful tool to diagnose LM, in particular when there are concomitant brain metastases.

In conclusion, the newly developed CD146/MCSP immunoflow cytometry assay is a promising tool for detection of melanoma cells in CSF and diagnose LM. Driver mutation analysis with ddPCR can be used to detect *BRAFV600E* mutation in both cfCSF and CMC isolated from CSF. Both assays need further validation for diagnostic accuracy in a larger patient cohort.

## References

1. Le Rhun E, Weller M, Brandsma D, et al. EANO-ESMO Clinical Practice Guidelines for diagnosis, treatment and follow-up of patients with leptomeningeal metastasis from solid tumours. *Ann Oncol*. 2017;28(suppl\_4):iv84-iv99.
2. Harstad L, Hess KR, Groves MD. Prognostic factors and outcomes in patients with leptomeningeal melanomatosis. *Neuro Oncol*. 2008;10(6):1010-1018.
3. Geukes Foppen MH, Brandsma D, Blank CU, van Thienen J V., Haanen JB, Boogerd W. Targeted treatment and immunotherapy in leptomeningeal metastases from melanoma. *Ann Oncol Off J Eur Soc Med Oncol*. 2016;27(6):1138-1142.
4. Le Rhun E, Taillibert S, Chamberlain MC. Carcinomatous meningitis: Leptomeningeal metastases in solid tumors. *Surg Neurol Int*. 2013;4(Suppl 4):S265-88.
5. Raizer JJ, Hwu W-J, Panageas KS, et al. Brain and leptomeningeal metastases from cutaneous melanoma: survival outcomes based on clinical features. *Neuro Oncol*. 2008;10(2):199-207.
6. Straathof CS, de Bruin HG, Dippel DW, Vecht CJ. The diagnostic accuracy of magnetic resonance imaging and cerebrospinal fluid cytology in leptomeningeal metastasis. *J Neurol*. 1999;246(9):810-814.
7. Wasserstrom WR, Glass JP, Posner JB. Diagnosis and treatment of leptomeningeal metastases from solid tumors: experience with 90 patients. *Cancer*. 1982;49(4):759-772.
8. van Oostenbrugge RJ, Twijnstra A. Presenting features and value of diagnostic procedures in leptomeningeal metastases. *Neurology*. 1999;53(2):382-385.
9. Tu Q, Wu X, Le Rhun E, et al. CellSearch technology applied to the detection and quantification of tumor cells in CSF of patients with lung cancer leptomeningeal metastasis. *Lung Cancer*. 2015;90(2):352-357.
10. Lee JS, Melisko ME, Magbanua MJ, et al. Detection of cerebrospinal fluid tumor cells and its clinical relevance in leptomeningeal metastasis of breast cancer. *Breast Cancer Res Treat*. 2015;154(2):339-349.
11. Nayak L, Fleisher M, Gonzalez-Espinoza R, et al. Rare cell capture technology for the diagnosis of leptomeningeal metastasis in solid tumors. *Neurology*. 2013;80(17):1598-605; discussion 1603.
12. Jiang B-Y, Li Y-S, Guo W-B, et al. Detection of Driver and Resistance Mutations in Leptomeningeal Metastases of NSCLC by Next-Generation Sequencing of Cerebrospinal Fluid Circulating Tumor Cells. *Clin Cancer Res*. 2017;23(18):5480-5488.
13. Milojkovic Kerklaan B, Pluim D, Bol M, et al. EpCAM-based flow cytometry in cerebrospinal fluid greatly improves diagnostic accuracy of leptomeningeal metastases from epithelial tumors. *Neuro Oncol*. 2016;18(6):855-862.
14. Subira D, Serrano C, Castanon S, et al. Role of flow cytometry immunophenotyping in the diagnosis of leptomeningeal carcinomatosis. *Neuro Oncol*. 2012;14(1):43-52.
15. Subira D, Simo M, Illan J, et al. Diagnostic and prognostic significance of flow cytometry immunophenotyping in patients with leptomeningeal carcinomatosis. *Clin Exp Metastasis*. 2015;32(4):383-391.
16. Le Rhun E, Tu Q, De Carvalho Bittencourt M, et al. Detection and quantification of CSF malignant cells by the CellSearch technology in patients with melanoma leptomeningeal metastasis. *Med Oncol*. 2013;30(2):538.



17. Rao C, Bui T, Connelly M, et al. Circulating melanoma cells and survival in metastatic melanoma. *Int J Oncol.* 2011;38(3):755-760.
18. Breuer J, Korpos E, Hannocks M-J, et al. Blockade of MCAM/CD146 impedes CNS infiltration of T cells over the choroid plexus. *J Neuroinflammation.* 2018;15(1):236.
19. Duda DG, Cohen KS, Di Tomaso E, et al. Differential CD146 expression on circulating versus tissue endothelial cells in rectal cancer patients: Implications for circulating endothelial and progenitor cells as biomarkers for antiangiogenic therapy. *J Clin Oncol.* 2006;24(9):1449-1453.
20. Natali PG, Giacomini P, Russo C, Steinbach G, Fenoglio C, Ferrone S. Antigenic profile of human melanoma cells. Analysis with monoclonal antibodies to histocompatibility antigens and to melanoma-associated antigens. *J Cutan Pathol.* 1983;10(4):225-237.
21. de Bruyn M, Rybczynska AA, Wei Y, et al. Melanoma-associated Chondroitin Sulfate Proteoglycan (MCSP)-targeted delivery of soluble TRAIL potentially inhibits melanoma outgrowth in vitro and in vivo. *Mol Cancer.* 2010;9(1):301.
22. Yadavilli S, Hwang EI, Packer RJ, Nazarian J. The Role of NG2 Proteoglycan in Glioma. *Transl Oncol.* 2016;9(1):57-63.
23. Eisenmann KM, McCarthy JB, Simpson MA, et al. Melanoma chondroitin sulphate proteoglycan regulates cell spreading through Cdc42, Ack-1 and p130cas. *Nat Cell Biol.* 1999;1(8):507-513.
24. Yang J, Price MA, Gui YL, et al. Melanoma proteoglycan modifies gene expression to stimulate tumor cell motility, growth, and epithelial-to-mesenchymal transition. *Cancer Res.* 2009;69(19):7538-7547.
25. Dawson MRL, Levine JM, Reynolds R. NG2-expressing cells in the central nervous system: are they oligodendroglial progenitors? *J Neurosci Res.* 2000;61(5):471-479.
26. van Ginkel JH, van den Broek DA, van Kuik J, et al. Preanalytical blood sample workup for cell-free DNA analysis using Droplet Digital PCR for future molecular cancer diagnostics. *Cancer Med.* 2017;6(10):2297-2307.
27. van Bussel MTJ, Pluim D, Bol M, Beijnen JH, Schellens JHM, Brandsma D. EpCAM-based assays for epithelial tumor cell detection in cerebrospinal fluid. *J Neurooncol.* 2018;137(1):1-10.
28. Ballester LY, Glitza Oliva IC, Douse DY, et al. Evaluating Circulating Tumor DNA From the Cerebrospinal Fluid of Patients With Melanoma and Leptomeningeal Disease. *J Neuropathol Exp Neurol.* 2018;77(7):628-635.
29. Pan W, Gu W, Nagpal S, Gephart MH, Quake SR. Brain tumor mutations detected in cerebral spinal fluid. *Clin Chem.* 2015;61(3):514-522.
30. Momtaz P, Pentsova E, Abdel-Wahab O, et al. Quantification of tumor-derived cell free DNA(cfDNA) by digital PCR (DigPCR) in cerebrospinal fluid of patients with BRAFV600 mutated malignancies. *Oncotarget.* 2016;7(51):85430-85436.

## Supplement to:

### **Circulating melanoma cell detection and driver mutation analysis in cerebrospinal fluid in melanoma patients with suspected leptomeningeal metastases**

#### **Development and validation of MCSP/CD146 immunoflow cytometry assay**

##### **Reagents and chemicals**

Milli-Q grade (Millipore, USA) water was used. Phosphate buffered saline (PBS) and RPMI medium were purchased from GIBCO BRL (Gaithersburg, USA). Neutral buffered methanol-free 40% formaldehyde was prepared from paraformaldehyde purchased from Merck (Darmstadt, Germany). Hoechst33258 was obtained from Sigma (St. Louis, USA). Anti-human MCSP-Micro-Beads, MS Magnetic antibody cell sorting (MACS®) columns, Fc-Receptor block (FcR), mouse clone 5B1 IgG2a anti-human CD45 labelled with fluorescein isothiocyanate (FITC) or allophycocyanin (APC), mouse clone EP-1 IgG1 MCSP-phycoerythrin (PE), and mouse clone 541-10B2 IgG1 CD146-APC were purchased from Miltenyi (Bergisch Gladbach, Germany). Perm/Wash™ (P/W) was purchased from Becton Dickinson (Heidelberg, Germany). Beads buffer (BB) is PBS containing 0.5% bovine serum albumin (BSA) and 2 mM EDTA degassed by sonication for 10 min. All buffers and formaldehyde solution were filtered through 0.22 µm filters before use.

##### **Cell culture and spiking experiments**

Human melanoma cell lines M19MEL and SK-MEL-28 (from ATCC, Rockville, USA) were cultured as monolayer in RPMI medium supplemented with 10% fetal calf serum. SK-MEL-28 is BRAFV600E mutated and has a MCSP expression of 99.8%.<sup>1</sup> For spiking experiments cells were counted and sorted by a FACSAria™ cell sorter (BD Biosciences, USA).

##### **Centrifugation and pellet resuspension**

Unless stated otherwise, all centrifugations were performed in 2 mL eppendorf tubes in a centrifuge equipped with a swing-out rotor at 1,000g for 4 min at 4°C. After centrifugation the supernatant was removed with a 1 mL pipet leaving 100 µL on the cell pellet. The pellet was resuspended in the remaining supernatant by vortex mixing at 50% speed setting.

### Sample pre-processing

CPT tubes containing 8 mL of whole blood were centrifuged in a swing-out rotor at 1,500g for 25 min at room temperature (RT). Next, the upper CPT layer was transferred to a 50 mL tube. The CPT tubes were washed with 3 mL physiologic salt, which was pooled with the rest of the sample. CSF was collected in 50 mL tubes. Sample volume was adjusted to 9 mL with physiological salt and 1 mL of 40% formaldehyde was added. After vortex mixing at half speed for 10 s, samples were incubated for 15 min at RT. Next, sample volume was adjusted to 50 mL using physiologic salt, followed by centrifugation at 1,000g for 10 min at 4°C. The supernatant was decanted, followed by placing the tubes upside down on filter paper for 5 s, after which the samples were chilled on ice. Next, the cell pellets were resuspended in 1 mL of ice-cold 50% (v,v%) methanol/PBS by vortex mixing for 10 s at the highest setting. The samples were stored at -80°C for future analysis.

### Cell recovery optimization

M19MEL cells were spiked at 10,000 cells in 35 CPT tubes each containing 8 mL of blood from healthy volunteers. Samples were pre-processed as described above and incubated with 40 µL of FcR-block for 1 h at RT. Next, 24 samples were incubated in triplicate at 0 °C and 37 °C for 1 h with, respectively, 10 µL, and 0, 0.25, 0.5, 1, 2.5, 5, 10 µL of anti-MCSP-Micro-Beads. An additional 21 samples were incubated in triplicate at RT with 2.5 µL of anti-MCSP-Micro-Beads for 0, 0.08, 0.25, 0.5, 1, 2, and 4 h. Next, the tumor cells were isolated by tumor cell enrichment (see paragraph below). The input control samples consisted of 10,000 M19MEL cells in 100 µL P/W. After immunofluorescent staining, the cell recovery and total event counts were determined by fluorescence-activated cell sorting (FACS).

### Tumor cell enrichment

CMC underwent an immunomagnetic enrichment using anti-MCSP-Micro-Beads, and FcR-block, with the following modifications to the manufacturer's protocol: samples stored at - 80°C were defrosted on ice. After centrifugation, the supernatant was removed and the cell pellets were washed twice with ice-cold BB. After centrifugation, the pellets were resuspended in the remaining 100 µL BB. Next, 40 µL of FcR was added and the samples were incubated for 1 h at RT. Subsequently, a volume of 2.5 µL of anti-MCSP-Micro-Beads was added, and the samples were incubated for an additional 1 h at RT. Next, samples were washed twice with 1 mL of BB, followed by centrifugation. After discarding the supernatant, the cell pellets were resuspended in 500 µL of BB. Subsequently, labelled cells were separated using a MACS column. After removal of the column from the magnetic field, the retained MCSP-positive cells were

eluted into 2 mL eppendorf tubes using two volumes of 1 mL BB. After centrifugation the supernatant was removed and the pellet was resuspended.

### **Immunofluorescence staining**

The CMC enriched samples were stained in 100  $\mu$ L P/W containing 10  $\mu$ M Hoechst33258, 0.25  $\mu$ L CD146-APC, 5  $\mu$ L anti-MCSP-PE, and 5  $\mu$ L anti-CD45-FITC for 1 h at RT. Next, samples were washed twice with 1 mL of P/W followed by centrifugation. CD45, MCSP, CD146 and DNA staining linearity were measured in triplicate in samples spiked with 10,000 SK-MEL-28 cells in CPT tubes containing 8 mL whole blood from a healthy volunteer. Subsequently, samples were stained with 0, 0.25, 0.5, 1, 2, 5, 10, and 20  $\mu$ L of anti-CD45-FITC and anti-MCSP-PE, 0, 0.025, 0.05, 0.1, 0.25, 0.5, 1.0, and 2.0  $\mu$ L of anti-CD146-APC, and 10  $\mu$ M of Hoechst33258 for 1h at RT. Next, samples were washed twice with 1 mL P/W and mean fluorescence intensity (MFI) was measured by FACS.

### **Fluorescence-activated cell sorting**

Fluorescence-activated cell sorting (FACS) analysis was performed using a CyAn ADP™ (Beckman Coulter, Brea, USA) and a Becton Dickinson LSR Fortessa™. Hoechst33258, FITC, PE, and APC were collected through 450  $\pm$  25 nm, 530  $\pm$  40 nm, 575  $\pm$  25 nm, and 665  $\pm$  25 nm band pass filters, respectively. Data analysis was performed with Summit v4.3.01 software (Dako Cytomation, Fort Collins, USA).

### **Specificity**

In order to assess the background levels in blood, three CPT tubes containing 8 mL peripheral blood were drawn from 20 healthy volunteers. Background levels in CSF were determined in non-oncological patients with a suspicion on an infectious or auto-immune meningitis or subarachnoid hemorrhage and a clinical indication for a diagnostic lumbar puncture.

### **Within- and between-day precision and recovery**

The between-day (BDP) and within-day precision (WDP) and recovery of the MCSP flow cytometry assay were determined as described previously.<sup>2</sup> CPT tubes containing 8 mL of whole blood were spiked with 10, 100, 1,000, and 5,000 SK-MEL-28, and M19MEL cells with 10 times less expression of MCSP.

### **Lower limit of quantification (LLOQ)**

The LLOQ was determined by spiking in six-fold 1, 2, 3, 4, 5, and 10 SK-MEL-28 cells in CPT tubes containing 8 mL of whole blood from six different healthy volunteers. The LLOQ was defined as the cell concentration that could be determined with a precision of 0 - 20%, and a recovery between 80 - 120% of the nominal value.

### Sample stability

Long term storage stability was assessed by spiking 21 CPT tubes, containing 8 mL whole blood from a healthy volunteer, with 1000 SK-MEL-28 cells each. Three samples per time point were processed and stored in 50% MeOH at  $-80^{\circ}\text{C}$  for 0, 1, 14, 30, 60, 180, and 360 days until analysis. We also assessed the stability of stained samples in triplicate after storage at  $4 - 7^{\circ}\text{C}$  in the refrigerator for 0, 4, and 24 until analysis.

### CMC assay validation in blood

Subjects asked for study participation included 20 healthy volunteers  $\geq 21$  years of age, not known with cancer, not treated with investigational or other drugs within 30 days before start of the study, and who had not undergone surgery within the past six months. Blood samples from 11 cancer patients with stage III or IV advanced melanoma were used for determination of the method sensitivity. Patients had not been on treatment for at least 4 weeks before whole blood was drawn for determination of CMC counts. For each subject three 8 mL cell preparation tubes (BD Vacutainer<sup>®</sup> CPT<sup>™</sup>) were used containing a Ficoll-Hypaque density fluid separated by a polyester gel barrier from a sodium citrate anticoagulant.

Discrimination of CMC from blood cells with red blood cell lysis is impossible due to more than 90% reduction of MCSP staining (data not shown). Therefore, density gradient centrifugation with CPT tubes was used. The gel barrier in these tubes separates the blood cells over two compartments. The lower compartment contains red blood cells and granulocytes. The upper compartment consists of CMC, leucocytes, and platelets. Further, enrichment of CMC was achieved by MACS using anti-human MCSP-Micro-Beads. For removal of protein aggregates that can bind nonspecifically to antibodies, which resulted in false positive CMC counts (data not shown), all antibody solutions except FcR-block and MCSP-Micro Beads were centrifuged at  $10,000g$  for 10 min at  $4^{\circ}\text{C}$ . Furthermore, buffers were filtered through  $0.2\ \mu\text{m}$  syringe filters. The use of swing-out rotors for centrifugations prevented the loss of 10% of cells observed with fixed angle rotors. CMC were identified based on double positivity for MCSP and CD146 in combination with CD45 negativity (Figure 1A). Release of adherent cells from the culture plates by trypsinisation reduced MCSP recognition by more than 90% (data not shown). Therefore, we used 10 mM EDTA for 5 min at  $37^{\circ}\text{C}$  to release adherent cells from the culture plates. Negative and positive quality controls were prepared by spiking, respectively, 0 and 1,000 SK-MEL-28 in the upper layer of centrifuged CPT tubes containing 8 mL of whole blood from a healthy volunteer. Quality Controls (QCs) were formaldehyde fixed and stably stored for a maximum of 360 days in 50% methanol/PBS at  $-80^{\circ}\text{C}$ . The background from negative QCs was always  $\leq 1$ , and the recovery of SK-MEL-28 cells from positive QCs was always  $\geq 90 \pm 6\%$ . CMC were considered

to be nucleated if the Hoechst33258 MFI was above the indicated DNA cut-off level determined from endogenous leucocytes present in the same sample (Figure 1A).

### ***Staining linearity***

Staining linearity was determined in triplicate in samples containing 10,000 SK-MEL-28 cells spiked in CPT tubes containing 8 mL of whole blood from a healthy volunteer. CD146 and MCSP were maximally stained with, respectively, a MFI of  $2545 \pm 182$  and  $771 \pm 31$  using 0.25 and 5  $\mu$ L of anti-CD146-APC and anti-MCSP-PE. Staining did not significantly increase at higher antibody concentrations.

### ***Specificity***

The amount of background counts in the CMC gate during FACS analysis was  $4 \pm 0.6$  false positive CMC per 8 mL of whole blood ( $n = 18$  healthy volunteers in triplicate) if MCSP positivity in combination with CD45 negativity were used as criteria for CMC identification after the FS/SSC gating. Specificity strongly improved to  $0.3 \pm 0.8$  CMC per 8 mL of whole blood (range 0 - 1) false positive CMC counts when CD146 positivity was included as marker for CMC identification. All control patients were negative for CMC ( $n=10$ ) (Figure 1A).

### ***Cell recovery optimization***

The recovery of M19MEL cells after the anti-MCSP-Micro-Beads enrichment step was significantly affected by the amount of anti-MCSP-Micro-Beads and incubation temperature (Supplementary Figure S1). The use of an extra volume of 1 mL of BB for elution of CMC from the MACS<sup>®</sup> columns resulted in 11% increase of cell recovery ( $P = 0.002$ , data not shown). The maximum M19MEL recovery of 28.1% was obtained after 1 h of incubation using 2.5  $\mu$ L of anti-MCSP-Micro-Beads (Supplementary Figure S1B). Under these conditions recovery of SK-MEL-28, with about 10 times higher MCSP levels as compared to M19MEL, was 70 -80% (Supplementary Table S1). Cell recovery did not significantly increase after prolonged incubation, or with more anti-MCSP-Micro-Beads.

### ***Lower limit of quantification (LLOQ)***

The lower limit of quantification (LLOQ) was determined in 8 mL whole blood samples from six different volunteers spiked with 0, 1, 2, 3, 4, and 5 SK-MEL-28 cells per CPT. The determined LLOQ of the method was 2 cells in 8 mL of whole blood. At this LLOQ the recovery was 105% and the precision 16.9%.

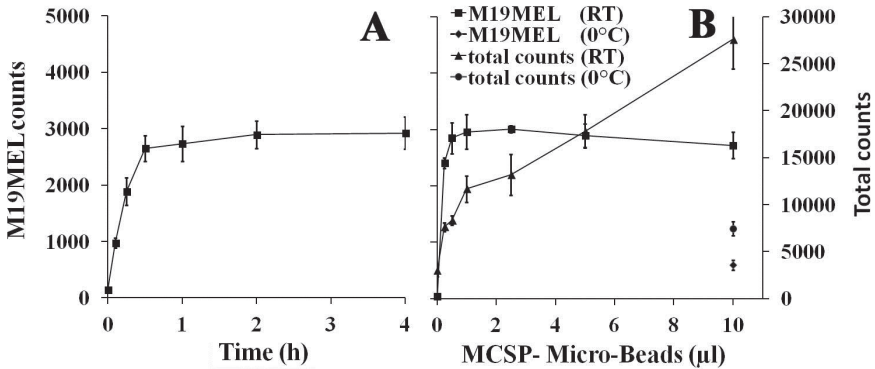
### ***Within- and between-day precision and recovery***

The precision and recovery of the method were determined by analyses of samples spiked with SK-MEL-28 at four different cell concentrations in triplicate in three

consecutive analytical runs. From these results we calculated the within-day and between-day precision and recovery (Supplementary Table S1). In all cases the precision and recoveries were well within the limits that are considered acceptable for bio-analytical methods.<sup>3</sup> An exception was the low recovery of M19MEL cells.

**Sample stability**

We determined the stability of CD146, MCSP, CD45, DNA, and cell counts for SK-MEL-28 cells spiked in 8 mL whole blood samples after storage at -80 °C for incremental time periods. All parameters were stable for at least 12 months. The fluorescent signals from stained CD146, MCSP, CD45, DNA, and SK-MEL-28 cell counts were also stable during the tested 24 h storage period at 4 - 7 °C.



**Supplementary Figure S1. Background events and recovery of M19MEL cells**

Total background events and recovery of 10,000 M19MEL cells spiked in 8 mL peripheral blood from a healthy volunteer, respectively, indicated incubation time using 4 µL of anti-MCSP-Micro-Beads (Figure S1A), or different amounts of anti-MCSP-Micro-Beads (Figure S1B). Data is expressed as means ± S.D. of three different samples.

**Supplementary Table S1. Recovery, within-day precision and between-day precision**

		M19MEL			SK-MEL-28			
Nominal spiked cells	Measured spiked cells	Recovery (%)	WDP (%)	BDP (%)	Measured spiked cells	Recovery (%)	WDP (%)	BDP (%)
10	2	20	9.9	7.2	8	80	14.2	10.2
100	24	24	11.3	6.5	74	74	11.5	7.7
1000	267	27	14.4	10.0	72	72	9.6	4.7
10000	2569	26	10.8	4.8	71	71	10.3	5.4

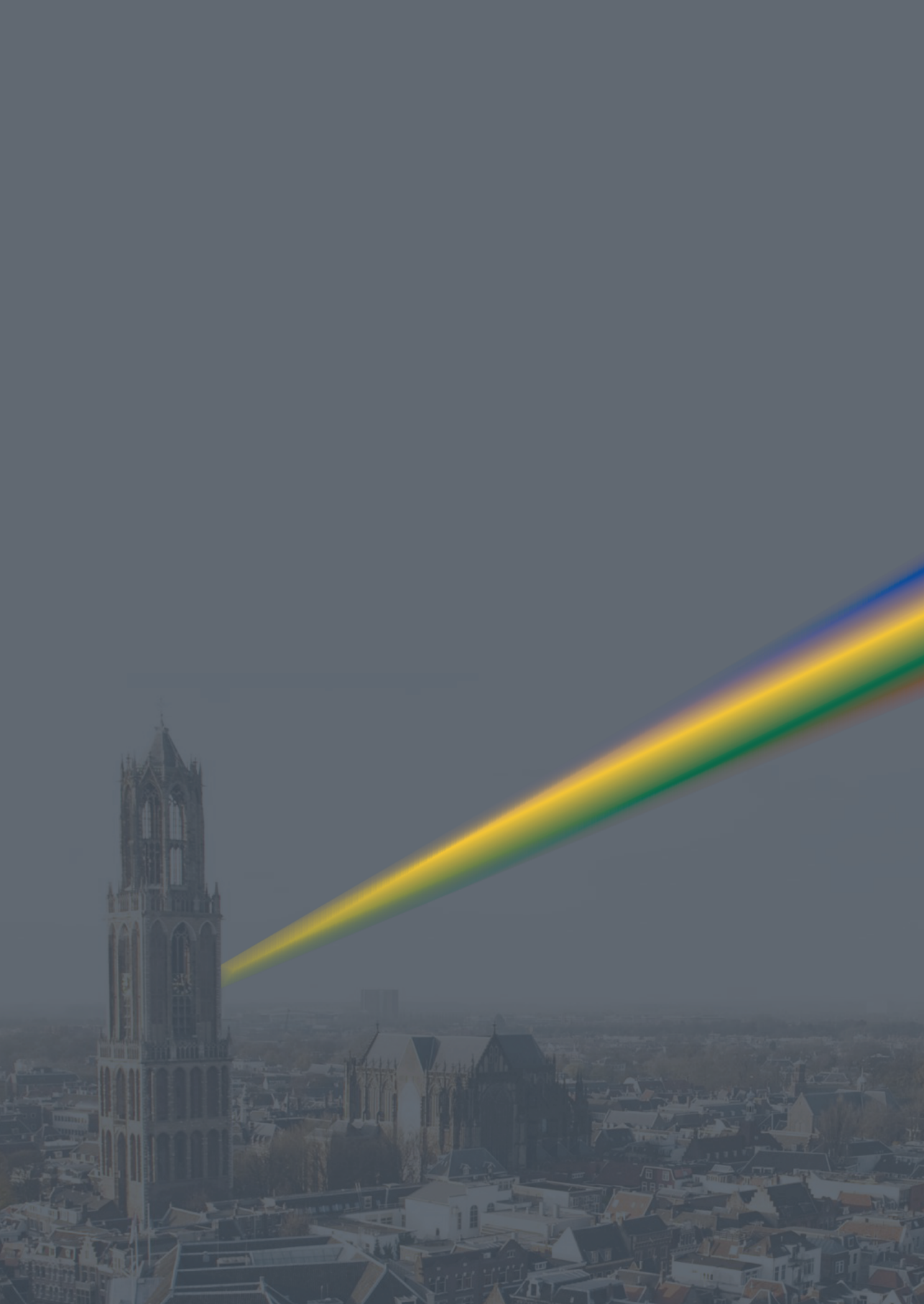
Recovery, within-day precision (WDP) and between-day precision (BDP) for determination of the number of SK-MEL-28 and M19MEL cells spiked in cell preparation tubes (CPT) tubes containing 8 mL peripheral blood from a healthy volunteer. Three replicate measurements were performed at each spike level. Within- and between-day precision were calculated using one-way analysis of variance (ANOVA).

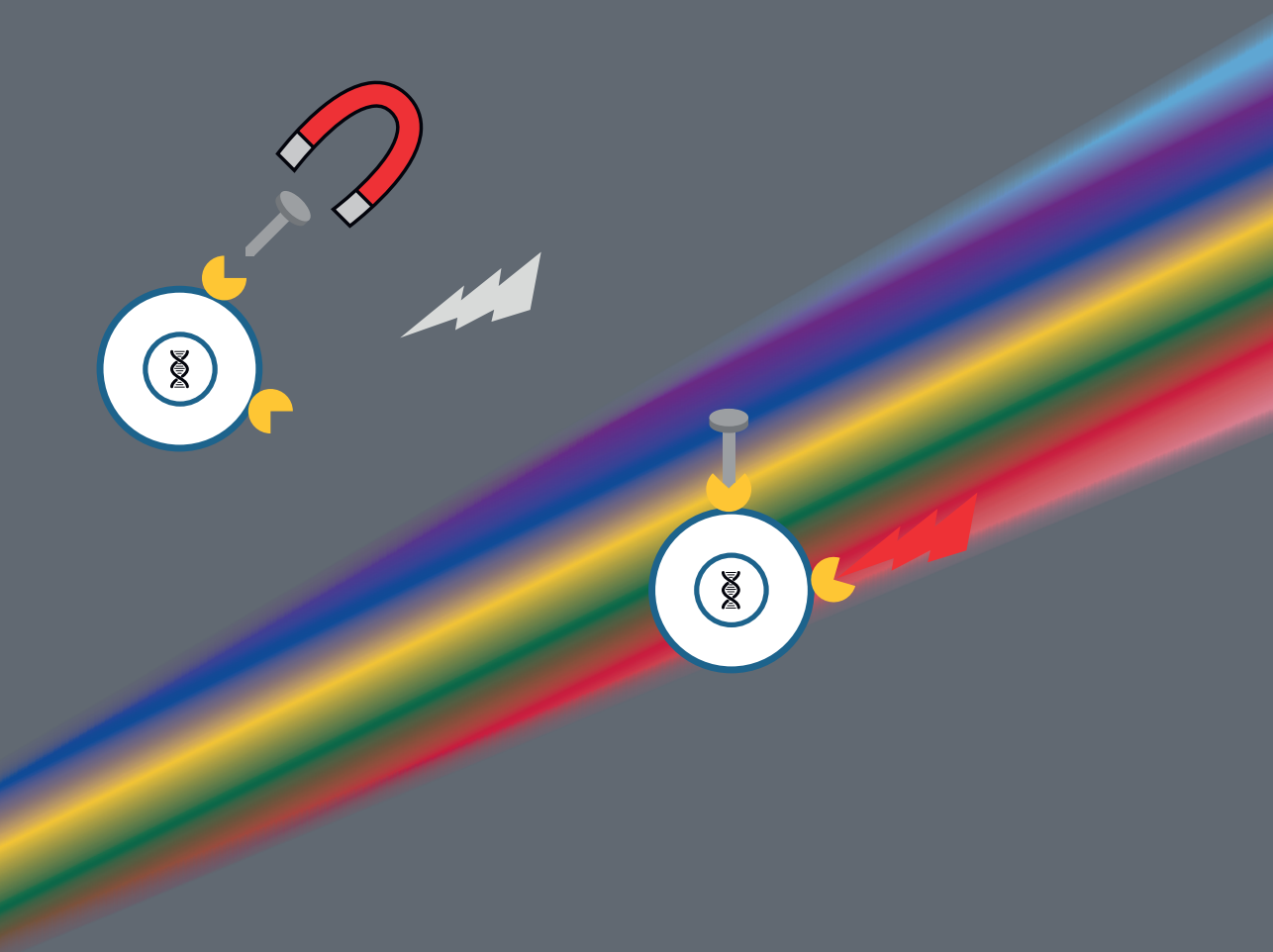
## References

1. Yu L, Favoino E, Wang Y, Ma Y, Deng X, Wang X. The CSPG4-specific monoclonal antibody enhances and prolongs the effects of the BRAF inhibitor in melanoma cells. *Immunol Res.* 2011;50(2-3):294-302.
2. Pluim D, Devriese LA, Beijnen JH, Schellens JHM. Validation of a multiparameter flow cytometry method for the determination of phosphorylated extracellular-signal-regulated kinase and DNA in circulating tumor cells. *Cytometry A.* 2012;81(8):664-671.
3. Chandran S, Singh RSP. Comparison of various international guidelines for analytical method validation. *Pharmazie.* 2007;62(1):4-14.



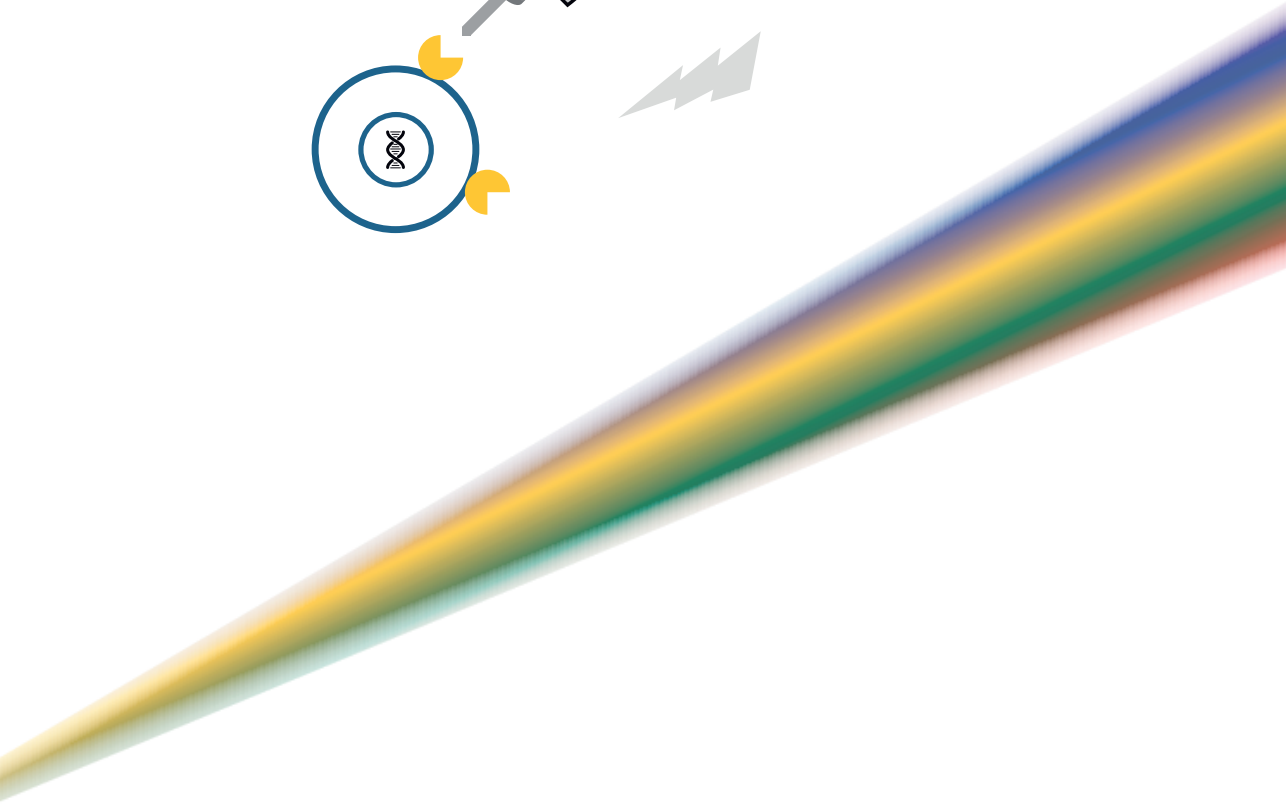
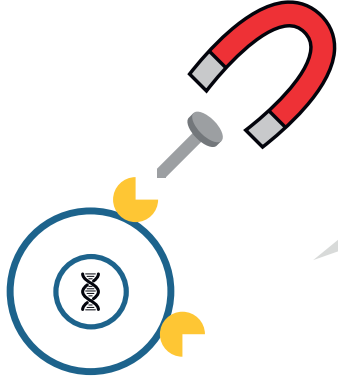


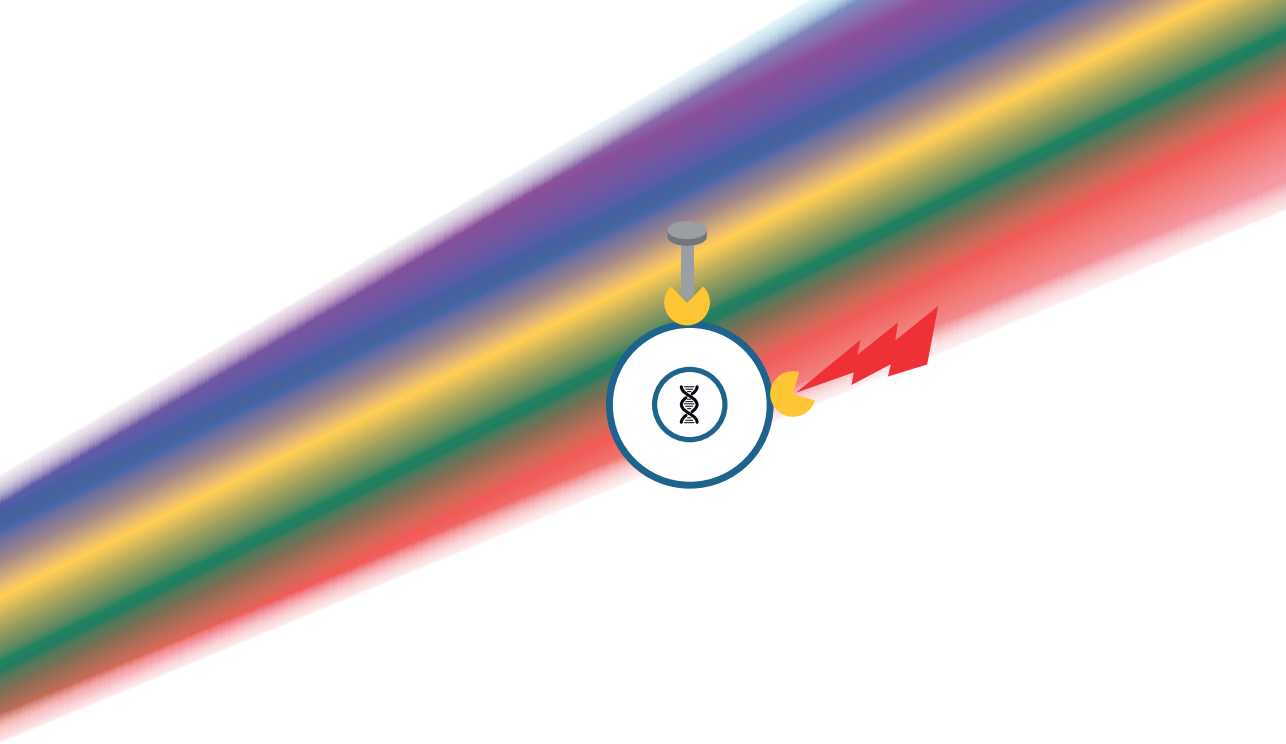




# Part 2

Clinical pharmacology of anticancer agents





# Chapter 4

## Intracranial antitumor responses of nivolumab and ipilimumab: a pharmacodynamic and pharmacokinetic perspective, a scoping systematic review

Mark T.J. van Bussel  
Jos H. Beijnen  
Dieta Brandsma

*BMC Cancer. 2019;19(1):519.*

## Summary

### Background

Recently, two phase II trials showed intracranial activity of the immune checkpoint inhibitors nivolumab and ipilimumab in patients with melanoma brain metastases. However, it is generally assumed that large molecules like monoclonal antibodies nivolumab and ipilimumab cannot penetrate and pass an intact blood brain barrier (BBB). In this systematic review we provide a pharmacodynamic and pharmacokinetic consideration of the clinical activity of the immune checkpoint inhibitors nivolumab and ipilimumab in melanoma brain metastases.

### Methods

Pubmed was systematically searched for prospective phase II and III studies on nivolumab and ipilimumab in melanoma brain metastases and cerebrospinal fluid (CSF) levels of nivolumab and ipilimumab. Results were discussed and a perspective on the pharmacodynamics and pharmacokinetics for the intracranial activity of these agents was given.

### Results

Two phase II studies with the combination nivolumab and ipilimumab and one phase II study with ipilimumab monotherapy in melanoma brain metastases were included in this review. One article reported drug levels of nivolumab in CSF. Intracranial responses were achieved in 16 of 35 patients (46%; 95% confidence interval (CI) 29-63) in a phase II study cohort treated with nivolumab and ipilimumab. In a second phase II study in 94 patients, the rate of intracranial clinical benefit was 57% (95% CI 47-68). The CSF/serum ratio of nivolumab was 0.88-1.9% in a cohort of metastatic melanoma patients treated with nivolumab 1-3 mg/kg. Nivolumab concentrations ranged from 35-150 ng/ml in CSF of these patients, which is in the range of the half maximal effective concentration (EC50) of 0.64 nM.

### Conclusions

Ipilimumab and nivolumab are active in melanoma brain metastases. Nivolumab penetrates into the CSF. Based on the described findings the general consensus that monoclonal antibodies do not penetrate into the central nervous system (CNS) and cannot have a direct intracranial effect needs to be reconsidered.

## Background

Immunotherapy with immune checkpoint inhibitors has become first line therapy in patients with metastatic melanoma.<sup>1</sup> Nivolumab (MDX-1106) is a human immunoglobulin G4 (IgG4) monoclonal antibody which binds to the programmed death-1 (PD-1) receptor and blocks its interaction with PD-L (programmed death ligand) 1 and PD-L2.<sup>2</sup> Activation of the PD-1 receptor inhibits T cell activity which is important in the inhibition and thus regulation of T cell immune responses. PD-L1 and PD-L2 are expressed by antigen presenting cells and can be expressed by tumors cells.<sup>3,4</sup> Nivolumab potentiates T cell responses against tumor cells through blockade of PD-1 receptor binding to PD-L1 and PD-L2. Ipilimumab is a fully human anti-cytotoxic T lymphocyte associated antigen 4 (CTLA-4) IgG1κ monoclonal antibody.<sup>5</sup> CTLA-4 present on activated T cells can induce T cell inhibitory signals.<sup>6</sup> The combination of intravenous nivolumab and ipilimumab had a higher efficacy than intravenous nivolumab monotherapy in a randomized, double-blind, phase III study with 945 previously untreated patients with unresectable stage III or IV melanoma.<sup>7</sup> The general consensus with regard to antibody pharmacokinetics is that monoclonal antibodies cannot penetrate an intact BBB due to their large molecular size and thereby may lack clinical activity in the CNS.<sup>8-13</sup> However, the BBB of blood vessels in brain metastases is partially disrupted leading to a higher permeability.<sup>14</sup> Recently, two phase II studies have shown intracranial efficacy of nivolumab and ipilimumab in patients with melanoma with untreated brain metastases.<sup>15,16</sup> With regard to the highly promising intracranial effects of immune checkpoint inhibitors administered intravenously in melanoma patients with brain metastases, we would like to give a perspective of the pharmacokinetics and pharmacodynamics on the intracranial antitumor activity of nivolumab and ipilimumab. In this paper, we argue against the consensus that monoclonal antibodies such as immune checkpoint proteins inhibitors cannot penetrate an intact BBB and thereby cannot be efficacious against CNS tumors via this direct intracranial mechanism. We show a concise mechanistic insight on the pharmacodynamics of the intracranial activity of nivolumab and ipilimumab.

### The immune system in brain metastases

One of the characteristics of the CNS is the lack of a classical lymphatic drainage system. However, based on recent research, it is now accepted that the CNS undergoes constant immune surveillance within the meningeal compartment.<sup>17-19</sup> Soluble antigens derived from tumors within the CNS can reach the deep cervical lymph nodes via CSF drainage. Antigen presenting cells take up neo-antigens from the intracranial tumor and present them in the cervical lymphnodes to lymphocytes. To mediate a pharmacodynamic therapeutic effect in the brain, the systemically

activated effector immune cells or the checkpoint inhibiting antibody has to reach the intracranial tumor site. Lymphocytes activated in the cervical lymph node can enter the brain and CSF via the blood. Tumor cells are able to evade these activated lymphocytes by expressing PD-L1 to inhibit the activated T cell. Tumor infiltrating lymphocytes (TILs) are present in melanoma brain metastases.<sup>3,20,21</sup> In a retrospective cohort of 43 melanoma brain metastases CD3+ TILs were present in 77% of the samples and CD8+ TILs were present in 91% of the samples.<sup>3</sup> Fifty-one percent of melanoma brain metastases expressed PD-L1.<sup>3</sup> The ligand and the effector immune cells are thus present in the tumor brain environment.

## Methods

First Pubmed was searched using the following terms: nivolumab OR ipilimumab OR nivolumab AND ipilimumab AND melanoma brain metastases NOT radiotherapy up to 24 December 2018. Prospective phase II-III studies in melanoma brain metastases were included. Modified Response Evaluation Criteria in Solid Tumors (RECIST) criteria for brain lesions or modified WHO response criteria were extracted from the clinical studies to assess efficacy. A second search was performed for (ipilimumab AND cerebrospinal fluid) OR (nivolumab AND cerebrospinal fluid) to identify additional papers in which CSF levels of nivolumab or ipilimumab are reported.

## Results

The Pubmed search resulted in 84 hits. Two prospective phase II studies with the combination nivolumab and ipilimumab and one prospective phase II study with ipilimumab monotherapy in melanoma brain metastases were included for this review as shown in Figure 1. No nivolumab or ipilimumab levels in CSF were reported in the phase II studies. Therefore, a second Pubmed search was performed specifically for nivolumab and CSF or ipilimumab and CSF. The search resulted in 16 hits as shown in Figure 2. One article was found in which drug levels of nivolumab in CSF were reported. No articles reported ipilimumab levels in CSF.



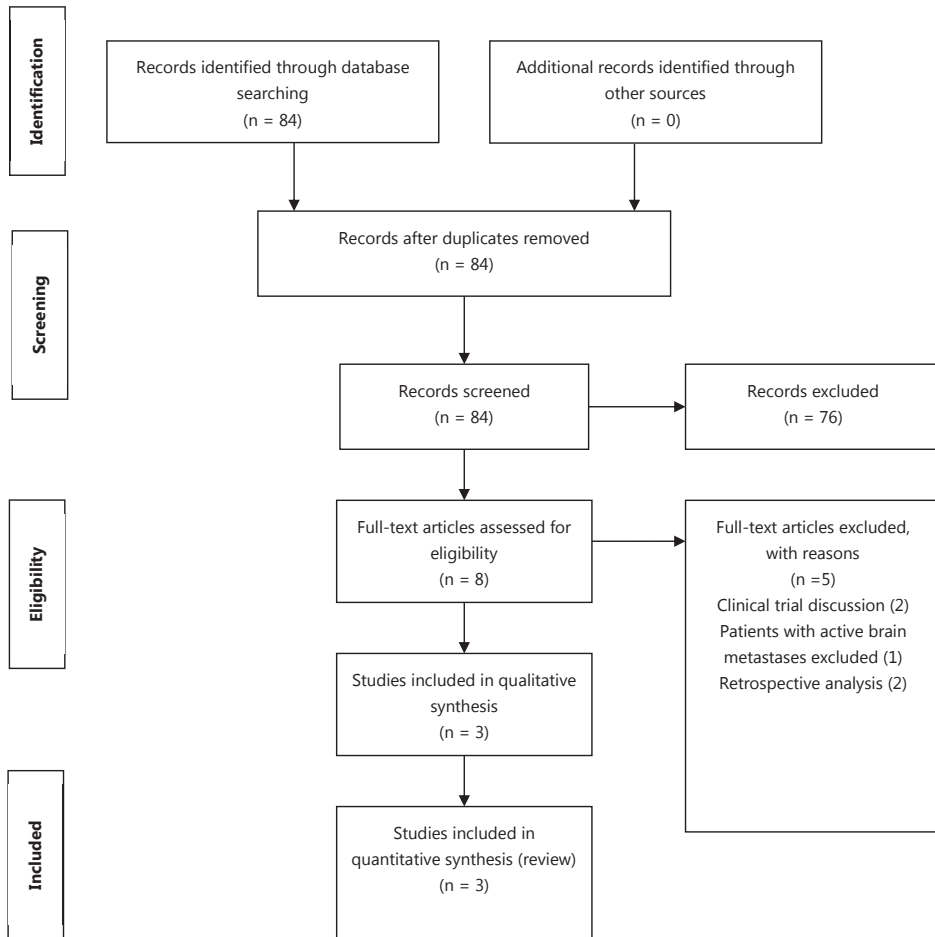


Figure 1. PRISMA diagram of clinical study selection

## Clinical studies

In the first clinical study 63 immunotherapy-naïve patients with asymptomatic brain metastases were randomized to intravenous nivolumab 1 mg/kg combined with intravenous ipilimumab 3 mg/kg every 3 weeks for four doses and were subsequently treated with nivolumab 3 mg/kg every 2 weeks in cohort A or nivolumab 3 mg/kg every 2 weeks patients in cohort B.<sup>16</sup> In the non-randomized cohort C, patients with progressive brain metastases after local therapy, patients with symptomatic brain metastases or with leptomeningeal disease were treated with nivolumab 3 mg/kg every 2 weeks. The primary endpoint was intracranial response defined as the percentage of patients with a confirmed intracranial complete or partial response at week 12. At the data cutoff with a median follow up of 17 months (IQR 8-25)

intracranial responses were achieved by 16 of 35 patients (46%; 95% CI 29-63) in cohort A, five of 25 (20%; 95% CI 7-41) in cohort B and one of 16 (6%; 95% CI 0-30) in cohort C. The median intracranial progression free survival has not been reached in cohort A. The intracranial progression-free survival at 6 months was 53%.

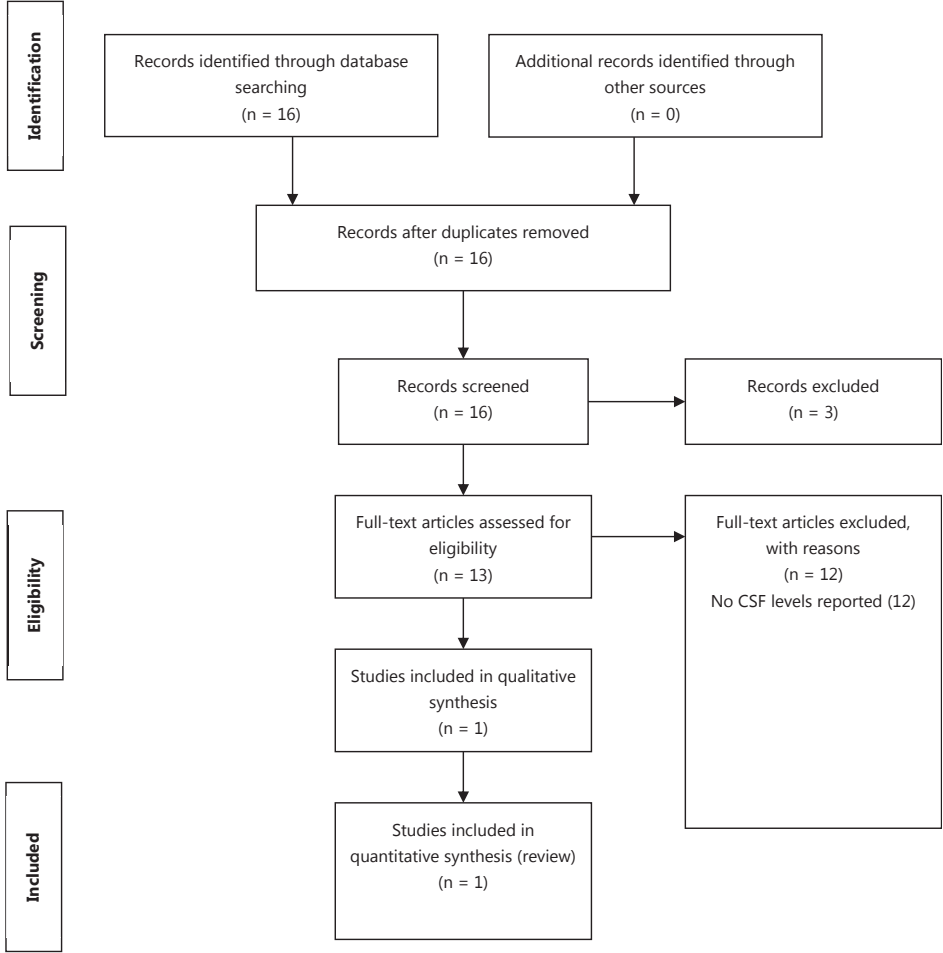


Figure 2. PRISMA diagram of study selection with reported CSF levels for nivolumab or ipilimumab

In the second clinical study, 94 patients with metastatic melanoma and at least one measurable, non-irradiated asymptomatic brain metastasis received nivolumab (1 mg/kg) plus ipilimumab (3 mg/kg) every 3 weeks for up to four doses, followed by nivolumab (3 mg/kg) every 2 weeks until progression or unacceptable toxicity.<sup>15</sup> The primary endpoint was the rate of intracranial clinical benefit, defined as the percentage of patients who had stable disease for at least 6 months or a partial

response or a complete response. At a median follow-up of 14 months the rate of intracranial clinical benefit was 57% (95% CI 47-68), the complete intracranial response rate was 26% and the partial intracranial response rate was 30%. This resulted in an intracranial objective response of 55% (95% CI 45-66). The median duration of intracranial response has not been reached.

Ipilimumab monotherapy has been studied in a phase II study in 72 patients with melanoma and brain metastases.<sup>22</sup> Patients received four doses of 10 mg/kg intravenous ipilimumab once every 3 weeks. Patients who were clinically stable at week 24 were eligible to receive 10 mg/kg ipilimumab every 12 weeks. Patients in cohort A were neurologically asymptomatic and were not receiving corticosteroids at inclusion. Patients in cohort B were symptomatic and received a stable dose of corticosteroids. The primary endpoint was the proportion of patients with disease control, defined as complete response, partial response or stable disease after 12 weeks, assessed with modified WHO criteria. CNS disease control assessed in 51 patients in cohort A was 24% (95% CI 13-38) and 10% (95% CI 1-30) in cohort B, which consisted of 21 patients.

The above mentioned clinical trials clearly demonstrated intracranial responses of patients with melanoma brain metastases treated intravenously with immune checkpoint inhibitors. Four other clinical trials with nivolumab and ipilimumab in patients with melanoma brain metastases are ongoing.<sup>23</sup> In a phase II trial nivolumab and ipilimumab is combined with radiotherapy (NCT03340129). In a phase III trial nivolumab and ipilimumab are combined with fotemustine (NCT02460068). Recently, a phase I/Ib trial (NCT03025256) of concurrent intravenous and intrathecal nivolumab for patients with leptomeningeal metastases has started.

### **Nivolumab pharmacodynamics**

Nivolumab is a human IgG4 monoclonal antibody. IgG4 antibodies can undergo Fab (Fragment antigen binding)-arm exchange.<sup>24,25</sup> Fab-exchange can be prevented by introducing a mutation in the hinge region of the antibody, as has been done for nivolumab.<sup>25,26</sup> The constant region fragment (Fc) of the antibody determines the effector functions and kinetics.<sup>27</sup> Antibodies with neonatal Fc receptor (FcRn) binding can enter cells via endocytosis and are prevented from degradation by the FcRn, resulting in a prolonged elimination half-life.<sup>27-29</sup> Nivolumab is an IgG4 antibody with FcRn binding.<sup>30</sup> IgG4 antibodies like nivolumab have a low potential to induce antibody dependent cell mediated cytotoxicity (ADCC) or complement dependent cytotoxicity (CDC).<sup>27,30</sup> This prevents toxic effects of nivolumab on the lymphocytes themselves and thereby preserves T cell function. Nivolumab binds to native PD-1 molecules expressed on activated T cells with an EC<sub>50</sub> of 0.64 nM.<sup>30</sup> No dose response relation

has been observed in melanoma patients treated with intravenous nivolumab dosed from 0.1 to 10 mg/kg. The receptor occupancy of nivolumab has been investigated at a dose range from 0.1-10 mg/kg. The median PD-1 receptor occupancy by nivolumab was 64-70% across all dose levels. These results demonstrate that the majority of PD-1 receptors are bound by nivolumab at the lowest dose level tested (0.1 mg/kg). No effect between dose and receptor occupancy was observed within the studied dose range. A sustained receptor occupancy above 70% of nivolumab on PD-1 on circulating T cells has been observed for more than 2 months after nivolumab infusion despite a serum half-life of nivolumab of 12 to 20 days regardless of dose.<sup>26</sup>

### **Nivolumab pharmacokinetics**

Nivolumab is dosed intravenously and has linear pharmacokinetics within the studied dose range of 0.1-10 mg/kg.<sup>2</sup> Based on population pharmacokinetic analysis at steady state at dose level 3 mg/kg every 2 weeks, the clearance, terminal half-life and average exposure were 7.9 ml/h, 25.0 days and 86.6 µg/ml, respectively. The registered dose interval was initial biweekly. However, in melanoma and in renal cell carcinoma the dose interval has been doubled to 4 weeks based on modelling of dose/exposure efficacy and safety relationships.<sup>2</sup> The molecular weight of nivolumab is 146 kDa.<sup>31</sup> As stated earlier, the EC50 of nivolumab binding to native PD-1 molecules expressed on activated T cells is 0.64 nM.<sup>30</sup> In a cohort of metastatic melanoma patients with a clinical suspicion on leptomeningeal metastases, treated with nivolumab 1-3 mg/kg every 2-3 weeks, nivolumab CSF levels have been quantified with a validated enzyme-linked immunosorbent assay.<sup>32</sup> The nivolumab concentrations ranged from 35-150 ng/ml with a CSF/serum ratio of 0.88-1.9%.<sup>32</sup> The CSF levels of nivolumab are in the range of the EC50 with a molar range of 0.24-1.0 nM.

### **Ipilimumab pharmacodynamics**

CTLA-4 induces T cell inhibitory signals.<sup>6</sup> CTLA-4 is transiently expressed by a subset of activated T cells and binds to the B7 (CD80/CD86) receptor on antigen presenting cells.<sup>33,34</sup> Ipilimumab is an IgG1κ anti-CTLA-4 monoclonal antibody.<sup>5</sup> Ipilimumab has an EC50 of 0.2 µg/ml for the in-vitro binding of human CTLA-4 to B7.1 (CD80) and B7.2 (CD86) with maximal blockage between 6 to 20 µg/ml and 1 to 3 µg/ml respectively.<sup>33</sup> The target trough concentration for ipilimumab is 20 µg/ml based on in vitro studies. Intravenous ipilimumab induces a dose dependent increase in absolute lymphocyte counts (ALC).<sup>5,35</sup> This includes an increase of central memory CD4- and CD8 T cells and effector memory T cells.<sup>5</sup> Given the rise in ALC it is unlikely that ADCC does occur at biological relevant levels during ipilimumab treatment.<sup>33</sup> Partial and complete ongoing systemic responses of ipilimumab have been observed till months after the last ipilimumab administration.<sup>36</sup> The persisted pharmacodynamic effects have

been maintained by the immune system in the absence of therapeutic ipilimumab concentrations for more than 710 days.<sup>36</sup>

### **Ipilimumab pharmacokinetics**

Ipilimumab has dose proportional pharmacokinetics over the dose range of 0.3 mg/kg to 10 mg/kg.<sup>33</sup> The terminal half-life is 15.4 days.<sup>5</sup> Ipilimumab accumulates due to the dose interval of once every 3 weeks and an estimated elimination half-life of 2 weeks. The molecular weight of ipilimumab is 148 kDa.<sup>33</sup> Ipilimumab has a systemic clearance of 16.8 ml/h (percent coefficient of variation) (38.1%) and a volume of distribution of 7.47 l (10.1%) at steady-state. The average steady state trough serum concentration ( $\pm$ SD) of ipilimumab was 21.8  $\mu$ g/ml ( $\pm$  11.2) at the 3 mg/kg induction regimen. The FcRn binding properties of ipilimumab have not been assessed.<sup>37</sup> However, IgG1 binds to the FcRn and therefore it is assumed that ipilimumab also binds to the FcRn.<sup>27</sup> CTLA-4 immune checkpoint inhibitors block T cell inhibitory signals induced by the CTLA-4 pathway and increases the number of reactive T effector cells, which induce a direct T cell immune attack against tumor cells.<sup>5,35</sup> CTLA-4 blockade can also inhibit the function of regulatory T cells which may provide an antitumor immune response. As ipilimumab is an IgG1 monoclonal antibody, it is expected that ipilimumab can also reach the CSF via FcRn mediated transcytosis. However, to the best of our knowledge, no studies have been published on ipilimumab concentrations in CSF.

## **Discussion**

Clinical studies in the recent years have shown a high intracranial effect of the combination of ipilimumab and nivolumab (55% intracranial response) on melanoma brain metastases, which is considered to be mediated by an intracranial increase of activated lymphocytes by blocking the two immune checkpoint proteins on T cells.<sup>15,16</sup> The general consensus on the intracranial effect of immune checkpoint inhibitors is that the expected pharmacodynamics effect is caused by activated peripheral T cells which then cross the BBB. Monoclonal antibodies are not believed to penetrate an intact BBB due to their large molecular size of ~150 kDa.<sup>8-12,38</sup> A sustained receptor occupancy above 70% of nivolumab on PD-1 on circulating T cells has been observed for more than 2 months after infusion, despite a serum half-life of nivolumab of 12 to 20 days regardless of dose.<sup>26</sup> Nivolumab can bind the peripheral circulating T cells irreversibly which then cross the BBB. The antitumor effect of nivolumab is mediated by activated T cells given the low potential of nivolumab to induce ADCC or CDC activity.<sup>27,30</sup> However, both nivolumab and ipilimumab are IgG monoclonal antibodies with FcRn binding, which can cross an intact BBB. FcRn binding of antibodies is known

to mediate transport of IgG antibodies over the placenta from mother to child and is involved in other transcellular transport processes.<sup>39,40</sup> IgG antibodies with FcRn binding like nivolumab can enter cells, like macrophages in the choroid plexus and reach the CSF via endocytosis via FcRn mediated transcytosis.<sup>41,42</sup> 80% of the total CSF production of 500-600 ml per day is produced by the choroid plexus via filtration of the blood.<sup>41</sup> Microglial cells, macrophages and dendritic cells reside in the choroid plexus and can mediate the nivolumab transport of the blood to the CSF. The proposed mechanism of nivolumab transport via the choroid plexus to the CSF is depicted in Figure 3.

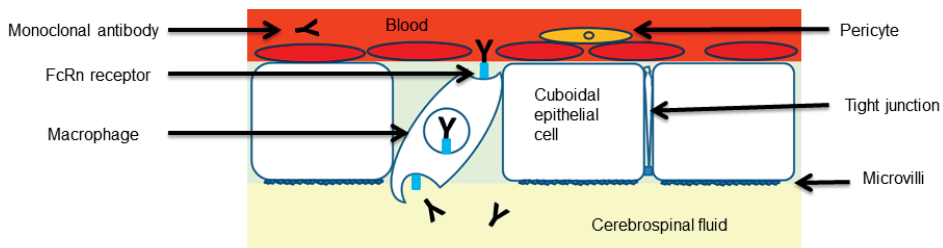


**Figure 3. Proposed mechanism of nivolumab transport to the CSF**

Neonatal Fc receptor mediated antibody transport from the blood vessels in the choroid plexus to the CSF. The choroid plexus consists of a monolayer of cuboidal epithelial cells in which macrophages reside.<sup>41</sup> The epithelial cells have microvilli and are interconnected via tight junctions forming the blood-CSF barrier. The proposed mechanism of FcRn mediated endocytosis of IgG4 monoclonal antibodies with FcRn binding like nivolumab is via macrophages residing in the choroid plexus.<sup>29,41</sup> Monoclonal antibodies with FcRn binding like nivolumab are prevented from degradation by the FcRn.<sup>29</sup> The FcRn mediates antibody transport to the CSF. *Abbreviations:* FcRn=neonatal Fc receptor, CSF=cerebrospinal fluid, IgG4=immunoglobulin G4.

The FcRn mediated transcellular transport is a saturable system.<sup>38</sup> High IgG concentrations will increase the antibody fraction that is being catabolized, leading to a decrease in the elimination half-life. IgG has an elimination half-life of 25 days and a plasma clearance of 10 ml/h.<sup>38</sup> IgG4 is the least common antibody subclass in of the IgG subclasses 1-4 with a serum concentration of 0.5 mg/ml.<sup>43</sup> Nivolumab has a clearance of 7.9 ml/h.<sup>2</sup> This indicates that the FcRn receptor mediated transcytosis has not yet been saturated at therapeutic concentrations and that the maximum physiological capacity of this transport system has not been reached.<sup>27,28</sup> The combination of nivolumab and ipilimumab has a higher systemic efficacy than monotherapy in a randomized, double-blind, phase III study with 945 previously untreated patients with unresectable stage III or IV melanoma.<sup>7</sup> The systemic response rate for nivolumab monotherapy was 43.7% (95% CI 38.1-49.3), for ipilimumab monotherapy 19.0% (95% CI 14.9-23.8) and for the combination 57.6% (95% CI 52.0-63.2). In the CNS, a similar increase of antitumor activity has been observed for the combination of nivolumab

and ipilimumab, with intracranial responses of 46% (95% CI 29-63) for the combination of nivolumab and ipilimumab and 20% (95% CI 7-41) for nivolumab monotherapy.<sup>16</sup> Currently, the pharmacodynamic effect of ipilimumab is considered to be on the peripheral T cells which then cross the BBB.<sup>10</sup> The sustained pharmacological effect of ipilimumab can be attributed to an increase of central memory CD4 and CD8 T cells and effector memory T cells.<sup>5</sup> Whether an additional, direct effect of ipilimumab in the brain occurs is unknown, as no data are available on ipilimumab FcRn binding and ipilimumab concentrations in the CSF.

## Conclusions

Based on the described findings the general consensus that monoclonal antibodies do not penetrate into the CNS and that this mechanism does not contribute to intracranial activity of these agents needs to be reconsidered. The intracranial effects of immune checkpoint inhibitors can be due to a dual mechanism: they can bind irreversibly PD1 or bind to CTLA-4 on peripheral circulating lymphocytes which can subsequently penetrate the BBB (mechanism 1) and the antibodies themselves can cross the BBB and inhibit the TILs, being already present in the intracranial tumor (mechanism 2). For adequate brain penetration of antibodies, they need to be selected for the optimal IgG subclass with FcRn binding and favorable pharmacokinetics in the early drug development process. The highly promising clinical antitumor activity combined with the described mechanism of penetration of monoclonal antibodies into the CSF opens novel strategies to treat malignant diseases in the CNS.

## Conflict of interest

The authors declare that they have no competing interests related to this study.

## References

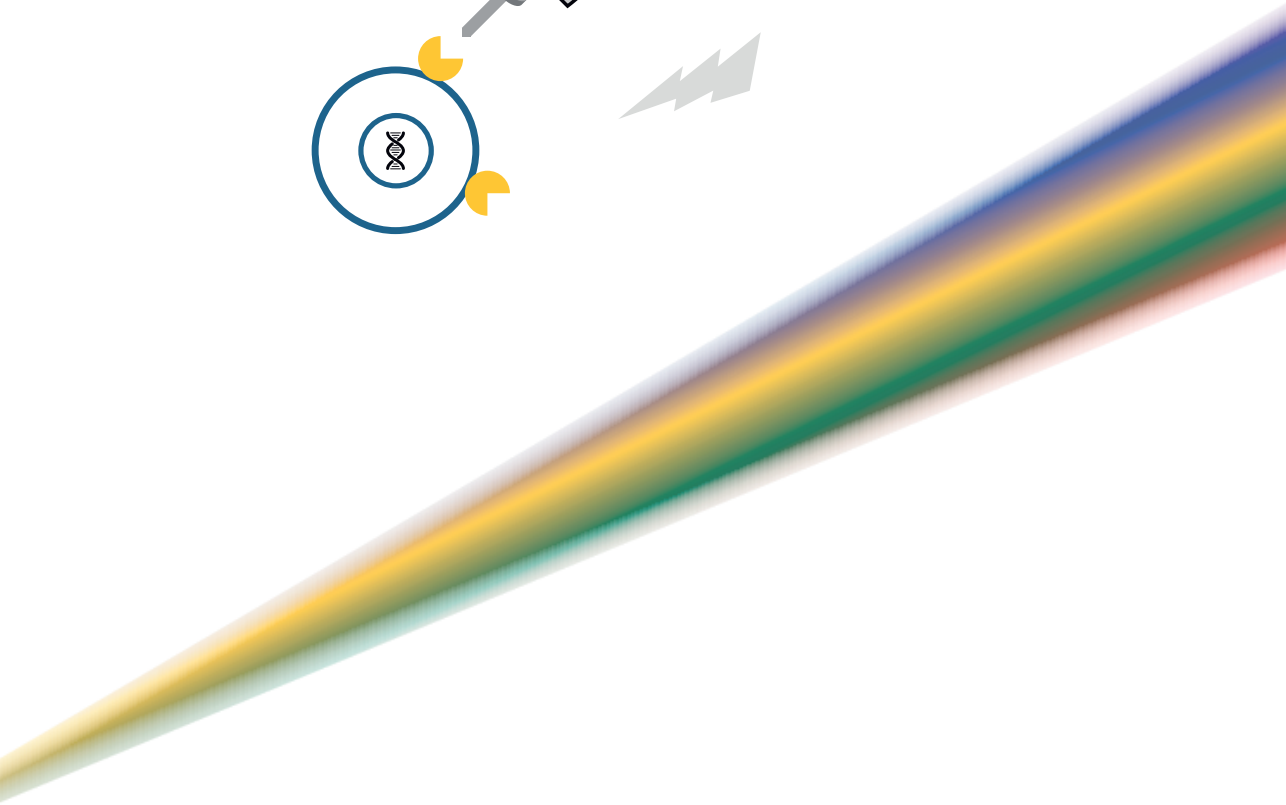
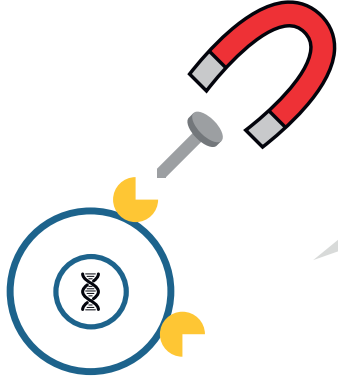
1. Dummer R, Hauschild A, Lindenblatt N, Pentheroudakis G, Keilholz U, ESMO Guidelines Committee. Cutaneous melanoma: ESMO Clinical Practice Guidelines for diagnosis, treatment and follow-up. *Ann Oncol Off J Eur Soc Med Oncol*. 2015;26 Suppl 5:v126-32.
2. European Medicines Agency. Summary of Product Characteristics Nivolumab. Available at <http://www.ema.europa.eu>. Accessed 12 Sep 2018.
3. Berghoff AS, Ricken G, Widhalm G, et al. Tumour-infiltrating lymphocytes and expression of programmed death ligand 1 (PD-L1) in melanoma brain metastases. *Histopathology*. 2015;66(2):289-299.
4. Morales-Betanzos CA, Lee H, Gonzalez Ericsson PI, et al. Quantitative Mass Spectrometry Analysis of PD-L1 Protein Expression, N-glycosylation and Expression Stoichiometry with PD-1 and PD-L2 in Human Melanoma. *Mol Cell Proteomics*. 2017;16(10):1705-1717.
5. Summary of Product Characteristics Ipilimumab. Available at <http://www.ema.europa.eu>. Accessed 14 Sep 2018.
6. Waterhouse P, Penninger JM, Timms E, et al. Lymphoproliferative disorders with early lethality in mice deficient in Ctlα-4. *Science*. 1995;270(5238):985-988.
7. Larkin J, Chiarion-Sileni V, Gonzalez R, et al. Combined Nivolumab and Ipilimumab or Monotherapy in Untreated Melanoma. *N Engl J Med*. 2015;373(1):23-34.
8. Kim M, Kizilbash SH, Laramy JK, et al. Barriers to Effective Drug Treatment for Brain Metastases: A Multifactorial Problem in the Delivery of Precision Medicine. *Pharm Res*. 2018;35(9):177.
9. Bechmann I, Galea I, Perry VH. What is the blood-brain barrier (not)? *Trends Immunol*. 2007;28(1):5-11.
10. Chamberlain MC, Baik CS, Gadi VK, Bhatia S, Chow LQM. Systemic therapy of brain metastases: non-small cell lung cancer, breast cancer, and melanoma. *Neuro Oncol*. 2017;19(1):i1-i24.
11. Levin VA. Relationship of octanol/water partition coefficient and molecular weight to rat brain capillary permeability. *J Med Chem*. 1980;23(6):682-684.
12. Pardridge WM. Delivery of Biologics Across the Blood-Brain Barrier with Molecular Trojan Horse Technology. *BioDrugs*. 2017;31(6):503-519.
13. Zhao YH, Abraham MH, Ibrahim A, et al. Predicting penetration across the blood-brain barrier from simple descriptors and fragmentation schemes. *J Chem Inf Model*. 2007;47(1):170-175.
14. Gampa G, Vaidyanathan S, Sarkaria JN, Elmquist WF. Drug delivery to melanoma brain metastases: Can current challenges lead to new opportunities? *Pharmacol Res*. 2017;123:10-25.
15. Tawbi HA, Forsyth PA, Algazi A, et al. Combined Nivolumab and Ipilimumab in Melanoma Metastatic to the Brain. *N Engl J Med*. 2018;379(8):722-730.
16. Long G V., Atkinson V, Lo S, et al. Combination nivolumab and ipilimumab or nivolumab alone in melanoma brain metastases: a multicentre randomised phase 2 study. *Lancet Oncol*. 2018;19(5):672-681.
17. Ransohoff RM, Engelhardt B. The anatomical and cellular basis of immune surveillance in the central nervous system. *Nat Rev Immunol*. 2012;12(9):623-635.
18. Louveau A, Smirnov I, Keyes TJ, et al. Structural and functional features of central nervous system lymphatic vessels. *Nature*. 2015;523(7560):337-341.

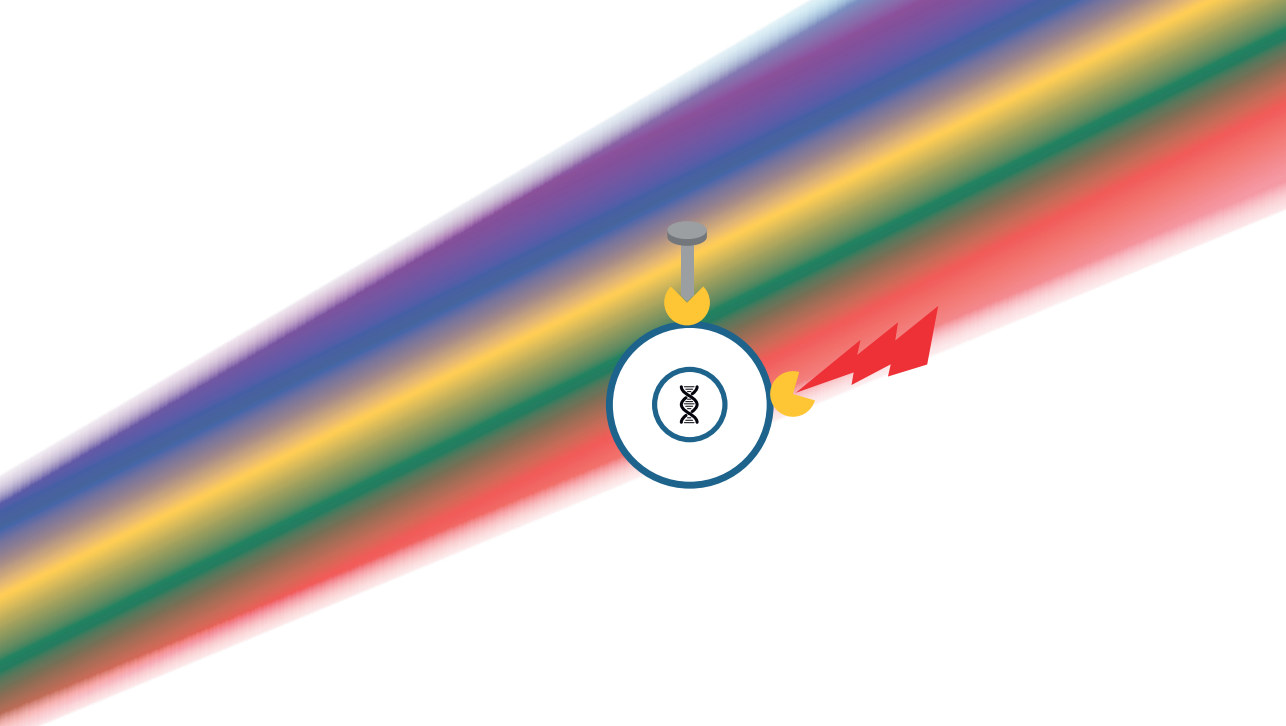


19. Louveau A, Herz J, Alme MN, et al. CNS lymphatic drainage and neuroinflammation are regulated by meningeal lymphatic vasculature. *Nat Neurosci*. 2018;21(10):1380-1391.
20. Amit M, Laidler-Trejo L, Shalom V, Shabtay-Orbach A, Krelin Y, Gil Z. Characterization of the melanoma brain metastatic niche in mice and humans. *Cancer Med*. 2013;2(2):155-163.
21. Berghoff AS, Lassmann H, Preusser M, Höftberger R. Characterization of the inflammatory response to solid cancer metastases in the human brain. *Clin Exp Metastasis*. 2013;30(1):69-81.
22. Margolin K, Ernstoff MS, Hamid O, et al. Ipilimumab in patients with melanoma and brain metastases: An open-label, phase 2 trial. *Lancet Oncol*. 2012;13(5):459-465.
23. <https://clinicaltrials.gov/ct2/results?term=nivolumab+ipilimumab&type=Intr&cond=melanoma+brain+metastases&rank=4#rowid3>. Accessed 2 Jan 2019.
24. Aalberse RC, Stapel SO, Schuurman J, Rispen T. Immunoglobulin G4: an odd antibody. *Clin Exp Allergy*. 2009;39(4):469-477.
25. van der Neut Kolfschoten M, Schuurman J, Losen M, et al. Anti-inflammatory activity of human IgG4 antibodies by dynamic Fab arm exchange. *Science*. 2007;317(5844):1554-1557.
26. Brahmer JR, Drake CG, Wollner I, et al. Phase I study of single-agent anti-programmed death-1 (MDX-1106) in refractory solid tumors: safety, clinical activity, pharmacodynamics, and immunologic correlates. *J Clin Oncol*. 2010;28(19):3167-3175.
27. Brennan FR, Morton LD, Spindeldreher S, et al. Safety and immunotoxicity assessment of immunomodulatory monoclonal antibodies. *MAbs*. 2010;2(3):233-255.
28. Jefferis R. Isotype and glycoform selection for antibody therapeutics. *Arch Biochem Biophys*. 2012;526(2):159-166.
29. Hendrikk JJMA, Haanen JBAG, Voest EE, Schellens JHM, Huitema ADR, Beijnen JH. Fixed Dosing of Monoclonal Antibodies in Oncology. *Oncologist*. 2017;22(10):1212-1221.
30. Sancho-Lopez A, de Graeff P, European Medicines Agency, Assessment report nivolumab EMA/CHMP/76688/2015.
31. Food and Drug Administration. Prescribing information nivolumab. 2015.
32. Pluim D, Ros W, van Bussel MTJ, Brandsma D, Beijnen JH, Schellens JHM. Enzyme linked immunosorbent assay for the quantification of nivolumab and pembrolizumab in human serum and cerebrospinal fluid. *J Pharm Biomed Anal*. 2019;164:128-134.
33. van Zwieten-Boot B, Sancho-Lopez EMA. Assessment report ipilimumab EMA/CHMP/557664/2011.
34. Lindsten T, Lee KP, Harris ES, et al. Characterization of CTLA-4 structure and expression on human T cells. *J Immunol*. 1993;151(7):3489-3499.
35. Wolchok JD, Neyns B, Linette G, et al. Ipilimumab monotherapy in patients with pretreated advanced melanoma: a randomised, double-blind, multicentre, phase 2, dose-ranging study. *Lancet Oncol*. 2010;11(2):155-164.
36. Weber JS, O'Day S, Urba W, et al. Phase I/II study of ipilimumab for patients with metastatic melanoma. *J Clin Oncol*. 2008;26(36):5950-5956.
37. Department of Health and Ageing Australian Government. Australian Public Assessment Report for Ipilimumab. August. 2011.
38. Wang W, Wang EQ, Balthasar JP. Monoclonal antibody pharmacokinetics and pharmacodynamics. *Clin Pharmacol Ther*. 2008;84(5):548-558.

39. Medesan C, Radu C, Kim JK, Ghetie V, Ward ES. Localization of the site of the IgG molecule that regulates maternofetal transmission in mice. *Eur J Immunol.* 1996;26(10):2533-2536.
40. Brazil MI, Chung H, Maxfield FR. Effects of incorporation of immunoglobulin G and complement component C1q on uptake and degradation of Alzheimer's disease amyloid fibrils by microglia. *J Biol Chem.* 2000;275(22):16941-16947.
41. Benarroch EE. Choroid plexus-CSF system: Recent developments and clinical correlations. *Neurology.* 2016;86(3):286-296.
42. Hulse RE, Swenson WG, Kunkler PE, White DM, Kraig RP. Monomeric IgG is neuroprotective via enhancing microglial recycling endocytosis and TNF-alpha. *J Neurosci.* 2008;28(47):12199-12211.
43. Scott-Taylor TH, Axinia S-C, Amin S, Pettengell R. Immunoglobulin G; structure and functional implications of different subclass modifications in initiation and resolution of allergy. *Immunity, Inflamm Dis.* 2018;6(1):13-33.







# Chapter 5

## Enzyme linked immunosorbent assay for the quantification of nivolumab and pembrolizumab in human serum and cerebrospinal fluid

Dick Pluim  
Willeke Ros  
Mark T.J. van Bussel  
Dieta Brandsma  
Jos H. Beijnen  
Jan H. M. Schellens

*Journal of Pharmaceutical and Biomedical Analysis* 2019;164:128-134.

## Summary

Immunotherapy with monoclonal antibodies targeting the programmed-death-1 (PD-1) receptor has become standard of care for an increasing number of tumor types. Pharmacokinetic studies may help to optimize anti-PD-1 therapy. Therefore, accurate and sensitive determination of antibody concentrations is essential. Here we report an enzyme linked immunosorbent assay (ELISA) capable of measuring nivolumab and pembrolizumab concentrations in serum and cerebrospinal fluid (CSF) with high sensitivity and specificity. The assay was developed and validated based on the specific capture of nivolumab and pembrolizumab by immobilized PD-1, with subsequent enzymatic chemiluminescent detection by anti-IgG4 coupled with horse radish peroxidase (HRP). The lower limit of quantification for serum and CSF was 2 ng/mL for both anti-PD-1 agents. The ELISA method was validated and showed long term sample stability of >1 year. This method is reliable, relatively inexpensive and can be used in serum and CSF from pembrolizumab and nivolumab treated patients.

## Introduction

Nivolumab and pembrolizumab are both monoclonal antibodies against Programmed-Death-1 (PD-1), which received FDA and EMA approval for immunotherapeutical treatment of a wide range of tumors including non-small cell lung cancer (NSCLC), melanoma, renal cell, urothelial, and microsatellite instability (MSI) high colorectal cancer. In the phase III trials both compounds showed better response rates with increased overall and progression free survival compared to standard chemotherapy.<sup>1,2</sup> Furthermore, nivolumab and pembrolizumab were associated with fewer high-grade treatment-related adverse events than other second-line therapy.<sup>3</sup> Little is known, however, about the impact of immunotherapy in patients with metastatic disease to the central nervous system. Clinical trials of immunotherapy excluded patients with active brain metastases due to a poor prognosis and uncertainty about the ability of the drugs to cross the blood brain barrier (BBB). However, current studies suggest that systemically administered immunotherapeutic antibodies demonstrate a similar durable response in the brain as in extra-cerebral sites.<sup>4</sup> Studies with other monoclonal antibodies indicate that median concentrations of monoclonal antibodies may be up to 400-fold lower in the central nervous system (CNS) than in serum, due to the BBB limiting penetration of molecules with molecular weights up to 200 kDa (nivolumab 144 kDa, pembrolizumab 146 kDa).<sup>4-6</sup> To the best of our knowledge no data has been published of nivolumab and pembrolizumab levels in cerebrospinal fluid (CSF). CSF is relatively easily accessible, and clinical studies suggest that drug concentrations in CSF are reasonably accurate in predicting CNS exposure.<sup>7</sup> Therefore, CSF may be used as a surrogate for the interstitial fluid (ISF) in the CNS and may be used for assessing CNS exposure because tumor biopsies are considered unethical to collect for pharmacokinetic purposes.

Monitoring of nivolumab and pembrolizumab concentrations in serum and CSF may enable individualized treatment strategies and lead to a better understanding of pharmacokinetic (PK) -pharmacodynamic (PD) effect relationships of these agents. Puzkiel et al. recently reported the development and validation of an ELISA for the quantification of nivolumab in plasma from NSCLC patients.<sup>8</sup> This assay has a lower limit of quantification (LLQ) of 5 µg/mL. Although this is sensitive enough for the quantification of trough plasma levels, a more sensitive assay is needed for the quantification in CSF. A five-fold more sensitive Liquid Chromatography-Mass Spectrometry (LC/MS) method has been developed that shows a LLQ of 0.977 µg/mL.<sup>9</sup> Although this method is more sensitive, it may still be not possible to accurately determine trough concentrations in CSF. In addition, LC/MS is unable to show if the measured antibodies are functionally active. Furthermore, this assay relies on

costly lab equipment that is not readily available at standard clinical laboratories. When properly optimized, chemiluminescent ELISA is one of the most sensitive immunoassays available with typical detection ranges of 0.01-0.04 fmole per mL.<sup>10</sup> Here, we report the successful development and validation of an ELISA with a lower limit of quantification of 2 ng/mL, which enables the accurate quantification of both nivolumab and pembrolizumab in serum and CSF. The applicability of the presented assay is demonstrated with the analysis of serum and CSF samples from cancer patients treated with these drugs.

## Materials and methods

### Reagents and chemicals

BD Vacutainer® SST II 5 mL tubes were obtained from Becton Dickinson (Franklin lakes, NJ, USA). Ficoll-paque™PLUS was obtained from General Electric Healthcare (Little Chalfont, UK). Nunc MaxiSorp™ white 96-well plates were purchased from VWR (Amsterdam, the Netherlands). Phosphate buffered saline (PBS) was purchased from GIBCO BRL (Gaithersburg, MD, USA). Protifar Plus low fat milk powder (ELK) was from Danone (Amsterdam, the Netherlands). Eppendorf® LoBind micro-centrifuge 2.0 mL tubes, bovine serum albumin (BSA), fetal calf serum (FCS), glycerol, thimerosal, and Tween-20 were purchased from Sigma (St. Louis, MO, USA). PBSTF consisted of PBS with 0.1% (v/v) Tween-20 and 1% (v/v) Ficoll. Ipilimumab, nivolumab and pembrolizumab were a kind gift from the Antoni van Leeuwenhoek hospital pharmacy. Mouse anti-human IgG4 Fc antibody-HRP conjugate originated from Thermo Fisher (Landsmeer, the Netherlands) as 200 µg lyophilized powder per vial, which was stored at -20 °C after reconstitution with 200 µl of 50% (v/v) glycerol, 0.05% (w/v) thimerosal, and 1% (w/v) BSA. Recombinant human PD-1 (His Tag) protein was purchased from Sino Biological Inc. (Beijing, China) as 100 µg of lyophilized powder, which was stored at -80 °C in small aliquots after reconstitution with 5.0 mL PBS. Pierce™ standard Electro Chemical Luminescence (ECL) western blotting substrate was from Pierce (Waltham, MA, USA). The ECL reagent PeroxyGlow™ was from Trevigen (Gaithersburg, MD, US). Biorad Clarity ECL was from Biorad (Veenendaal, the Netherlands). Unless stated otherwise, serum used was pooled from 6 healthy human volunteers.

### Nivolumab and pembrolizumab concentrations in the clinical stocks

The concentrations of nivolumab and pembrolizumab in the clinical stock vials were determined spectrophotometrically at 280 nm with a DS-11 (DeNovix, Wilmington, DE, USA) using the following formula:



$$c_{Ab} = 10 \cdot A_{280nm} / (\epsilon_{Ab} \cdot L)$$

$A_{280}$  = measured absorbance of nivolumab and pembrolizumab solution at 280 nm

$c_{Ab}$  = concentration of nivolumab and pembrolizumab (mg/mL)

$\epsilon_{Ab}$  = extinction coefficient of human IgG<sub>4</sub> ( $13.6A^{280nm} \cdot 1\%^{-1} \cdot cm^{-1}$ )<sup>11</sup>

L = optical path length DS-11 (1 cm)

### Serum preparation

Blood was collected in 5 mL BD Vacutainer® SST II tubes. Tubes were immediately inverted 5 times. After 30 min of coagulation at room temperature (RT), tubes were centrifuged at 1200 g for 10 min in a swing-out rotor. Next, serum was snap-frozen in liquid nitrogen in 2.0 mL vials before storage at  $-80^{\circ}C$ .

### ELISA

Nunc MaxiSorp™ white 96-well flat-bottom plates were coated overnight at  $4^{\circ}C$  with 50  $\mu$ l of 2  $\mu$ g/mL PD-1. The next day, wells were emptied and washed 4 times with 300  $\mu$ l of PBSTF.

Standard curves were prepared in 2 mL Eppendorf® LoBind vials on the day of analysis by serial dilution of a 11.0 mg/mL nivolumab clinical stock solution to 100, 50, 20, 10, 5, 2, and 0 ng/mL in ice-cold 10% (v/v) serum in PBSTF. Quality controls (QCs) were prepared from different nivolumab and pembrolizumab stock solutions, independently from the standard curves, at 5, 20, and 160  $\mu$ g/mL in serum, and stored at  $-80^{\circ}C$ . On the day of analysis, patient serum and QCs were diluted 10-fold with PBSTF, and CSF was diluted 2-fold with 20% serum (v/v) in PBSTF, in order to have the same 10% serum (v/v) in PBSTF final matrix. If necessary, CSF and serum were additionally diluted 2- and 100-fold, respectively, with 10% (v/v) serum in PBSTF. The 10-fold diluted QCs were additionally diluted 100-fold to 5, 20, and 160 ng/mL with 10% (v/v) serum in PBSTF. Next, QC160 was further diluted 2-fold to 80 ng/mL with 10% serum (v/v) in PBSTF. Patient serum, CSF, and QCs were analyzed as 50  $\mu$ l duplicates per plate. Samples were added as 50  $\mu$ l triplicates per plate, which was subsequently sealed and incubated for 2 h at RT. Then, the plate was emptied and washed 4 times with 300  $\mu$ l of PBSTF. After addition of 50  $\mu$ l of 1  $\mu$ g/mL anti-human IgG4-HRP in PBSTF, plates were sealed and incubated for 1 h at RT. Next, plates were emptied and washed 4 times with 300  $\mu$ l of PBSTF. Subsequently, 100  $\mu$ l of Pierce standard ECL was added and

luminescence was measured within 15 min using a Tecan Infinite 200 Pro plate reader at 1 s per well of read time.

### **Optimization of anti-human IgG4-HRP concentration**

Nivolumab standard curves were prepared at concentrations of 100, 50, 20, 10, 5, 2, and 0 ng/mL in ice-cold 10% (v/v) serum in PBSTF. In triplicate 50 µl of each standard was incubated for 2 h at RT on plate. After 3 washes with 300 µl of PBSTF, 50 µl of 1:500, 1:1000, and 1:2000 in PBSTF diluted anti-human IgG4-HRP was added and incubated for 1 h at RT. Subsequently, the plate was washed and luminescence was measured after addition of ECL, as described in the ELISA section.

### **Serum matrix effect**

The effect of different concentrations of serum on the quantification of nivolumab was determined in triplicate in standard curves prepared in 2 mL Eppendorf® LoBind vials on the day of analysis by serial dilution of 11.0 mg/mL nivolumab clinical stock solution to 100, 50, 20, 10, 5, and 2 ng/mL in ice-cold PBSTF containing 0, 10%, and 20% (v/v) serum. To assess the dilution integrity, nivolumab was spiked in triplicate at 1000 µg/mL in serum and 2 µg/mL in CSF. Next, serum and CSF were diluted 1000 and 2-fold to 1 µg/mL, respectively, as described in ELISA. Further 2-fold serial dilutions with 10% serum (v/v) in PBSTF were then applied to serum and CSF to a final nominal nivolumab concentration of 62.5 ng/mL. The accuracies of the back-calculated nivolumab concentrations relative to the nominal spike concentrations at each serial dilution level were determined.

### **Specificity and limit of detection**

Wells coated with and without PD-1 were incubated in triplicate with 100 µl of 0 and 100 ng/mL nivolumab in PBSTF. Next, plates were washed and incubated with secondary antibody as described under ELISA. After 4 washes, 100 µl of Pierce standard, Biorad Clarity, and Trevigen Peroxyglow™ ECL were added and luminescence was measured. The effect of three of the most commonly used blocking agents was tested. Wells coated with PD-1 were incubated for 3 h at RT with 300 µl of 2% and 5% (w/v) BSA in PBS, 2% and 5% (w/v) ELK in PBS, 40% and 100% (v/v) FCS in PBS, and PBS as negative control. Next, wells were emptied and incubated for 2 h with 50 µl of 10% (v/v) serum in PBSTF. Treatment of nivolumab is sometimes combined with ipilimumab, which is a fully human monoclonal antibody against cytotoxic T-lymphocyte-associated antigen-4 (CTLA-4). Although its target is different, a possible analytical interference cannot be ruled out. Therefore, we spiked 0, 20, and 80 ng/mL of nivolumab in 10% (v/v) serum in PBSTF and 50% (v/v) CSF containing 10% (v/v) serum in PBSTF. After addition of 0, 100, 200, and 500 ng/mL of ipilimumab, these samples were analyzed by ELISA, as

described. The limit of detection (LOD) was defined as the average background level plus 5 times the standard deviation and was determined in serum from 10 healthy volunteers and in CSF from 10 immunotherapy naïve cancer patients.

### Standard curve fitting

Calibration curves are commonly fit using polynomial or logistic models.<sup>12</sup> We compared the goodness of fit of a quadratic and 4-parameter logistic model on 21 standard curves using Graphpad Prism 6. Net luminescence was calculated as the luminescence of samples minus the average luminescence of the duplicate blank samples. Net luminescence of standards 2-100 ng/mL was plotted against the nominal nivolumab concentration. Curve fits were not forced through 0, and back-calculated concentrations had to be within 15% of the nominal concentrations for all 7 calibration standards.

### Lower limit of quantification

The lower limit of quantification (LLQ) was determined in triplicate in ice-cold PBSTF, containing 10% (v/v) serum from 7 different volunteers, spiked with 1, 2, 3, 4, 5 ng/mL of nivolumab or pembrolizumab. CSF from 6 immunotherapy naïve patients was diluted 2-fold with ice-cold PBSTF containing 20% (v/v) serum, which was spiked with 1, 2, 3, 4, and 5 ng/mL of nivolumab or pembrolizumab. The LLQ was defined as the nominal input level at which the nivolumab and pembrolizumab concentrations could be determined with a precision  $\leq 20\%$  and an accuracy of 80-120%. Furthermore, the analyte response at the LLQ should be at least five times the response compared to the blank response.

### Between- and within-day precision and accuracy

Samples containing 5, 20 or 80 ng/mL nivolumab in 10% (v/v) serum in PBSTF were measured in triplicate on six consecutive days. The between-day (BDP) and within-day precision (WDP) were calculated by one-way analysis of variance (ANOVA) for each spike level using the run day as classification variable using the software package SPSS v15.0 for windows (SPSS, Chicago, USA). The day mean square (DayMS), error mean square (ErrMS) and the grand mean (GM) of the observed concentrations across run days were used.

The WDP% and BDP% for each spike level were calculated using the formulas:

$$\text{WDP}\% = (\text{ErrMS})^{0.5} / \text{GM} \times 100\%$$

$$\text{BDP}\% = [(\text{DayMS} - \text{ErrMS}) / n]^{0.5} / \text{GM} \times 100\%$$

With  $n$  being the number of replicates within each run.

Accuracy was determined as the relative difference between the nominal input concentration and measured concentration. Imprecisions  $\leq 15\%$  and accuracy between 85-115% were considered acceptable.

### **Pembrolizumab quantification**

Standard curves were prepared in 2 mL Eppendorf® LoBind vials on the day of analysis by serial dilution of 11.0 mg/mL nivolumab and 27.8 mg/mL pembrolizumab clinical stock solutions to 100, 50, 20, 10, 5, and 2 ng/mL in ice-cold 10% (v/v) serum in PBSTF. These standards were analyzed in triplicate on three consecutive days. The concentrations of the pembrolizumab standards ( $M_w = 146,286$  Da) were back-calculated from the nivolumab ( $M_w = 143,597$  Da) standard curves. After correction for the 1.87% difference in molecular weight, the back-calculated pembrolizumab concentrations had to be within 15% of the nominal pembrolizumab concentrations.

### **Stability**

To assess the long-term storage stability, nivolumab and pembrolizumab were spiked at 0.1, 1, 10, and 100  $\mu\text{g/mL}$  in serum. This largely covers the whole range of concentrations found in patient serum along the PK curve. Aliquots of 50  $\mu\text{L}$  of spiked serum were snap-frozen in liquid nitrogen and stored for 0, 7, 120, 360, and 480 days at  $-80^\circ\text{C}$ . At these time points nivolumab and pembrolizumab concentrations were determined in triplicate, after dilution to 50 ng/mL in ice-cold 10% (v/v) serum in PBSTF. Stability of nivolumab and pembrolizumab at 10 and 50 ng/mL, diluted in ice-cold 10% (v/v) serum in PBSTF, was tested after 0, 6, and 24 h on ice, using freshly prepared nivolumab standard curves.

Freeze-thaw stability was tested for nivolumab and pembrolizumab spiked at 10 and 100  $\mu\text{g/mL}$  in serum. Nivolumab and pembrolizumab concentrations were determined after 0, 1, 2, and 3 snap-freeze/thaw cycles, after dilution to 100 ng/mL with 10% (v/v) serum in PBSTF. Nivolumab and pembrolizumab concentrations were considered stable if the determined concentrations were within 15% of the nominal concentrations.

### **Clinical applicability**

The clinical application of the ELISA method was demonstrated in serum from seven patients treated once every 2 weeks with nivolumab ( $n=4$ ) or once every 3 weeks with pembrolizumab ( $n=3$ ). Patient 1 received concomitantly ipilimumab at 3.3 mg/kg (Table 3). Blood was drawn from these patients at day 0 (predose+end of infusion), and predose at cycle 2. To demonstrate clinical applicability of the ELISA

for determination of nivolumab in CSF, CSF was collected from 15 patients with a solid tumor and a clinical suspicion of leptomeningeal metastases but a normal or equivocal MRI who underwent a diagnostic lumbar puncture (LP). All patients have been included in a diagnostic CSF study at the NKI comparing the sensitivity and specificity of immunoflowcytometry assays for circulating tumor cells (CTC) detection with CSF cytology. Five patients were treated with nivolumab. Three out of these five patients had melanoma and concomitantly received ipilimumab at 3 mg/kg (Table 4). The other 10 patients had not received any immunotherapy prior to sampling and served as a negative control group. An aliquot of 1-2 mL of CSF was collected in 2.0 mL vials and stored at  $-80^{\circ}\text{C}$ . Both clinical studies have been approved by the Ethics Committee of the Netherlands Cancer Institute and subjects provided whole blood and CSF samples after written informed consent.

### Statistical analysis

Statistical evaluation was performed using the unpaired two-tailed student *t*-test in Excel, unless indicated otherwise. Matrix effects were analyzed using the paired two-tailed *t*-test in Excel. The slopes and intercept of nivolumab and pembrolizumab standard curves were compared using linear regression analysis in Graphpad Prism 6. *P*-values of  $\leq 0.05$  were considered to be significant.

### Method validation

Validation of the ELISA method was performed based on the guidelines for bioanalytical assays provided by the FDA.<sup>13</sup>

## Results

### Optimization of anti-human IgG4-HRP concentration

We tested anti-human IgG4-HRP at dilutions of 1:500, 1:1000, and 1:2000 in PBSTF. The 1:1000 dilution resulted in a significantly higher ( $P < 0.001$ ) signal to noise ratio, as compared to the other dilutions, over the whole range of spiked nivolumab concentrations from 2 to 100 ng/ml (Supplementary Table 1).

### Serum matrix effect

We found that addition of 10% and 20% (v/v) serum to PBSTF had a significant effect on the accuracy of nivolumab quantification over the whole standard curve concentration range with an average of decrease in nivolumab concentration of 14.1% at 10% (v/v) serum to PBSTF ( $P < 0.001$ ) and 21.4% at 20% serum to PBSTF ( $P < 0.001$ ) (Supplementary Table 2). Therefore, we used 10% (v/v) serum in PBSTF, for both

serum and CSF samples, as well as for the standard curves and quality controls (QCs), to assure accurate quantification of nivolumab. Next, dilution integrity was assessed in triplicate in quality controls, spiked with nivolumab at 160 µg/mL, after a standard 1000-fold dilution followed by an additional 2-fold dilution. The back-calculated nivolumab concentration did not deviate more than 15% from the nominal spike concentration, which indicates good dilution integrity. Furthermore, samples spiked with nivolumab at 1000 and 2 µg/mL in serum and CSF, respectively, which required an additional 16-fold dilution after the standard 1000-fold dilution, also showed adequate dilution integrity (Table 1).

**Table 1.**

Dilution integrity was assessed, after indicated number of serial 2-fold dilutions with 10% (v/v) serum in PBSTF, for serum spiked at 160 (Quality Control) and 1000 µg/mL, and CSF spiked at 2 µg/mL nivolumab. Results are the average of three replicate measurements. PBSTF=phosphate buffered saline supplemented with 0.1% Tween-20 and 1% Ficoll.

Nivolumab spiked	Total dilution factor	Number of 2-fold serial dilutions	Nominal conc. ng/mL	Determined conc. ±SD µg/mL	Accuracy ±SD (%)
QC at 160 µg/mL	2000	1	80	153 ± 9.6	95.6 ± 6.0
Serum at 1000 µg/mL	1000	1	1000	129 ± 5.7	13.4 ± 1.7
	2000	2	500	251 ± 14.9	25.5 ± 5.3
	4000	4	250	483 ± 21.7	48.2 ± 3.2
	8000	8	125	880 ± 21.4	87.9 ± 3.4
	16000	16	62.5	921 ± 44.4	94.9 ± 9.0
CSF at 2 µg/mL	2	1	1000	0.26 ± 0.011	12.9 ± 4.4
	4	2	500	0.50 ± 0.030	25.1 ± 5.9
	8	4	250	0.97 ± 0.043	48.3 ± 4.5
	16	8	125	1.75 ± 0.085	87.2 ± 4.9
	32	16	62.5	1.84 ± 0.089	96.3 ± 3.2

### Specificity

The signal to noise ratios of nivolumab using Pierce standard ECL, Biorad Clarity, and Trevigen Peroxyglow were 363, 100, and 2000, respectively. Although, Peroxyglow showed superior signal to noise ratio, we chose to develop the ELISA with about 10-fold less expensive Pierce standard ECL.

The detection of nivolumab was very specific: wells coated with PD-1 showed luminescence of 5762 ± 182, which was not significantly higher than the luminescence of 5439 ± 454 for wells not coated with PD-1. This ensures the absence of any meaningful interaction between the secondary antibody and PD-1, and indicates that

net luminescence, defined as measured luminescence minus background signal from ECL, originates only from the reaction of the secondary antibody with nivolumab. There was a large difference in background signal after blocking with different agents (PBS only, BSA, FCS, ELK). The lowest background of  $10.2 \times 10^3 \pm 552$  arbitrary luminescent units (ALU) was obtained without blocking, which are the wells incubated with PBS only. In sequence of increasing background signal, 2% BSA, 40 and 100% FCS, 5% BSA, and 2 and 5% ELK, resulted in significant ( $P < 0.001$ ) higher backgrounds of  $270 \times 10^3$ ,  $338 \times 10^3$ ,  $363 \times 10^3$ ,  $423 \times 10^3$ ,  $823 \times 10^4$ , and  $842 \times 10^4$  ALU, respectively (Figure 1). To put this in perspective, 100 ng/mL nivolumab resulted on average in net luminescence of  $240 \times 10^4$  ALU. Based on these results, we concluded, that blocking should be omitted in this ELISA.

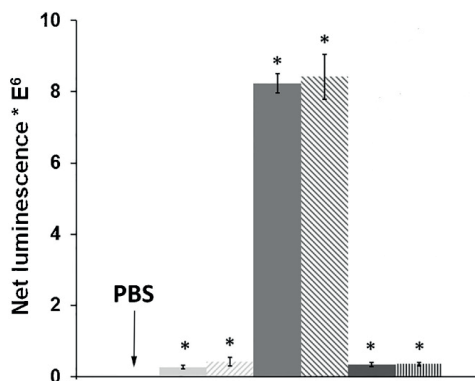


**Figure 1.**

Background signal after 3 h of incubation with 300  $\mu$ l of the following blocking solutions in phosphate buffered saline (PBS): PBS as control  $\blacksquare$ ; 2%  $\square$  and 5%  $\text{▨}$  bovine serum albumin (BSA); 2%  $\blacksquare$  and 5%  $\text{▨}$  low fat milk powder; 40%  $\blacksquare$  and 100%  $\text{▨}$  fetal calf serum (FCS). Results  $\pm$  SD of 3 different samples are shown. \*Indicates significant  $P < 0.05$  higher background relative to PBS.

Addition of ipilimumab had no significant effect on the quantification of nivolumab in both serum and CSF (Supplementary Table 3). Furthermore, the background level was not significantly increased by 500 ng/mL of ipilimumab (data not shown). The mean background level of 10% (v/v) serum from 10 different volunteers in PBSTF was  $0.22 \pm 0.039$  (range 0.089-0.37) ng/mL. The mean background of 50% (v/v) CSF in PBSTF containing 10% (v/v) serum from 10 patients was  $0.31 \pm 0.011$  (range 0.21-0.45) ng/mL. From these backgrounds, limits of detection (LOD) for nivolumab in serum and CSF of 0.65 ng/mL, and 0.75 ng/mL, respectively, were calculated.

### Lower limit of quantification (LLQ)

The LLQ of nivolumab and pembrolizumab in serum and CSF was 2 ng/mL. In serum, nivolumab was determined at the LLQ with a mean accuracy of 101% (range

97.4%-110%, n=7), and mean precision of 3% (range 0%-9.5%). Pembrolizumab was determined at LLQ with a mean accuracy of 100% (range 91.4%-105%, n=7), and mean precision of 3.9% (range 1.6%-5.8%). In CSF, nivolumab was determined at LLQ with a mean accuracy of 103% (range 101%-106%, n=6) and mean precision of 2.2% (range 0.4%-4.2%). Pembrolizumab was determined at LLQ with mean accuracy of 102% (range 98.9%-105%, n=6), and mean precision of 3.4% (range 0.4%-4.2%).

### Between- and within-day precision

Nivolumab was measured at 6 consecutive days in triplicate at 5, 20, 80 ng/mL spiked in 10% (v/v) serum in PBSTF. The mean within- and between day imprecisions, and the nivolumab quantification accuracy at these nominal input levels were within 15%, and 85-115%, respectively (Table 2).

**Table 2.**

Imprecisions and accuracy at indicated nivolumab and pembrolizumab nominal input levels after dilution of quality control samples prepared in 100% serum to a final matrix composition of 10% (v/v) serum in PBSTF. Imprecisions were calculated from triplicate measurements on three consecutive days by one-way analysis of variance (ANOVA) for each spike level using the run day as classification variable. Accuracy is determined as the ratio between the measured and nominal concentration. WDP = within-day precision, BDP = between-day precision.

Nominal input ng/mL	Nivolumab			Pembrolizumab		
	WDP %	BDP %	accuracy %	WDP %	BDP %	accuracy %
5	3.3	4.1	102.5	6.1	5.3	98.1
20	3.4	4.1	99.5	6.5	6.6	101.9
80	4.2	4.6	100.8	5.1	0.6	105.7

**Table 3.**

Patients and treatment characteristics used to demonstrate applicability of the ELISA in serum. Patients received indicated dose of nivolumab at day 1 of every course. In addition, melanoma patients received 3 mg/kg ipilimumab, NSCLC=non-small cell lung cancer, q2w and q3w=administration every 2 and 3 weeks, respectively.

Patient #	Tumor type	Therapeutic antibody	Dosing regime	Dose mg/kg	Dose mg
1	Melanoma	Nivolumab	q2w	1.3	100
2	Melanoma	Pembrolizumab	q3w	2.1	200
3	NSCLC	Nivolumab	q2w	2.8	140
4	NSCLC	Nivolumab	q2w	5.7	240
5	NSCLC	Pembrolizumab	q3w	3.0	200
6	Melanoma	Pembrolizumab	q3w	2.5	150
7	NSCLC	Nivolumab	q2w	2.6	240



**Table 4.**

Measured nivolumab concentrations in serum and CSF from 5 patients receiving the indicated dose of nivolumab at day 1 of every course. In addition, melanoma patients received 3 mg/kg ipilimumab. Results are the average of three replicate measurements  $\pm$  SD. CSF=cerebrospinal fluid, NSCLC=non-small cell lung cancer, PK=pharmacokinetics, C=course, D=day, q2w and q3w=administration of nivolumab every 2 and 3 weeks, respectively.

Patient #	Tumor type	Nivolumab dosing regime	PK sample	Dose mg/kg	Dose mg	Measured nivolumab concentration $\pm$ SD in		Ratio serum/CSF
						serum	CSF	
137	Breast cancer	q3w	C1D16	1	61	4481 $\pm$ 287	15 $\pm$ 0.9	299
123	Melanoma	q3w	C1D21	1	80	1831 $\pm$ 138	35 $\pm$ 0.9	52
113	Melanoma	q3w	C1D21	1	77	4410 $\pm$ 324	39 $\pm$ 1.9	113
135	Melanoma	q2w	C1D12	3	245	13,759 $\pm$ 311	150 $\pm$ 2.5	92
114	NSCLC	q3w	C3D14	3	240	33,454 $\pm$ 705	304 $\pm$ 11	110

### Pembrolizumab quantification

Concentrations of nivolumab and pembrolizumab, back-calculated from nivolumab standard curves, were compared by linear regression analysis. No significant differences in slope and intercept were found, which indicates that assay response over the investigated standard curve concentration range is the same for both antibodies (Supplementary Table 4). In addition, the Pearson correlation coefficient (*r*) of 1.00 indicates good correlation between the quantification of both antibodies. Therefore, we conclude that pembrolizumab can be accurately quantified against standard curves prepared from nivolumab if the 1.87% molecular weight difference is taken into account.

### Stability

Nivolumab and pembrolizumab were stable at 0.1, 1, 10, and 100  $\mu$ g/mL spiked in PBSTF containing serum, in storage at  $-80^{\circ}$ C for at least 480 days. Furthermore, samples containing nivolumab and pembrolizumab, at 10 and 50 ng/mL in 10% (v/v) serum in PBSTF, could be stored on ice for 6 h without significant decrease in concentration of both antibodies. However, after 24 h of storage on ice nivolumab and pembrolizumab concentrations decreased significantly by 13% ( $P=0.026$ ) and 19% ( $P=0.005$ ), respectively. Samples containing 10 and 100  $\mu$ g/mL of nivolumab and pembrolizumab spiked in 10% (v/v) serum in PBSTF were subjected to 3 freeze-thaw cycles. The measured drug concentrations, after 1000-fold dilution of samples in 10% (v/v) serum in PBSTF, did not differ significantly from the spiked concentrations (Supplementary Table 5).

### Clinical applicability

Nivolumab (n=4 patients) and pembrolizumab (n=3 patients) serum concentrations were determined in seven patients treated with different doses of nivolumab and pembrolizumab (Figure 2). Predose nivolumab and pembrolizumab serum concentrations for all seven patients were below the limit of detection. At end of infusion, we found nivolumab C<sub>max</sub> concentrations of 43.9-65.1 µg/mL for two patients treated with nivolumab at 2.6 and 2.8 mg/kg, which is within the concentration range reported by EMA of 61.3±26.4 µg/mL for patients treated with nivolumab at 3 mg/kg (n=13 patients).<sup>14</sup> Patients 1 and 4 were treated with nivolumab doses that were about a factor 2 below and above this 3 mg/kg level, which resulted in nivolumab serum concentrations of 19.6 and 107 µg/mL, respectively. Trough nivolumab serum concentrations ranged from 3.1 for patient 1 (1.3 mg/kg) to 56.2 µg/mL for patient 4 (5.7 mg/kg). Pembrolizumab serum concentrations at end of infusion were 43.9, 46.5, and 65.1 µg/mL for the three patients treated with a 200 mg dose of pembrolizumab, which is within the range reported by EMA of 67.5±23 µg/mL (n=150) for patients treated at this dose.<sup>15</sup> Trough pembrolizumab concentrations ranged from 8.01 to 22.8 µg/mL.

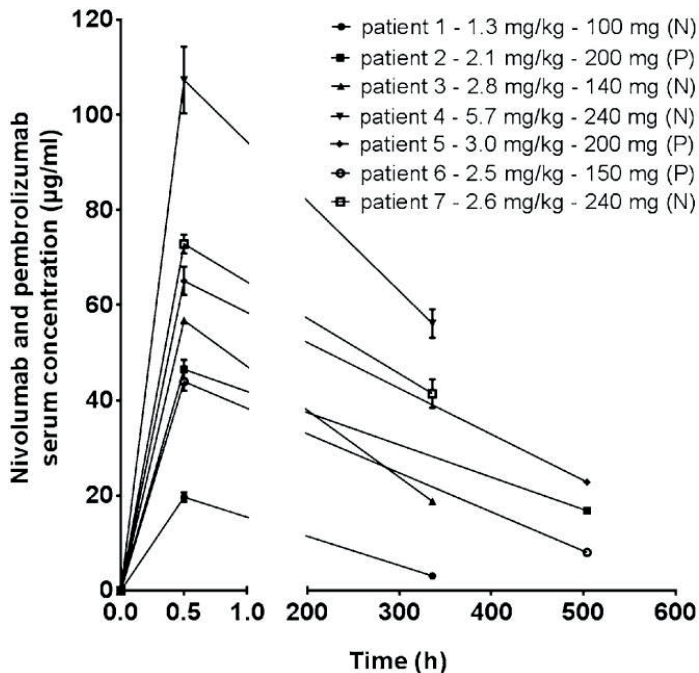


**Figure 2.**

Pharmacokinetics of nivolumab (N; n=4) and pembrolizumab (P; n=3) in serum from 7 patients treated with indicated doses (mg/kg). Blood was drawn at baseline (0min), end of infusion (30min), and predose course 2 (336 and 504h). Results are expressed as the means±SD of 3 different samples.

The concentrations of nivolumab in CSF of five patients treated with 1 or 3 mg/kg nivolumab ranged from 14.5 to 304 ng/mL and levels of nivolumab in concomitantly drawn serum ranged from 1.8 to 33.5 µg/mL (Table 4). The serum/CSF ratios of nivolumab ranged from 52-299. Although, the sample size is small and inter-patient variability in nivolumab levels in CSF is substantial, these data indicate that there is a low penetration of nivolumab in the brain.

## Discussion

Pembrolizumab and nivolumab are both anti-PD-1 monoclonal IgG4 antibodies, which have been approved for various advanced cancers, showing improved overall and progression free survival compared to standard-of-care in phase III trials.<sup>16-20</sup> Intracranial activity of these agents has been observed in progressing brain metastases in patients with melanoma and NSCLC.<sup>21,22</sup> Studies show a rapid and durable brain metastasis response rate of 22% in 18 melanoma patients and 33% in 18 NSCLC patients. Despite these encouraging data, many patients fail to respond to anti-PD-1 treatment in the brain or on extra-cerebral sites. Additional combination therapies and biomarker development will be important, particularly in patients with brain metastases who may have a different disease biology than patients with extra-cerebral disease. It is unclear whether the effect of anti-PD-1 agents in brain metastases is due to systematically activated T-cells that cross the blood-brain barrier or whether the anti-PD-1 agent actually has its action mechanism in the brain itself and therefore has to cross the BBB.<sup>21</sup> Our data now show that only minimal nivolumab concentrations reach the brain/CSF with serum to CSF ratios of 52-299. Recently, Puszkiel et al. reported the first ELISA for the determination of nivolumab in plasma.<sup>8</sup> Puszkiel et al. have demonstrated that their ELISA is sensitive enough to measure trough nivolumab levels in patients receiving nivolumab at 3 mg/kg. However, our results indicate that treatment of patients with nivolumab at 1-1.3 mg/kg can result in trough levels below the 5000 ng/mL lower quantification limit of their ELISA (Figure 2 and Table 4).

Here, we report the development and validation of a sensitive, quick and inexpensive ELISA which can be used to measure both nivolumab and pembrolizumab concentrations in biological fluids. Most ELISAs describe the use of time consuming blocking steps with BSA, FCS, and ELK-based protein solutions to prevent nonspecific binding of antibodies.<sup>8</sup> These blocking agents, however, prevented the sensitive detection of nivolumab in our ELISA due to an increase of background signal that originates from nonspecific binding of the secondary anti-IgG4-HRP antibody. Therefore, we tried the highly branched hydrophilic polysaccharide Ficoll as an alternative blocking agent,

as suggested by Huber et al.<sup>23</sup> Furthermore, the original developers of the ELISA described that addition of Tween-20 in the antibody and washing solutions is sufficient to reduce nonspecific binding.<sup>24</sup> Based on these findings, we omitted a separate blocking step and combined both the Ficoll and Tween-20 in the antibody and washing solutions. Further enhancement in sensitivity was obtained through chemiluminescent detection of the anti-IgG4-HRP. An advantage of this assay is a 100-fold reduction in the amount of recombinant PD-1 used for coating the ELISA plates, which significantly reduces the cost of the assay. The method has a LLQ of 2 ng/mL for both nivolumab and pembrolizumab, which will most likely be sensitive enough to allow quantification of both peak and trough levels of nivolumab and pembrolizumab in serum and CSF from most patients.

Clinical trials are showing promising results from the combination of nivolumab and pembrolizumab with ipilimumab.<sup>25,26</sup> We showed that quantification of nivolumab with our ELISA was not affected by analytical interference from an 25-fold excess of ipilimumab. Moreover, the background of the assay was not significantly increased by 500 ng/mL of ipilimumab. Therefore, our ELISA can be used to accurately quantify nivolumab and pembrolizumab in plasma and CSF from patients receiving combination therapy.

## Conclusions

We developed and validated a sensitive ELISA for the quantitative determination of nivolumab and pembrolizumab in serum and CSF. The ELISA has a LLQ of 2 ng/mL, which enables accurate quantification of the low levels of these anti-PD-1 antibodies found in CSF. To our knowledge, this is the first evaluation of nivolumab concentration levels in CSF. The concentrations of nivolumab in CSF ranged from 14.5 to 304 ng/mL, at trough nivolumab serum levels in 5 patients receiving nivolumab at 1 and 3 mg/kg, respectively. The method is accurate, precise, and shows good long-term sample storage stability using standard laboratory equipment and techniques. This quantitative ELISA for nivolumab and pembrolizumab can be used in future clinical trials.

## Conflict of interest

The authors declare no conflict of interest.

## References

1. Larkin J, Minor D, D'Angelo S, et al. Overall Survival in Patients With Advanced Melanoma Who Received Nivolumab Versus Investigator's Choice Chemotherapy in CheckMate 037: A Randomized, Controlled, Open-Label Phase III Trial. *J Clin Oncol*. July 2017;JCO.2016.71.802.
2. Sul J, Blumenthal GM, Jiang X, He K, Keegan P, Pazdur R. FDA Approval Summary: Pembrolizumab for the Treatment of Patients With Metastatic Non-Small Cell Lung Cancer Whose Tumors Express Programmed Death-Ligand 1. *Oncologist*. 2016;21(5):643-650.
3. Shu CA, Rizvi NA. Into the Clinic With Nivolumab and Pembrolizumab. *Oncologist*. 2016;21(5):527-528.
4. Yushak ML, Chiang VL, Kluger HM. Clinical trials in melanoma patients with brain metastases. *Pigment Cell Melanoma Res*. 2015;28(6):741-743.
5. Stemmler H-J, Schmitt M, Willems A, Bernhard H, Harbeck N, Heinemann V. Ratio of trastuzumab levels in serum and cerebrospinal fluid is altered in HER2-positive breast cancer patients with brain metastases and impairment of blood-brain barrier. *Anticancer Drugs*. 2007;18(1):23-28.
6. Pestalozzi BC, Brignoli S. Trastuzumab in CSF. *J Clin Oncol*. 2000;18(11):2349-2351.
7. Lin J. CSF as a Surrogate for Assessing CNS Exposure: An Industrial Perspective. *Curr Drug Metab*. 2008;9(1):46-59.
8. Puszkiel A, Noé G, Boudou-Rouquette P, et al. Development and validation of an ELISA method for the quantification of nivolumab in plasma from non-small-cell lung cancer patients. *J Pharm Biomed Anal*. 2017;139:30-36.
9. Iwamoto N, Shimada T, Terakado H, Hamada A. Validated LC-MS/MS analysis of immune checkpoint inhibitor Nivolumab in human plasma using a Fab peptide-selective quantitation method: nano-surface and molecular-orientation limited (nSMOL) proteolysis. *J Chromatogr B*. 2016;1023-1024:9-16.
10. Zhang S, Garcia-D'Angeli A, Brennan JP, Huo Q. Predicting detection limits of enzyme-linked immunosorbent assay (ELISA) and bioanalytical techniques in general. *Analyst*. 2014;139(2):439-445.
11. Nikolayenko I V, Galkin OY, Grabchenko NI, Spivak MY. Preparation of highly purified human IgG , IgM , and IgA for immunization and immunoanalysis. *Ukr Bioorganica Acta*. 2005;2:3-11.
12. Herman RA, Scherer PN, Shan G. Evaluation of logistic and polynomial models for fitting sandwich-ELISA calibration curves. *J Immunol Methods*. 2008;339(2):245-258.
13. FDA, Food and Drug Administration, Guidance for Industry: Bioanalytical method validation. 2001.
14. Sancho-Lopez A, de Graeff P, European Medicines Agency, Assessment report nivolumab EMA/CHMP/76688/2015.
15. Melchiorri D, Mueller-Berghaus J. European Medicines Agency. Assessment report pembrolizumab EMA/CHMP/16441/2017.
16. Robert C, Schachter J, Long G V, et al. Pembrolizumab versus Ipilimumab in Advanced Melanoma. *N Engl J Med*. 2015;372(26):2521-2532.
17. Robert C, Long G V, Brady B, et al. Nivolumab in previously untreated melanoma without BRAF mutation. *N Engl J Med*. 2015;372(4):320-330.

18. Brahmer J, Reckamp KL, Baas P, et al. Nivolumab versus Docetaxel in Advanced Squamous-Cell Non-Small-Cell Lung Cancer. *N Engl J Med.* 2015;373(2):123-135.
19. Borghaei H, Paz-Ares L, Horn L, et al. Nivolumab versus Docetaxel in Advanced Nonsquamous Non-Small-Cell Lung Cancer. *N Engl J Med.* 2015;373(17):1627-1639.
20. Garon EB, Rizvi NA, Hui R, et al. Pembrolizumab for the Treatment of Non-Small-Cell Lung Cancer. *N Engl J Med.* 2015;372(21):2018-2028.
21. Dudnik E, Yust-Katz S, Nechushtan H, et al. Intracranial response to nivolumab in NSCLC patients with untreated or progressing CNS metastases. *Lung Cancer.* 2016;98:114-117.
22. Goldberg SB, Gettinger SN, Mahajan A, et al. Pembrolizumab for patients with melanoma or non-small-cell lung cancer and untreated brain metastases: early analysis of a non-randomised, open-label, phase 2 trial. *Lancet Oncol.* 2016;17(7):976-983.
23. Huber D, Rudolf J, Ansari P, et al. Effectiveness of natural and synthetic blocking reagents and their application for detecting food allergens in enzyme-linked immunosorbent assays. *Anal Bioanal Chem.* 2009;394(2):539-548.
24. Engvall E, Perlmann P. Enzyme-linked immunosorbent assay, Elisa. 3. Quantitation of specific antibodies by enzyme-labeled anti-immunoglobulin in antigen-coated tubes. *J Immunol.* 1972;109(1):129-135.
25. Kirchberger MC, Hauschild A, Schuler G, Heinzerling L. Combined low-dose ipilimumab and pembrolizumab after sequential ipilimumab and pembrolizumab failure in advanced melanoma. *Eur J Cancer.* 2016;65:182-184.
26. Hodi FS, Chesney J, Pavlick AC, et al. Combined nivolumab and ipilimumab versus ipilimumab alone in patients with advanced melanoma: 2-year overall survival outcomes in a multicentre, randomised, controlled, phase 2 trial. *Lancet Oncol.* 2016;17(11):1558-1568.

## Supplement to:

## Enzyme linked immunosorbent assay for the quantification of nivolumab and pembrolizumab in human serum and cerebrospinal fluid

Supplementary Table 1.

Effect of indicated secondary antibody dilutions on the signal to noise ratio of the mean luminescence at different spiked (nominal) nivolumab concentrations in 10% (v/v) serum in PBSTF. Results are the average of three replicate measurements  $\pm$  SD, \*indicates a significant difference. ALU=arbitrary luminescence unit, S/N=signal to noise ratio i.e. ALU of nivolumab standard : ALU of standard 0.

Nominal nivolumab conc. ng/mL	Secondary antibody dilutions					
	1:500		1:1000		1:2000	
	ALU	S/N	ALU	S/N	ALU	S/N
100	3026518	348 $\pm$ 5.05	2460188	452 $\pm$ 5.23*	1165947	202 $\pm$ 2.28
50	1382593	159 $\pm$ 6.46	1277491	235 $\pm$ 20.0*	609230	106 $\pm$ 0.58
20	496599	57.1 $\pm$ 0.96	429751	79.0 $\pm$ 0.93*	305220	53.0 $\pm$ 0.01
10	249029	28.6 $\pm$ 0.22	213621	39.3 $\pm$ 0.17*	153399	26.6 $\pm$ 0.26
5	128316	14.7 $\pm$ 0.09	106484	19.6 $\pm$ 0.08*	74215	12.9 $\pm$ 0.14
2	55591	6.4 $\pm$ 0.05	45401	8.3 $\pm$ 0.09*	35591	6.2 $\pm$ 0.05
0	8701		5442		5764	

Supplementary Table 2.

Effect of 0, 10, and 20% serum on the measured concentrations of nivolumab relative to the spiked (nominal) concentrations of nivolumab in PBSTF (\* indicates a significant difference). Results are the average of three replicate measurements  $\pm$  SD. PBSTF=phosphate buffered saline supplemented with 0.1% Tween-20 and 1% Ficoll.

Nominal	Measured nivolumab concentrations $\pm$ SD in ng/mL in PBSTF + serum		
	0% serum	10% serum	20% serum
100	98.8 $\pm$ 4.05	87.5 $\pm$ 1.89 *	78.8 $\pm$ 3.57 *
50	52.3 $\pm$ 0.59	46.6 $\pm$ 0.70 *	43.6 $\pm$ 0.68 *
20	18.8 $\pm$ 0.02	15.9 $\pm$ 0.45 *	14.6 $\pm$ 0.25 *
10	10.1 $\pm$ 0.46	8.6 $\pm$ 0.07 *	7.9 $\pm$ 0.08 *
5	5.1 $\pm$ 0.06	4.1 $\pm$ 0.03 *	3.8 $\pm$ 0.02 *
2	2.0 $\pm$ 0.03	1.8 $\pm$ 0.03 *	1.6 $\pm$ 0.01 *
1	1.0 $\pm$ 0.03	0.8 $\pm$ 0.03 *	0.7 $\pm$ 0.04 *

**Supplementary Table 3.**

Influence of indicated nominal concentrations of ipilimumab on the quantification of nivolumab spiked at 20 and 80 ng/mL in 10% (v/v) serum, and 50% (v/v) cerebrospinal fluid (CSF) in PBSTF containing 10% (v/v) serum. Results are the average of three replicate measurements  $\pm$  SD. PBSTF=phosphate buffered saline supplemented with 0.1% Tween-20 and 1% Ficoll.

Nominal ipilimumab conc. ng/mL	Measured nivolumab concentrations $\pm$ SD in ng/mL at 20 and 80 ng/ml nivolumab spike level			
	10% serum		50% CSF	
	20	80	20	80
0	18.5 $\pm$ 1.5	87.2 $\pm$ 2.5	20.4 $\pm$ 0.8	79.1 $\pm$ 2.5
100	18.5 $\pm$ 2.6	79.3 $\pm$ 4.1	20.6 $\pm$ 1.4	79.1 $\pm$ 3.9
200	19.4 $\pm$ 1.3	82.8 $\pm$ 3.9	20.2 $\pm$ 1.6	76.5 $\pm$ 5.5
500	18.9 $\pm$ 1.1	77.8 $\pm$ 3.3	20.9 $\pm$ 2.7	76.5 $\pm$ 2.6

**Supplementary Table 4.**

Comparison of assay response for nivolumab and pembrolizumab. Standard curves containing 2, 5, 10, 20, 50, and 100 ng/mL nivolumab and pembrolizumab were measured in triplicate on three consecutive days. Concentrations, expressed in pM  $\pm$  between day standard deviation, of both antibodies were back-calculated from the nivolumab standard curves. Subsequently, pembrolizumab concentrations were corrected by 1.87% to adjust for its higher molecular weight in comparison with nivolumab.

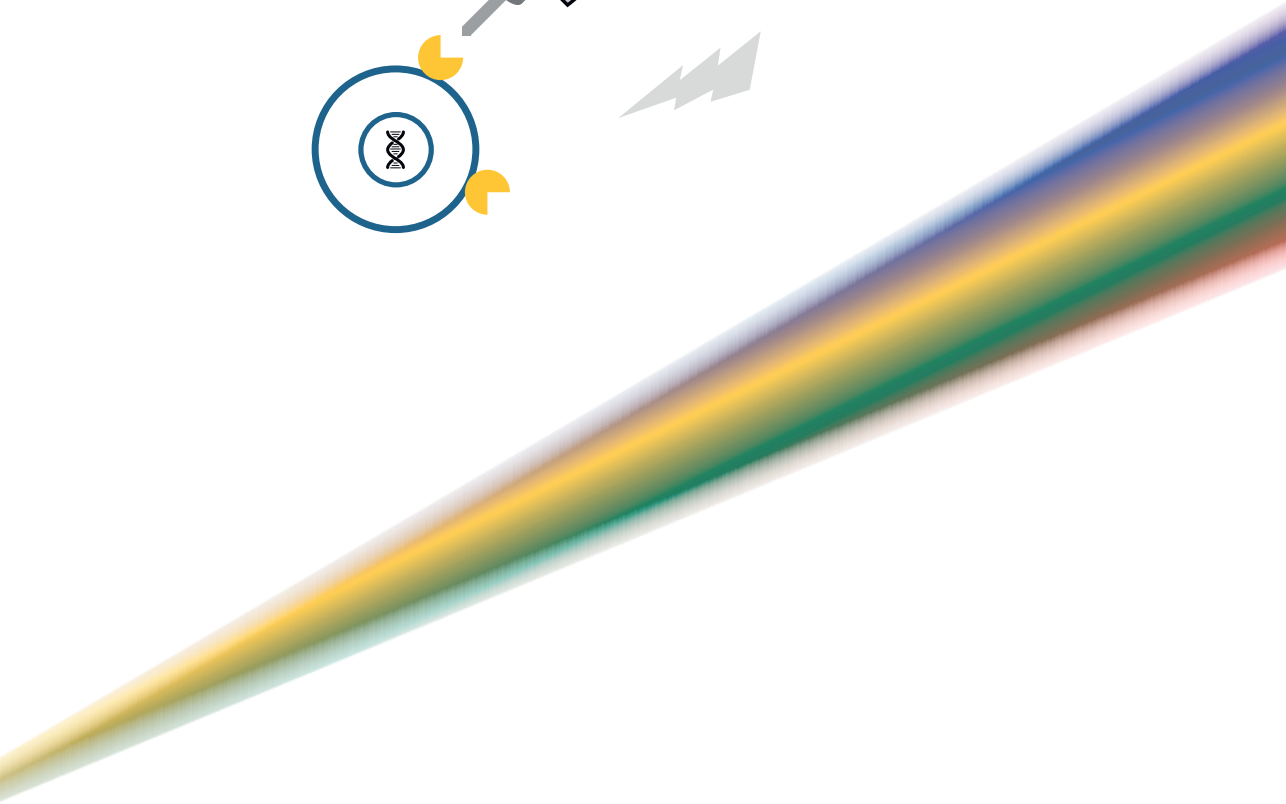
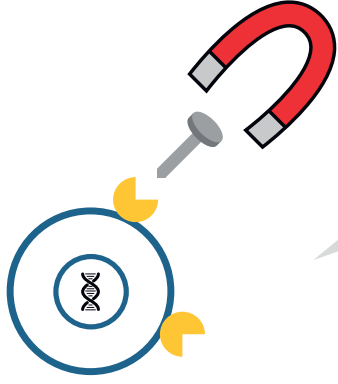
Nominal input concentration		Back-calculated concentrations (n = 3)			
Nivolumab pM	Pembrolizumab pM	Nivolumab		Pembrolizumab	
		pM $\pm$ SD	Accuracy %	pM $\pm$ SD	Accuracy %
696	684	675 $\pm$ 9.0	-3.1	672 $\pm$ 16.6	-1.7
348	342	361 $\pm$ 15	3.7	361 $\pm$ 20.7	5.7
139	137	143 $\pm$ 5.0	2.5	141 $\pm$ 8.7	3.3
69.6	68.4	68.5 $\pm$ 3.7	-1.7	68.4 $\pm$ 5.0	0.1
34.8	34.2	34.3 $\pm$ 1.8	-1.6	34.5 $\pm$ 2.2	0.9
13.9	13.7	14.1 $\pm$ 0.1	0.9	14.0 $\pm$ 0.3	2.6

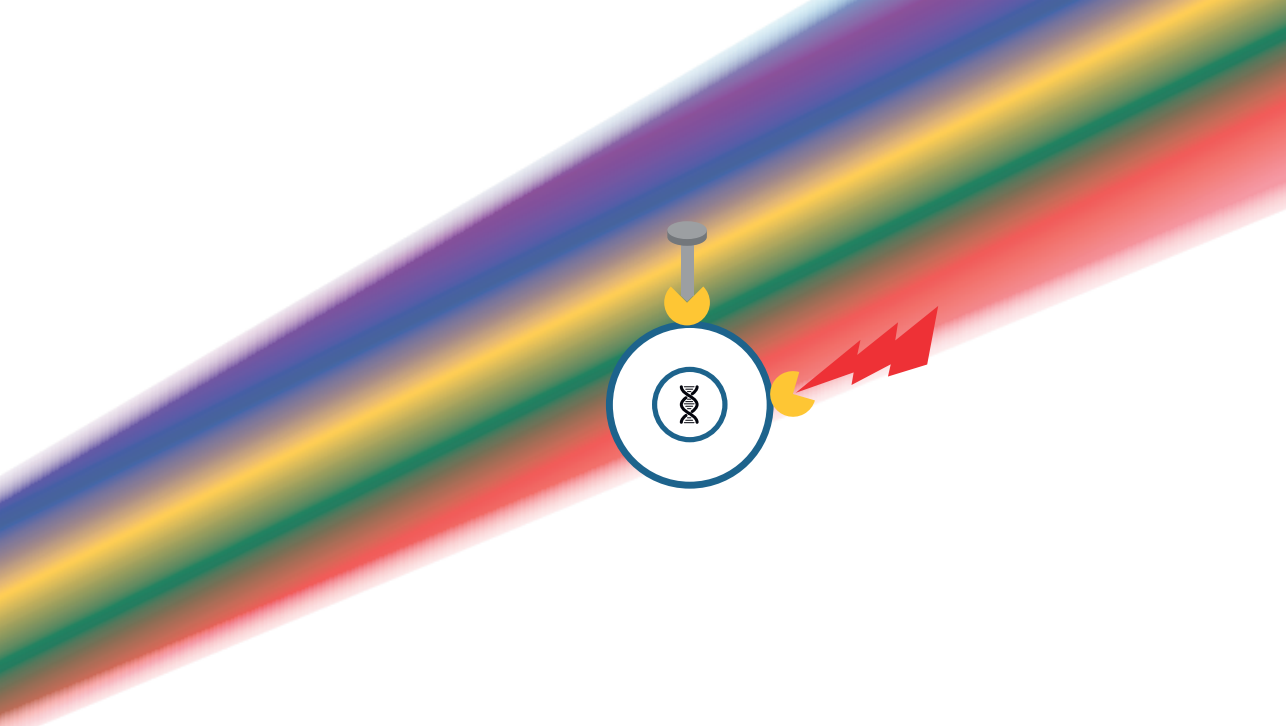


**Supplementary Table 5.**

Effect of indicated number of freeze-thaw cycles on the measured concentrations of nivolumab and pembrolizumab spiked at 10 and 100 µg/mL in 10% (v/v) serum in PBSTF. Samples were measured after 1000-fold dilution in 10% (v/v) serum in PBSTF. Results are the average of three replicate measurements ± SD.

Freeze-thaw cycle	Spike concentration in µg/mL of			
	Nivolumab		Pembrolizumab	
	10	100	10	100
	Measured concentrations ± SD in ng/mL			
0	9.57 ± 0.52	99.5 ± 5.6	9.64 ± 0.33	98.0 ± 2.4
1	10.3 ± 0.22	99.4 ± 2.4	9.68 ± 0.35	97.9 ± 5.5
2	9.64 ± 0.58	98.5 ± 7.8	9.39 ± 0.75	104 ± 4.1
3	9.87 ± 0.47	95.2 ± 7.7	9.51 ± 0.53	99.5 ± 3.2





# Chapter 6

## Liquid chromatography-tandem mass spectrometric assay for the T790M mutant EGFR inhibitor osimertinib (AZD9291) in human plasma

Johannes J.M. Rood  
Mark T.J. van Bussel  
Jan H. M. Schellens  
Jos H. Beijnen  
Rolf W. Sparidans

*Journal of Chromatography B.* 2016;1031:80-85.

## Summary

A method for the quantitative analysis by ultra-performance liquid chromatography-tandem mass spectrometry of the highly selective irreversible covalent inhibitor of EGFR-TK, osimertinib in human plasma was developed and validated, using pazopanib as an internal standard. The validation was performed in a range from 1 to 1000 ng/ml, with the lowest level corresponding to the lower limit of quantitation. Gradient elution was performed on a 1.8  $\mu\text{m}$  particle trifunctional bonded C18 column by 1% (v/v) formic acid in water, and acetonitrile as mobile phase. The analyte was detected in the selected reaction monitoring mode of a triple quadrupole mass spectrometer after positive ionization with the heated electrospray interface. Within-day precisions ranged from 3.4 to 10.3%, and between-day precisions from 3.8 to 10.4%, accuracies were 95.5 to 102.8%. Plasma (either lithium heparin or sodium EDTA) pretreatment was performed by salting-out assisted liquid-liquid extraction using acetonitrile and magnesium sulfate. This method was used to analyze the osimertinib blood plasma levels of five adult patients with metastatic T790M mutated non-small cellular lung carcinoma for therapeutic drug monitoring purposes.

## Introduction

With the first generation epidermal growth factor receptor-tyrosine kinase inhibitors (EGFR-TKI), advanced non-small cell lung carcinoma (NSCLC) patients harboring a sensitizing EGFR mutation (EGFRm(+)) were provided an initial significant improvement in terms of treatment.<sup>1</sup> Unfortunately, most of these patients ultimately develop disease progression due to the acquiring of a second mutation in the EGFR-TK gene. In approximately 60% of these patients a T790M mutation leads to decreased affinity of the current TKIs.<sup>2</sup> Osimertinib (AZD9291, Merelitinib, Tagrisso®; Figure 1) is a third generation, highly selective, irreversible covalent inhibitor of EGFR-TK, selective for both the EGFRm(+) sensitizing, as well as the T790M, L858R (IC<sub>50</sub>: 11.4 nM), and exon 19 deletion (IC<sub>50</sub>: 12.9 nM) EGFR-TKI resistance mutations, leaving the wild-type EGFR-TK (IC<sub>50</sub>: 493.8 nM) untouched.<sup>1,3-5</sup>

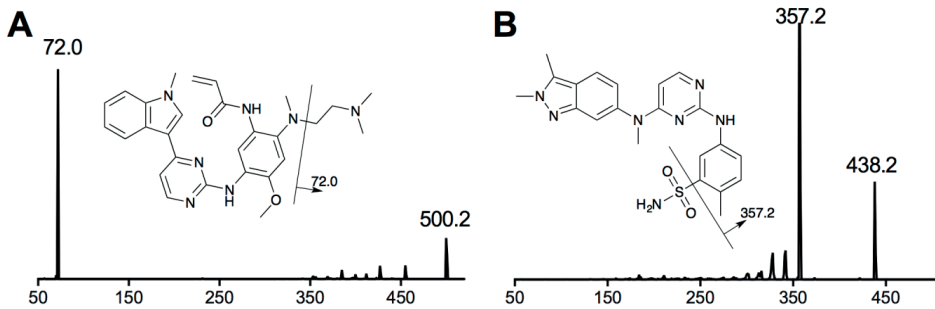


**Figure 1.**

**Product spectra, chemical structures and proposed fragmentation patterns**

A. Osimertinib (m/z 500.2) at -25V collision energy.

B. Internal standard pazopanib (m/z 438.2) at -30V.

Osimertinib was granted accelerated approval by the US-FDA for patients with advanced T790M mutated tumors, and developed disease progression after treatment with other EGFR-blocking therapy.<sup>6</sup> Osimertinib has a relatively long plasma half-life of 48 hours, with the main metabolites circulating at approximately 10% of the parent compounds geometric mean exposure. The main active metabolites are the desmethyl metabolites AZ7550 and AZ5104.<sup>3</sup> These metabolites could not be included in the assay due to the lack of analytical standards. To the best of our knowledge, one LC-MS/MS method for the determination of osimertinib and metabolite concentrations in biological samples has been published hitherto, giving very little detail about the materials, procedure, and validation.<sup>7</sup> This paper describes the development and validation of an ultra-performance liquid chromatographic tandem mass spectrometric method for the quantitative analysis of osimertinib in human plasma, using pazopanib as an internal standard. Samples were pretreated by an optimized salting-out assisted

liquid-liquid extraction (SALLE), using a system of plasma, acetonitrile and magnesium sulfate ( $\text{MgSO}_4$ ). This method provides a simple, fast and accurate method for the quantitative analysis of osimertinib. In this paper we describe the osimertinib blood plasma levels of five adult patients who have received 80 mg osimertinib once daily to support treatment with the drug.

## Materials and methods

### Chemicals and reagents

Osimertinib (>98% purity) and pazopanib (99.1% purity) were acquired from Sequoia Research Products (Pangbourne, UK). Water (LC-MS grade), and acetonitrile (HPLC-S grade) were purchased from Biosolve (Valkenswaard, The Netherlands). Anhydrous magnesium sulfate was supplied by Sigma Aldrich (St. Louis, MO). Formic acid was of analytical grade and originated from Merck (Darmstadt, Germany). Analytical grade dimethyl sulfoxide (DMSO) was supplied by Acros (Geel, Belgium). Pooled human lithium-heparinized plasma and EDTA plasma was obtained from Sera Laboratories (Haywards Heath, West Sussex, UK). For the evaluation of selectivity and matrix effect, lithium-heparinized plasma and EDTA plasma of six individual human donors was obtained from Innovative Research (Novi, MI, USA). Pure water used for other uses than mobile phase was prepared in house using a Synergy UV apparatus (Merck Millipore, Darmstadt, Germany).

### Chromatography and MS/MS method

The UHPLC-MS/MS equipment consisted of an Accela pump and auto-injector, coupled through a diverter valve to a TSQ Quantum Ultra triple quadrupole mass spectrometer with a heated electrospray ionization interface (HESI; all from Thermo Fisher Scientific, San Jose, CA, USA). Partial loop injections of 10  $\mu\text{l}$  were made onto a Waters® Acquity UPLC® BEH300 C18 column (50 mm  $\times$  2.1 mm, 1.7  $\mu\text{m}$ , Waters, Milford, USA). The components were eluted by a gradient of A) 1.0% formic acid in water and B) acetonitrile. The 2-minute gradient was running linearly from 10% B to 55% B in 1.2 min after injection, after which an 100% organic flush with acetonitrile of 0.3 min was performed. The flush-period was followed by a 0.5 min re-equilibration of the column. The whole eluate was introduced into the HESI source in positive ionization mode, starting at 0.6 min after injection by switching the diverter valve, up to 1.3 min. For initial tuning of the MS parameters, a 10  $\mu\text{g}/\text{ml}$  solution of osimertinib was infused at 5  $\mu\text{l}/\text{min}$ , while introducing a 600  $\mu\text{l}/\text{min}$  flow mixture of 0.1% (v/v) formic acid in water, and methanol (1:1; v:v). The highest response was obtained with a 5000 V spray voltage, 400 °C spray temperature, and a 329 °C capillary temperature.

The nitrogen sheath, ion sweep and auxiliary gasses were set at respectively 60, 0 and 5 arbitrary units; the skimmer voltage was set off (0 V). The SRM mode with 0.2 s dwell times was used with argon as the collision gas at 1.5 mTorr. The tube lens offset was 114 V for osimertinib and 130 V for pazopanib. Osimertinib was monitored at  $m/z$  500.2  $\rightarrow$  72.1 at -31 V collision energy, the internal standard pazopanib at  $m/z$  438.2  $\rightarrow$  377.15 at -28 V collision energy. The mass resolutions were set at  $m/z$  0.7 for both separating quadrupoles.

### Data processing

For acquiring chromatography-mass spectrometric data, Thermo Fisher Xcalibur software (version 2.0.7 SP1) was used. For further data processing Microsoft Excel (Office 2016, Version 15.11.2) was used. Averages ( $\pm$ SD), and outcomes of the validation were calculated using MS Excel.

### Standard solutions and quality controls

For osimertinib, a stock solution was made by weighing an amount of osimertinib, which was dissolved in an appropriate volume of DMSO, giving a final concentration of 500  $\mu$ g/ml. The same method was used to create a 500  $\mu$ g/ml stock solution of the internal standard pazopanib, which was then diluted to 25 ng/ml using acetonitrile. Serial dilution of the osimertinib stock standards using blank human plasma was performed to produce calibration standards at 1000, 500, 100, 50, 10, 5, and 1 ng/ml. From a separate stock solution, the QC samples of 800 (high), 200 (medium), 3 (low) and 1 ng/ml (LLOQ) were produced. Calibration and QC samples were aliquoted in 0.5 ml polypropylene reaction tubes, and stored at -30 °C until further use.

### Sample preparation

Samples were prepared by SALLE. For this method, 20  $\mu$ l of plasma was transferred to a 1.5 ml polypropylene reaction vial. Subsequently, 20  $\mu$ l of a 2M MgSO<sub>4</sub> solution and 100  $\mu$ l of 25 ng/ml pazopanib in acetonitrile were added. The tubes were closed and vortex mixed for approximately 10 s after which they were mixed further by inverting on a Rotamix RM1 mixer (ELMI, Riga, Latvia) at 45 RPM for 15 minutes. The reaction vials were then centrifuged for 5 min at 15,000  $\times$  g at 22 °C to aid phase separation. Of the upper organic liquid, 75  $\mu$ l was transferred to an injection vial with a 200  $\mu$ l insert. Before closing the vial, 75  $\mu$ l water was added to ensure compatibility with the chromatographic system.

### Analytical method validation

A laboratory scheme based on international guidelines, published by the EMA and FDA was used for the validation procedures.<sup>8,9</sup>

### **Calibration and carry-over**

The calibration samples were prepared and were processed for each daily calibration. Least squares linear regression ( $1/X^2$  weighted) was used to define the calibration curve, using the analyte/IS peak ratio. Auto injector carry-over was determined by injecting the highest calibration standard, followed by injection of three blank samples. The response of the blanks was then compared to the LLOQ.

### **Precision and accuracy**

Separate stock solutions of 500,000 ng/ml of osimertinib were used to obtain validation samples in human heparin plasma (800, 200, 3, and 1 ng/ml). Precisions and accuracies were determined by sextuple analysis of each QC sample in three analytical runs on three separate days for all QCs (total:  $n = 18$  per QC). Relative standard deviations and accuracies were calculated for both within- and between-day precisions. For EDTA samples precisions and accuracies were determined by sextuple analysis of each QC sample ( $n=6$  per QC).

### **Selectivity**

Selectivity of the method was determined by comparing the response of six individual human lithium heparin plasma samples and six individual human EDTA plasma samples. The relative and absolute effect was measured by processing samples spiked at LLoQ level (1 ng/ml), and blank samples with (blank) and without (double blank) internal standard.

### **Recovery and matrix effect**

To determine the recovery of osimertinib, processed QC samples (high, medium, and low,  $n=4$ ) were compared to blank plasma extracts spiked with reference solutions at the same levels, representing 100% extraction efficiency. For evaluation of the matrix effect, the responses of the spiked reference solutions were compared to matrix-free solutions, at QC levels high, medium, and low. Relative matrix effects for both lithium heparin and EDTA were determined at the high and low QC levels. Matrix-free solutions consisted of acetonitrile with water in the same proportions as the sample to insure the compatibility with the chromatographic system. Additionally, an infusion experiment was performed, where the MS response was monitored while continuously infusing osimertinib and pazopanib (both 5  $\mu\text{g}/\text{ml}$ , at 5  $\mu\text{l}/\text{min}$ ), during which extracted blank plasma samples were injected.



## Stability

### ***Benchmark stability***

Quadruplicate stability tests at room temperature were evaluated for heparinized plasma by comparing the response of QC samples at the low, medium, and high levels stored at room temperature for four hours, with fresh samples.

### ***Freeze-thaw stability***

Quadruplicate analysis of human heparin plasma samples from separate tubes was performed after storage at 20 °C for 8 h, followed by three freeze-thaw cycles (thawing at 20 °C during ca. 2 h and freezing again at -30 °C for at least 12 hours).

### ***Long term stability***

QC samples at low, medium, and high levels were produced in lithium heparin, and stored at -30 °C for an extended period of 75 days. These samples were analyzed, and the relative responses were compared to freshly prepared QC samples.

### ***Auto injector stability***

An analytical run of 18 QC samples was re-injected after 24 hours. The auto injector cooling was turned off during this period, mimicking device failure.

### ***Stock stability***

The responses of osimertinib from the stock solutions in DMSO, after 2 months at -30 °C (n = 2) were compared to fresh stock solutions with LC-MS/MS after appropriate dilution of the samples with 50% (v/v) acetonitrile, and adding internal standards. Of the diluted stock, 500 µl was transferred to a vial, and 500 µl water was added before closing the vial to increase the compatibility with the chromatographic system.

### ***Patient samples***

The method was used to determine blood-plasma levels for 34 patients receiving oral osimertinib therapy, 80 mg once daily. Drug analysis was part of a therapeutic drug monitoring service to support therapy. Sodium-EDTA plasma samples were taken after 24 h (trough levels), and were analyzed in duplo. The samples were analyzed in two separate runs to evaluate the incurred sample analysis.

## Results and discussion method development

### Chromatography and LC-MS/MS method

The settings for ESI-MS/MS were optimized for osimertinib as to obtain maximal sensitivity; a product spectrum of osimertinib is presented in Figure 1 Formic acid provided the maximum response compared to other MS compatible additives, such as ammonium hydroxide and ammonium acetate. Acetonitrile resulted in narrower, sharper peaks than methanol when used as eluent. Gradient elution was optimized to facilitate the 10  $\mu$ l injection volume and was therefore started at a relatively low percentage of 10% acetonitrile. Representative chromatograms of extracted human plasma, with and without analyte and/or IS are shown in Figure 2.

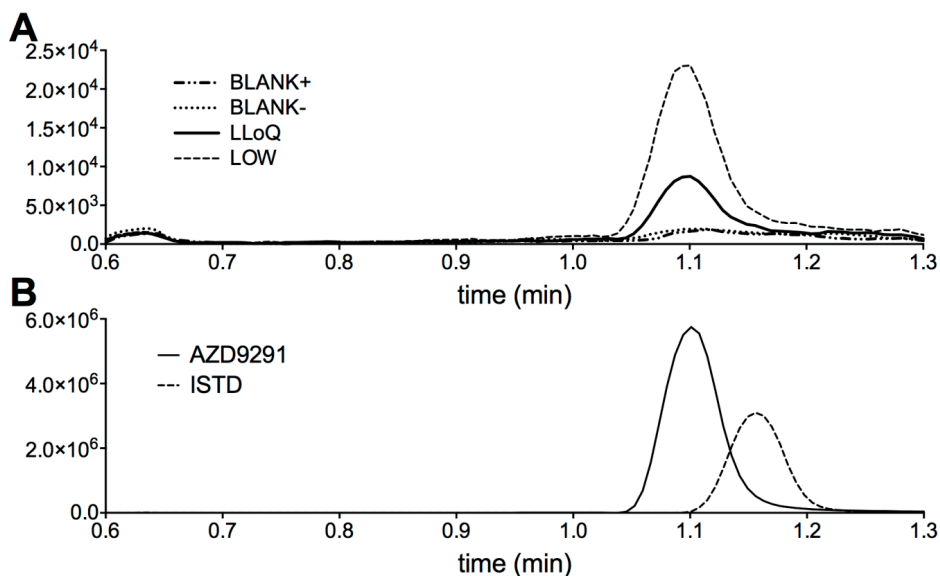


Figure 2. Chromatograms of extracted human plasma

A. With and without analyte and/or IS.

B. Representative chromatogram, showing the retention times and overlap of osimertinib and the internal standard (pazopanib).

Column equilibration for 0.5 min (with an additional between run time of *ca.* 0.5 min for the autosampler duty cycle) showed sufficient equilibration based on retention time stability (RSD <0.5%). Osimertinib eluted at 1.09 minutes, the internal standard pazopanib at 1.14 min.

Incorporation of a high organic flush at the end of each run prevented the build-up of strongly retained plasma-components that could cause long term suppressive effects on ion formation, such as phospholipids. Positive ESI-MS/MS settings were optimized

for protonated osimertinib and the internal standard, pazopanib. The product spectrum of osimertinib is shown in Figure 1. Because the stable isotope labeled osimertinib was commercially unavailable at the time, pazopanib was chosen as an internal standard because it is not co-administered with osimertinib and because it shows similar retention under the selected conditions.

### Sample preparation

Various methods have been used in the bioanalysis of small-molecule tyrosine kinase inhibitors, following either LC-MS/MS or less common, LC-UV.<sup>10</sup> The most commonly used methods are simple crash-dilute-and-shoot protein precipitation or the more labor intensive and more selective liquid-liquid extraction and solid-phase extraction, following evaporation of non LC-MS/MS compatible solvents.<sup>11</sup> Recently, another method emerged in this field: Salting-out Assisted Liquid-Liquid Extraction (SALLE).<sup>12</sup> The present SALLE method uses three simple steps, and avoids laborious steps, such as evaporation of non-compatible solvents.

### SALLE optimization

SALLE was chosen as the pretreatment method over protein precipitation (PP) and the more laborious regular liquid extraction (LLE) and solid-phase extraction (SPE). Extraction methods provide a cleaner sample compared to PP, and LLE uses organic solvents like TBME, whereas SALLE uses ACN that is more common and often less toxic for personnel and/or environmental impact. For 'wetting', equilibration and elution SPE usually uses up to 1 mL of solvent, whereas for PP and SALLE less than 100  $\mu\text{L}$  is sufficient. The reduced volume, and LC-compatible solvent removes the need for solvent evaporation resulting in an improved handling speed of SALLE over LLE and SPE.<sup>10</sup>

Various salts were tested during optimization (namely  $\text{CH}_3\text{COONH}_4$ ,  $\text{KH}_2\text{PO}_4$ ,  $\text{K}_2\text{HPO}_4$ ,  $\text{NaCl}$ ,  $\text{MgCl}_2$ ,  $\text{MgSO}_4$ ,  $\text{ZnSO}_4$ ), in multiple concentrations. The concentration ranged from 0.3 to 1.5 M final concentration, or a saturated solution when saturation occurred below 3.0 M.  $\text{MgSO}_4$  provided the optimal signal-to-noise. Although some other salts showed comparable results, the advantage of  $\text{MgSO}_4$  over other salts is that after centrifugation a layer of precipitated protein is formed between the two liquid layers, effectively sealing the two layers from each other. This layer stabilizes the phase-separation and provides a good visual aid in pipetting off the upper layer. For the SALLE method, the volume ratio of acetonitrile versus water was determined experimentally by varying the amounts of both, as well as the concentration of  $\text{MgSO}_4$  (Figure 3). The optimization was focused on minimizing the acetonitrile volume to limit sample dilution by maximizing salt concentration, whilst avoiding

precipitation of salts. Based on the volume of the upper phase (mostly acetonitrile), a sample:saline:acetonitrile ratio of 1:1:5; v/v was used for sample pretreatment, with a saline concentration of 2.0 M  $\text{MgSO}_4$ . The selected ratio resulted in a sufficient recovery of osimertinib.

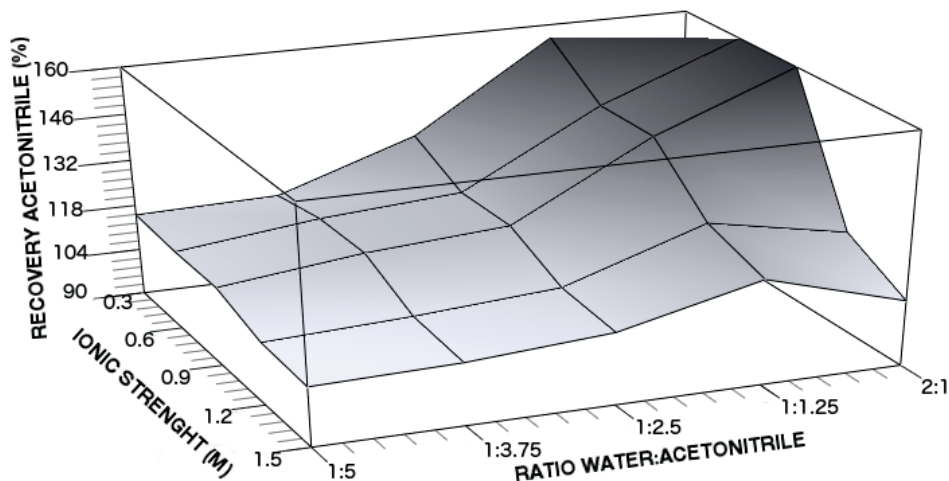


Figure 3. Effect of  $\text{MgSO}_4$  concentration and water to acetonitrile ratio on partitioning of water acetonitrile mixture  
At an ionic strength of 0.3 M and a ratio of 0.2, no phase separation occurred.

### Analytical method validation

For this assay, the upper limit of quantitation was proposed at 1,000 ng/ml because initial drug levels were reported at approximately 50 to 1000 ng/ml.<sup>1,4</sup> A range of 1000 orders of magnitude was deemed suitable for quantifying osimertinib in patients, so the validation was performed at a range from 1 to 1000 ng/ml. The sensitivity reported by Planchard et al. (25 pg/ml) was far below the therapeutic range and was not required for our TDM application.<sup>7</sup>

### Calibration

The calibration curves ( $n=5$ ) were linear over the range examined, with a coefficient of determination ( $R^2$ ) of  $0.993 \pm 0.004$ . Since the calibration curves of osimertinib did not show non-linearity (data not shown), a linear-regression model using least squares regression (quadratic weighting,  $1/X^2$ ) was used. The linear functions were  $Y = (0.00151 \pm 0.00055) * X + (0.000398 \pm 0.000090)$  for osimertinib. Here, X is the ratio of the analyte response versus the internal standard response, and Y the concentration in ng/ml. Auto injector carry-over from the highest calibration sample was found to be less than 20% of the LLOQ, as required by the EMA and FDA guidelines.<sup>8,9</sup>

## Precision and accuracy

In Tables 1 and 2, the accuracy and precision of the method in human lithium heparin and EDTA plasma are shown. The precisions and accuracies for three analytical runs were within the  $\pm 15\%$  for high, medium, and low QC's, and  $\pm 20\%$  for the LLOQ QC's, as required.<sup>8,9</sup> For the spiked EDTA plasma samples the within day accuracy and precision were similar to heparin plasma samples.

**Table 1.** Within and between day precision, and accuracy of osimertinib in lithium heparin spiked human plasma samples (n=18)

Level (ng/ml)	Within-day precision (%)	Between-day precision (%)	Accuracy (%)
800	3.4	3.8	95.5
200	2.8	3.6	96.9
3	6.5	10.2	99.5
1	10.3	10.4	102.8

**Table 2.** Within day precision, and accuracy of osimertinib in spiked human sodium-EDTA plasma samples (n=6)

Level (ng/ml)	Within-day precision (%)	Accuracy (%)
800	2.6	101.5
200	5.3	103.7
3	4.5	102.2
1	4.4	101.2

## Selectivity

The analysis of six independent blank human plasma samples of both heparin and EDTA showed no interfering peaks in the SRM traces for osimertinib or the internal standard (data not shown). Blank osimertinib responses were all  $<20\%$  of the LLOQ response ( $9.8\% \pm 3.6\%$ ) as required.<sup>8</sup> Blank IS responses were below 1% ( $0.11\% \pm 0.05\%$ ) of the normal response. At the LLOQ of 1 ng/ml (n = 6) a mean concentration of  $0.96 \pm 0.07$  ng/ml for osimertinib in heparinized plasma ( $95.7 \pm 7.6\%$ ) was found, and  $1.05 \pm 0.10$  ng/ml for EDTA plasma ( $105.3 \pm 9.9\%$ ) with one value  $>20\%$  (120.2%), justifying the investigated LLOQ level in human plasma.<sup>9</sup> The results of six different spiked plasma samples (lithium heparin and sodium EDTA) are shown in Table 3.

## Recovery and matrix effect

By performing infusion experiments, it was shown that along with chromatographic separation, any remaining endogenous substance does not cause any effect on ionization of osimertinib and internal standard. As shown in Table 4, the extraction recoveries showed no losses for both target compound and IS and ranged from 94% to 104% in

**Table 3. Selectivity for six spiked plasma samples at LLOQ level (1 ng/ml)**

Replicate	Lithium Heparin		Sodium EDTA	
	Calculated	Diff.	Calculated	Diff.
	Amount	Spec. Amount.	Amount	Spec. Amount.
	(ng/ml)	(%)	(ng/ml)	(%)
1	0.90	89.8	1.05	105.4
2	1.03	102.8	1.04	103.9
3	1.01	100.5	1.20	120.2
4	0.92	91.7	0.88	88.4
5	1.03	103.0	1.03	103.0
6	0.86	86.5	1.11	110.7
Average	0.96	95.7	1.05	105.3
%VC	7.6	7.6	9.9	9.9

lithium heparin. No substantial matrix effects were observed, and recovery ranged from 87 to 89% for osimertinib at the investigated levels. Relative matrix effects for both matrices were determined (Table 5), and were found to be within the limits set in the international guidelines for analytical method validation. The high extraction recovery and low matrix effects aided the successful validation of the method. The low matrix effect can be attributed to the efficient sample pre-treatment procedure.

**Table 4. Recovery and matrix effect for osimertinib in human plasma in lithium heparin (mean±SD; n = 4)**

Level (ng/ml)	Extraction Recovery			Matrix Effect		
High (800)	93.9%	±	5.5%	88.8%	±	9.2%
Med (200)	98.9%	±	2.7%	88.5%	±	1.7%
Low (3)	103.7%	±	9.8%	87.2%	±	13.7%

**Table 5. Relative matrix effect**

Relative matrix effect at high (800 ng/ml) and low (3 ng/ml) QC levels for six spiked individual lithium heparin and sodium EDTA samples.

Indiv.	Heparin		EDTA	
	High (%)	Low (%)	High (%)	Low (%)
1	92.3	115.5	94.1	110.8
2	96.9	102.0	92.3	97.5
3	93.8	100.4	96.3	105.5
4	90.7	96.8	97.8	106.3
5	96.0	101.1	88.2	95.0
6	95.3	95.8	98.1	101.2
Average	94.2	101.9	94.5	102.7
RSD	2.5	7.0	4.0	5.7

## Stability

Quadruplicate stability tests at room temperature was (22 °C) for six hours, compared with fresh samples showed minimal degradation of osimertinib. Analysis of samples after three freeze-thaw cycles (thawing at room temperature (ca 22 °C), during ca. 4 h and freezing again at -30 °C for at least 12 hours) resulted in less than 15% degradation. Based on these findings we concluded that osimertinib could undergo multiple freeze-thaw cycles. The final results are noted in Table 6. For long term stability QC samples (low, medium, and high levels) were stored at -30 °C for an extended period of 75 days. These samples were analyzed, and the relative response was compared to freshly prepared QC samples. This experiment indicated that osimertinib is stable in human plasma at -30 °C. The complete results are shown in Table 6.

**Table 6. Stability of osimertinib**

Stability of osimertinib at 4 hours at room temperature, after three freeze thaw cycles, and -30 °C for 75 days (mean±SD, n = 4)

Level (ng/ml)	Short term stability (%)	Freeze-thaw stability (%)	Long term stability (%)
High (800)	88.6 ± 1.9	95.7 ± 2.4	92.5 ± 4.7
Med (200)	92.6 ± 10.1	91.8 ± 1.8	97.7 ± 9.8
Low (3)	89.8 ± 6.5	89.1 ± 10.0	89.1 ± 2.5

## Auto injector stability

An analytical run of 18 QC samples was re-injected after 24 hours at room temperature, showing similar results for osimertinib, with no QC exceeding ±15% (data not shown). Osimertinib and the internal standards proved stable in the auto-sampler under the tested conditions.

## Stock stability

The responses of osimertinib from the stock solutions in DMSO, after 2 months at -30 °C (n = 2) compared to fresh stock solutions resulted in unchanged concentrations (99.3% recovery) proving the stability of osimertinib under the tested condition.

## Patient samples

Plasma levels were analyzed for all 34 patients (66.1±11.5 y) receiving oral osimertinib therapy (80 mg once daily) to support drug treatment. The average plasma-levels were 301.6±164.1 ng/ml with none of the samples showing a concentration outside the set range of 1 to 1,000 ng/ml. These findings are in line with previous literature and a plot of the measured plasma concentrations of the 34 plasma-samples are shown in Figure 4B.<sup>1,4</sup> The available plasma samples were collected using EDTA as an anticoagulant, opposed to heparin. To show the validity of the change in anticoagulant,

additional experiments were performed, including precision and accuracy, selectivity, and relative matrix effect. Incurred sample analysis of these initial samples showed that the method can reliably report the subject sample analyte concentrations with less than 20% difference ( $4.6 \pm 3.3\%$  difference).<sup>8</sup>

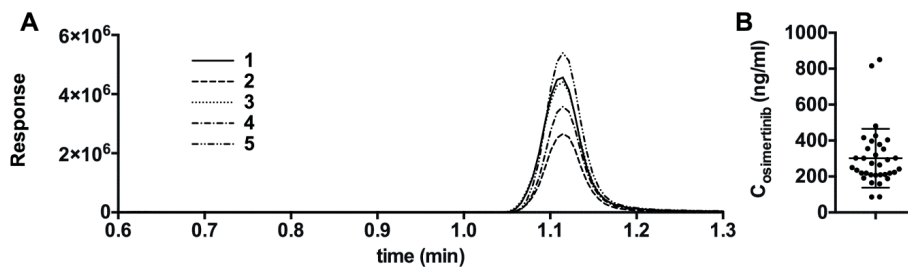


Figure 4.

A. Chromatograms from five initial patient samples.

B. Average plasma-concentrations of osimertinib in 34 patients (two replicates per sample).

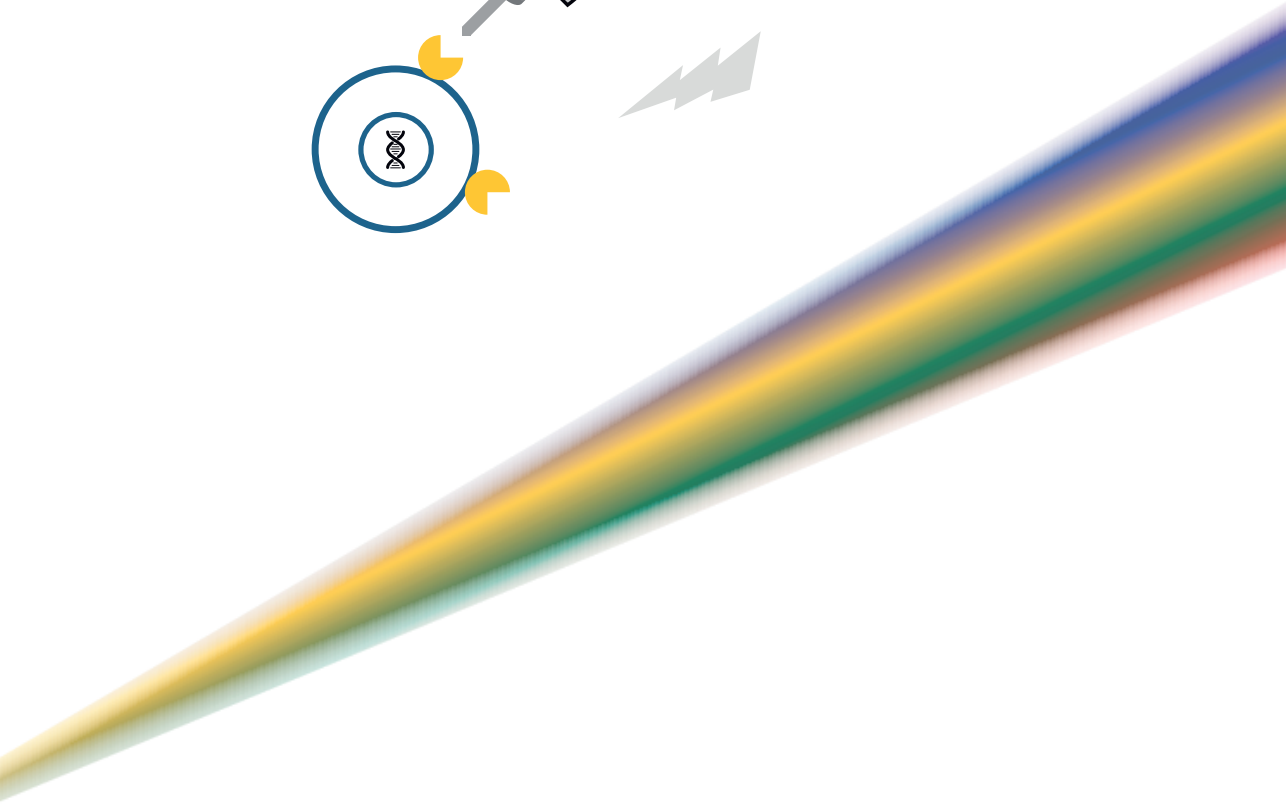
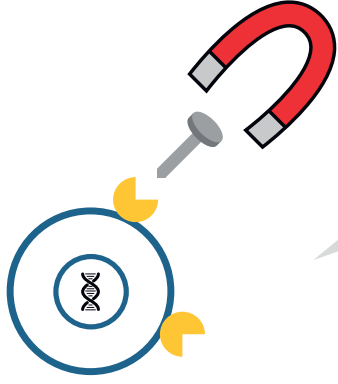
## Conclusions

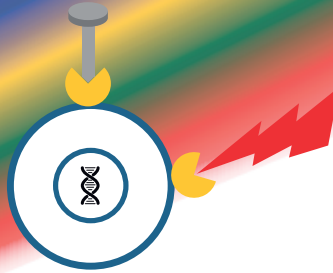
An LC-ESI-MS/MS method has been developed and validated for the rapid and precise quantitation of osimertinib in human plasma. The method can be used for both lithium heparin samples, as well as sodium EDTA samples. The method used was successfully validated, was shown adequate in the analysis of osimertinib in samples from patients with a T790 EFGR mutated form of NSCLC, and is the first published validated assay for this drug. Accuracy and precision met the limits as they are described in international guidelines. Long-term, bench-top, freeze-thaw and auto-sampler stability of the samples met these criteria as well. In the analysis of osimertinib in human plasma we found no samples out of the validated range showing that the chosen range is adequate.



## References

1. Cross DE, Ashton SE, Ghiorghiu S, et al. AZD9291, an irreversible EGFR TKI, overcomes T790M-mediated resistance to EGFR inhibitors in lung cancer. *Cancer Discov.* 2014;4:1046-1061.
2. Yu HA, Arcila ME, Rekhtman N, et al. Analysis of tumor specimens at the time of acquired resistance to EGFR-TKI therapy in 155 patients with EGFR-mutant lung cancers. *Clin Cancer Res.* 2013;19(8):2240-2247.
3. Drug label Tagrisso available at: [http://www.accessdata.fda.gov/drugsatfda\\_docs/label/2015/208065s000lbl.pdf](http://www.accessdata.fda.gov/drugsatfda_docs/label/2015/208065s000lbl.pdf). Accessed 03 Dec 2015.
4. Jänne P, Yang JC-H, Kim D-W, et al. AZD9291 in EGFR Inhibitor-Resistant Non-Small-Cell Lung Cancer. *N Engl J Med.* 2015;372(18):1689-1699.
5. Butterworth S, Finlay MR V, Ward RA, et al. 2 - (2, 4, 5 - substituted -anilino) pyrimidine derivatives as egfr modulators useful for treating cancer WO2013014448A1. January 2013.
6. Food and Drug Administration (FDA) Approves New Pill to Treat Certain Patients with Non-small Cell Lung Cancer, <http://www.fda.gov/NewsEvents/Newsroom/PressAnnouncements/ucm472525>. Accessed 20 Nov 2015.
7. Planchard D, Brown KH, Kim D-W, et al. Osimertinib Western and Asian clinical pharmacokinetics in patients and healthy volunteers: implications for formulation, dose, and dosing frequency in pivotal clinical studies. *Cancer Chemother Pharmacol.* 2016;77(4):767-776.
8. European Medicines Agency (EMA), Guideline on bioanalytical method validation [http://www.ema.europa.eu/ema/index.jsp?curl=pages/includes/document/document\\_detail](http://www.ema.europa.eu/ema/index.jsp?curl=pages/includes/document/document_detail). Accessed 09 Dec 2014.
9. Food and Drug Administration (FDA) Guidance for Industry: Bioanalytical Method Validation. <http://www.fda.gov/downloads/drugs/guidancecomplianceregulatoryinformation/guidances/ucm070107.pdf>. Accessed 09 December 2014.
10. Rood JJ, Schellens JHM, Beijnen JH, Sparidans RW. Recent developments in the chromatographic bioanalysis of approved kinase inhibitor drugs in oncology. *J Pharm Biomed Anal.* 2016;130:244-263.
11. Chang MS, Ji Q, Zhang J, El-Shourbagy TA. Historical review of sample preparation for chromatographic bioanalysis: pros and cons. *Drug Dev Res.* 2007;68(3):107-133.
12. Tang YQ, Weng N. Salting-out assisted liquid-liquid extraction for bioanalysis. *Bioanalysis.* 2013;5(12):1583-1598.





# Chapter 7

**A phase Ib/II multi-center, open label,  
dose escalation study of WNT974,  
encorafenib and cetuximab in patients  
with BRAFV600-mutant KRAS wild-type  
metastatic colorectal cancer harboring  
WNT pathway mutations**

Mark T.J. van Bussel

*To be submitted*

## Summary

More than 90% of colorectal cancers (CRC) have alterations in WNT signaling. Eight to ten percent of patients with metastatic KRAS-WT colorectal cancer have BRAF mutations and do not benefit from EGFR antibodies like cetuximab and panitumumab. In two phase I studies the combination of the BRAF inhibitor vemurafenib or encorafenib and cetuximab induced response rates of 35% and 19% in this patient population. Addition of a WNT inhibitor seems an attractive approach to increase the response rate in patients with BRAFV600 mutated KRAS-WT CRC with WNT alterations. Patients with BRAFV600E mutated KRAS-WT CRC with WNT alterations in RNF43 and/or RSPO fusion were treated with a BRAF inhibitor (encorafenib), plus a monoclonal antibody targeting EGFR (cetuximab) and a porcupine inhibitor (WNT974). The primary objective was to determine the maximum tolerated dose (MTD) or a recommended phase II dose. The triplet combination (WNT974 + encorafenib + cetuximab) demonstrated clinical activity with a confirmed overall response rate of 10% and a disease control rate of 85%. Overall, the combination of encorafenib plus WNT974 and cetuximab was associated with a high incidence of bone toxicities. These observations led to the decision to discontinue the study.

## Introduction

In total 774 000 people died from colon cancer worldwide in 2015.<sup>1</sup> Eight to ten percent of patients with metastatic colorectal cancer (mCRC) have a v-Raf murine sarcoma viral oncogene homolog B (BRAF) mutation.<sup>2-4</sup> Patients with BRAFV600E mCRC have a poor prognosis with a median overall survival (OS) of less than 1 year.<sup>3-5</sup> Patients with mCRC with BRAF mutations in the absence of Kirsten rat sarcoma viral oncogene homolog (KRAS) mutations lack treatment benefit of epidermal growth factor receptor (EGFR) antibodies like cetuximab and panitumumab.<sup>2</sup> In two phase I studies the combination of the BRAF inhibitor vemurafenib or encorafenib and cetuximab induces response rates of 35% and 19% in this patient population.<sup>6,7</sup> In colon cancer, WNT signaling is often upregulated.<sup>8,9</sup> WNT ligands stimulate multiple signaling cascades in various tissues, including the 'canonical' B-catenin pathway and are being classified as 'canonical' on the basis of their ability to inhibit glycogen synthase kinase 3 phosphorylation of B-catenin.<sup>10</sup> Up to 94% of 224 colorectal tumors had alterations in WNT signaling.<sup>8</sup> Mutations in the WNT pathway frequently co-occur with BRAF-mutations and induce tumor growth.<sup>11</sup> Inhibition of the WNT pathway in addition to BRAF and EGFR inhibition therefore seems to be an attractive approach to increase the response rate of targeted agents in mCRC. WNT974/LGK974 is an inhibitor of the WNT pathway via porcupine inhibition.<sup>12</sup> Porcupine is a membrane bound O-acyl transferase which adds a palmitoyl group to WNT ligands. Palmitoylation of WNT ligands is necessary for release of WNT ligands from the Golgi membrane to the cell plasma.<sup>13</sup> WNTs bind to receptor complexes containing one of 10 frizzled (Fzd) receptors and also to the low-density lipoprotein receptor-related protein (LRP) 5 or 6 co-receptors. Under normal conditions the E3 ubiquitin-protein ligase RING finger 43 (RNF43) inhibits WNT signaling.<sup>14</sup> Mutations in RNF43 lead to activation of WNT signaling. R-spondin (RSPO) gene fusions in RSPO2 and RSPO3 have a prevalence of 10% in colon cancer and potentiate WNT signaling.<sup>15</sup> Combination therapy with EGFR-inhibitors, BRAF-inhibitors and WNT-inhibitors could potentially inhibit tumor growth in patients with KRAS-WT mCRC with mutations in BRAF and in the WNT-pathway. This strategy has been explored in the phase IB/II clinical trial NCT02278133. In this phase 1b study patients with BRAFV600-mutant KRAS-WT metastatic colorectal cancer harboring WNT pathway mutations in RNF43 and/or RSPO fusion received a fixed dose of cetuximab at the recommended dose as defined in its label and encorafenib 200 mg once daily together with WNT974. The starting dose of WNT974 was 10 mg once daily and was escalated to determine the MTD or the recommended phase 2 dose (RP2D). In this phase 1b trial the safety and efficacy of this drug combination was assessed. Here, we report the results of the phase 1b trial.

## Methods

### Study design

The primary objective of phase Ib was to determine the MTD and/or RP2D of the triple combination of WNT974, encorafenib and cetuximab in patients with BRAFV600-mutant KRAS wild-type metastatic colorectal cancer harboring WNT pathway mutations. Adult patients with mCRC were enrolled on the basis of documented wild-type KRAS and a BRAF v600 mutation with RNF43 mutations and/or RSPO fusions. Eligibility criteria included Eastern Cooperative Oncology Group performance status (ECOG PS) of  $\leq 2$ , progression of disease after at least one prior standard of care regimen or intolerance to irinotecan based regimens. All patients gave written informed consent per declaration of Helsinki recommendations, and the protocol was reviewed and approved by a properly constituted institutional review board prior to study start. The study is registered with ClinicalTrials.gov (NCT02278133).

### Study treatment

Cetuximab was dosed intravenously according to the label for patients with mCRC: a 400 mg/m<sup>2</sup> loading dose (cycle 1 day 1) and 250 mg/m<sup>2</sup> for subsequent weekly doses. The recommended phase II dose of encorafenib 200 mg once daily was given orally.<sup>7</sup> Treatment cycles were 28 days. The starting dose of 10 mg WNT974 orally was based on the recommended dose for expansion cohorts in the NCT01351103 study.<sup>16</sup> The MTD was not determined in the phase 1 single agent study of WNT974. Several dose ranges and schedules of 5-30 mg QD; 30-45 mg QD 4 days on, 3 days off; and 5 mg BID have been explored in the single agent study. Preclinical data indicated a potential drug drug interaction (DDI) between WNT974 and encorafenib due to CYP3A4 interactions. WNT974 is primarily metabolized by CYP3A4 and encorafenib is a strong inducer of CYP3A4. Simcyp modeling at several doses of WNT974 (10 to 50 mg QD) and encorafenib (100 to 450 mg QD) indicated that WNT974 exposure was expected to decrease by approximately 90% in the presence of encorafenib. The starting of WNT974 was based on pharmacokinetic (PK), pharmacodynamic (PD) and tolerability data.

Selection of the actual dose for the next cohort of patients was guided by the Bayesian logistic regression model (BLRM) with escalation overdose control (EWOC) criteria. Dose-escalation decisions were based on data from all evaluable patients, including safety information, DLTs, together with medical review of available relevant clinical, PK, PD and laboratory data. A DLT was defined as an adverse event (AE) or abnormal laboratory value assessed as unrelated to disease, disease progression, inter-current illness, or concomitant medications that occurs within the first 28 days of treatment

with the triple combination of WNT974, LGX818 and cetuximab and meets any of the criteria included in supplementary table S1.

### Study assessments

Tumor response was evaluated locally by the investigator according to guidelines based on RECIST version 1.1. Each patient was evaluated for all potential sites of tumor lesions at screening/baseline and every 6 weeks after starting study treatment until disease progression. All complete responses (CR) and partial responses (PR) were to be confirmed by a second assessment at least 4 weeks after the initial assessment. The disease control rate (DCR) was defined as: CR + PR + stable disease (SD). Safety was assessed at screening and throughout the treatment period by physical examination and collection of AEs. AEs were assessed according to the CTCAE version 4.03. Serial PK blood samples were collected on day 1 and day 15 of cycle 1, and predose blood samples were collected on day 2, 8, 16 and day 22 of cycle 1 and day 1 of cycles 2 through 4. Samples were analyzed using validated liquid chromatography (LC) mass spectrometry (MS) (LC/MS-MS). PK parameters were defined as follows: Area Under the plasma Concentration-time curve during a dosing interval (tau) ( $AUC_{\tau}$ ) (amount x time x volume<sup>-1</sup>);  $C_{\max}$ : maximum (peak) observed plasma concentration (mass x volume<sup>-1</sup>);  $T_{\max}$ : time to reach maximum peak plasma concentration;  $C_{\min,ss}$ : minimum drug concentration observed during a dosing interval at steady state (mass x volume<sup>-1</sup>);  $C_{\max,ss}$ : maximum drug concentration observed during a dosing interval at steady state (mass x volume<sup>-1</sup>);  $T_{1/2}$ : the elimination half-life associated with the terminal slope ( $\lambda_z$ ) of a semilogarithmic concentration-time curve. Pre and post treatment tumor biopsies were collected for immunohistochemistry assessments of changes in cMyc, Mucin and Ki67. For the biomarker cMyc (nuclear H-score), the median percent change from baseline was assessed with Alcian blue (percent tumor area) and Alcian blue (percent tumor cells) staining. Pre and post treatment matched skin biopsies were collected for biomarker assessments by reverse transcription polymerase chain reaction of a  $\beta$ -catenin target gene AXIN2.

### Statistical methods

An adaptive BLRM guided by the EWOC principle directed the dose escalation to the MTD/RP2D.<sup>17</sup> Selection of the actual dose for the next cohort of patients was guided by the BLRM with EWOC criteria. A 10 parameter BLRM for combination treatment was fitted on the cycle 1 DLT data accumulated throughout the dose escalation to model the dose-toxicity relationship of WNT974, encorafenib and cetuximab given in combination.

## Results

### Patient disposition and characteristics

A total of 138 patients were screened and 20 patients were assigned to treatment. Currently, all 20 patients discontinued treatment. The most common reasons for treatment discontinuation were disease progression in 15 patients (75%) and AEs in 3 patients (15%). There were two deaths (10%) during the study treatment period or within 30 days after treatment period. One death was reported during treatment and was noted as the primary reason for treatment discontinuation and one death occurred during the posttreatment phase. Both deaths were related to disease progression. The patient characteristics at baseline are shown in Table 1.

**Table 1. Patient characteristics at baseline**

Sex, n (%)	
Female	11 (55)
Male	9 (45)
Age, median (range), years	61 (50-75)
ECOG PS, n (%)	
0	9 (45)
1	10 (50)
2	1 (5)
Number of prior treatment regimens, n (%)	
1	1 (5)
2	11 (55)
3	3 (15)
>3	5 (25)
Best response to last prior therapy, n (%)	
Partial response	3 (15)
Stable disease	5 (25)
Progressive disease	6 (30)
Unknown / not applicable	5 (25) / 1(5)

*Abbreviations:* ECOG PS, Eastern Cooperative Oncology Group performance status.

### Dose escalation

Eighteen patients who were dosed with WNT974 + encorafenib + cetuximab were considered evaluable for dose-finding. Four patients were enrolled in cohort 1 at 10 mg QD WNT974 + 200 mg QD encorafenib + cetuximab. Two patients reported DLTs (increased lipase grade 4 and dysgeusia grade 2). Five patients were enrolled in cohort 2 at 5 mg QD WNT974 + 200 mg QD encorafenib + cetuximab. No patients reported a DLT. Six patients were enrolled in cohort 3 at 7.5 mg QD WNT974 + 200



mg QD encorafenib + cetuximab. One patient reported a DLT (hypercalcaemia grade 3). Once cohort 3 was completed, an enrichment cohort was reopened for further elaboration of safety and PK parameters at dose level 5 mg QD WNT974 + 200 mg QD encorafenib + cetuximab. Five patients were enrolled. No further DLTs were reported. After a review of the efficacy and safety data from the ongoing study, the sponsor decided to discontinue further enrollment in the study. Therefore, the MTD for the triplet combination was not determined.

## Safety

There were fifteen (75%) patient deaths in the study of which two (10%) occurred while the patient was on study treatment or within 30 days of discontinuing study treatment. Both fatalities were attributed to CRC and were related to disease progression. There were 15 serious adverse events (SAEs) reported (75% of patients). Nine patients (45%) had SAEs suspected to be study drug related. The most frequently reported study drug related SAEs for  $\geq 10\%$  of patients were rib fracture (n=3, 15%) spinal compression fracture (n=3, 15%) and hypercalcaemia (n=2, 10%). All 20 patients experienced at least 1 AE that was suspected to be drug related and of those, 13 patients (65%) experienced AEs that were of grade 3 or 4 severity. An overview of AEs occurring in  $>20\%$  of patients is given in Table 2.

## Bone-related (serious) adverse events

There were 9 patients (45%) with reported bone-related SAEs (6 bone fractures and 3 other bone-related SAEs). The median(range) study day of bone-related SAE occurrence was 127 (29-344). There were 9 patients (45%) with at least 1 bone fracture, including rib fracture (7 patients 35%), spinal compression fracture (4 patients 20%), pathological fracture (2 patients 10%), foot fracture (1 patient 5%), hip fracture (1 patient 5%) and lumbar vertebral fracture (1 patient 5%). Other bone-related AEs occurred in 16 patients (80%) overall and included hypercalcaemia (14 patients 70%), hypocalcaemia (5 patients 25%), osteoporosis (5 patients 25%), bone pain (2 patients 10%) and osteopenia (2 patients 10%).

## Efficacy

The phase 2 part of the study was not initiated, there was no primary efficacy endpoint assessed. The secondary efficacy endpoints included overall response rate (ORR) and the DCR and are presented in Table 3. Based on confirmed responses, the ORR was 10% (95% confidence interval 1-32%). Most patients achieved SD (75%) and the confirmed DCR was 85%.

Table 2. Adverse events, regardless of treatment attribution, occurring in &gt;20% of patients

Adverse event n (%)	WNT974 5 mg QD+ Encorafenib 200 mg QD+ Cetuximab n = 10		WNT974 7.5 mg QD+ Encorafenib 200 mg QD+ Cetuximab n = 6		WNT974 10 mg QD+ Encorafenib 200 mg QD+ Cetuximab n = 4		All Patients n = 20	
	All grades	Grade 3/4	All grades	Grade 3/4	All grades	Grade 3/4	All grades	Grade 3/4
Hypercalcaemia	5 (50)	1 (10)	5 (83)	2 (33)	4 (100)	4(100)	14 (70)	7 (35)
Arthralgia	5 (50)	0	4 (67)	4(100)	4 (100)	0	13 (65)	0
Fatigue	6 (60)	0	2 (33)	0	3 (75)	0	11 (55)	0
Anaemia	5 (50)	1 (10)	2 (33)	0	3 (75)	2 (50)	10 (50)	3 (15)
Constipation	5 (50)	0	2 (33)	0	2 (50)	0	9 (45)	0
Nausea	4 (40)	0	4 (67)	0	1 (25)	0	9 (45)	0
Back pain	3 (30)	1 (10)	3 (50)	1 (17)	2 (50)	0	8 (40)	2 (10)
Hypophosphatemia	4 (40)	3 (30)	2 (33)	1 (17)	2 (50)	1 (25)	8 (40)	5 (25)
Pyrexia	5 (50)	0	2 (33)	0	1 (25)	0	8 (40)	0
Vomiting	4 (40)	0	2 (33)	0	1 (25)	0	8 (40)	0
Decreased appetite	3 (30)	0	2 (33)	1 (17)	2 (50)	0	7 (35)	1 (5)
Dysgeusia	2 (20)	0	2 (33)	0	3 (75)	0	7 (35)	0
Hypokalaemia	3 (30)	0	2 (33)	0	2 (50)	1 (25)	7 (35)	1 (5)
Hypomagnesaemia	3 (30)	0	1 (17)	0	3 (75)	1 (25)	7 (35)	1 (5)
Myalgia	3 (30)	0	2 (33)	0	2 (50)	0	7 (35)	0
Oedema peripheral	3 (30)	0	0	0	4 (100)	0	7 (35)	0
Rib fracture	4 (40)	1 (10)	2 (33)	1(17)	1 (25)	0	6 (30)	0
Abdominal pain	2 (20)	0	2 (33)	0	2 (50)	0	5 (25)	0
Diarrhoea	3 (30)	0	1 (17)	0	1 (25)	0	5 (25)	0
Hypocalcaemia	1 (10)	0	1 (17)	0	3 (75)	1 (25)	5 (25)	1 (5)
Osteoporosis	2 (20)	0	2 (33)	0	1 (25)	0	5 (25)	0
Pain in extremity	2 (20)	0	1 (17)	0	2 (50)	1 (25)	5 (25)	1 (5)
Weight decreased	1 (10)	0	2 (33)	0	2 (50)	0	5 (25)	0

Abbreviation: QD=once daily.

Table 2. Continued

Adverse event n (%)	WNT974 5 mg QD+ Encorafenib 200 mg QD+ Cetuximab		WNT974 7.5 mg QD+ Encorafenib 200 mg QD+ Cetuximab		WNT974 10 mg QD+ Encorafenib 200 mg QD+ Cetuximab		All Patients	
	n = 10	n = 6	n = 6	n = 6	n = 4	n = 4	n = 20	n = 20
	All grades	Grade 3/4	All grades	Grade 3/4	All grades	Grade 3/4	All grades	Grade 3/4
Aspartate aminotransferase increased	2 (20)	0	1 (17)	1 (25)	1 (25)	4 (20)	4 (20)	4 (20)
Blood bilirubin increased	1 (10)	0	2 (33)	1 (17)	1 (25)	1 (25)	4 (20)	2 (10)
Blood creatinine increased	0	0	1 (17)	0	3 (75)	1 (25)	4 (20)	1 (5)
Chills	2 (20)	0	1 (17)	0	1 (25)	0	4 (20)	0
Dyspnoea	2 (20)	0	2 (33)	1 (17)	0	0	4 (20)	1 (5)
Headache	2 (20)	1(10)	2 (33)	1 (17)	1 (25)	0	4 (20)	1 (5)
Infusion related reaction	1 (10)	0	2 (33)	1 (17)	1 (25)		4 (20)	1 (5)
Musculoskeletal pain	4 (40)	0	0	0	0	0	4 (20)	0
Peripheral sensory neuropathy	1 (10)	0	2 (33)	0	0	1 (25)	4 (20)	0
Spinal compression fracture	2 (20)	0	1 (17)	0	1 (25)	1 (25)	4 (20)	1 (5)

Table 3. Best overall response to treatment

Response, n (%)	
Complete response (CR)	0
Partial response (PR)	2 (10.0)
Stable disease (SD)	15 (75.0)
Progressive disease (PD)	1 (5.0)
Unknown	2 (10.0)
Overall response rate (CR + PR) (%)	10
Disease control rate (CR +PR + SD) (%)	85

### Biomarker analyses

For cMyc the median percent change from baseline was -28%. For mucin, the median percent change from baseline was 0%. For Ki67 the median percent change from baseline was 33%. There was no significant correlation between the best percentage

change from baseline in sum of longest diameters of tumor size and RNF43 mutation status. No dose-effect of WNT974 on skin AXIN2 expression was observed.

### Pharmacokinetics

Exposure to WNT974 was approximately dose-proportional (Supplementary Table S2). Following a fixed oral dose of encorafenib at 200 mg QD in combination with WNT974 oral doses ranging from 5 to 10 mg QD, PK parameters were generally comparable across all WNT974 dose levels. Mean  $C_{\min,ss}$  for WNT974 ranged from 1.30 to 2.59 ng/mL across all dose groups on day 15 with the statistical assessment indicating that steady state was achieved approximately on day 8. Median  $T_{\max}$  ranged from 1.0 to 4.0 hours across all WNT974 doses, and mean  $T_{1/2}$  was similar with increasing doses of WNT974, ranging from 3.8 to 5.4 hours. Mean  $C_{\min,ss}$  for the active metabolite of WNT974 LHA333 ranged from 1.22 to 2.54 ng/mL across all dose groups on day 15 with the statistical assessment indicating that steady state was achieved by day 15. Median  $T_{\max}$  and ranged from 1.9 to 4.0 hours across all dose groups, and mean  $T_{1/2}$  was similar across all WNT974 dose levels, ranging from 7.28 to 7.95 hours. For encorafenib, the mean AUC and values were generally comparable across all WNT974 dose levels. Median  $T_{\max}$  was observed at approximately 2 hours for all cohorts, and mean  $T_{1/2}$  was similar with increasing doses of WNT974, at 3.95 and 4.29 hours.

### Discussion

The combination of encorafenib plus WNT974 and cetuximab in patients with KRAS-WT and BRAFV600E mutated CRC harboring RNF43 mutations or RSPO fusions was associated with a high incidence of bone toxicities, demonstrated by increased susceptibility to fractures, including SAEs of spinal compression fracture, hip fracture and pathological fracture. SAEs of bone pain and hypercalcaemia were also reported. An indirect comparison of the triplet treatment combination (WNT974 + encorafenib + cetuximab) versus the doublet treatment combination (encorafenib + cetuximab) demonstrated limited improvement in clinical activity relative to the efficacy observed with the doublet treatment combination in patients with BRAF v600 mutated mCRC in a separate ongoing clinical phase 1b trial.<sup>7</sup> The ORR with doublet treatment combination was 19% and the DCR 77%. The ORR for the triplet treatment was 10% and the DCR 85%. The safety profile observed with the triplet combination, suggested that more restrictive patient selection, additional on-treatment monitoring and, potentially, prophylactic treatments to prevent bone resorption were indicated. This would have hampered the further development of the combination. The time of onset of the severe bone related toxicities ranged from 29-344 days. The early onset

of some of these SAEs was not expected based on the experience of the phase I single agent study of WNT974 (NCT01351103).<sup>16</sup> In the phase I single agent trial of WNT974 the MTD was not determined. The median duration of exposure was 29 days with a range of 1-119 days. In the study abstract of the single agent study no specific bone related toxicity was mentioned. However, hypercalcaemia occurred in 13% of the patients. The incidence of fractures in patients with mCRC cancer is unknown. Colon cancer and rectum cancer (n=3869) was not associated with an increased fracture risk in a case control study of fracture risk in patients with different types of cancer.<sup>18</sup> In a retrospective study with 104 colorectal cancer patients with bone metastases the median time from bone metastasis to the first skeletal related event was 1 month and fractures occurred in 10% of the patients.<sup>19</sup> The reported frequency of bone related AEs or hypocalcaemia was below 20% in the phase Ib study of encorafenib and cetuximab in BRAF-mutant mCRC.<sup>7</sup> A high rate of hypophosphatemia (27%, with 19% grade 3-4) was observed with this doublet which can lead to secondary bone resorption. Prolonged hypophosphatemia results in decreased bone mineralization and osteomalacia. The triplet combination with WNT974 was associated with a high rate of hypophosphatemia of 40% (25% grade 3-4). In the Food and Drug Administration (FDA) drug label of cetuximab the incidence of bone pain is described.<sup>20</sup> The incidence of grade 1-4 bone pain was 15% (4% grade 3-4) in mCRC patients treated with cetuximab monotherapy versus 8% (2% grade 3-4) of patients who received best supportive care. In patients with squamous cell carcinoma of the head and neck treated with cetuximab plus platinum-based therapy with 5-FU or platinum-based therapy with 5-FU alone the incidence of grade 1-4 hypocalcaemia was 12% (4% grade 3-4) versus 5% (1% grade 3-4). No further bone or skeleton related toxicities were mentioned. In the summary of product characteristics of the European Medicines Agency (EMA) hypocalcaemia is described as a common undesirable effect of cetuximab.<sup>21</sup> No further bone or skeleton related toxicities were mentioned.

WNT ligands are a large family of 19 secreted cysteine rich glycoproteins that trigger multiple signaling cascades essential for control of gene expression, cell fate determination, proliferation and migration.<sup>22,23</sup> WNT ligands are required for several processes such as embryonic development, tissue regeneration and protein synthesis and are also involved in bone remodeling.<sup>22,24-26</sup> Palmitoylation of WNT ligands is necessary for release of WNT ligands from the Golgi membrane to the cell plasma.<sup>13</sup> An overview of WNT signaling in bone homeostasis has been published.<sup>24</sup> WNT ligands stimulate multiple signaling cascades in various tissues, including the 'canonical'  $\beta$ -catenin pathway and are being classified as 'canonical' on the basis of their ability to inhibit glycogen synthase kinase 3 phosphorylation of  $\beta$ -catenin.<sup>10</sup> WNT ligands bind to receptor complexes containing one of 10 Fzd receptors and also to the LRP

5 or 6 co-receptors.<sup>25</sup> In bone phosphorylation of  $\beta$ -catenin results in its subsequent degradation and prevents translocation of  $\beta$ -catenin to the nucleus to stimulate bone formation and to inhibit bone resorption. WNT activation leads to bone formation, whereas WNT-inhibition leads to bone resorption. The increase in bone resorption could elucidate the high incidence of hypercalcaemia. WNT974/LGK974 inhibits porcupine<sup>27</sup>, a membrane bound O-acyl transferase which adds a palmitoyl group to WNT ligands. Inhibition of palmitoylation of WNT ligands could have contributed to the severe bone toxicity seen in this trial. In mice it has recently been shown that porcupine inhibition by WNT974/LGK974 induces deleterious effects on bone mass and strength.<sup>28</sup> These effects could be mitigated by the addition of the bisphosphonate alendronate in mice.<sup>29</sup> Further clinical trials with WNT pathway inhibitors need to coincide with intensive monitoring of bone homeostasis and include bone protective measurements in their clinical trial protocols. It would also be of interest to analyze the LRP 5/6 receptors for possibly molecular differences between tumor cells and osteoblast. This would enable a more specific targeting of tumor cells rather than osteoblasts.

The results and conclusions of the PK for WNT974 should be interpreted with caution due to a potential PK sample stability issue. Overall, 129 (29%) of 446 WNT974 and LHA333 samples were analyzed between 348 and 614 days after sample collection, which was outside of the validated storage stability range of 345 days. Of these, 91 (20%) were included in the calculation of the WNT974 and LHA333 PK parameters.

Taken together, the decision was made to discontinue enrollment and to not initiate phase 2 of the study. Therefore, the MTD for the triplet combination was not determined and there was no primary efficacy endpoint assessed.

**Role of the funding source:**

The trial was planned, initiated, and sponsored by Novartis Pharmaceuticals and Array BioPharma.

## References

1. WHO, cancer, 2018. Available at: <http://www.who.int/news-room/fact-sheets/detail/cancer>. Accessed 14 May 2018.
2. van Brummelen EMJ, de Boer A, Beijnen JH, Schellens JHM. BRAF Mutations as Predictive Biomarker for Response to Anti-EGFR Monoclonal Antibodies. *Oncologist*. 2017;22(7):864-872.
3. Tol J, Nagtegaal ID, Punt CJ a. BRAF mutation in metastatic colorectal cancer. *N Engl J Med*. 2009;361(1):98-99.
4. Souglakos J, Philips J, Wang R, et al. Prognostic and predictive value of common mutations for treatment response and survival in patients with metastatic colorectal cancer. *Br J Cancer*. 2009;101(3):465-472.
5. Van Cutsem E, Köhne CH, Láng I, et al. Cetuximab plus irinotecan, fluorouracil, and leucovorin as first-line treatment for metastatic colorectal cancer: Updated analysis of overall survival according to tumor KRAS and BRAF mutation status. *J Clin Oncol*. 2011;29(15):2011-2019.
6. Hong DS, Morris VK, El Osta B, et al. Phase IB Study of Vemurafenib in Combination with Irinotecan and Cetuximab in Patients with Metastatic Colorectal Cancer with BRAFV600E Mutation. *Cancer Discov*. 2016;6(12):1352-1365.
7. Van Geel RMJM, Taberner J, Elez E, et al. A phase 1b dose-escalation study of encorafenib and cetuximab with or without alpelisib in metastatic BRAF-mutant colorectal cancer. *Cancer Discov*. 2017;7(6):610-619.
8. Cancer Genome Atlas Network, Muzny DM, Bainbridge MN, et al. Comprehensive molecular characterization of human colon and rectal cancer. *Nature*. 2012;487(7407):330-337.
9. Giannakis M, Hodis E, Jasmine Mu X, et al. RNF43 is frequently mutated in colorectal and endometrial cancers. *Nat Genet*. 2014;46(12):1264-1266.
10. Lerner UH, Ohlsson C. The WNT system: Background and its role in bone. *J Intern Med*. 2015;277(6):630-649.
11. Bond CE, McKeone DM, Kalimutho M, et al. RNF43 and ZNRF3 are commonly altered in serrated pathway colorectal tumorigenesis. *Oncotarget*. 2016;7(43):1-12.
12. Jiang X, Hao H, Growney JD, et al. Inactivating mutations of RNF43 confer Wnt dependency in pancreatic ductal adenocarcinoma. *Proc Natl Acad Sci U S A*. 2013;110(31):12649-12654.
13. Proffitt KD, Madan B, Ke Z, et al. Pharmacological inhibition of the Wnt acyltransferase PORCN prevents growth of WNT-driven mammary cancer. *Cancer Res*. 2013;73(2):502-507.
14. Koo BK, Spit M, Jordens I, et al. Tumour suppressor RNF43 is a stem-cell E3 ligase that induces endocytosis of Wnt receptors. *Nature*. 2012;488(7413):665-669.
15. Seshagiri S, Stawiski EW, Durinck S, et al. Recurrent R-spondin fusions in colon cancer. *Nature*. 2012;488(7413):660-664.
16. Janku F, Connolly R, LoRusso P, et al. Abstract C45: Phase I study of WNT974, a first-in-class Porcupine inhibitor, in advanced solid tumors. *Mol Cancer Ther*. 2016;14(12 Supplement 2):C45 LP-C45.
17. Neuenschwander B, Branson M, GsPoner T. Critical aspects of the Bayesian approach to phase I cancer trials. *Stat Med*. 2008;27(13):2420-2439.
18. Vestergaard P, Rejnmark L, Mosekilde L. Fracture risk in patients with different types of cancer. *Acta Oncol (Madr)*. 2009;48(1):105-115.

19. Hong R, Lin Q, Luo J, Dai Z, Wang W. Clinical features and prognosis in 104 colorectal cancer patients with bone metastases. *Zhonghua Zhong Liu Za Zhi*. 2013;35(10):787-791.
20. Drug label Erbitux available at [https://www.accessdata.fda.gov/drugsatfda\\_docs/label/2018/125084Orig1s268lbl.pdf](https://www.accessdata.fda.gov/drugsatfda_docs/label/2018/125084Orig1s268lbl.pdf) accessed 23 May 2018.
21. Summary of product characteristics Erbitux available at [http://www.ema.europa.eu/docs/en\\_GB/document\\_library/EPAR\\_-\\_Product\\_Information/human/000558/WC500029119.pdf](http://www.ema.europa.eu/docs/en_GB/document_library/EPAR_-_Product_Information/human/000558/WC500029119.pdf) accessed 24 May 2018.
22. Rijsewijk F, Schuermann M, Wagenaar E, Parren P, Weigel D, Nusse R. The *Drosophila* homology of the mouse mammary oncogene int-1 is identical to the segment polarity gene wingless. *Cell*. 1987;50(4):649-657.
23. Miller JR. The Wnts. *Genome Biol*. 2002;3(1):3001.1-3001.15.
24. Baron R, Kneissel M. WNT signaling in bone homeostasis and disease: from human mutations to treatments. *Nat Med*. 2013;19(2):179-192.
25. Niehrs C. The complex world of WNT receptor signalling. *Nat Rev Mol Cell Biol*. 2012;13(12):767-779.
26. Fathke C, Wilson L, Shah K, et al. Wnt signaling induces epithelial differentiation during cutaneous wound healing. *BMC Cell Biol*. 2006;7:4.
27. Ho SY, Keller TH. The use of porcupine inhibitors to target Wnt-driven cancers. *Bioorganic Med Chem Lett*. 2015;25(23):5472-5476.
28. Funck-Brentano T, Nilsson KH, Brommage R, et al. Porcupine inhibitors impair trabecular and cortical bone mass and strength in mice. *J Endocrinol*. 2018;238(1):13-23.
29. Madan B, McDonald MJ, Foxa GE, Diegel CR, Williams BO, Virshup DM. Bone loss from Wnt inhibition mitigated by concurrent alendronate therapy. *Bone Res*. 2018;6(1):17.



## Supplement to:

**A phase Ib/II multi-center, open label, dose escalation study of WNT974, encorafenib and cetuximab in patients with BRAFV600-mutant KRAS wild-type metastatic colorectal cancer harboring WNT pathway mutations**

## Supplementary Table S1.

Table S1. Criteria for defining dose-limited toxicities

Toxicity	DLT criteria
Blood and lymphatic system disorders	Febrile neutropenia CTCAE Grade $\geq 3$ (ANC $< 1.0 \times 10^9/L$ or $1000/mm^3$ with a single temperature of $>38.3^\circ C$ ( $101^\circ F$ ) or a sustained temperature of $\geq 38^\circ C$ ( $100.4^\circ F$ ) for more than one hour)
Investigations (Blood)	Neutrophils count CTCAE Grade $\geq 3$ for $> 7$ consecutive days Neutrophils count CTCAE Grade 4 Platelet count CTCAE Grade 3 for $> 7$ consecutive days and/or with signs of bleeding Platelet count CTCAE Grade 4
Vascular disorders Hypertension	Persistent hypertension CTCAE Grade 3 for $> 7$ consecutive days despite treatment. Hypertension CTCAE Grade 4
Nervous system disorders	Dysgeusia Grade 2 that results in clinically significant anorexia and/or dehydration.
General disorders and administration site conditions	Fatigue CTCAE Grade $\geq 3$ for $> 7$ consecutive days
Ophthalmologic	Eye disorders-Retinopathy/Uveitis -CTCAE Grade 3 for $> 21$ consecutive days confirmed by ophthalmologic examination -CTCAE Grade 4 confirmed by ophthalmologic examination Eye disorders - Retinal Vein Occlusion -Any grade Eye disorders- any other - CTCAE Grade 3 for $> 14$ consecutive days - CTCAE Grade 4
Skin and subcutaneous tissue disorders: Rash, Hand foot skin reaction (HFSR) and/or photosensitivity	Rash, HFSR or photosensitivity HFSR CTCAE Grade $\geq 3$ for $> 7$ consecutive days despite skin toxicity treatment Rash, HFSR or photosensitivity Grade 4

Table S1. (continued)

Toxicity	DLT criteria
Gastrointestinal disorders	Diarrhea <sup>b</sup> CTCAE Grade 3 for $\geq 2$ days, despite the optimal use of anti-diarrhea therapy Diarrhea <sup>b</sup> CTCAE Grade 4 Nausea/ vomiting CTCAE Grade $\geq 3$ for $\geq 2$ days, despite the optimal use of anti-emetic therapy Pancreatitis CTCAE Grade $\geq 3$
Investigations (Renal)	Serum creatinine CTCAE Grade $\geq 3$
Investigations (Hepatic)	Blood bilirubin <sup>c</sup> CTCAE Grade $\geq 3$ AST or ALT CTCAE Grade $\geq 3$ in conjunction with blood bilirubin CTCAE Grade $\geq 2$ of any duration AST or ALT CTCAE Grade $\geq 3$ for $> 7$ consecutive days AST or ALT CTCAE Grade 4 Serum alkaline phosphatase CTCAE Grade 4 for $> 7$ consecutive days
Investigations (Metabolic)	Serum lipase and/or serum amylase (asymptomatic) CTCAE Grade 3 for $> 7$ consecutive days Serum lipase and/or serum amylase (asymptomatic) CTCAE Grade 4 Serum CK/CPK CTCAE Grade $\geq 3$ for $> 7$ consecutive days Serum CK/CPK CTCAE Grade 4
Infections	Infection or fever in the absence of neutropenia if they are CTCAE Grade 3 and last $> 5$ days Infection or fever in the absence of neutropenia if they are CTCAE Grade 4
Electrolytes	CTCAE Grade 3 electrolyte abnormalities if they persist $> 7$ days despite treatment or are clinically significant CTCAE Grade 4 electrolyte abnormalities
Other toxicities	Any other CTCAE Grade $\geq 3$ toxicity except: - Grade 3 laboratory values that are deemed clinically insignificant by the investigator - Cetuximab-induced infusion reactions will not be considered a DLT
Other adverse events	Other clinically significant toxicities, including a single event or multiple occurrences of the same event that lead to a dosing delay of $> 7$ days in Cycle 1, may be considered to be DLTs by the Investigators and the Sponsor, even if not CTCAE Grade 3 or higher
Infections	Infection or fever in the absence of neutropenia if they are CTCAE Grade 3 and last $> 5$ days Infection or fever in the absence of neutropenia if they are CTCAE Grade 4
Electrolytes	CTCAE Grade 3 electrolyte abnormalities if they persist $> 7$ days despite treatment or are clinically significant CTCAE Grade 4 electrolyte abnormalities

Table S1. (continued)

Toxicity	DLT criteria
Other toxicities	Any other CTCAE Grade $\geq$ 3 toxicity except: - Grade 3 laboratory values that are deemed clinically insignificant by the investigator - Cetuximab-induced infusion reactions will not be considered a DLT
Other adverse events	Other clinically significant toxicities, including a single event or multiple occurrences of the same event that lead to a dosing delay of > 7 days in Cycle 1, may be considered to be DLTs by the Investigators and the Sponsor, even if not CTCAE Grade 3 or higher

*Abbreviations:* ALT=alanine aminotransferase, ANC=absolute neutrophil count, AST=aspartate aminotransferase, CK/CPK=creatinine kinase, CTCAE=Common Terminology Criteria for Adverse Events, DLT=dose-limiting toxicity, HFSR=hand foot skin reaction.

Note: CTCAE version 4.03 will be used for all grading.

<sup>a</sup> G-CSF may be used to treat patients who have developed dose-limiting neutropenia, as per institutional guidelines, following discontinuation of WNT974 and LGX818 treatment.

<sup>b</sup> Optimal therapy for vomiting or diarrhea will be based in institutional guidelines, with consideration of the prohibited medications listed in this protocol.

<sup>c</sup> Refers to total bilirubin.

## Supplementary Table S2.

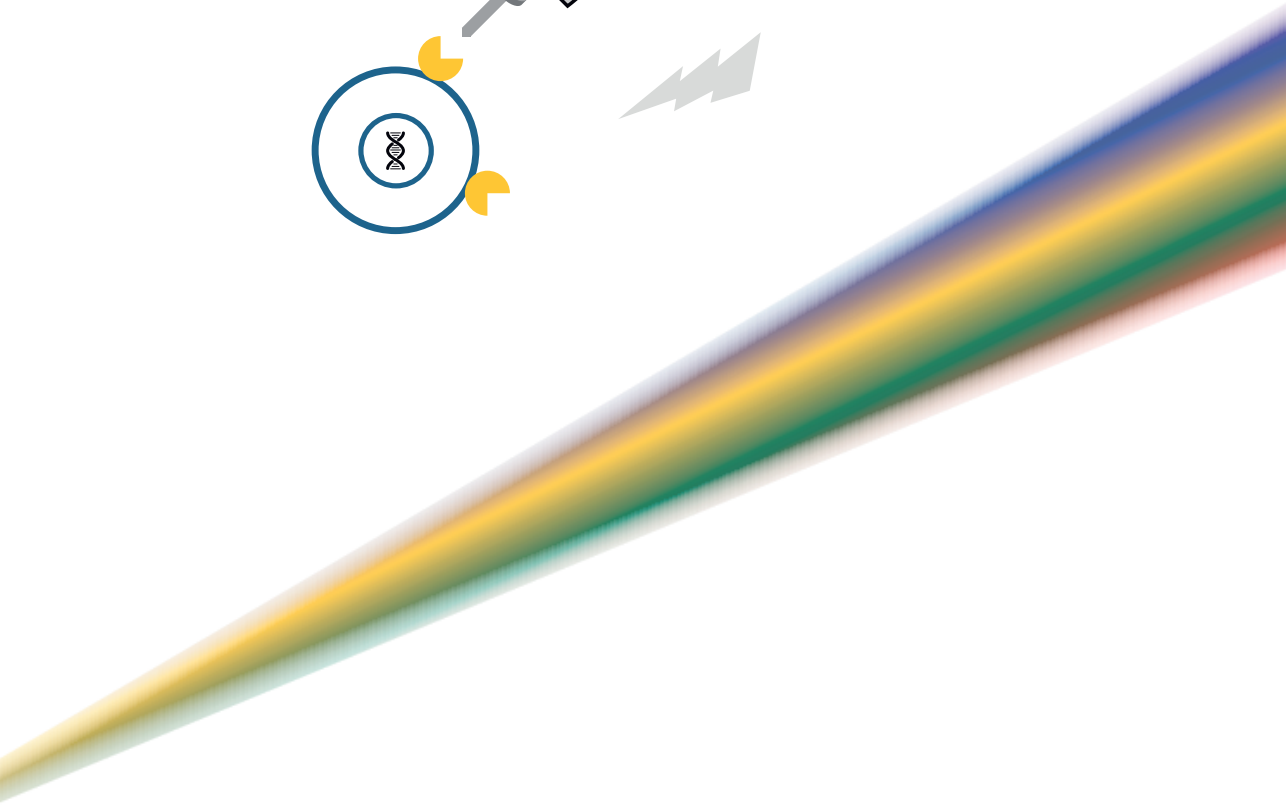
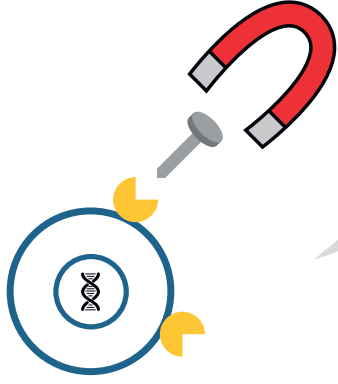
Table S2. Pharmacokinetic parameters of WNT974, LHA333 and encorafenib in patients at steady state (cycle 1 day 15)

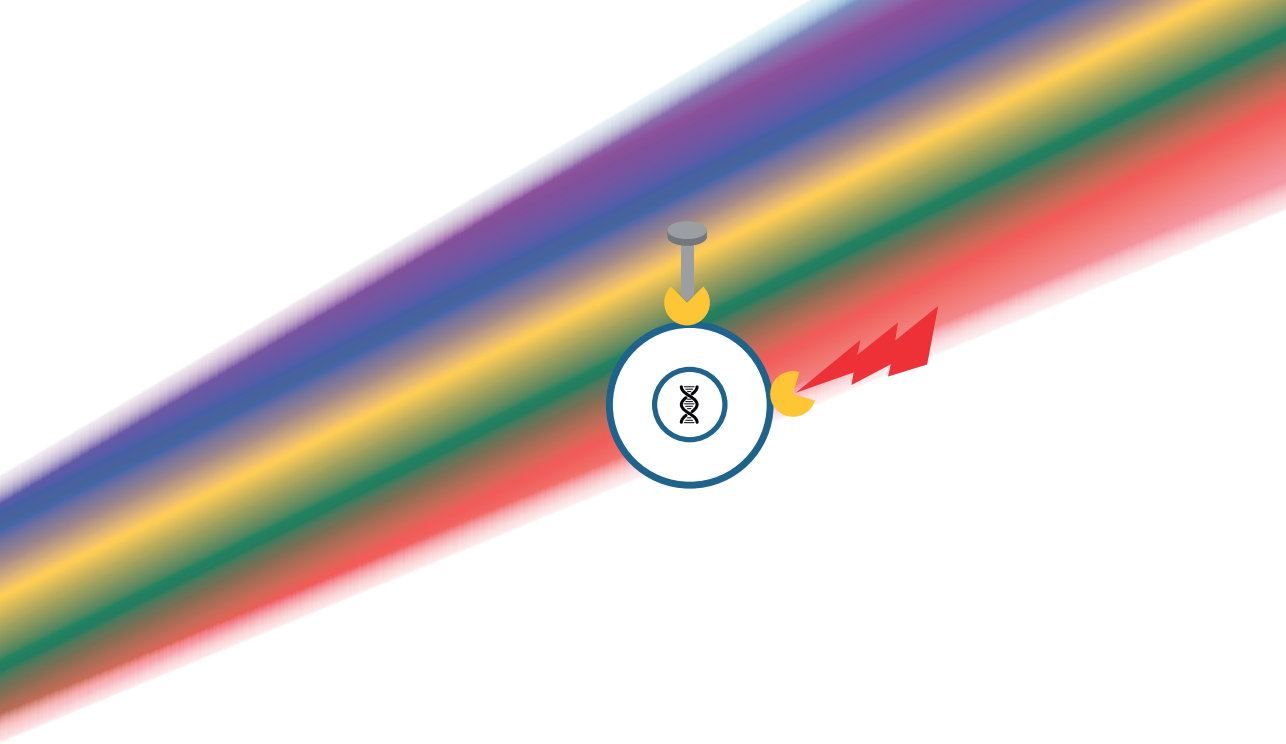
Treatment	C <sub>max</sub> (ng/mL)*	T <sub>max</sub> (h)†	AUC <sub>tau</sub> (h.ng/mL)*
WNT974 PK			
5 mg WNT974 (n = 9)	51.0 (23.2)	1.0 (0.5-5.5)	227 (83.1)
7.5 mg WNT974 (n = 5)	93.4 (55.7)	1.0 (0.5-3.0)	384 (109)
10 mg WNT974 (n = 3)	42.9 (37.1)	4.0 (1.0-7.2)	542 (101)
LHA333 PK			
5 mg WNT974 (n = 9)	13.3 (7.48)	2.0 (0.9-6.5)	141 <sup>a</sup> (96.7)
7.5 mg WNT974 (n = 5)	25.5 (8.03)	2.0 (0.5-4.0)	241 (63.7)
10 mg WNT974 (n = 3)	14.0 (12.9)	4.0 (2.0-7.2)	291 <sup>b</sup> (101)
Encorafenib PK			
5 mg WNT974 (n = 9)	3080 (1440)	2.0 (0.5-5.5)	13500 (5380)
7.5 mg WNT974 (n = 5)	3250 (1170)	1.0 (1.0-4.0)	13000 (3450)
10 mg WNT974 (n = 3)	1440 (1340)	4.0 (1.0-7.2)	17400 <sup>b</sup> (7470)

\*Mean (SD)

†Median (minimum, maximum) *Abbreviations:* AUC<sub>tau</sub>, area under the plasma concentration time curve for a dosing interval, C<sub>max</sub>, maximum plasma concentration, PK, pharmacokinetics; T<sub>max</sub>, time of maximum plasma concentration.<sup>a</sup> n=8<sup>b</sup> n=2







# Chapter 8

**Observations of severe bone toxicity in  
a phase 1 dose escalation combination  
trial of anticancer agents to inhibit  
EGFR, BRAF and WNT pathways in colon  
carcinoma**

Mark T.J. van Bussel

*To be submitted*

## Summary

More than 90% of colorectal cancers (CRC) have alterations in WNT signaling. Eight to ten percent of patients with metastatic KRAS-WT colorectal cancer have BRAF mutations and do not benefit from EGFR antibodies like cetuximab and panitumumab. Addition of a porcupine inhibitor seems an attractive approach to increase the response rate in patients with BRAFV600 mutated KRAS-WT metastatic (mCRC) with WNT alterations. Patients with BRAFV600E mutated KRAS-WT CRC with WNT alterations in RNF43 and/or RSPO fusion were treated with a BRAF inhibitor (encorafenib), plus a monoclonal antibody targeting EGFR (cetuximab) and a porcupine inhibitor (WNT974). The combination of encorafenib plus WNT974 and cetuximab was associated with severe bone toxicities. A 66-year-old male patient with BRAF V600E mutated KRAS<sup>wt</sup> mCRC and a RNF43 mutation and a 70-year-old man diagnosed with stage IV BRAF V600E mutated KRAS<sup>wt</sup> mCRC and a RNF43 mutation are described in this case report. Limited efficacy data, safety concerns and the need for more restrictive patient selection led to the decision to discontinue the enrolment. Moreover, additional on-treatment monitoring and, potentially, prophylactic treatments to prevent bone resorption could have been required, which would have hindered further development of the combination. Therefore, the decision was made to discontinue enrollment and to not initiate phase 2 of study CWNT974X2102C.



## Introduction

WNTs are a large family of 19 secreted cysteine rich glycoproteins that trigger multiple signaling cascades essential for control of gene expression, cell fate determination, proliferation and migration.<sup>1,2</sup> WNTs are required for several processes such as embryonic development, tissue regeneration and protein synthesis and are also involved in bone remodeling.<sup>1,3-5</sup> Palmitoylation of WNT-ligands is necessary for release of WNT ligands from the Golgi membrane to the cell plasma.<sup>6</sup> WNTs bind to receptor complexes containing one of 10 Frizzled (Fzd) receptors and also to the low-density lipoprotein receptor-related protein (LRP) 5 or 6 co-receptors where they stimulate multiple signaling cascades in various tissues, including the “canonical”  $\beta$ -catenin pathway and are being classified as “canonical” on the basis of their ability to inhibit glycogen synthase kinase 3 phosphorylation of  $\beta$ -catenin.<sup>4,7</sup> In bone, phosphorylation of  $\beta$ -catenin results in its degradation and prevents translocation of  $\beta$ -catenin to the nucleus to stimulate bone formation and to inhibit bone resorption.<sup>3</sup> WNT inhibition can therefore result in a reduced bone formation and an increased resorption. Since the discovery of the WNT pathway, many attempts have been explored to address this pathway as a therapeutic target to reduce tumor growth and to treat osteoporosis. However, finding a tissue specific WNT inhibitor is challenging. In colon carcinoma, WNT signaling is often upregulated.<sup>8,9</sup> Accordingly, WNT974 (formerly LGK974) has been developed, which is an inhibitor of the WNT pathway by porcupine inhibition.<sup>10</sup> Porcupine is a membrane bound O-acyl transferase which adds a palmitoyl group to WNT ligands. WNT974/LGK974 inhibits porcupine and can inhibit WNT signaling. E3 ubiquitin-protein ligase RNF43 inhibits WNT-signaling under normal conditions.<sup>11</sup> Mutations in RNF43 lead to activation of WNT signaling. Mutations in the WNT pathway co-occur frequently with BRAF-mutations and induce tumor growth.<sup>12</sup> Combination therapy with EGFR inhibitors, BRAF inhibitors and WNT inhibitors could potentially inhibit tumor growth in patients with mutations in BRAF and in the WNT pathway. This strategy has been explored in the phase IB/II clinical trial NCT02278133. Unfortunately, some patients in this trial developed severe bone toxicity. Two of these patients are described in this case report.

### Patient 1 (115)

This patient was initially diagnosed with stage IIIB colorectal cancer (CRC). The 66-year-old male patient underwent hemicolectomy with adjuvant capecitabine-oxaliplatin treatment for colon carcinoma. After 11 months he developed progressive disease with liver metastasis. Next, the patient was treated with irinotecan-bevacizumab. The patient had stable disease for 14 months. At disease progression, stage IVB, the patient was referred to The Netherlands Cancer Institute to explore

treatment opportunities in clinical trials. The patient was screened for a phase I clinical trial with an EGFR inhibitor, a BRAF inhibitor and a porcupine inhibitor in CRC because of his tumor type. Molecular prescreening revealed a KRAS<sup>wt</sup> and a RNF43 mutation besides the BRAF V600E mutation therefore, the patient was eligible for the trial and treated with the EGFR inhibitor cetuximab, the BRAF inhibitor encorafenib and the porcupine inhibitor WNT974. The patient's best response was stable disease after 4 treatment cycles (16 weeks). Nonetheless, he gradually developed back pain after treatment initiation, due to vertebral collapse of Th10, which had not been present at the baseline CT-scan. No DEXA scan or data at baseline for this patient regarding bone density status was available. After two months of treatment, a grade 2 hypercalcemia developed and zoledronic acid was administered as a single infusion, rapidly resolving the hypercalcemia but inducing hypocalcemia as well. WNT974, encorafenib, cetuximab and perindopril were temporarily interrupted. Thereafter, the patient developed an acute renal dysfunction with elevated creatinine and a hypocalcemia. The patient also developed a hypophosphatemia two days after study drug interruption. Calcium and cholecalciferol treatment were started eight days after the treatment interruption. Four days later cetuximab was restarted followed by encorafenib two days later followed by the restart of WNT974 two days later. A relationship of the hypercalcemia with the study drugs is suspected due to a decrease in calcium levels which rapidly increased again after rechallenge, despite recent zoledronic acid administration. The calcium levels were above the reference range without the presence of bone metastasis. See Figure 1 for the calcium levels of patient 1 before and during the study.

A CT-scan confirmed the osteoporotic thoracic 10 collapse and a thoracic 11 increased collapse. Thereafter, he received an analgesic corset. On cycle 5 day 8 the patient was hospitalized due to back-pain, dyspnea and pleural fluid right. By then, severe bone toxicity in this trial was evident, however, the patient decided to continue the treatment. Due to a pleural drainage the study medication was shortly interrupted, but was reintroduced the next day. Due to progressive disease (malignant ascites) and clinical deterioration the patient stopped treatment 4 days later. Because of excessive pain palliative sedation was started and the patient died a few hours later. Autopsy revealed 6 rib fractures right, 3 rib fractures left and thoracic 10 and 11 collapse. Metastases were not observed at the sites of the bone fractures. Bone histology of two fragments of the iliac crest, showed a thin and porous cortex and a poor trabecular structure (see Figure 2).

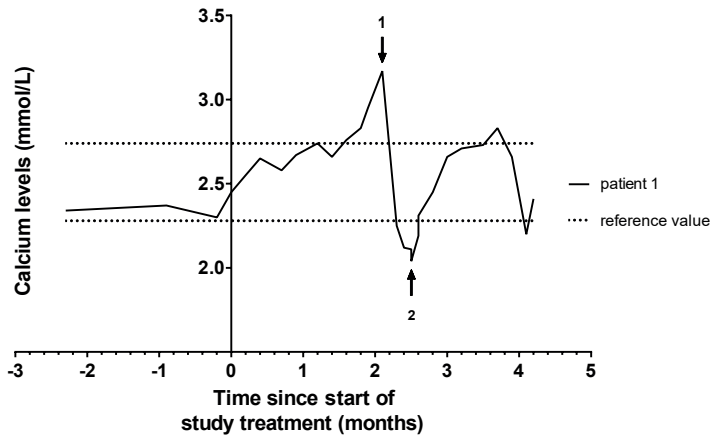


**Figure 1.** Calcium levels of patient 1

Patient 1 received zoledronic acid, furosemide and rehydration therapy with saline therapy due to hypercalcemia 2.1 months after the start of the study treatment. WNT974, encorafenib, cetuximab and perindopril were temporary interrupted (arrow 1). The patient developed an acute renal dysfunction with elevated creatinine and a hypophosphatemia two days after study drug interruption. Calcium and cholecalciferol treatment were started eight days after the treatment interruption. Four days later cetuximab was restarted followed by encorafenib two days later followed by the restart of WNT974 two days later (arrow 2). The reported calcium reference laboratory values are 2.28-2.74 mmol/L.

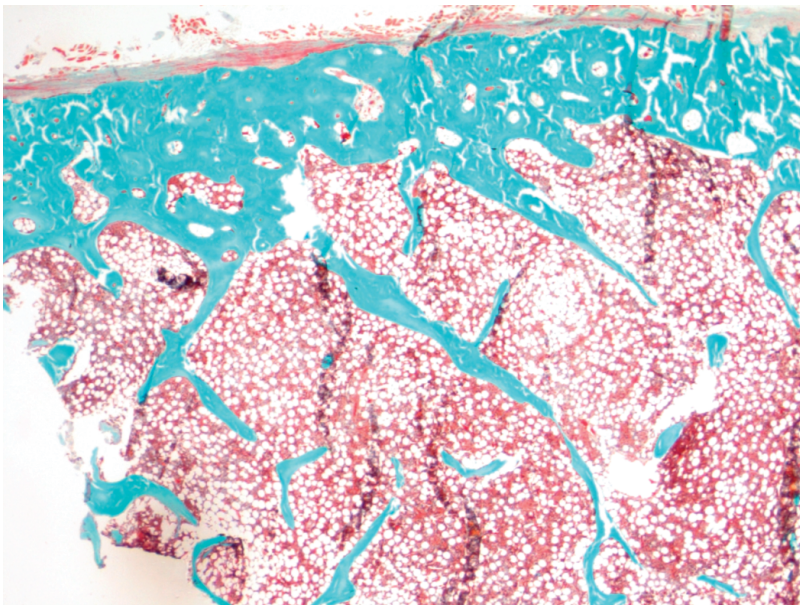


**Figure 2.**

Bone specimen showing a thin porous cortex bone and impaired trabecular structure with thin trabeculae and low connectivity. Goldner's trichrome staining, magnification 10x.

Goldner's trichrome staining total osteoid surface (bone surface covered with non-mineralized bone). Total osteoclast number was low indicating a low turnover state, as can be expected after bisphosphonate therapy. Immunohistochemistry was performed to detect the presence of known factors involved in the WNT signaling pathway including sclerostin, a bone specific endogenous WNT-antagonist, LRP5 and non-phospho  $\beta$ -catenin (Figure 3 - 5).<sup>13</sup> Sclerostin expression was normal (Figure 3).

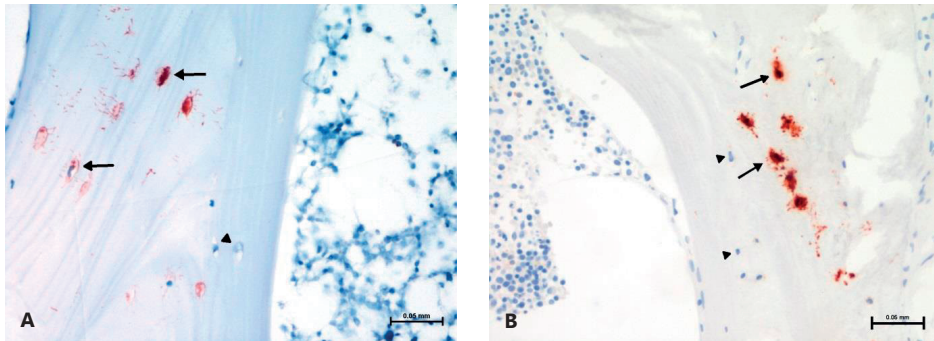


**Figure 3. Immunohistochemical detection of sclerostin in cortical bone**  
Black arrows point to osteocytes expressing sclerostin and arrow heads point to the osteocytes negative for sclerostin. Note the similar expression pattern in which both positive and negative osteocytes are shown in the cortical bone of the patient (3A) and the control bone (3B).

Since osteoblasts, the cell type expressing LRP5, were rarely observed, LRP5 expression was low (Figure 4).

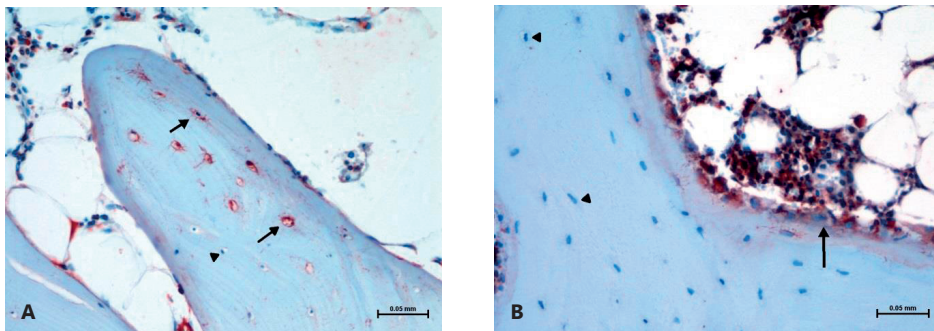


**Figure 4. Immunohistochemical detection of LRP5 in trabecular bone of patient 1**  
(A) and control bone (B). In control bone LRP5 is expressed in osteoblasts covering bone surface as indicated by the arrow in figure 4B. In the patient osteoblasts were hardly present and thus no LRP5 expression in osteoblasts was observed. However, osteocytes expressed LRP5 instead as indicated by the arrows in figure 4A. Arrow heads indicate negative osteocytes.

Non-phospho  $\beta$ -catenin, a sign of activated WNT signaling in bone, expression was seen in osteocytes (Figure 5), but not in osteoblasts since osteoblast numbers were low.

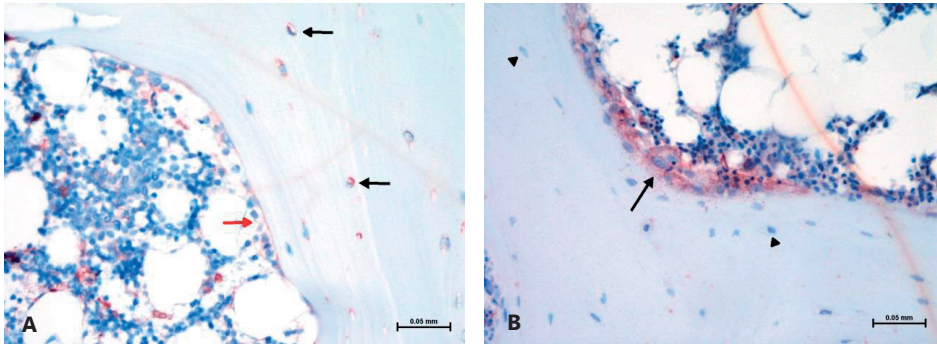


**Figure 5.**

Shows an immunohistochemical staining in bone for non phospho  $\beta$ -catenin in patient 1 (A) and a transiliac bone biopsy from an osteoporosis patient as control (B). Note the presence of non phospho  $\beta$ -catenin in the osteocytes of the patient as indicated by the black arrows in Figure 5A. Osteoblasts show a low expression of non phospho  $\beta$ -catenin as indicated by the red arrows in Figure 5A. Regularly non phospho  $\beta$ -catenin is expressed in osteoblasts as is demonstrated in the control biopsy (arrows in 5B) but not in osteocytes (arrowheads). This indicates low bone formation in the patient.

In conclusion we observed increased skeletal fragility with multiple severe osteoporotic fractures with histological signs of extreme low turnover and biochemical signs of increased resorption on treatment (hypercalcemic episodes).

### Patient 2 (117)

A 70-year-old man was diagnosed with stage IV BRAF V600E mutated metastasized CRC. The patient was treated with folinic acid, fluorouracil and oxaliplatin (FOLFOX). At the second cycle bevacizumab was added. The patient progressed after 3 months and was screened for a phase I clinical trial with an EGFR-inhibitor, a BRAF inhibitor and a porcupine inhibitor in colon carcinoma because of his tumor type. The molecular profile of the tumor showed KRAS<sup>wt</sup>, a BRAF V600E mutation and a RNF43 mutation. The patient was therefore treated with the EGFR inhibitor cetuximab, the BRAF inhibitor LGX818 and the porcupine inhibitor WNT974, which has resulted in a Partial Response (PR) for 1.5 years. Similar to patient 1, this patient also developed severe bone toxicity. Four months after initiation of the combination therapy the patient experienced a toe fracture. One month later the patient had several rib fractures. The patient had not experienced trauma or bone metastases. A DEXA scan of lumbar spine and hips showed osteopenia of the right hip and lumbar spine, normal bone density of the left hip and no indication of vertebral compression (no DEXA scan had been performed at baseline). WNT974 treatment was stopped and zoledronic acid was started, encorafenib and cetuximab were continued. A similar pattern as in patient 1 was observed. Initiation of the triple combination study treatment induced a rise

in calcium levels which was reversed after stopping WNT974 definitely and starting zoledronic acid (Figure 6).

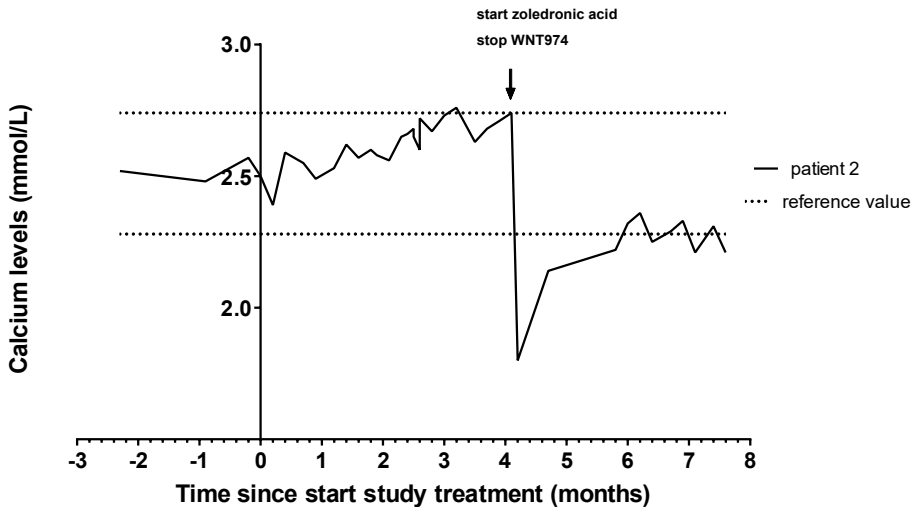


Figure 6. Calcium levels of patient 2

Calcium levels during treatment. The reported calcium reference laboratory values are 2.28-2.74 mmol/L. Patient 2 received zoledronic acid and WNT974 was stopped, encorafenib and cetuximab were continued. WNT974 was not resumed. Abbreviations used: WNT974=porcupine inhibitor.

In this patient we were able to evaluate biochemical markers of bone turnover before zoledronic acid administration. The patient gave written informed consent and donated additional fasted blood during regular laboratory visits, in order to further investigate the effect of study treatment on bone homeostasis. Bone metabolism was monitored by measuring serum levels of specific collagen fragments which are released into the circulation during bone remodeling.<sup>14</sup> Procollagen type 1 amino-terminal Propeptide (P1NP) is a bone formation marker specific for proliferating osteoblasts and fibroblasts.<sup>15</sup> Carboxy-Terminal cross-linked telopeptides of type 1 collagen (CTX) is cleaved from type 1 collagen by cathepsin-K during bone resorption and is used as a bone resorption marker. Bone biomarkers in serum may be affected by circadian rhythm and food effects therefore fasting blood samples were obtained at the same time of the day in the morning. The levels of P1NP and CTX are shown in Figure 7.

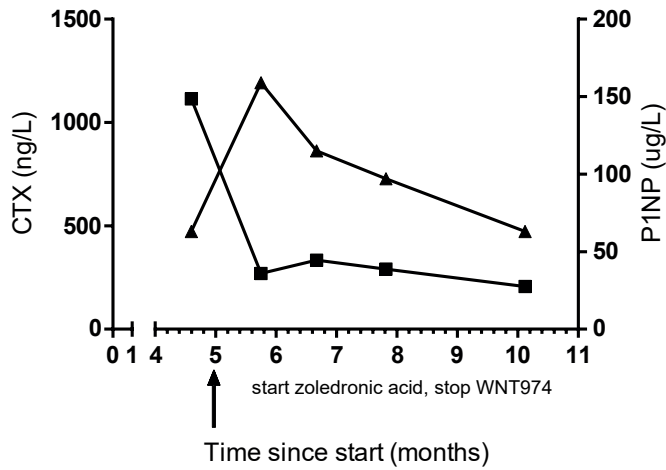


Figure 7.

The levels of the bone biomarkers P1NP (▲) and CTX (■) of patient 2. Propeptide (P1NP) is a bone formation marker specific for proliferating osteoblasts and fibroblasts. The reference value of P1NP is 22-87  $\mu\text{g/L}$ . Carboxy-Terminal cross-linked telopeptides of type 1 collagen (CTX) is a bone resorption marker and cleaved from type 1 collagen by cathepsin-K during bone resorption. CTX values below 854  $\text{ng/L}$  are considered normal. WNT974=porcupine inhibitor.

During treatment with encorafenib, cetuximab and WNT974 CTX was up to 1.3x the upper limit of normal, although no baseline value was measured. P1NP was low during treatment, but increased after stopping WNT974 and starting zoledronic acid to 1.8x the upper limit of reference values. Furthermore, we measured serum sclerostin levels at time of starting zoledronic acid and twice during bisphosphonate therapy at 2.2 and 2.3 months since the start of study treatment which were 36  $\text{pg/mL}$ , 31  $\text{pg/mL}$  and 49  $\text{pg/mL}$  respectively indicating that changes in sclerostin did not cause the change in bone turnover (reference value sclerostin 40.0  $\text{pg/mL}$ ; 95% CI 37.2 to 42.9  $\text{pg/mL}$ ).<sup>16</sup> The changes in bone turnover markers after starting zoledronic acid are consistent with its known effects. On study day 210 a DEXA scan of the lumbar spine and hips showed normal bone density of both hips and osteopenia of the lumbar spine without indication of vertebral compression. On study day 211, approximately 2 months after discontinuation of WNT974 and initiation of zoledronic acid, a CT of the chest and abdomen showed stable disease with unchanged liver metastases and three rib fractures right and two rib fractures left. The patient continued on doublet therapy with encorafenib and cetuximab and on study day 253, a repeated CT scan of the chest and abdomen showed stable disease and a large number of rib fractures of varying ages bilaterally. In summary, this patient developed skeletal fragility with biochemical signs of suppressed bone formation and increased bone resorption, thus uncoupling of formation and resorption during study treatment.

## Discussion

Detailed overviews about WNT signaling in bone homeostasis have been published.<sup>3</sup> WNT activation leads to bone formation, whereas WNT inhibition leads to bone resorption. WNT974/LGK974 inhibits porcupine, a membrane bound O-acyl transferase which adds a palmitoyl group to WNT ligands.<sup>10</sup> The palmitoylation of WNT ligands is necessary for release of WNT-ligands from the Golgi membrane to the plasma. Inhibition of palmitoylation of WNT ligands could have contributed to the severe bone toxicity seen in this trial. Since the biopsy material was gathered post mortem and especially post-bisphosphonate therapy we have to rely on the biochemistry obtained during treatment since zoledronic acid induces osteoclast apoptosis.<sup>17</sup> However, the specimens obtained are still very useful to fully comprehend the observed toxicity. In mice it has been shown that porcupine inhibition increased bone marrow adiposity.<sup>18</sup> Inhibition of DNA methylation by 5-aza-2'-deoxycytidine in preadipocytes inhibited adipogenesis and promoted osteoblastogenesis.<sup>19</sup> This coincided with up-regulation of Wnt10a. The effects of 5-aza-2'-deoxycytidine on osteoblastogenesis were prevented by the porcupine inhibitor IWP-2. Perhaps alterations of bone cell differentiation by the study treatment in patient 1 could explain the observation that osteoblasts were hardly present in trabecular bone of patient 1 shown in Figure 4. Osteocytes have a long-life span and constitute 90% of the bone cells and express LRP5 and were present in trabecular bone of patient 1.<sup>20,21</sup> In patient 2 bone turnover makers (BTMs) P1NP a marker for bone formation and CTX, a marker for bone resorption were measured while on study treatment, after starting zoledronic acid and starting WNT974. Bone resorption was high while bone formation was low during study treatment, suggesting there might be an uncoupling between bone formation and resorption. However, baseline values were not available so the attribution to study treatment is unclear. In mice it has been shown that WNT974 had detrimental effects on bone and reduced the serum levels of P1NP and increased the serum levels of CTX.<sup>22</sup> Considering these biochemical findings we hypothesize that WNT974 induced this uncoupling and accordingly is responsible for the high calcium levels and severe osteoporosis, shown in the biopsy material. Importantly, however, a contribution of encorafenib and cetuximab to this process cannot be excluded, particularly as this doublet combination was reported to result in high rates of hypophosphatemia, which can lead to secondary bone resorption.<sup>23</sup> Moreover, the rate of hypercalcemia reported in patients treated with encorafenib, cetuximab, and WNT974 was 70%, compared to 13% in patients treated with single agent WNT974.<sup>24</sup>

The CTX levels in patient 2 after zoledronic acid therapy cannot be considered a reliable marker of the effects of WNT974 withdrawal since zoledronic acid is known



to be a very potent anti-bone resorption drug. Nevertheless, bone formation markers are higher than to be expected after antiresorptive therapy which further supports our hypothesis of a disruption of the bone formation/resorption balance in patients treated with the combination of cetuximab, encorafenib and WNT974.<sup>25</sup> A similar phenomenon has been observed after cessation of anti-RANKL therapy.<sup>26</sup> Upfront we did not expect this severe bone toxicity in the adult population. The results of the phase 1 monotherapy study of WNT974 were published in an abstract.<sup>24</sup> A maximum tolerated dose was not determined and 10 mg WNT974 once daily was chosen for the expansion cohorts based on pharmacokinetics, pharmacodynamics and tolerability. Of the 68 patients enrolled in the trial one patient had stable disease with tumor shrinkage of -27% at time of data cut-off. Bone toxicity was not reported in the abstract. However in 13% of the patients hypercalcemia was reported. By contrast, the combination of encorafenib, cetuximab and WNT974 resulted in hypercalcemia in 70% of the patients (35% grade 3-4).

The incidence of fractures in patients with mCRC cancer is unknown. Colon cancer and rectum cancer (n=3869) was not associated with an increased fracture risk in a case control study of fracture risk in patients with different types of cancer.<sup>27</sup> In a retrospective study with 104 colorectal cancer patients with bone metastases the median time from bone metastasis to the first skeletal related event was 1 month and fractures occurred in 10% of the patients.<sup>28</sup> The reported frequency of bone related AEs or hypocalcaemia was below 20% in the phase Ib study of encorafenib and cetuximab in BRAF-mutant mCRC.<sup>23</sup> A high rate of hypophosphatemia (27%, with 19% grade 3-4) was observed with this doublet, which can lead to secondary bone resorption. Prolonged hypophosphatemia results in decreased bone mineralization and osteomalacia. The triplet combination of encorafenib, cetuximab, and WNT974 resulted in a high rate of hypophosphatemia of 40% (25% grade 3-4). Although the single agent WNT974 report included only suspected related adverse events of any grade occurring in >10% of patients, hypophosphatemia was not reported.

In the Food and Drug Administration (FDA) drug label of cetuximab the incidence of bone pain is described.<sup>29</sup> The incidence of grade 1-4 bone pain was 15% (4% grade 3-4) in mCRC patients treated with cetuximab monotherapy versus 8% (2% grade 3-4) of patients who received best supportive care. In patients with squamous cell carcinoma of the head and neck treated with cetuximab plus platinum-based therapy with 5-FU or platinum-based therapy with 5-FU alone the incidence of grade 1-4 hypocalcaemia was 12% (4% grade 3-4) versus 5% (1% grade 3-4). No further bone or skeleton related toxicities were mentioned. In the summary of product characteristics of the European

Medicines Agency (EMA) hypocalcaemia is described as a common undesirable effect of cetuximab.<sup>30</sup> No further bone or skeleton related toxicities were mentioned.

Adult bone homeostasis is a dynamic process in which 2-5% of cortical bone is being remodeled each year in a normal situation.<sup>31</sup> In elderly cancer patients, several treatments will influence bone remodeling that will make them already more prone to fractures. Disruption of the bone remodeling process by the combination of cetuximab, encorafenib and WNT974 may therefore cause effects leading to toxicity as observed in this trial with excessive fracture incidence. The supportive function of the skeleton becomes affected by inhibiting bone formation during the remodeling process. Drugs altering the WNT pathway need detailed pre-clinical investigation before initiating clinical studies, particularly when used in combination with other agents that may affect bone homeostasis. Possibly molecular differences between LRP5/6 receptors between tumor cells and osteoblasts exist, enabling more specific targeting of tumor cells rather than osteoblasts. In mice it has recently been shown that porcupine inhibition by WNT974/LGK974 induces deleterious effects on bone mass and strength, and that these effects could be mitigated by the addition of the bisphosphonate alendronate.<sup>18,22</sup>

In conclusion, combined inhibition of porcupine, BRAF, and EGFR seems to have detrimental effects on the skeleton and should be proceeded with caution in patients with mCRC. The safety profile observed with the triplet combination, suggested that more restrictive patient selection, additional bone biomarker monitoring and concurrent treatment with bisphosphonates needs to be considered.

### **Acknowledgements**

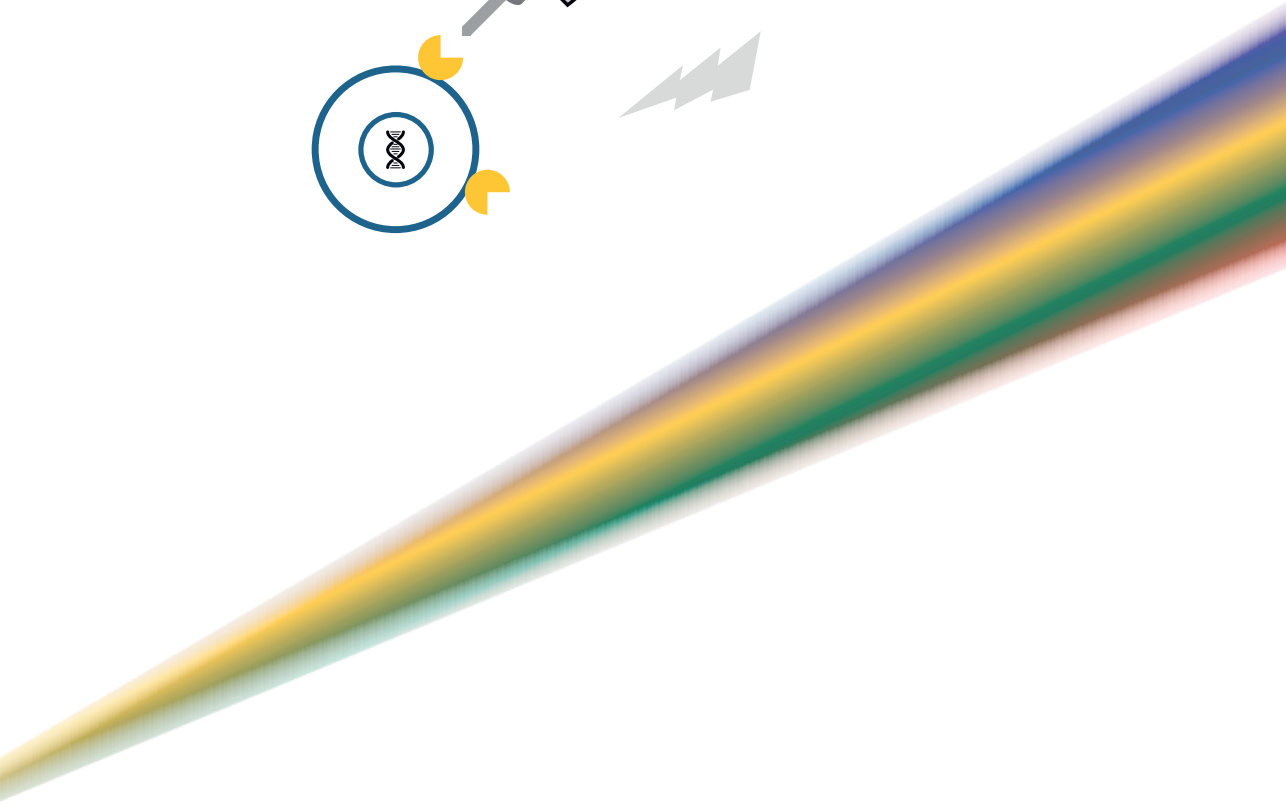
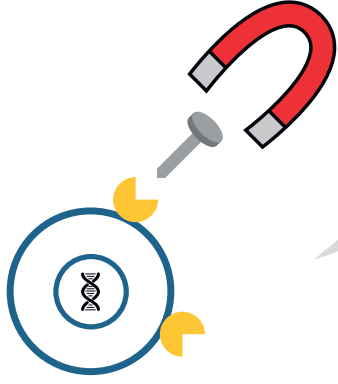
I would like to acknowledge Nathalie Bravenboer and Huib van Essen from The Department of Clinical Chemistry, VU University Medical Center, Research Institute MOVE, Amsterdam University Medical Center. I would like to acknowledge Natasha Appelman-Dijkstra from the Department of Medicine, Division of Endocrinology & Centre for Bone Quality, Leiden University Medical Center, Leiden, the Netherlands. I would like to acknowledge Petur Snaebjornsson from The Department of Pathology, The Netherlands Cancer Institute - Antoni van Leeuwenhoek Hospital, Amsterdam, The Netherlands. I would like to acknowledge NKI-AVL Core Facility Molecular Pathology & Biobanking (CFMPB) for supplying NKI-AVL Biobank material and laboratory support.

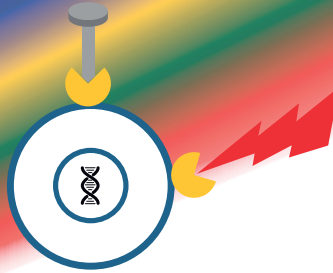
## References

1. Rijsewijk F, Schuermann M, Wagenaar E, Parren P, Weigel D, Nusse R. The Drosophila homology of the mouse mammary oncogene int-1 is identical to the segment polarity gene wingless. *Cell*. 1987;50(4):649-657.
2. Miller JR. The Wnts. *Genome Biol*. 2002;3(1):3001.1-3001.15.
3. Baron R, Kneissel M. WNT signaling in bone homeostasis and disease: from human mutations to treatments. *Nat Med*. 2013;19(2):179-192.
4. Niehrs C. The complex world of WNT receptor signalling. *Nat Rev Mol Cell Biol*. 2012;13(12):767-779.
5. Fathke C, Wilson L, Shah K, et al. Wnt signaling induces epithelial differentiation during cutaneous wound healing. *BMC Cell Biol*. 2006;7:4.
6. Proffitt KD, Madan B, Ke Z, et al. Pharmacological inhibition of the Wnt acyltransferase PORCN prevents growth of WNT-driven mammary cancer. *Cancer Res*. 2013;73(2):502-507.
7. Lerner UH, Ohlsson C. The WNT system: Background and its role in bone. *J Intern Med*. 2015;277(6):630-649.
8. Cancer Genome Atlas Network, Muzny DM, Bainbridge MN, et al. Comprehensive molecular characterization of human colon and rectal cancer. *Nature*. 2012;487(7407):330-337.
9. Giannakis M, Hodis E, Jasmine Mu X, et al. RNF43 is frequently mutated in colorectal and endometrial cancers. *Nat Genet*. 2014;46(12):1264-1266.
10. Jiang X, Hao H, Growney JD, et al. Inactivating mutations of RNF43 confer Wnt dependency in pancreatic ductal adenocarcinoma. *Proc Natl Acad Sci U S A*. 2013;110(31):12649-12654.
11. Koo BK, Spit M, Jordens I, et al. Tumour suppressor RNF43 is a stem-cell E3 ligase that induces endocytosis of Wnt receptors. *Nature*. 2012;488(7413):665-669.
12. Bond CE, McKeone DM, Kalimutho M, et al. RNF43 and ZNRF3 are commonly altered in serrated pathway colorectal tumorigenesis. *Oncotarget*. 2016;7(43):1-12.
13. Li X, Zhang Y, Kang H, et al. Sclerostin binds to LRP5/6 and antagonizes canonical Wnt signaling. *J Biol Chem*. 2005;280(20):19883-19887.
14. Naylor K, Eastell R. Bone turnover markers: use in osteoporosis. *Nat Rev Rheumatol*. 2012;8(510):379-38986.
15. Wheeler G, Elshahaly M, Tuck SP, Datta HK, van Laar JM. The clinical utility of bone marker measurements in osteoporosis. *J Transl Med*. 2013;11(1):201.
16. Van Lierop AH, Hamdy NAT, Hamersma H, et al. Patients with sclerosteosis and disease carriers: Human models of the effect of sclerostin on bone turnover. *J Bone Miner Res*. 2011;26(12):2804-2811.
17. Drug label Zometa available at [https://www.accessdata.fda.gov/drugsatfda\\_docs/label/2002/21386lbl.pdf](https://www.accessdata.fda.gov/drugsatfda_docs/label/2002/21386lbl.pdf). Accessed 20 April 2019
18. Madan B, McDonald MJ, Foxa GE, Diegel CR, Williams BO, Virshup DM. Bone loss from Wnt inhibition mitigated by concurrent alendronate therapy. *Bone Res*. 2018;6(1):17.
19. Chen YS, Wu R, Yang X, et al. Inhibiting DNA methylation switches adipogenesis to osteoblastogenesis by activating Wnt10a. *Sci Rep*. 2016;6(May):1-12.
20. Tu X, Delgado-Calle J, Condon KW, et al. Osteocytes mediate the anabolic actions of canonical Wnt/ $\beta$ -catenin signaling in bone. *Proc Natl Acad Sci*. 2015;112(5):E478-E486.
21. Cui Y, Niziolek PJ, MacDonald BT, et al. Lrp5 functions in bone to regulate bone mass. *Nat Med*. 2011;17(6):684-691.

22. Funck-Brentano T, Nilsson KH, Brommage R, et al. Porcupine inhibitors impair trabecular and cortical bone mass and strength in mice. *J Endocrinol.* 2018;238(1):13-23.
23. Van Geel RMJM, Tabernero J, Elez E, et al. A phase Ib dose-escalation study of encorafenib and cetuximab with or without alpelisib in metastatic BRAF-mutant colorectal cancer. *Cancer Discov.* 2017;7(6):610-619.
24. Janku F, Connolly R, LoRusso P, et al. Abstract C45: Phase I study of WNT974, a first-in-class Porcupine inhibitor, in advanced solid tumors. *Mol Cancer Ther.* 2016;14(12 Supplement 2):C45 LP-C45.
25. Chen F, Dai Z, Kang Y, Lv G, Keller ET, Jiang Y. Effects of zoledronic acid on bone fusion in osteoporotic patients after lumbar fusion. *Osteoporos Int.* 2016;27(4):1469-1476.
26. Anastasilakis AD, Polyzos SA, Makras P, Aubry-Rozier B, Kaouri S, Lamy O. Clinical Features of 24 Patients With Rebound-Associated Vertebral Fractures After Denosumab Discontinuation: Systematic Review and Additional Cases. *J Bone Miner Res.* 2017;32(6):1291-1296.
27. Vestergaard P, Rejnmark L, Mosekilde L. Fracture risk in patients with different types of cancer. *Acta Oncol (Madr).* 2009;48(1):105-115.
28. Hong R, Lin Q, Luo J, Dai Z, Wang W. Clinical features and prognosis in 104 colorectal cancer patients with bone metastases. *Zhonghua Zhong Liu Za Zhi.* 2013;35(10):787-791
29. Drug label Erbitux available at [https://www.accessdata.fda.gov/drugsatfda\\_docs/label/2018/125084Orig1s268lbl.pdf](https://www.accessdata.fda.gov/drugsatfda_docs/label/2018/125084Orig1s268lbl.pdf). Accessed 23 May 2018
30. Summary of product characteristics Erbitux available at [http://www.ema.europa.eu/docs/en\\_GB/document\\_library/EPAR\\_Product\\_Information/human/000558/WC500029119.pdf](http://www.ema.europa.eu/docs/en_GB/document_library/EPAR_Product_Information/human/000558/WC500029119.pdf). Accessed 24 May 2018.
31. Hadjidakis DJ, Androulakis II. Bone remodeling. *Ann N Y Acad Sci.* 2006;1092:385-396.







# Chapter 9

## A first-in-man phase I study of the DNA-dependent protein kinase inhibitor M3814 in patients with advanced solid tumors

Mark T.J. van Bussel  
Ahmad Awada  
Maja J.A. de Jonge  
Morten Mau-Sørensen  
Dorte Nielsen  
Patrick Schöffski  
Henk Verheul  
Barbara Sarholz  
Karin Berghoff  
Samer El Bawab  
Mirjam Kuipers  
Ivan Diaz-Padilla  
Lars Damstrup  
Jan H.M. Schellens

*Submitted*

## Summary

### Purpose

This open-label phase I trial (NCT02316197) aimed to determine the maximum-tolerated dose (MTD) and/or recommended phase II dose (RP2D) of M3814, a DNA-dependent protein kinase inhibitor in patients with advanced solid tumors. Secondary/exploratory objectives were to explore the safety, tolerability, pharmacokinetic and pharmacodynamic profiles, and clinical activity.

### Patients and Methods

Patients aged  $\geq 18$  years with advanced solid tumors received M3814 continuously in 21-day cycles starting at 100 mg once daily (QD). Subsequent cohorts received: 200 mg QD; 150 mg twice daily (BID); 200 mg BID; 300 mg BID; and 400 mg BID.

### Results

Thirty-one patients were included (median age 66 years, 61% male, 87% Caucasian). One dose-limiting toxicity was reported (300 mg BID cohort): a combination of non-serious adverse events (AEs) and a long recovery duration following treatment discontinuation. Nausea ( $n=8$ ), vomiting ( $n=6$ ), fatigue ( $n=6$ ), and pyrexia ( $n=5$ ) were the most frequently reported M3814-related AEs. The most common grade 3 M3814-related AEs were maculo-papular rash ( $n=4$ ) and nausea ( $n=2$ ). M3814 was quickly absorbed into the systemic circulation (median  $T_{max}$ : 1.1-2.5 hours). Overall, a consistent and marked decrease in the pharmacodynamic biomarker (phospho-DNA-PK/total DNA-PK) level was observed in peripheral blood mononuclear cells at 3 and 6 hours after intake. Twelve patients (39%) had a best overall response of stable disease (seven of these patients experienced stable disease for  $\geq 12$  weeks).

### Conclusions

M3814 showed an acceptable safety profile. The MTD of M3814 was not reached at 400 mg BID. The RP2D for M3814 monotherapy was declared as 400 mg BID.



## Introduction

DNA double-strand breaks (DSBs) are the most cytotoxic type of DNA lesions, which if left unrepaired, can cause cell-cycle arrest via checkpoint activation and subsequent cell death.<sup>1</sup> Complex signaling pathways, collectively termed the DNA damage response (DDR), exist within cells to detect and repair DNA damage, including DNA DSBs.<sup>1</sup> Defects in DDR pathways can lead to the accumulation of non-lethal DNA damage and genomic instability, which is a hallmark of many cancers and drives tumorigenesis.<sup>2</sup> Many anticancer treatments, such as radiotherapy and some chemotherapies, work by inducing DNA DSBs in tumor cells. The efficacy of such treatments can be compromised by the efficient repair of DNA damage through activation of the DDR, including DNA-dependent protein kinase (DNA-PK).<sup>3</sup> DNA-PK is a serine/threonine protein kinase that plays a critical role in the DDR and regulates DNA DSB repair via the non-homologous end joining (NHEJ) pathway.<sup>4,5</sup> M3814 (previously known as MSC2490484A) is an orally administered, small-molecule, selective DNA-PK inhibitor that blocks DNA-PK kinase activity at sub-nanomolar concentrations, inhibiting its ability to function in the DNA repair process leading to the persistence of DNA DSBs and subsequent cell death.<sup>6-8</sup> M3814 demonstrated selectivity against a broad panel of kinases, including wild-type and mutant kinases belonging to the phosphoinositide 3 kinase (PI3K) family, which were affected by strongly reduced potency (>100-fold split).<sup>7</sup> Additionally, M3814 demonstrated synergy with radiotherapy and selected chemotherapies in preclinical studies, by preventing the repair of radiation- or chemotherapy-induced DNA DSBs via the NHEJ pathway.<sup>6-10</sup> The purpose of this first-in-man, open-label phase I trial (NCT02316197) was to determine the maximum-tolerated dose (MTD) and/or the recommended phase II dose (RP2D) of M3814, and to explore the safety, tolerability, pharmacokinetic (PK) and pharmacodynamic (PD) profiles, and clinical activity of M3814 administered as a single agent in patients with advanced tumors likely to have alterations in DNA repair mechanisms. To our knowledge, this is the first full report of an oral DNA-PK inhibitor in humans. The results of this study have been partially presented at the American Society for Clinical Oncology Annual Meeting in 2017 and the European Society for Clinical Oncology Annual Meeting in 2018.<sup>11,12</sup>

## Patients and Methods

### Trial design

This phase I, first-in-man, open-label, dose-escalation study (NCT02316197) was designed to explore the safety, tolerability, PK and PD profile, and clinical activity of M3814 administered daily as a single agent to patients with advanced solid tumors

likely to have alterations in DNA repair mechanisms. Following screening and baseline evaluations, patients received M3814 until disease progression, unacceptable toxicity, withdrawal of consent, or other reasons necessitating withdrawal (Supplementary Figure 1).

Dose escalation was by use of a standard “3+3” design, based on the presence/absence of dose-limiting toxicities (DLTs). Patients in the first dose cohort received M3814 continuously in 21-day cycles at a starting dose of 100 mg once daily (QD). This starting dose was considered to have acceptable safety and be close to the predicted biological effective dose range of 200-800 mg daily (100-400 mg BID) in the monotherapy setting based on predicted human PK parameters and the results of nonclinical PK/PD modeling (unpublished data). Patients in the second cohort received M3814 at a dose of 200 mg QD. Subsequent cohorts received ascending doses of M3814 as follows: 150 mg twice daily (BID); 200 mg BID; 300 mg BID; and 400 mg BID. The study was conducted in accordance with the ethical principles of the International Council for Harmonisation guideline for Good Clinical Practice and the Declaration of Helsinki, as well as with applicable local regulations.

## **Patients**

Patients aged  $\geq 18$  years with advanced solid tumors, preferably those likely to harbor alterations in DNA repair mechanisms (triple-negative breast, serous epithelial ovary, bladder, microsatellite instability-high colon, lung, castration-resistant prostate, stomach, or uterine cancer) for whom no other standard surgical, radiation, or systemic anticancer therapies were available, and with tumor accessible for biopsies, and measurable or evaluable disease by Response Evaluation Criteria in Solid Tumors (RECIST) version 1.1<sup>13</sup> were eligible for inclusion in the study. Patients were excluded from the study if they had an Eastern Cooperative Oncology Performance Status (ECOG PS)  $>1$ ; had received any anticancer therapy (except for luteinizing hormone-releasing hormone analogs) or any other investigational agent within 28 days of the first dose of M3814; had received extensive radiotherapy on  $>30\%$  of bone marrow reserves or prior bone marrow/stem cell transplantation within 5 years of study start; or were receiving medications/herbal supplements known to be potent inhibitors or inducers of CYP3A. All patients provided written informed consent. As preclinical studies found M3814 to have a weak inhibitory effect after ADP-induced platelet aggregation, but not after arachidonic acid activation (data not shown), the clinical relevance of this observation was evaluated in six aspirin-naïve patients (defined as being off aspirin for at least 14 days before study Day 1) treated at the RP2D were tested for alterations in platelet aggregation.

## Study objectives and endpoints

The primary objective was to determine the MTD and/or the RP2D of M3814 assessed as the proportion of patients who experienced at least one DLT during the first 21-day treatment cycle. The MTD was to be determined as the dose level below the dose at which two out of six patients experienced a DLT. Once the MTD was established, the RP2D was to be defined by the Safety Monitoring Committee (SMC), either at the MTD level or another dose level, depending on the available safety, efficacy, PK, and PD data. A DLT was defined as any of the following toxicities considered to be possibly related to M3814 by the sponsor and/or investigator during Cycle 1: a treatment-emergent adverse event (TEAE) of potential clinical significance such that further dose escalation would expose patients to unacceptable risk; evidence of possible treatment-related hepatocellular injury for  $\geq 3$  days, any grade 4 liver enzyme elevation; any grade  $\geq 3$  toxicity (defined according to National Cancer Institute Common Terminology Criteria for Adverse Events [NCI CTCAE] version 4.03, and excluding diarrhea, nausea, and vomiting of  $< 3$  days duration following adequate therapy, grade 3 skin toxicity resolving to grade  $\leq 2$  with supporting measures within 7 days, fatigue or headache of  $< 7$  days duration following initiation of adequate supportive care, any other single laboratory value out of the normal range that was not correlated to clinically significant symptoms, grade 3 thrombocytopenia without bleeding; neutropenia lasting for  $\geq 5$  days and not associated with fever); any toxicity related to study drug resulting in  $\geq 20\%$  of the planned dose to be missed in Cycle 1. In addition, a DLT could be identified by the SMC as any TEAE that impaired daily function or abnormality occurring in patients treated with M3814 at any time during the dose escalation part of the study. Secondary objectives included evaluation of the safety and tolerability of M3814, assessment of PK, and exploration of antitumor activity. Safety was assessed through the recording, reporting, and analysis of baseline medical conditions, AEs, physical examination findings, including vital signs and monitoring for bleeding, laboratory tests, ECOG PS, and 12-lead electrocardiograms. PK was assessed using blood samples collected pre-treatment and on-treatment. The following PK parameters were evaluated: maximum observed concentration ( $C_{max}$ ); dose-normalized  $C_{max}$  ( $C_{max}/\text{dose}$ ); time to  $C_{max}$  ( $t_{max}$ ); area under the plasma concentration-time curve (AUC) from 0 to 12 hours ( $AUC_{0-12}$ ); dose-normalized  $AUC_{0-12}$  ( $AUC_{0-12}/\text{dose}$ ); AUC from 0 to infinity ( $AUC_{0-\infty}$ ; Day 1 only); apparent elimination half-life ( $t_{1/2}$ ); apparent total body clearance of drug ( $C_{L/f}$ ); apparent total body clearance at steady state of drug ( $C_{Lss/f}$ ; Cycle 2 only); apparent volume of distribution during terminal phase ( $V_{z/f}$ ); accumulation ratio for AUC ( $R_{acc(AUC)}$ ); and accumulation ratio for  $C_{max}$  ( $R_{acc(Cmax)}$ ). Tumor response was evaluated according to RECIST (version 1.1). Target and nontarget lesions were measured by computed tomography or magnetic resonance imaging. Exploratory objectives included assessing the PD of M3814 in

peripheral blood mononuclear cells (PBMCs), isolated from serial blood samples collected pre-treatment and on-treatment. PBMCs were stimulated *ex vivo* with the DNA-damaging agent bleomycin to induce DNA-PK activity. The PD biomarker of M3814 was the level of autophosphorylated form of DNA-PK on Ser<sup>2056</sup> (p-DNA-PK) normalized by the total DNA-PK (t-DNA-PK), as measured by the Erenna® Immunoassay System in the PBMC lysates, and was calculated as the p-DNA-PK concentration (ng/mL)/t-DNA-PK concentration (ng/mL). DNA-PK inhibition by M3814 on-treatment was expressed as the percentage change of the PD biomarker versus pre-treatment value.

## Analyses

The cut-off for the final analysis was when the last patient completed the dose-escalation phase. The All Patients Analysis Set comprised all patients who provided informed consent (screening failures plus enrolled patients) and used to describe patient disposition and deaths. The Safety Analysis Set included patients who received at least one dose of M3814 and used for all baseline and safety (except for DLTs) summaries. The Efficacy Analysis Set, including patients who received at least one treatment dose, was used for all efficacy summaries. The Dose-Escalation Analysis Set included patients treated in dose-escalation cohorts who received at least 80% of M3814 planned doses in the first treatment cycle or who experienced a DLT during the first treatment cycle regardless of the amount of drug received (used for DLT summary). The PK Analysis Set (Cycles 1 and 2) included patients who received at least the first dose of M3814 and provided PK samples as per protocol for at least 24 hours following the first dose on Day 1 of Cycle 1 for the QD regimen, or for at least 12 hours following first dose on Day 1 of Cycle 1 for the BID regimen. The Biomarker/ Pharmacogenomics Analysis Set included patients who received at least the first dose of study drug and provided at least one pre-dose sample and one post-dose sample. TEAEs, defined as AEs observed from the first dose of M3814 to 30 days after the last dose, were summarized according to MedDRA (v20.0) preferred term and system organ class. All statistical analyses (except for PK) were performed using SAS 9.1.3 or higher. Tumor assessments, based on investigator evaluations of target, non-target, and new lesions according to RECIST (version 1.1) were used to derive the best overall response. Trial data were summarized by dose level.

## Results

### Patient baseline demographics and disease characteristics

Patient disposition is shown in Figure 1. Overall, 39 patients were screened. Eight patients did not receive M3814: six did not meet the eligibility criteria, one withdrew

consent, and one did not continue beyond screening due to a serious adverse event (intestinal obstruction). Thirty-one patients were included in the study (100 mg QD,  $n = 3$ ; 200 mg QD,  $n = 3$ ; 150 mg BID,  $n = 3$ ; 200 mg BID,  $n = 3$ ; 300 mg BID,  $n = 9$ ; 400 mg BID,  $n = 4$ ; 400 mg BID [declared as the RP2D], aspirin-naïve,  $n = 6$ ). The numbers of patients included in each of the analysis sets were as follows: Safety/Efficacy Analysis Set,  $n = 31$ ; Dose-Escalation Analysis Set,  $n = 21$ ; PK Analysis Set,  $n = 31$ ; Biomarker Analysis Set,  $n = 31$ .

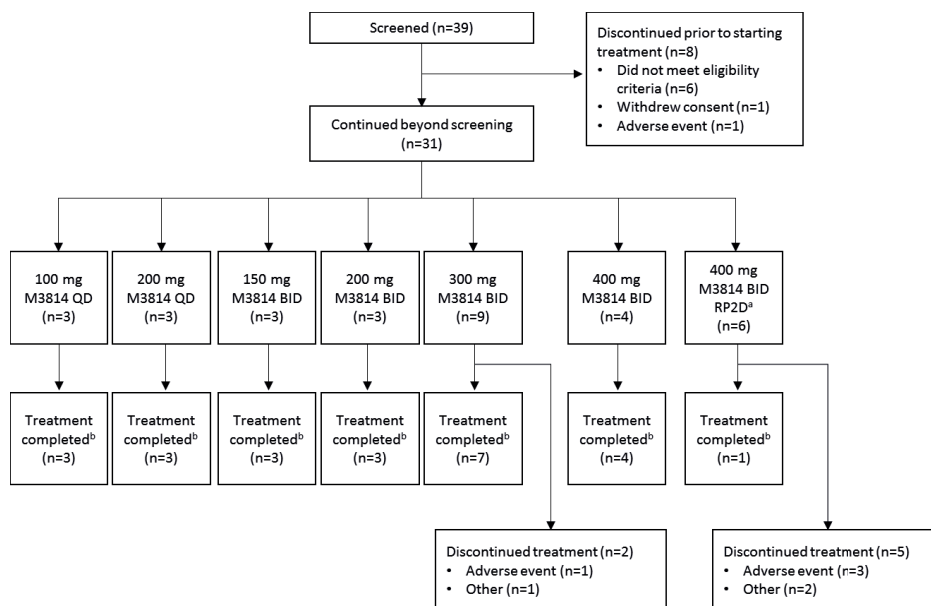


**Figure 1. Patient disposition**

<sup>a</sup>The six patients in the RP2D cohort were aspirin-naïve.

<sup>b</sup>Patients were treated until disease progression or death.

*Abbreviations:* BID=twice daily, RP2D=recommended phase II dose, QD=once daily.

Baseline characteristics are presented in Table 1. The median (range) age was 66 (25-78) years; 19/31 (61%) patients were male; 27/31 (87%) were Caucasian; ECOG PS at baseline was 0 in 32% of patients and 1 in 68% of patients.

All patients were treated until disease progression or death, except for two patients in the 300 mg BID cohort (one discontinued due to an AE [DLT, due to a combination of non-serious AEs and the long duration of recovery following treatment discontinuation] and the other due to patient request), and five patients in the 400 mg BID (RP2D) cohort who discontinued due to AEs ( $n = 3$ ; colitis in one patient [unrelated to M3814]; maculo-papular rash in one patient [related to M3814]; nausea and papular rash in one patient [both related to M3814]; all were considered serious and all were grade 3)

and other reasons ( $n = 2$ ; both clinical progressive disease). The study was terminated once the RP2D was declared.

**Table 1. Baseline patient demographics and disease characteristics**

Parameter	Categories/characteristics	Total
Sex, n (%)	Male	19 (61)
	Female	12 (39)
Race, n (%)	Caucasian	27 (87)
	Other	4 (13)
Age (years)	Mean (SD)	62 (12)
Primary tumor location*, n (%)	Colorectal	10 (33)
	Head and neck	3 (10)
	Liver	3 (10)
	Lung	2 (6)
	Bone	2 (6)
	Skin	2 (6)
	Bladder	1 (3)
	Breast	1 (3)
	Kidney	1 (3)
	Lymph nodes	1 (3)
	Ovary	1 (3)
	Pancreas	1 (3)
	Urinary system	1 (3)
Uterus	1 (3)	

\*Site of primary tumor not recorded for 1 patient. Abbreviations: SD=standard deviation.

### Dose-limiting toxicities and maximum tolerated dose

Safety evaluation was based on M3814 exposure of up to a maximum of 484 days (69 weeks). One DLT was reported for one patient in the 300 mg BID cohort: no individual AE qualified as a DLT; however, a combination of non-serious AEs (stomatitis, decreased appetite, dysgeusia, erythema, urticaria, fatigue, and nausea) and a long recovery duration following treatment discontinuation was considered as a DLT. The MTD of M3814 was not reached at 400 mg BID (dose expansion was stopped at 400 mg BID), and it was decided not to conduct the dose-expansion part of the study as the tumor response to M3814 dose escalation did not support a monotherapy dose-expansion cohort. As there were no DLTs reported at the 400 mg BID dose level, this dose was declared as an acceptable RP2D. Six aspirin-naïve patients (see above) were enrolled at the RP2D to confirm the safety and tolerability and to explore the PK and PD profile of M3814.

### Safety

The median (range) treatment duration with M3814 was 6.0 (0.3-69.0) weeks. All 31 patients had at least one TEAE and most (71%) had at least one TEAE related to M3814.

Nausea ( $n = 17$ ), fatigue ( $n = 14$ ), pyrexia ( $n = 11$ ) and constipation ( $n = 10$ ) were the most common TEAEs. Nausea ( $n = 8$ ), vomiting ( $n = 6$ ), fatigue ( $n = 6$ ), and pyrexia ( $n = 5$ ) were the most frequently reported TEAEs related to M3814 (Table 2). Twenty-one patients (68%) had at least one TEAE of grade  $\geq 3$ . M3814-related grade 3 TEAEs occurred in seven (23%) patients. The most common grade 3 M3814-related TEAEs were maculo-papular rash ( $n = 4$ ) and nausea ( $n = 2$ ). There were no M3814-related grade 4 TEAEs. Seventeen patients (55%) had a serious TEAE. M3814-related serious TEAEs occurred in four (13%) patients, all at the highest dose level of 400 mg BID. M3814-related serious TEAEs were rash maculo-papular in two patients; pyrexia and rash maculo-papular in one patient; and nausea and rash maculo-papular in one patient. One patient in the 400 mg BID cohort had a TEAE leading to death (grade 5 general physical health deterioration considered unrelated to M3814). Three patients died due to disease progression; there were no treatment-related deaths (Supplementary Table 1). In the aspirin-naïve cohort (400 mg BID, RP2D) a very weak effect on platelet aggregation was observed, which was not considered a safety signal.

### Pharmacokinetics

Following oral administration, M3814 was quickly absorbed into the systemic circulation with a median  $t_{\max}$  of 1.1-2.5 hours. The exposure parameters of M3814 showed high inter-individual variability across all doses as indicated by moderate to high geometric mean %CV values (15.5-117% for  $C_{\max}$ ; 12.5-124% for  $AUC_{0-12}$ ). Minimal to slight accumulation of M3814 after QD and BID dosing, respectively, was observed on Cycle 2 Day 1, following multiple dosing, in line with the observed mean  $t_{1/2}$  of ~5.5 hours (Figure 2, Supplementary Table 2). Plasma exposure of M3814 increased with increasing doses. However, high inter-individual variability in dose-normalized exposure prevented conclusive estimation of dose-proportionality (Figure 2; Supplementary Table 2).

### Pharmacodynamics

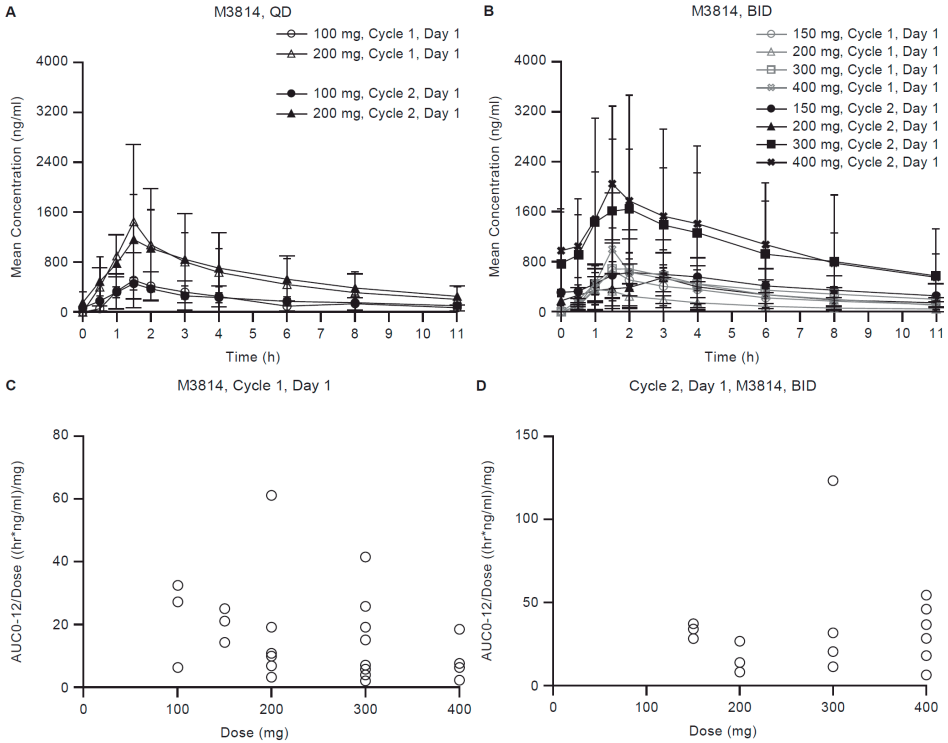
Overall, a consistent and marked dose-dependent decrease in the PD biomarker level (p-DNA-PK/total DNA-PK ratio) was observed in peripheral blood mononuclear cells (PBMCs, as a surrogate of tissue) at early time points (3 and 6 hours) after M3814 administration (Figure 3). A typical profile is shown in Figure 3A. In addition, M3814 concentration-dependent p-DNA-PK inhibition could be clearly established (Figure 3B) with half-maximal inhibition ( $IC_{50}$ ) observed at M3814 concentrations of approximately 200 ng/mL (95% confidence intervals, 149-286). These results demonstrate that M3814 inhibits DNA-PK in a time- and concentration-dependent manner, providing evidence of target engagement.

Table 2. Most common treatment-related treatment-emergent adverse events by worst grade

Preferred term n (%)	Grade*	M3814 dose (mg)/ frequency of administration										Total n = 31
		100/ QD n = 3	200/ QD n = 3	150/ BID n = 3	200/ BID n = 3	300/ BID n = 9	400/ BID n = 4	400/ BID (RP2D) n = 6	400/ BID (RP2D) n = 6			
<b>Patients with ≥ 1 event</b>												<b>22 (71)</b>
Nausea	Any	0 (0)	0 (0)	0 (0)	0 (0)	2 (22)	2 (50)	4 (67)	8 (26)		2 (6)	
	Grade 3	0 (0)	0 (0)	0 (0)	0 (0)	0 (0)	1 (25)	1 (17)	2 (6)		0 (0)	
Vomiting	Any	0 (0)	0 (0)	0 (0)	0 (0)	2 (22)	2 (50)	2 (33)	6 (19)		0 (0)	
	Grade 3	0 (0)	0 (0)	0 (0)	0 (0)	0 (0)	0 (0)	0 (0)	0 (0)		0 (0)	
Fatigue	Any	0 (0)	0 (0)	1 (33)	0 (0)	5 (56)	0 (0)	0 (0)	6 (19)		0 (0)	
	Grade 3	0 (0)	0 (0)	0 (0)	0 (0)	1 (11)	0 (0)	0 (0)	1 (3)		0 (0)	
Pyrexia	Any	0 (0)	0 (0)	0 (0)	0 (0)	1 (11)	1 (25)	3 (50)	5 (16)		0 (0)	
	Grade 3	0 (0)	0 (0)	0 (0)	0 (0)	0 (0)	1 (25)	0 (0)	1 (3)		0 (0)	
Stomatitis	Any	0 (0)	0 (0)	0 (0)	0 (0)	2 (22)	1 (25)	1 (17)	4 (13)		0 (0)	
	Grade 3	0 (0)	0 (0)	0 (0)	0 (0)	0 (0)	1 (25)	0 (0)	1 (3)		0 (0)	
Rash maculo-papular	Any	0 (0)	0 (0)	0 (0)	0 (0)	1 (11)	1 (25)	2 (33)	4 (13)		0 (0)	
	Grade 3	0 (0)	0 (0)	0 (0)	0 (0)	1 (11)	1 (25)	2 (33)	4 (13)		0 (0)	
Constipation	Any	0 (0)	1 (33)	0 (0)	0 (0)	2 (22)	0 (0)	0 (0)	3 (10)		0 (0)	
	Grade 3	0 (0)	0 (0)	0 (0)	0 (0)	0 (0)	0 (0)	0 (0)	0 (0)		0 (0)	
Diarrhea	Any	0 (0)	1 (33)	1 (33)	0 (0)	0 (0)	0 (0)	1 (17)	3 (10)		0 (0)	
	Grade 3	0 (0)	0 (0)	0 (0)	0 (0)	0 (0)	0 (0)	0 (0)	0 (0)		0 (0)	
Rash	Any	0 (0)	0 (0)	0 (0)	0 (0)	2 (22)	0 (0)	1 (17)	3 (10)		0 (0)	
	Grade 3	0 (0)	0 (0)	0 (0)	0 (0)	1 (11)	0 (0)	1 (17)	2 (6)		0 (0)	
Periorbital edema	Any	0 (0)	0 (0)	0 (0)	0 (0)	1 (11)	0 (0)	1 (17)	2 (6)		0 (0)	
	Grade 3	0 (0)	0 (0)	0 (0)	0 (0)	0 (0)	0 (0)	0 (0)	0 (0)		0 (0)	
Dry mouth	Any	0 (0)	0 (0)	0 (0)	0 (0)	2 (22)	0 (0)	0 (0)	2 (6)		0 (0)	
	Grade 3	0 (0)	0 (0)	0 (0)	0 (0)	0 (0)	0 (0)	0 (0)	0 (0)		0 (0)	
Decreased appetite	Any	0 (0)	0 (0)	1 (33)	0 (0)	1 (11)	0 (0)	0 (0)	2 (6)		0 (0)	
	Grade 3	0 (0)	0 (0)	0 (0)	0 (0)	0 (0)	0 (0)	0 (0)	0 (0)		0 (0)	

MedDRA Version 20.0. \*No treatment-related grade 4 or 5 TEAEs were observed in any treatment group. TEAE=treatment-emergent adverse event.





**Figure 2.**

Plasma concentration-time profiles of M3814 following daily (QD, A) and twice-daily (BID, B) dosing (linear scale). Dose-normalized AUC<sub>0-12h</sub> for M3814 by dose on (C) Cycle 1 Day 1 (QD and BID; PK Analysis Set; n = 25) and (D) Cycle 2 Day 1 (BID; PK Analysis Set; n = 17).

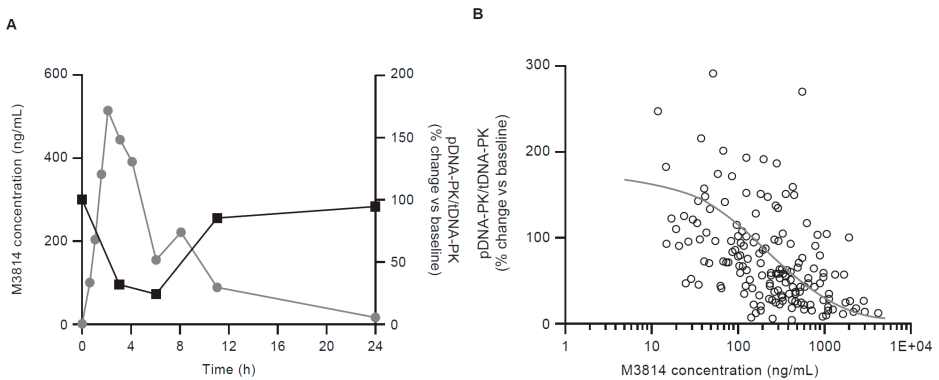


**Figure 3.**

DNA-PK inhibition by M3814. In (A) typical time-course profiles of PK (grey circles) and DNA-PK inhibition (black squares) after M3814 treatment from one patient treated with M3814 100 mg QD. DNA-PK inhibition on treatment is expressed as percentage change of p-DNA-PK/t-DNA-PK from the pretreatment value (time h=0) In (B) concentration-dependent inhibition of DNA-PK in response to M3814 treatment. Experimental concentration-response data are shown as (o) and the line represents the E<sub>max</sub> model fit to the data.

## Efficacy

No objective tumor responses (complete responses or partial responses) were reported. Twelve patients (39%) had a best overall response of stable disease during treatment and/or follow-up (7 of these patients experienced stable disease for  $\geq 12$  weeks), 14 patients (45%) had a best response of progressive disease, and five patients (16%) were not evaluable (tumor assessment at screening only) (Figure 4).

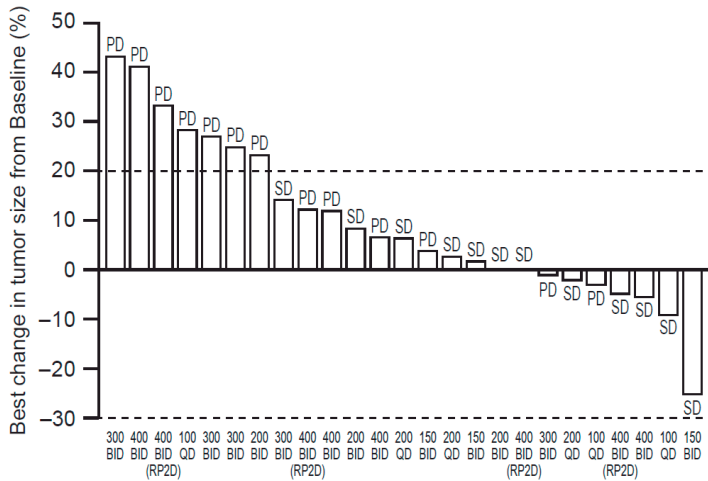


**Figure 4.**

Waterfall plot showing best percentage change in tumor size from baseline and best overall response. M3814 dose (mg)/frequency of administration is shown for each patient on the x axis. Dashed lines show the 20% threshold for disease progression and the 30% threshold for partial response. *Abbreviations:* PD=progressive disease, SD=stable disease.

## Discussion

M3814 is a sub-nanomolar potent and selective inhibitor of DNA-PK catalytic activity.<sup>6-8</sup> In this first-in-man study, M3814 showed an acceptable safety profile when given orally QD or BID to patients with advanced solid tumors. The MTD of M3814 was not reached at 400 mg BID (dose expansion was stopped at 400 mg BID), and it was decided not to conduct the dose-expansion part of the study as the response to M3814 dose escalation did not support a monotherapy dose-expansion cohort. Therefore, the RP2D for M3814 monotherapy was declared as 400 mg BID. A combination of non-serious AEs and the long duration of recovery after treatment discontinuation was considered a DLT in one patient treated with 300 mg M3814 BID. Based on an extrapolation from preclinical data available at the time of study initiation, no unexpected clinical safety signals

for M3814 were observed. Doses up to 400 mg M3814 BID were tolerated and AEs were manageable.

M3814 may cause an inhibitory, yet reversible effect, on platelet aggregation; therefore, platelet function was evaluated in this study, and only a weak effect on platelet aggregation in some patients was observed. These findings do not support the exclusion of patients taking oral anticoagulation medication from receiving M3814 treatment. In preclinical studies, M3814 was shown to inhibit PI3K lipid kinases with strongly reduced potency, despite the high similarity in their kinase domain.<sup>7</sup> Nevertheless, the occurrence of rash has been observed with clinical PI3K inhibitors, and grade 3 maculo-papular rashes were reported in the present study.<sup>14</sup> Further data are required to confirm any association between the occurrence of rash and PI3K inhibition by M3814. Together, these data indicate that the safety and tolerability of M3814 in humans are consistent with the results of preclinical studies, and as expected based on its mechanism of action.

To date, the use of DNA-PK inhibitors in clinical studies has been limited by the pharmacokinetic profiles of currently available molecules.<sup>15</sup> Here, we show that the tested M3814 formulation was quickly absorbed into the systemic circulation, with slight accumulation observed with multiple QD and BID dosing. M3814 plasma exposure increased with increasing dose, but dose proportionality could not be evaluated due to the large inter-patient variability in exposure. A novel formulation will be developed for future clinical trials.

DNA-PK is a component of the DDR and a key driver of DNA DSB repair via the NHEJ pathway; this mechanism is functional throughout all phases of the cell cycle and repairs the majority of DSBs induced by radiotherapy in cancer cells.<sup>16</sup> DNA-PK autophosphorylation and subsequent activation is essential for the repair process.<sup>5,17</sup> In preclinical studies, M3814 was shown to inhibit DNA DSB repair and enhance existing sensitivity to radiation in cancer cells through inhibition of DNA-PK kinase activity, consistent with studies in cervical cancer cells and mouse embryonic fibroblasts showing that loss of DNA-PK activity leads to radiosensitization.<sup>6,7,18-20</sup> Consistent with this, high expression of the DNA-PK catalytic subunit (DNA-PKcs) has been reported in patient tumor samples, and has been associated with resistance to radiotherapy.<sup>26,27</sup> In addition, combination drug profiling of M3814 with antitumor agents revealed synergy with chemotherapeutics that work by generating DNA DSBs.<sup>7,10, 21-25</sup> These data indicate that M3814 may function predominantly through the inhibition of NHEJ repair.<sup>7</sup> However, the prognostic effect of increased DNA-PK expression appears to be context-dependent.<sup>22-24</sup> The lack of partial response according to RECIST (version 1.1)

with M3814 monotherapy is consistent with its mechanism of action, and with the findings of preclinical studies, which support combining M3814 with DNA DSB-inducing agents such as radiotherapy and DNA-DSB-inducing chemotherapeutic agents.<sup>6,7,10</sup> These results, along with preclinical data, support further clinical evaluation of M3814 and a phase I trial in combination with radiotherapy/chemotherapy is ongoing in patients with advanced solid tumors (NCT02516813).<sup>6,10,28</sup>

In conclusion, M3814 showed an acceptable safety profile and the RP2D for M3814 monotherapy was declared as 400 mg BID.

### **Acknowledgments**

The authors would like to thank patients, investigators, co-investigators, and the study teams at each of the participating centers and at Merck KGaA, Darmstadt, Germany. Medical writing assistance was provided by Lisa Jolly, PhD, and Jen Lewis, PhD of Bioscript Science, Macclesfield, UK and funded by Merck KGaA, Darmstadt, Germany. The trial was sponsored by Merck KGaA, Darmstadt, Germany.

### **Conflict of interest**

Barbara Sarholz, Karin Berghoff, Samer El Bawab, Mirjam Kuipers, Ivan Diaz-Padilla, and Lars Damstrup are current or past employees of Merck KGaA, Darmstadt, Germany. J.H.M. Schellens is patent holder on development of oral taxanes and shareholder of Modra Pharmaceuticals BV.

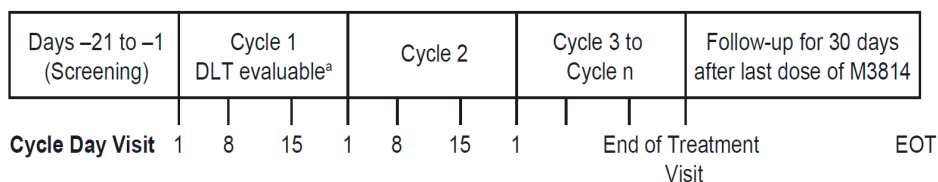
## References

1. O'Connor MJ. Targeting the DNA Damage Response in Cancer. *Mol Cell* 2015; 60(4): 547-60.
2. Hanahan D, Weinberg RA. Hallmarks of cancer: the next generation. *Cell* 2011; 144(5): 646-74.
3. Desai A, Yan Y, Gerson SL. Advances in therapeutic targeting of the DNA damage response in cancer. *DNA Repair (Amst)* 2018; 66-67: 24-9.
4. Davis AJ, Chen BP, Chen DJ. DNA-PK: a dynamic enzyme in a versatile DSB repair pathway. *DNA Repair (Amst)* 2014; 17: 21-9.
5. Salles B, Calsou P, Frit P, Muller C. The DNA repair complex DNA-PK, a pharmacological target in cancer chemotherapy and radiotherapy. *Pathol Biol (Paris)* 2006; 54(4): 185-93.
6. Fuchss T, Mederski WW, Emde U, et al. Abstract 4198: Highly potent and selective DNA-PK inhibitor M3814 with sustainable anti-tumor activity in combination with radiotherapy. *Cancer Res* 2017; 77(13 Suppl).
7. Zenke F. [Preclinical M3814 manuscript]. *TBC* 2019.
8. Zenke FT, Zimmermann A, Sirrenberg C, et al. Abstract 1658: M3814, a novel investigational DNA-PK inhibitor: enhancing the effect of fractionated radiotherapy leading to complete regression of tumors in mice. *Cancer Res* 2016; 76(14 Suppl)(Abstract nr 1658).
9. Klein C, Dokic I, Mairani A, et al. Overcoming hypoxia-induced tumor radioresistance in non-small cell lung cancer by targeting DNA-dependent protein kinase in combination with carbon ion irradiation. *Radiat Oncol* 2017; 12(1): 208.
10. Sirrenberg C, Zimmermann A, Grombacher T, et al. Abstract 4183: A novel selective DNA-PK inhibitor, M3814, as a potential combination partner of Etoposide and Cisplatin in the therapy of lung cancer. *Cancer Res* 2017; 77 (13 Suppl).
11. van Bussel MTJ, Mau-Soerensen M, Damstrup L, et al. Abstract 2556: A multicenter phase I trial of the DNA-dependent protein kinase (DNA-PK) inhibitor M3814 in patients with solid tumors. *J Clin Oncol* 2017; 35 (15\_Suppl): 2556.
12. Mau-Sorensen M, van Bussel MTJ, Kuipers M, Nielsen DL, Verheul HM, Aftimos P, de Jonge MJA, van Triest, B, Falkenius J, Debus J, Troost E, Samuels M, Sarholz B, Budach V, Goel S, Locatelli G, Geertsens PF. Safety, clinical activity and pharmacological biomarker evaluation of the DNA-dependent protein kinase (DNA-PK) inhibitor M3814: Results from two phase I trials. *Annals of Oncology* 2018; 29 (Suppl\_8).
13. Eisenhauer EA, Therasse P, Bogaerts J, et al. New response evaluation criteria in solid tumours: revised RECIST guideline (version 1.1). *Eur J Cancer* 2009; 45(2): 228-47.
14. Sarker D, Ang JE, Baird R, et al. First-in-human phase I study of pictilisib (GDC-0941), a potent pan-class I phosphatidylinositol-3-kinase (PI3K) inhibitor, in patients with advanced solid tumors. *Clinical cancer research* 2015; 21(1): 77-86.
15. Davidson D, Amrein L, Panasci L, Aloyz R. Small Molecules, Inhibitors of DNA-PK, Targeting DNA Repair, and Beyond. *Front Pharmacol* 2013; 4: 5.
16. Kakarougkas A, Jeggo PA. DNA DSB repair pathway choice: an orchestrated handover mechanism. *Br J Radiol* 2014; 87(1035): 20130685.
17. Dobbs TA, Tainer JA, Lees-Miller SP. A structural model for regulation of NHEJ by DNA-PKcs autophosphorylation. *DNA Repair (Amst)* 2010; 9(12): 1307-14.

18. Taccioli GE, Amatucci AG, Beamish HJ, et al. Targeted disruption of the catalytic subunit of the DNA-PK gene in mice confers severe combined immunodeficiency and radiosensitivity. *Immunity* 1998; 9(3): 355-66.
19. Dong J, Ren Y, Zhang T, et al. Inactivation of DNA-PK by knockdown DNA-PKcs or NU7441 impairs non-homologous end-joining of radiation-induced double strand break repair. *Oncol Rep* 2018; 39(3): 912-20.
20. Fuhrman CB, Kilgore J, LaCoursiere YD, et al. Radiosensitization of cervical cancer cells via double-strand DNA break repair inhibition. *Gynecol Oncol* 2008; 110(1): 93-8.
21. Hosoi Y, Watanabe T, Nakagawa K, et al. Up-regulation of DNA-dependent protein kinase activity and Sp1 in colorectal cancer. *Int J Oncol* 2004; 25(2): 461-8.
22. Perrone F, Baldassarre G, Indraccolo S, et al. Biomarker analysis of the MITO2 phase III trial of first-line treatment in ovarian cancer: predictive value of DNA-PK and phosphorylated ACC. *Oncotarget* 2016; 7(45): 72654-61.
23. Pinel B, Duchesne M, Godet J, et al. Mesenchymal subtype of glioblastomas with high DNA-PKcs expression is associated with better response to radiotherapy and temozolomide. *J Neurooncol* 2017; 132(2): 287-94.
24. Xing J, Wu X, Vaporciyan AA, Spitz MR, Gu J. Prognostic significance of ataxia-telangiectasia mutated, DNA-dependent protein kinase catalytic subunit, and Ku heterodimeric regulatory complex 86-kD subunit expression in patients with nonsmall cell lung cancer. *Cancer* 2008; 112(12): 2756-64.
25. Bouchaert P, Guerif S, Debiais C, Irani J, Fromont G. DNA-PKcs expression predicts response to radiotherapy in prostate cancer. *Int J Radiat Oncol Biol Phys* 2012; 84(5): 1179-85.
26. Beskow C, Skikuniene J, Holgersson A, et al. Radioresistant cervical cancer shows upregulation of the NHEJ proteins DNA-PKcs, Ku70 and Ku86. *Br J Cancer* 2009; 101(5): 816-21.
27. Shintani S, Mihara M, Li C, et al. Up-regulation of DNA-dependent protein kinase correlates with radiation resistance in oral squamous cell carcinoma. *Cancer Sci* 2003; 94(10): 894-900.
28. van Triest B, Damstrup L, Falkenius J, et al. A phase Ia/Ib trial of the DNA-PK inhibitor M3814 in combination with radiotherapy (RT) in patients (pts) with advanced solid tumors: Dose-escalation results. *J Clin Oncol* 2018; 36 (15\_Suppl): 2518.

## Supplement to:

## A first-in-man phase I study of the DNA-dependent protein kinase inhibitor M3814 in patients with advanced solid tumors



## Supplementary Figure 1. Study schematic

<sup>a</sup>The DLT observation period was 21 days of the first cycle of treatment. DLTs were evaluated in order to make decisions regarding dose escalation or evaluation of intermediate dose levels. *Abbreviations:* DLT=dose-limiting toxicity, EOT=End of trial visit.

## Supplementary Table 1. Overall summary of treatment-emergent adverse events

Number of patients, <i>n</i> (%), with:	M3814 dose (mg)/frequency of administration							Total <i>n</i> = 31
	100/ QD	200/ QD	150/ BID	200/ BID	300/ BID	400/ BID	400/ BID (RP2D)	
<i>n</i> = 3	<i>n</i> = 3	<i>n</i> = 3	<i>n</i> = 3	<i>n</i> = 3	<i>n</i> = 9	<i>n</i> = 4	<i>n</i> = 6	<i>n</i> = 31
Any TEAE	3 (100)	3 (100)	3 (100)	3 (100)	9 (100)	4 (100)	6 (100)	31 (100)
Any M3814-related TEAE	1 (33)	2 (67)	2 (67)	0 (0)	8 (89)	3 (75)	6 (100)	22 (71)
Any serious TEAE	1 (33)	1 (33)	2 (67)	1 (33)	5 (56)	3 (75)	4 (67)	17 (55)
Any M3814 related serious TEAE	0 (0)	0 (0)	0 (0)	0 (0)	0 (0)	1 (25)	3 (50)	4 (13)
Any grade $\geq 3$ TEAE	2 (67)	1 (33)	3 (100)	2 (67)	5 (56)	3 (75)	5 (83)	21 (68)
Any grade $\geq 4$ TEAE	0 (0)	0 (0)	0 (0)	0 (0)	0 (0)	2 (50) <sup>a</sup>	0 (0)	2 (6)
Any M3814 related grade $\geq 3$ TEAE	0 (0)	0 (0)	0 (0)	0 (0)	3 (33)	1 (25)	3 (50)	7 (23)
Any M3814 related grade $\geq 4$ TEAE	0 (0)	0 (0)	0 (0)	0 (0)	0 (0)	0 (0)	0 (0)	0 (0)
Any TEAE leading to study discontinuation	0 (0)	0 (0)	0 (0)	0 (0)	1 (11)	1 (25)	2 (33)	4 (13)
Any TEAE leading to death	0 (0)	0 (0)	0 (0)	0 (0)	0 (0)	1 (25)	0 (0)	1 (3)
Any M3814 related TEAE leading to death	0 (0)	0 (0)	0 (0)	0 (0)	0 (0)	0 (0)	0 (0)	0 (0)

<sup>a</sup>Adverse events of blood alkaline phosphatase increased were not considered a TEAE for one patient (occurred prior to the start of study treatment). *Abbreviations:* RP2D=recommended phase II dose, TEAE=treatment-emergent adverse event.

Supplementary Table 2. Key summary statistics of M3814 PK parameters by dose group on Cycle 1 Day 1 and Cycle 2 Day 1 (PK Analysis Set)

M3814 Dose group	$C_{max}$ (ng/mL)	$t_{max}$ (h)	$AUC_{0-\infty}$ (h*ng/mL) <sup>a</sup>	$AUC_{0-12h}$ (h*ng/mL)	$CL_{r/f}$ (L/h) <sup>a</sup>	$V_{z/f}$ (L) <sup>a</sup>	$t_{1/2}$ (h) <sup>a</sup>	$C_{max}/dose$ (ng/mL/mg)	$AUC_{0-24h}/dose$ (h*ng/mL/mg)	Racc $C_{max}$	Racc $AUC_{0-12}$
Cycle 1 Day 1											
100 mg QD	N	3	3	3	3	3	3	3	3	-	-
	Mean	561	1.7	2,920	2,220	54.2	508	6.6	5.6	22.2	-
	Min	161	1.5	908	670	21.8	194	4.4	1.6	6.7	-
	Median	512	1.6	3,270	2,730	30.6	273	6.7	5.1	27.3	-
	Max	1,010	2.1	4,590	3,250	110	1,060	8.7	10.1	32.5	-
	GeoMean	437	1.7	2,390	1,810	41.9	382	6.3	4.4	18.1	-
200 mg QD	N	3	3	3	3	3	3	3	3	-	-
	Mean	1,490	1.4	9,970	6,080	40.2	433	9.4	7.4	30.4	-
	Min	539	1.1	2,880	2,190	9.0	191	6.1	2.7	10.9	-
	Median	1,070	1.5	4,730	3,870	42.3	369	7.4	5.4	19.3	-
	Max	2,850	1.5	22,300	12,200	69.3	741	14.7	14.3	60.9	-
	GeoMean	1,180	1.3	6,730	4,690	29.7	374	8.7	5.9	23.4	-
150 mg BID	N	3	3	3	3	3	3	3	3	-	-
	Mean	695	1.3	3,770	3,040	40.5	304	5.1	4.6	20.3	-
	Min	330	1.0	3,320	2,170	33.0	202	3.5	2.2	14.5	-
	Median	594	1.5	3,460	3,180	43.3	218	4.2	4.0	21.2	-
	Max	1,160	1.5	4,550	3,770	45.2	492	7.6	7.7	25.2	-
	GeoMean	610	1.3	3,740	2,960	40.1	279	4.8	4.1	19.8	-
200 mg BID	N	3	3	3	3	3	3	3	3	-	-
	Mean	393	2.0	1,780	1,370	143	1,010	5.6	2.0	6.9	-
	Min	192	1.0	787	700	81.8	442	3.3	1.0	3.5	-
	Median	260	1.1	2,120	1,420	94.3	1,120	4.0	1.3	7.1	-
	Max	727	4.0	2,440	2,000	254	1,480	9.5	3.6	10.0	-
	GeoMean	331	1.7	1,600	1,260	125	901	5.0	1.7	6.3	-



Supplementary Table 2. (continued)

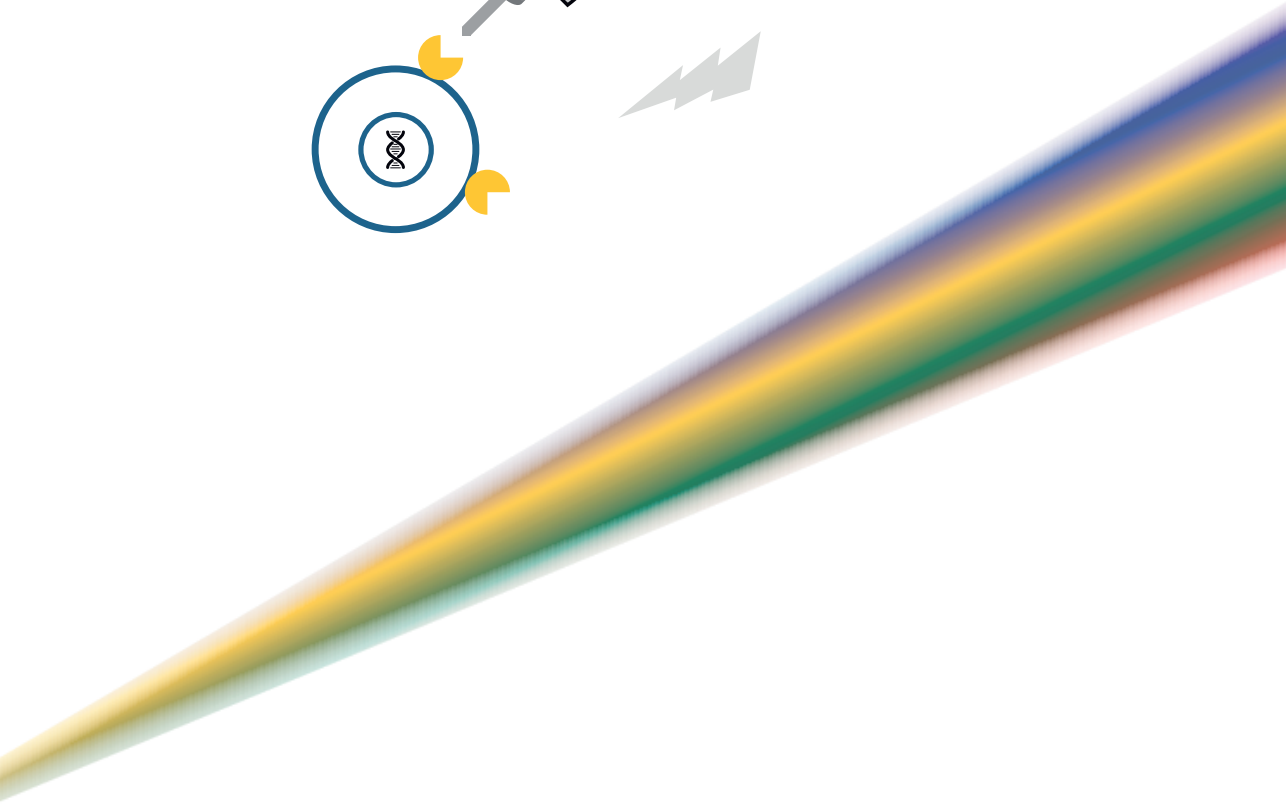
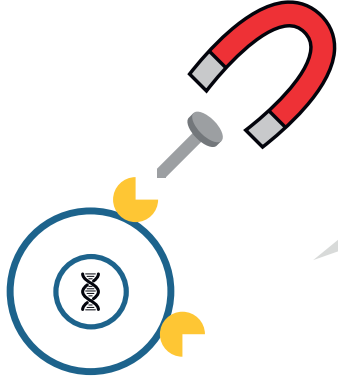
Dose group	$C_{max}$ (ng/mL)	$t_{max}$ (h)	$AUC_{0-\infty}$ (h*ng/mL) <sup>a</sup>	$AUC_{0-12h}$ (h*ng/mL)	$CL_{r/f}$ (L/h) <sup>a</sup>	$V_{z/f}$ (L) <sup>a</sup>	$t_{1/2}$ (h) <sup>a</sup>	$C_{max}/dose$ (ng/mL/mg)	$AUC_{0-12h}/dose$ (h*ng/mL/mg)	Racc $C_{max}$	Racc $AUC_{0-12}$
<b>300 mg BID</b>	<b>N</b>	<b>9</b>	<b>9</b>	<b>9</b>	<b>9</b>	<b>9</b>	<b>9</b>	<b>9</b>	<b>9</b>	-	-
	Mean	839	1.9	6,050	4,270	127	662	4.7	2.8	14.2	-
	Min	156	1.0	781	702	14.4	182	2.0	0.5	2.3	-
	Median	677	1.5	2,290	2,250	131	425	4.6	2.3	7.5	-
	Max	2,070	4.0	20,800	12,400	384	1,750	8.8	6.9	41.5	-
	GeoMean	654	1.7	3,690	2,950	81.4	489	4.2	2.2	9.9	-
<b>400 mg BID</b>	<b>N</b>	<b>4</b>	<b>4</b>	<b>4</b>	<b>4</b>	<b>4</b>	<b>4</b>	<b>4</b>	<b>4</b>	-	-
	Mean	717	2.4	4,140	3,580	172	511	3.0	1.8	8.9	-
	Min	451	0.5	1,020	1,020	44.5	290	1.3	1.1	2.6	-
	Median	493	2.5	3,280	2,920	126	517	3.1	1.2	7.3	-
	Max	1,430	4.0	8,990	7,450	391	720	4.5	3.6	18.6	-
	GeoMean	629	1.9	3,130	2,830	128	479	2.6	1.6	7.1	-
<b>Cycle 2 Day 1 (clearance is <math>CL_{ss}</math>)</b>											
<b>100 mg QD</b>	<b>N</b>	<b>3</b>	<b>3</b>	-	<b>3</b>	<b>3</b>	<b>3</b>	<b>3</b>	<b>3</b>	<b>3</b>	<b>3</b>
	Mean	440	1.8	-	2,290	39.3	276	5.5	4.4	22.9	1.3
	Min	390	1.5	-	1,630	24.3	241	2.9	3.9	16.3	0.4
	Median	408	1.6	-	2,130	36.2	264	6.2	4.1	21.3	1.0
	Max	523	2.4	-	3,100	57.3	322	7.5	5.2	31.0	2.4
	GeoMean	437	1.8	-	2,210	36.9	274	5.1	4.4	22.1	1.0
<b>200 mg QD</b>	<b>N</b>	<b>3</b>	<b>3</b>	-	<b>3</b>	<b>3</b>	<b>3</b>	<b>3</b>	<b>3</b>	<b>3</b>	<b>3</b>
	Mean	1,190	1.8	-	6,520	30.8	198	4.53	5.9	32.6	0.9
	Min	654	1.1	-	4,360	15.7	109	4.11	3.3	21.8	0.7
	Median	931	1.5	-	4,630	37.8	231	4.67	4.7	23.1	0.9
	Max	1,970	3.0	-	10,600	38.9	255	4.81	9.9	52.9	1.2
	GeoMean	1,060	1.7	-	5,970	28.5	186	4.52	5.3	29.9	0.9
<b>150 mg BID</b>	<b>N</b>	<b>3</b>	<b>3</b>	-	<b>3</b>	<b>3</b>	<b>3</b>	<b>3</b>	<b>3</b>	<b>3</b>	<b>3</b>
	Mean	699	2.7	-	5,000	30.3	294	6.8	4.7	33.3	1.3

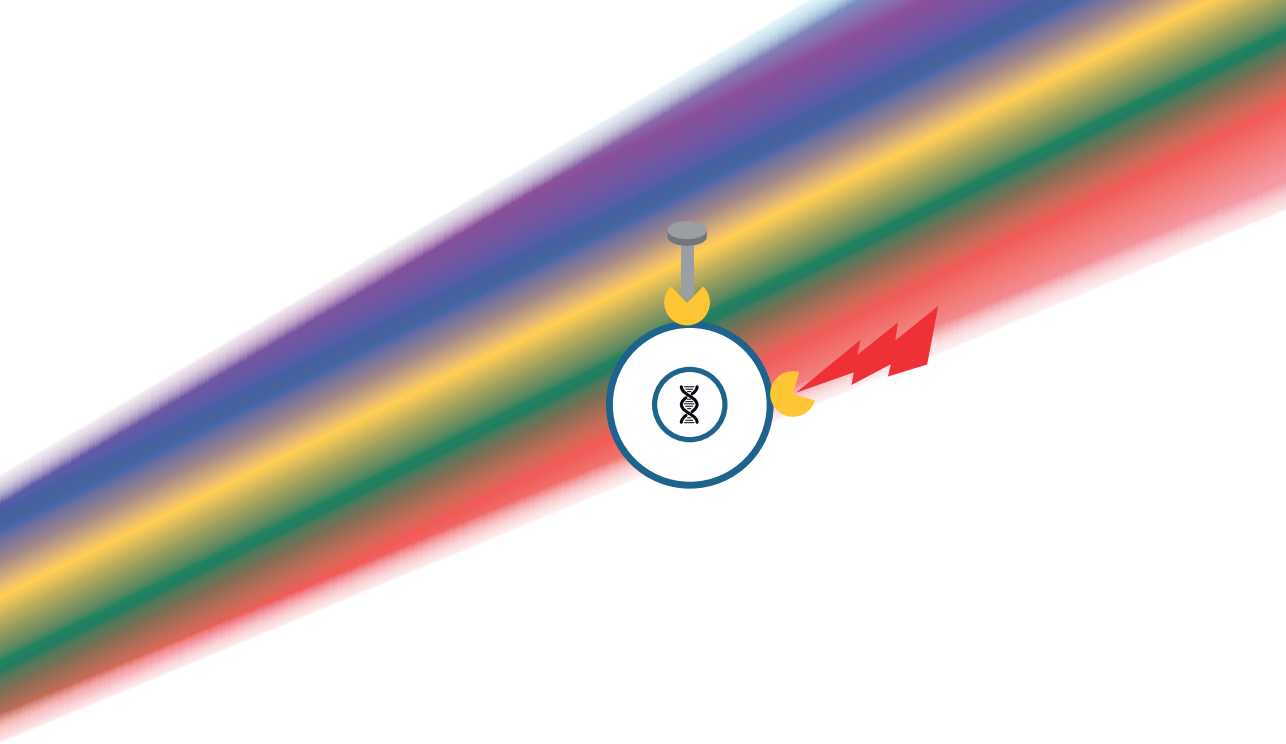
Supplementary Table 2. (continued)

Dose group	$C_{max}$ (ng/mL)	$t_{max}$ (h)	$AUC_{0-\infty}$ (h*ng/mL) <sup>a</sup>	$AUC_{0-12h}$ (h*ng/mL)	$CL_r$ (L/h) <sup>b</sup>	$V_z/f$ (L) <sup>a</sup>	$t_{1/2}$ (h) <sup>a</sup>	$C_{max}/dose$ (ng/mL/mg)	$AUC_{0-12h}/dose$ (h*ng/mL/mg)	Racc $C_{max}$	Racc $AUC_{0-12}$
Min	586	2.0	-	4,350	27.0	242	5.7	3.9	29.0	0.6	1.2
Median	720	2.1	-	5,090	29.5	314	6.3	4.8	33.9	1.0	1.6
Max	792	4.0	-	5,560	34.5	327	8.4	5.3	37.1	2.4	2.6
GeoMean	694	2.6	-	4,970	30.2	292	6.7	4.6	33.1	1.1	1.7
200 mg BID	N	3	3	3	3	3	3	3	3	3	3
Mean	671	2.1	-	3,320	74.4	447	4.4	3.4	16.6	2.8	2.9
Min	343	1.4	-	1,730	37.1	267	3.9	1.7	8.7	0.5	0.9
Median	599	2.1	-	2,830	70.7	431	4.2	3.0	14.1	2.3	3.8
Max	1,070	3.0	-	5,400	115	644	5.0	5.4	27.0	5.6	4.0
GeoMean	604	2.0	-	2,980	67.1	420	4.3	3.0	14.9	1.8	2.4
300 mg BID	N	5	5	5	5	5	5	5	5	5	5
Mean	1,730	1.7	-	11,900	51.1	448	6.21	5.8	39.8	2.7	4.2
Min	507	1.0	-	3,580	8.2	88.0	3.71	1.7	11.9	1.5	1.9
Median	1,000	2.0	-	6,180	48.6	394	5.62	3.3	20.6	2.4	3.4
Max	4,870	2.1	-	36,800	83.8	1,060	8.79	16.2	123	4.9	7.6
GeoMean	1,260	1.7	-	7,750	38.7	333	5.95	4.2	25.8	2.4	3.8
400 mg BID	N	6	6	6	6	6	6	6	6	3	3
Mean	1,930	1.5	-	12,800	50.1	252	4.7	4.8	31.9	1.9	3.2
Min	730	0.0 <sup>b</sup>	-	2,770	18.4	128	2.0	1.8	6.9	1.5	2.5
Median	2,060	1.7	-	13,100	31.0	233	5.4	5.1	32.8	1.6	2.7
Max	3,050	2.1	-	21,800	144	425	6.1	7.6	54.4	2.7	4.4
GeoMean	1,740	NC	-	10,600	37.9	235	4.3	4.4	26.4	1.87	3.1

<sup>a</sup>Diagnostic parameters indicated that  $\lambda_z$  and thus derived pharmacokinetic parameters could not be precisely estimated for most patients. <sup>b</sup>Pre-dose sample assigned a time of 0 h. Abbreviations:  $AUC_{0-12}$ =area under the concentration-time curve from 0 to 12 hours,  $AUC_{0-\infty}$ =area under the concentration-time curve from 0 to infinity,  $CL_r/f$ =apparent total body clearance of drug,  $CL_{ss}/f$ =apparent steady-state total body clearance of drug,  $C_{max}$ =maximum observed concentration,  $C_{max}/dose$ =dose-normalized maximum observed concentration (normalized using the actual dose, and the formula  $C_{max}/dose$ ), GeoMean=geometric mean, max=maximum, min=minimum, NC=not calculated, PK=pharmacokinetic, Racc  $AUC_{0-12}$ =accumulation ratio for  $AUC_{0-12}$ , Racc  $C_{max}$ =accumulation ratio for  $C_{max}$ ,  $t_{1/2}$ =apparent elimination half-life,  $t_{max}$ =time to  $C_{max}$ ,  $V_z/f$ =apparent volume of distribution during terminal phase.







**Conclusions and perspectives**



## Conclusions and perspectives

### Part I Biomarker development and assessment

Promising results are described in the review of circulating tumor cells (CTC) assays for the detection of epithelial cell adhesion molecule (EpCAM) positive CTC from cerebrospinal fluid (CSF) in **Chapter 1**. The reported sensitivities and specificities of the EpCAM-based CTC assays for the diagnosis of leptomeningeal metastases (LM) across the different studies are high and vary between 76-100%. In **Chapter 2** we investigated the diagnostic performance of an EpCAM based immunoflow cytometry CTC assay in patients clinically suspected for LM with a negative or equivocal magnetic resonance imaging (MRI). The results of this prospective study has led to the transfer of the CTC analysis from a research laboratory setting to the Department of Laboratory Medicine at The Netherlands Cancer Institute, Amsterdam, the Netherlands. This highlights the urgent unmet medical need for better diagnostic tools in this patient population. Due to the low sensitivities of both MRI and cytology these techniques should not be used for treatment response monitoring in LM in clinical trials. CTC analysis provides a quantitative tool which could be used as an early treatment response marker in CSF.<sup>1-3</sup> Slow patient accrual due to the diagnostic challenges and poor prognosis of patients with LM has hampered the development of LM specific treatments.<sup>4,5</sup> These difficulties could be overcome by introducing CTC analysis of CSF in clinical trials in patients with a clinical suspicion of LM. The disease could be diagnosed in an earlier stage at which patients could have sufficient time to respond to treatment. In **Chapter 3** we presented the first results of an immunoflow cytometry assay for circulating melanoma cells (CMC) in CSF. These CMC are captured and detected by melanoma-associated sulfate proteoglycan (MCSP) and CD146 based immunoflow cytometry. CMC were detected in CSF in 11 of 12 patients with confirmed LM. Control patients and non-LM patients were negative for CMC. Driver mutation analysis of *BRAFV600E* was performed on paired cell free CSF, isolated CMC from CSF and plasma samples in 15 patients with *BRAFV600E* mutated melanoma. Cell-free CSF samples of all four tested patients with *BRAFV600E* mutated melanoma and cytology confirmed LM were positive for the *BRAFV600E* driver mutation. CMC isolated from CSF in 2 of these patients with confirmed LM were *BRAFV600E* positive. Both assays need further validation for diagnostic accuracy in a larger patient cohort. Driver mutation analysis of cell free CSF and isolated CTC or CMC from CSF can be used to guide future therapy of central nervous system (CNS) metastases and unravel the pathophysiological and genetic mechanisms of tumor cells metastasizing to the CSF.

## Part II Clinical pharmacology of anticancer agents

Cancer in the CNS is difficult to treat due to the blood brain barrier (BBB) which normally protects the CNS from toxic agents. The general consensus with regard to antibody pharmacokinetics is that monoclonal antibodies cannot penetrate an intact BBB due to their large molecular size and thereby may lack clinical activity in the CNS.<sup>6-11</sup> Recently, two phase II trials showed intracranial activity of the immune checkpoint inhibitors nivolumab and ipilimumab in patients with melanoma brain metastases.<sup>12,13</sup> In **Chapter 4** a pharmacodynamic and pharmacokinetic perspective on the intracranial antitumor responses of immunotherapy with the monoclonal antibodies nivolumab and ipilimumab was given. The intracranial effects of these immune checkpoint inhibitors can be due to a dual mechanism: nivolumab can bind irreversibly to programmed death receptor 1 (PD1) and ipilimumab can bind to cytotoxic T lymphocyte associated antigen 4 (CTLA-4) on peripheral circulating lymphocytes which can subsequently penetrate the BBB or the antibodies themselves can cross the BBB and inhibit tumor infiltrating lymphocytes, being already present in the intracranial tumor. For adequate brain penetration of antibodies, they need to be selected for the optimal immunoglobulin G4 subclass with neonatal Fc receptor (FcRn) binding. FcRn binding mediates transcytosis of IgG antibodies. The highly promising clinical antitumor activity combined with the described mechanism of penetration of monoclonal antibodies into the CSF opens novel strategies to treat malignant diseases in the CNS. Based on the described findings the general consensus that monoclonal antibodies do not penetrate into the CNS needs to be reconsidered. In **Chapter 5** we described the method development and validation of an enzyme linked immunosorbent assay for the quantification of nivolumab and pembrolizumab in human serum and CSF. With this assay we can investigate the pharmacokinetics of nivolumab and pembrolizumab in both serum and CSF. The dose response curves of nivolumab and pembrolizumab have been poorly characterised. Together with the pharmacodynamics of these agents more rational and cost saving dosing regimens could be developed. In **Chapter 6** we presented a liquid chromatography-tandem mass spectrometric assay for the T790M mutant EGFR inhibitor osimertinib in human plasma. This method can be used for therapeutic drug monitoring for instance in the case of drug-drug interactions via the drug metabolizing cytochrome (CYP) P450 3A4 and CYP3A5 enzymes which metabolize osimertinib. In **Chapter 7** severe bone toxicities were observed with the treatment combination of WNT974, LGX818 and cetuximab in patients with *BRAFV600*-mutant *KRAS* wild-type metastatic colorectal cancer harbouring Wnt pathway mutations. The bone toxicities were not expected based on the experience of the phase I single agent study of WNT974 (NCT01351103).<sup>14</sup> The maximum tolerated dose (MTD) was not determined in the phase I single agent trial of WNT974, also known as LGK974. In the study abstract of the single agent study no specific bone related toxicity



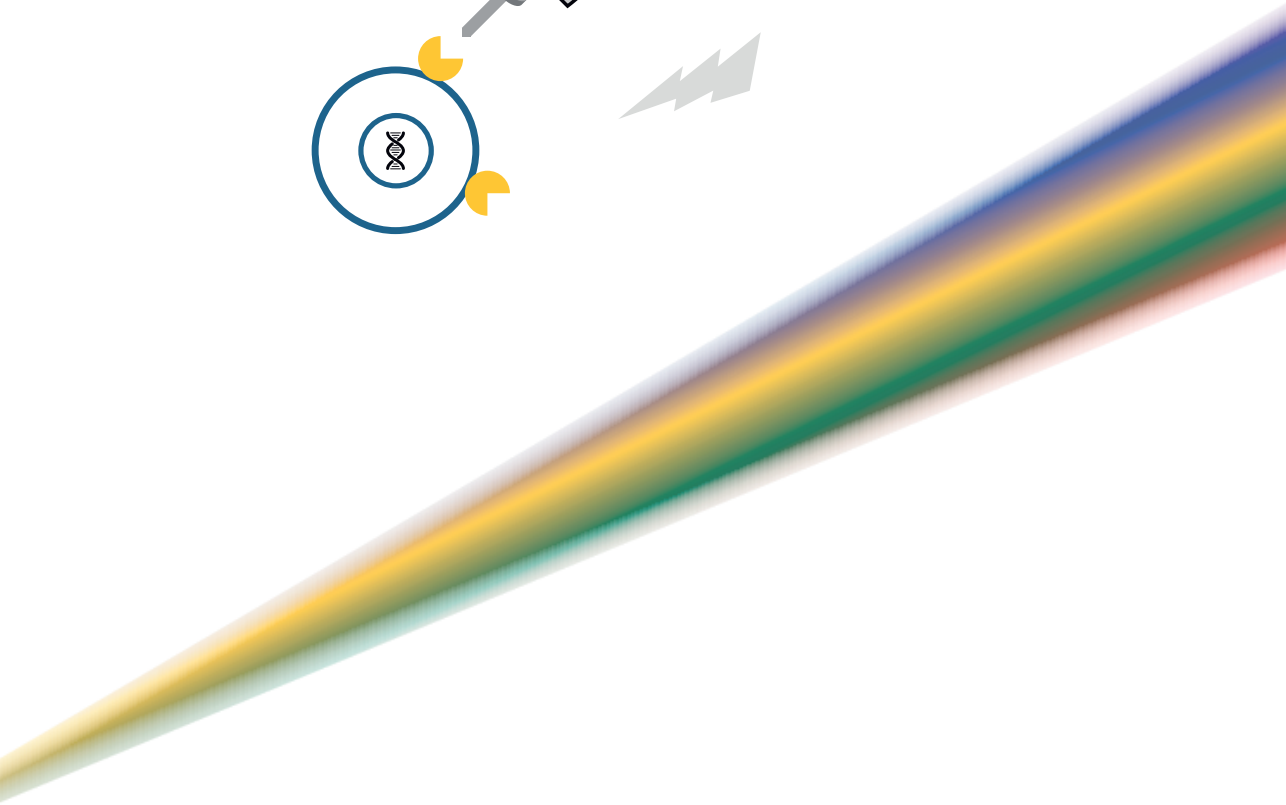
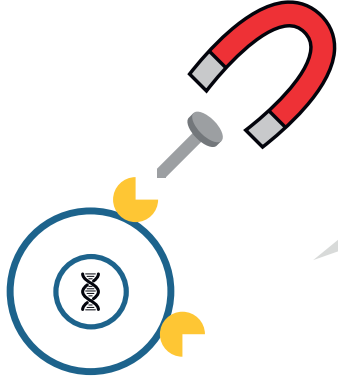
was mentioned. Two patients who experienced severe bone toxicity in the trial of WNT974, encorafenib and cetuximab were described in **Chapter 8**. Future clinical trials with WNT pathway inhibitors need to coincide with intensive monitoring of bone homeostasis and inclusion of bone protective measurements in their clinical trial protocols. WNT974 is still under clinical investigation in combination with PDR001, also known as spartalizumab, an anti-PD-1 monoclonal antibody.<sup>15</sup>

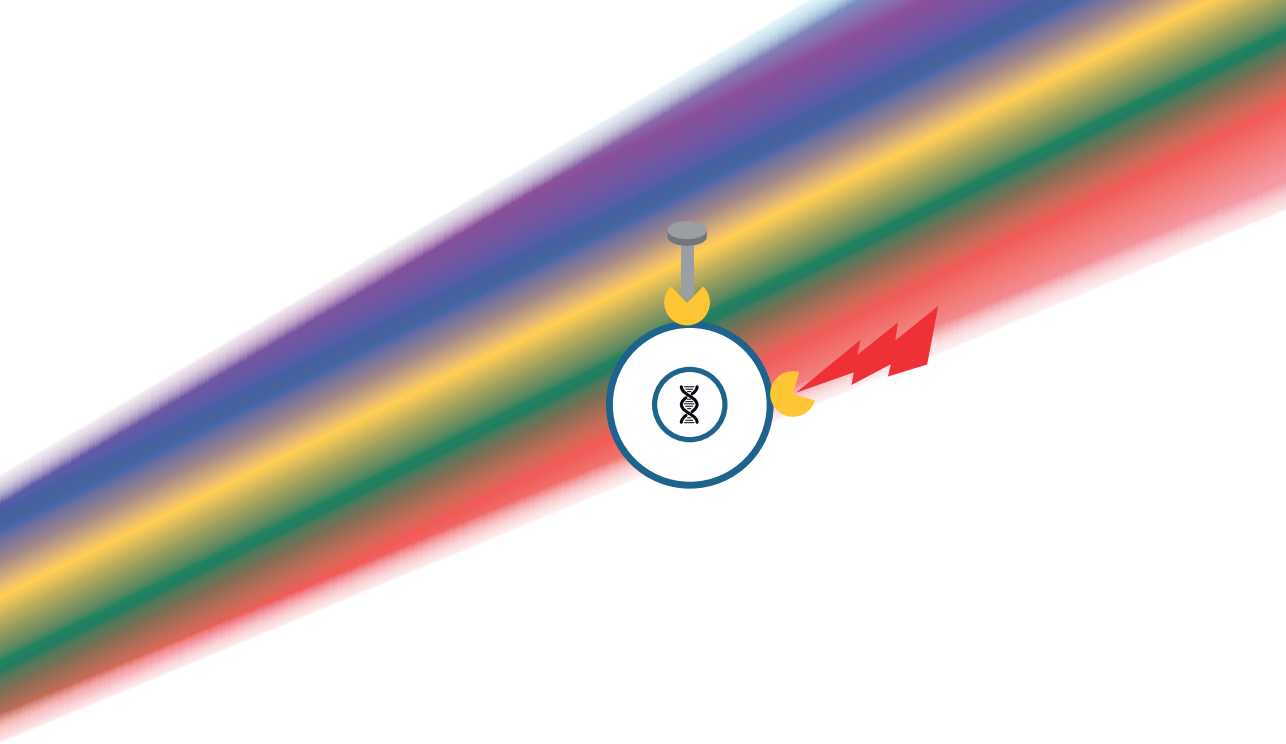
In **Chapter 9** we presented the first-in-man study of the DNA-protein kinase inhibitor M3814. The trial aimed to determine the MTD and/or recommended phase II dose (RP2D) of M3814, a DNA-dependent protein kinase inhibitor in patients with advanced solid tumors. Secondary and exploratory objectives were to explore the safety, tolerability, pharmacokinetic and pharmacodynamic profiles, and clinical activity. M3814 showed an acceptable safety profile. The MTD of M3814 was not reached at the dose level of 400 mg twice daily (BID). The RP2D for M3814 monotherapy was declared as 400 mg BID. The lack of partial responses as evaluated by Response Evaluation Criteria in Solid Tumors (RECIST) version 1.1 with M3814 monotherapy is consistent with its mechanism of action and the findings of preclinical studies. Preclinical studies support combining M3814 with DNA double-strand breaks (DSBs) inducing agents such as radiotherapy and DNA-DSB-inducing chemotherapeutic agents.<sup>16,17</sup> A phase I trial in combination with radiotherapy/chemotherapy is ongoing in patients with advanced solid tumors.<sup>18</sup> M3814 is currently under investigation in combination with avelumab, a monoclonal antibody directed against programmed death ligand 1 (PD-L1), with or without radiotherapy in patients with selected advanced solid tumors.<sup>19</sup> M3814 is also under investigation in combination with capecitabine and radiotherapy in rectal cancer.<sup>20</sup>

## References

1. Tu Q, Wu X, Le Rhun E, et al. CellSearch technology applied to the detection and quantification of tumor cells in CSF of patients with lung cancer leptomeningeal metastasis. *Lung Cancer*. 2015;90(2):352-357.
2. Lee JS, Melisko ME, Magbanua MJ, et al. Detection of cerebrospinal fluid tumor cells and its clinical relevance in leptomeningeal metastasis of breast cancer. *Breast Cancer Res Treat*. 2015;154(2):339-349.
3. Patel AS, Allen JE, Dicker DT, et al. Identification and enumeration of circulating tumor cells in the cerebrospinal fluid of breast cancer patients with central nervous system metastases. *Oncotarget*. 2011;2(10):752-760.
4. Jackman DM, Cioffredi LA, Jacobs L, et al. A phase I trial of high dose gefitinib for patients with leptomeningeal metastases from non-small cell lung cancer. *Oncotarget*. 2015;6(6):4527-4536.
5. Segura PP, Gil M, Balañá C, et al. Phase II trial of temozolomide for leptomeningeal metastases in patients with solid tumors. *J Neurooncol*. 2012;109(1):137-142.
6. Kim M, Kizilbash SH, Laramy JK, et al. Barriers to Effective Drug Treatment for Brain Metastases: A Multifactorial Problem in the Delivery of Precision Medicine. *Pharm Res*. 2018;35(9):177.
7. Bechmann I, Galea I, Perry VH. What is the blood-brain barrier (not)? *Trends Immunol*. 2007;28(1):5-11.
8. Chamberlain MC, Baik CS, Gadi VK, Bhatia S, Chow LQM. Systemic therapy of brain metastases: non-small cell lung cancer, breast cancer, and melanoma. *Neuro Oncol*. 2017;19(1):i1-i24.
9. Levin VA. Relationship of octanol/water partition coefficient and molecular weight to rat brain capillary permeability. *J Med Chem*. 1980;23(6):682-684.
10. Pardridge WM. Delivery of Biologics Across the Blood-Brain Barrier with Molecular Trojan Horse Technology. *BioDrugs*. 2017;31(6):503-519.
11. Zhao YH, Abraham MH, Ibrahim A, et al. Predicting penetration across the blood-brain barrier from simple descriptors and fragmentation schemes. *J Chem Inf Model*. 2007;47(1):170-175.
12. Tawbi HA, Forsyth PA, Algazi A, et al. Combined Nivolumab and Ipilimumab in Melanoma Metastatic to the Brain. *N Engl J Med*. 2018;379(8):722-730.
13. Long G V, Atkinson V, Lo S, et al. Combination nivolumab and ipilimumab or nivolumab alone in melanoma brain metastases: a multicentre randomised phase 2 study. *Lancet Oncol*. 2018;19(5):672-681.
14. Janku F, Connolly R, LoRusso P, et al. Abstract C45: Phase I study of WNT974, a first-in-class Porcupine inhibitor, in advanced solid tumors. *Mol Cancer Ther*. 2016;14(12 Supplement 2):C45 LP-C45.
15. <https://clinicaltrials.gov/ct2/show/NCT01351103?cond=lgk974&rank=1> Accessed November 26, 2018.
16. Fuchss T, Mederski WW, Emde U, et al. Abstract 4198: Highly potent and selective DNA-PK inhibitor M3814 with sustainable anti-tumor activity in combination with radiotherapy. *Cancer Res* 2017; 77(13 Suppl).

17. Sirrenberg C, Zimmermann A, Grombacher T, et al. Abstract 4183: A novel selective DNA-PK inhibitor, M3814, as a potential combination partner of Etoposide and Cisplatin in the therapy of lung cancer. *Cancer Res* 2017; 77 (13 Suppl).
18. van Triest B, Damstrup L, Falkenius J, et al. A phase Ia/Ib trial of the DNA-PK inhibitor M3814 in combination with radiotherapy (RT) in patients (pts) with advanced solid tumors: Dose-escalation results. *J Clin Oncol* 2018; 36 (15\_Suppl): 2518.
19. <https://clinicaltrials.gov/ct2/show/NCT03724890?term=m3814&rank=2> Accessed 03 May 2019.
20. <https://clinicaltrials.gov/ct2/show/NCT03770689?term=m3814&rank=3> Accessed 03 May 2019.





Appendix



## Author affiliations

A. Awada	Oncology Medicine Department, Jules Bordet Institute, Université Libre de Bruxelles, Brussels, Belgium
S. Bawab	Merck KGaA, Darmstadt, Germany
K. Berghoff	Merck KGaA, Darmstadt, Germany
J.H. Beijnen	Department of Pharmacy and Pharmacology, The Netherlands Cancer Institute, Amsterdam, the Netherlands and Division of Pharmacoepidemiology and Clinical Pharmacology, Department of Pharmaceutical Sciences, Faculty of Science, Utrecht University, Utrecht, the Netherlands
M. Bol	Department of Pathology, The Netherlands Cancer Institute, Amsterdam, the Netherlands
D. Brandsma	Department of Neuro-oncology, The Netherlands Cancer Institute, Amsterdam, the Netherlands
D. van den Broek	Department of Laboratory Medicine, Netherlands Cancer Institute - Antoni van Leeuwenhoek, Amsterdam, the Netherlands
M.T.J. van Bussel	Division of Pharmacology and Department of Clinical Pharmacology, Division of Medical Oncology, The Netherlands Cancer Institute, Amsterdam, the Netherlands
A. Compter	Department of Neuro-oncology, The Netherlands Cancer Institute, Amsterdam, the Netherlands
L. Damstrup	Merck KGaA, Darmstadt, Germany
I. Diaz-Padilla	Merck KGaA, Darmstadt, Germany
M.J.A. de Jonge	Medical Oncology, Erasmus MC Daniel den Hoed Cancer Center, Rotterdam, the Netherlands
M. Kuipers	Merck KGaA, Darmstadt, Germany
E. Le Rhun	Neuro-oncology, General and Stereotaxic Neurosurgery service, University Hospital of Lille, Lille cedex, France, Breast Cancer Department, Oscar Lambret Center, Lille cedex, France
T.C. Linders	Department of Laboratory Medicine, Netherlands Cancer Institute - Antoni van Leeuwenhoek, Amsterdam, the Netherlands

## Appendix

- M. Mau-Sørensen      Department of Oncology, Rigshospitalet, Copenhagen, Denmark
- B. Milojkovic Kerklaan      Division of Pharmacology and Department of Clinical Pharmacology,  
Division of Medical Oncology, The Netherlands Cancer Institute,  
Amsterdam, the Netherlands
- D. Nielsen      Department of Oncology, Herlev and Gentofte Hospital, Herlev, Denmark
- D. Pluim      Division of Pharmacology, The Netherlands Cancer Institute, Amsterdam,  
the Netherlands
- J.J.M. Rood      Faculty of Science, Department of Pharmaceutical Sciences, Division of  
Pharmacoepidemiology and Clinical Pharmacology, Utrecht University, the  
Netherlands
- W. Ros      Division of Pharmacology and Department of Clinical Pharmacology,  
Division of Medical Oncology, The Netherlands Cancer Institute,  
Amsterdam, the Netherlands
- B. Sarholz      Merck KGaA, Darmstadt, Germany
- J.H.M. Schellens      Division of Pharmacology and Department of Clinical Pharmacology,  
Division of Medical Oncology, The Netherlands Cancer Institute,  
Amsterdam, the Netherlands and Division of Pharmacoepidemiology and  
Clinical Pharmacology, Department of Pharmaceutical Sciences, Faculty of  
Science, Utrecht University, Utrecht, the Netherlands
- P. Schöffski      Department of General Medical Oncology Leuven Cancer Institute;  
University Hospitals Leuven, Leuven, Belgium
- K. Sikorska      Department of Biometrics, Netherlands Cancer Institute - Antoni van  
Leeuwenhoek, Amsterdam, the Netherlands
- R.W. Sparidans      Faculty of Science, Department of Pharmaceutical Sciences, Division of  
Pharmacoepidemiology and Clinical Pharmacology and Utrecht University,  
Faculty of Science, Department of Pharmaceutical Sciences, Division  
of Chemical Biology and Drug Development, Utrecht University, the  
Netherlands
- H. Verheul      Medical Oncology, Vrije University Medical Centre (VUMC), Amsterdam,  
the Netherlands



## Summary

### Part I Biomarker development and assessment

Leptomeningeal metastases (LM), also known as leptomeningeal carcinomatosis or neoplastic meningitis, is a diffuse dissemination of tumor cells into the cerebrospinal fluid (CSF) and leptomeninges. Approximately ten per cent of patients with cancer ultimately develop LM. Survival of patients with LM varies from several weeks to more than a year, depending on the tumor type, performance status and treatment of LM, consisting of radiotherapy of symptomatic sites and/or systemic therapy. The median survival is 6-8 weeks without treatment. Gadolinium enhanced magnetic resonance imaging (MRI) of the symptomatic sites of the central nervous system (CNS) is the radiological method of choice as diagnostic technique when LM is clinically suspected. The sensitivity of MRI with gadolinium for the diagnosis of LM is approximately 75% and the specificity approximately 77%. When MRI does not show equivocal abnormalities, CSF cytology needs to be performed. Sensitivity of CSF cytology is also low: 44-67% at first LP, increasing to 84-91% upon second sampling. Therefore, improved CSF diagnostics for LM are needed to either rule out the diagnosis or expedite treatment without further delay. The isolation, molecular characterization and quantification of circulating tumor cells (CTC) in CSF is described in patients with a suspicion on LM in part I of this thesis.

Epithelial cell adhesion molecule (EpCAM) is expressed by solid tumors of epithelial origin like non-small-cell lung cancer, breast cancer or ovarian cancer. An overview of the different EpCAM-based laboratory techniques for the enumeration of CTC in CSF is given and a comparison is made with CSF cytology for the diagnoses of LM from epithelial tumors in **Chapter 1**. The reported sensitivities and specificities of the EpCAM-based CTC assays for the diagnosis of LM across the different studies are highly promising and vary between 76-100%.

We report the results of the performance of an EpCAM based immunoflow cytometry CTC assay versus CSF cytology in a prospective study in 81 patients with a clinical suspicion of LM but a non-confirmatory MRI in **Chapter 2**. In a non-small cell lung cancer (NSCLC) subcohort we analyzed circulating tumor (ct)DNA of the selected driver mutations by digital droplet (dd)PCR. The sensitivity of the CTC assay was 94% (95% CI 80-99) and the specificity was 100% (95% CI 91-100) at the optimal cut-off of 0.9 CTC/ml. The sensitivity of cytology was 76% (95% CI 58-89). Twelve of the 23 NSCLC patients had a mutation in the epidermal growth factor receptor (EGFR). All five tested patients with LM demonstrated the primary EGFR driver mutation in cell free CSF. The driver mutation could also be detected in CTC isolated from CSF. It was

concluded that CTC in CSF are detected with a high sensitivity for the diagnosis of LM. ddPCR can determine EGFR mutations in both cell free CSF and isolated CTC from CSF of EGFR mutated NSCLC in patients with LM.

The enumeration of circulating melanoma cell (CMC) in CSF was investigated in 42 patients with a clinical suspicion of LM and described in **Chapter 3**. Thirty-six of them had a negative or equivocal MRI and 6 showed typical leptomeningeal contrast enhancement on MRI. Furthermore, CMC in CSF were enumerated in 10 non-oncological control patients. EANO-ESMO clinical practice guidelines were used to classify LM diagnosis. Driver mutation analysis of *BRAFV600E* was performed on paired cell free CSF, isolated CMC from CSF and plasma samples in 15 patients with *BRAFV600E* mutated melanoma. CMC were detected in CSF in 11 of 12 patients with confirmed LM in whom CSF was available (1.9 - 5587 CMC/ml). In one of 12 patients no CMC were found. One patient with probable LM had 180 CMC/ml and 2 out of 8 patients with possible LM had 9.8 CMC/ml and 3.5 CMC/ml, respectively. Control patients and non-LM patients had  $\leq 0.3$  CMC/ml. Cell-free CSF samples of all four patients with *BRAFV600E* mutated melanoma and cytology confirmed LM were positive for the *BRAFV600E* driver mutation. CMC isolated from CSF in 2 of these patients with confirmed LM were *BRAFV600E* positive. The newly developed MCSP/CD146 immunoflow cytometry assay is a promising tool to detect melanoma cells in CSF. Driver mutation analysis can be used to detect *BRAFV600E* mutations in both cell-free CSF and CMC isolated from CSF. Both assays need further validation for diagnostic accuracy in a larger patient cohort.

## **Part II Clinical pharmacology of anticancer agents**

A systematic Pubmed search for prospective phase II and III studies on nivolumab and ipilimumab in melanoma brain metastases and studies in which CSF levels of nivolumab and ipilimumab are reported is described in **Chapter 4**. Two phase II studies with the combination nivolumab and ipilimumab and one phase II study with ipilimumab monotherapy in melanoma brain metastases were included in this review. One article reported drug levels of nivolumab in CSF. Intracranial responses were achieved in 16 of 35 patients (46%; 95% confidence interval (CI) 29-63) in a phase II study with nivolumab and ipilimumab. The rate of intracranial clinical benefit was 57% (95% CI 47-68) in a second phase II study in 94 patients. The CSF/serum ratio of nivolumab was 0.88-1.9% in a cohort of metastatic melanoma patients treated with nivolumab 1-3 mg/kg. Nivolumab concentrations in CSF ranged from 35-150 ng/ml in these patients, which is in the range of the half maximal effective concentration (EC<sub>50</sub>) of 0.64 nM. The results are discussed and a perspective on the pharmacodynamics and pharmacokinetics for the intracranial activity of these agents was given. Ipilimumab and nivolumab are

active in melanoma brain metastases. Nivolumab penetrates into the CSF. Based on the described findings the general consensus that monoclonal antibodies do not penetrate into the CNS and cannot have a direct intracranial effect needs to be reconsidered.

Immunotherapy with monoclonal antibodies targeting the programmed-death-1 (PD-1) receptor has become standard of care for an increasing number of tumor types. Pharmacokinetic studies may help to optimize anti-PD-1 therapy. Therefore, accurate and sensitive determination of antibody concentrations is essential. We developed and validated an enzyme linked immunosorbent assay (ELISA) capable of measuring nivolumab and pembrolizumab concentrations in serum and CSF with high sensitivity and specificity as reported in **Chapter 5**. The assay was developed and validated based on the specific capture of nivolumab and pembrolizumab by immobilized PD-1, with subsequent enzymatic chemiluminescent detection by anti-IgG4 coupled with horse radish peroxidase (HRP). The lower limit of quantification for serum and CSF was 2 ng/ml for both anti-PD-1 agents. The ELISA method was validated and showed long term sample stability of >1 year. This method is reliable, relatively inexpensive and can be used in serum and CSF from pembrolizumab and nivolumab treated patients.

Another analytical technique for quantitative analysis is described in **Chapter 6**. A method for the quantitative analysis by ultra-performance liquid chromatography-tandem mass spectrometry of osimertinib, a highly selective covalent inhibitor of EGFR T790M mutated tyrosine kinase, in human plasma has been developed. The validation was performed in a range from 1 to 1000 ng/ml, with the lowest level corresponding to the lower limit of quantitation. Gradient elution was performed on a 1.8  $\mu\text{m}$  particle trifunctional bonded C18 column by 1% (v/v) formic acid in water, and acetonitrile as mobile phase. The analyte was detected in the selected reaction monitoring mode of a triple quadrupole mass spectrometer after positive ionization with the heated electrospray interface. Within-day precisions ranged from 3.4 to 10.3%, and between-day precisions from 3.8 to 10.4%, accuracies were 95.5 to 102.8%. Plasma (either lithium heparin or sodium-ethylenediaminetetraacetic acid (EDTA) pre-treatment was performed by salting-out assisted liquid-liquid extraction using acetonitrile and magnesium sulphate. This method was used to analyse the osimertinib blood plasma levels of adult patients with metastatic EGFR T790M mutated NSCLC for therapeutic drug monitoring purposes.

More than 90% of colorectal cancers (CRC) have alterations in WNT signalling. Eight to ten per cent of patients with metastatic Kirsten rat sarcoma viral oncogene homolog wild-type (KRAS-WT) colorectal cancer have v-Raf murine sarcoma viral oncogene homolog B (BRAF) mutations and do not benefit from EGFR antibodies like cetuximab

and panitumumab. In two phase I studies the combination of the BRAF inhibitor vemurafenib or encorafenib and cetuximab induced response rates of 35% and 19% in this patient population. Addition of a WNT inhibitor seems an attractive approach to increase the response rate in patients with *BRAFV600* mutated KRAS-WT CRC with WNT alterations. A phase Ib/II multi-centre, open label, dose escalation study of WNT974, encorafenib and cetuximab in patients with *BRAFV600*-mutant KRAS wild-type metastatic colorectal cancer harboring WNT pathway mutations is described in **Chapter 7**. Patients with *BRAFV600E* mutated KRAS-WT CRC with WNT alterations in RNF43 and/or RSPO fusion were treated with a BRAF inhibitor (encorafenib), plus a monoclonal antibody targeting EGFR (cetuximab) and a porcupine inhibitor (WNT974). The primary objective was to determine the maximum tolerated dose (MTD) or a recommended phase II dose (RP2D). The triplet combination (WNT974 + encorafenib + cetuximab) demonstrated clinical activity with a confirmed overall response rate of 10% and a disease control rate of 85%. Overall, the combination of encorafenib plus WNT974 and cetuximab resulted in a high incidence of bone toxicities. These observations led to the decision to discontinue the study.

A case report of two patients who experienced severe bone toxicity in the trial of WNT974, encorafenib and cetuximab is described in **Chapter 8**.

A first-in-man phase I study of the DNA-dependent protein kinase inhibitor M3814 in patients with advanced solid tumors is described in **Chapter 9**. The aim was to determine the MTD and/or RP2D of M3814, in patients with advanced solid tumors. Secondary objectives were to explore the safety, tolerability, pharmacokinetic and pharmacodynamic profiles, and clinical activity. M3814 was administered continuously in 21-day cycles starting at 100 mg once daily (QD). Subsequent cohorts received: 200 mg QD; 150 mg twice daily (BID); 200 mg BID; 300 mg BID; and 400 mg BID. Thirty-one patients were included. One dose-limiting toxicity was reported (300 mg BID cohort): a combination of non-serious adverse events (AEs) and a long recovery duration following treatment discontinuation. Nausea (n=8), vomiting (n=6), fatigue (n=6), and pyrexia (n=5) were the most frequently reported M3814-related AEs. The most common grade 3 M3814-related AEs were maculo-papular rash (n=4) and nausea (n=2). M3814 was quickly absorbed into the systemic circulation (median Tmax: 1.1-2.5 hours). Overall, a consistent and marked decrease in the pharmacodynamic biomarker (phospho-DNA-PK/total DNA-PK) level was observed in peripheral blood mononuclear cells at 3 and 6 hours after intake. Twelve patients (39%) had a best overall response of stable disease. M3814 showed an acceptable safety profile. The MTD of M3814 was not reached at 400 mg BID. The RP2D for M3814 monotherapy was declared as 400 mg BID.

## Nederlandse samenvatting

### Deel I Biomarker onderzoek

Leptomeningeale metastasen (LM) zijn uitzaaiingen van tumoren naar het hersen-/ ruggenvocht. Het stellen van de diagnose LM is lastig door de lage sensitiviteit van de huidige technieken die gebruikt worden in de klinische praktijk. 'Magnetic resonance imaging' (MRI) heeft een sensitiviteit van 76% voor het opsporen van LM. Bij een negatieve of twijfelachtige MRI-uitslag wordt middels een lumbaalpunctie (LP) hersenvocht afgenomen. Dit hersenvocht, ook wel de cerebrospinale vloeistof genoemd, wordt dan door de patholoog onderzocht op de aanwezigheid van tumor cellen middels cytologie. Cytologie heeft een sensitiviteit van 44-67% bij de eerste LP, die toeneemt naar 84-91% bij een tweede LP. Recent zijn een aantal nieuwe laboratoriumtechnieken ontwikkeld om circulerende tumor cellen (CTC) op te sporen in de cerebrospinale vloeistof. Deze technieken worden in deel I van dit proefschrift besproken. Deel II van dit proefschrift gaat over de klinische farmacologie van anti-kanker middelen.

**Hoofdstuk 1** geeft een overzicht van de literatuur van een aantal nieuwe laboratoriumtechnieken om CTC op te sporen zoals de CELLSEARCH® assay en diverse flowcytometrie assays. Deze laboratoriumtechnieken kunnen CTC opsporen die het epitheliale cel adhesie molecuul (EpCAM) tot expressie brengen. Tumoren die EpCAM tot expressie brengen zijn onder andere longkanker, borstkanker en ovariumkanker. De beschreven sensitiviteit en specificiteit van de op EpCAM gebaseerde CTC analyse methoden bij een verdenking op LM is veelbelovend en varieert van 76 tot 100%.

**Hoofdstuk 2** beschrijft een prospectieve studie naar de sensitiviteit en specificiteit van EpCAM+ CTC bepaling in de cerebrospinale vloeistof met immunoflow cytometrie in 81 patiënten met een klinische verdenking op LM en een negatieve of twijfelachtige MRI. Ook zijn de CTC en de cerebrospinale vloeistof onderzocht op de aanwezigheid van 'driver' mutaties in een subcohort van patiënten met niet-kleincellig longcarcinoom met mutaties in de epidermale groeifactor receptor (EGFR). De mutatieanalyse is uitgevoerd met behulp van 'digital droplet polymerase chain reactie' (dd)PCR technologie. In de controlegroep met 10 patiënten zonder kanker werden geen CTC gevonden. De gevonden sensitiviteit van de CTC bepaling bij patiënten met een klinische verdenking op LM was 94% (95% betrouwbaarheids interval (BI) 80-99) en de specificiteit was 100% (95% BI 91-100) bij de optimale afkapwaarde van 0.9 CTC/ml. De sensitiviteit van de cytologie was 76% (95% BI 58-89). Twaalf van de 23 patiënten met niet-kleincellig longkanker die geïnccludeerd waren in de studie hadden een mutatie in de EGFR. In vijf patiënten met LM is de 'driver' mutatie ook aangetoond

in de celvrije fractie van de cerebrospinale vloeistof. De ‘driver’ mutatie kon ook aangetoond worden in de CTC geïsoleerd uit de cerebrospinale vloeistof. De studie toont aan dat CTC met een hoge sensitiviteit gedetecteerd kunnen worden in de cerebrospinale vloeistof bij patiënten met een klinische verdenking op LM en een negatieve of twijfelachtige MRI.

In **Hoofdstuk 3** worden de initiële resultaten van circulerende melanoom cel bepaling met immunoflow cytometrie beschreven bij 42 patiënten met een klinische verdenking op LM. Eerst is een immunoflow cytometrie assay ontwikkeld voor het opsporen van circulerende melanoom cellen (CMC) met de celoppervlaktemarkers ‘melanoma-associated chondroitin sulfates proteoglycan’ (MCSP) en CD146. In een prospectieve studie is vervolgens de cerebrospinale vloeistof van patiënten met melanoom en een klinische verdenking op LM geanalyseerd. Tevens is de cerebrospinale vloeistof van 10 controlepatiënten zonder melanoom geanalyseerd voor CMC. Ook zijn de CMC en de cerebrospinale vloeistof onderzocht op ‘driver’ mutaties in een subcohort van patiënten met v-Raf muis sarcoom viraal oncogen homolog B (BRAF) *BRAFV600E* gemuteerd melanoom. In 11 van de 12 patiënten met een bevestigde diagnose LM werden CMC aangetoond. De CMC aantallen varieerde van 1.9 - 5587 CMC/ml. De controlepatiënten en de patiënten zonder LM hadden minder dan 0.3 CMC/ml in de cerebrospinale vloeistof. In vier patiënten met LM is de *BRAFV600E* ‘driver’ mutatie ook aangetoond in de celvrije fractie van de cerebrospinale vloeistof. Bij twee van deze patiënten werden ook CMC geïsoleerd en kon de *BRAFV600E* mutatie aangetoond worden in de CMC. Voor de gebruikte laboratoriumtechnieken is verdere klinische validatie in een groter patiënten cohort nodig.

## **Deel II Klinische farmacologie van anti-kanker middelen**

In **Hoofdstuk 4** wordt in een verkennend systematisch literatuuronderzoek de effectiviteit van nivolumab en ipilimumab beschreven bij naar de hersenen gemetastaseerd melanoom. Ook wordt een visie gegeven op de farmacokinetiek en farmacodynamiek van de antitumor activiteit van nivolumab en ipilimumab bij patiënten met naar de hersenen gemetastaseerd melanoom. Nivolumab en ipilimumab grijpen aan op het immuunsysteem door blokkade van immuuncontrole punten van de T-cellen. Nivolumab bindt irreversibel aan de geprogrammeerde celdood-1 (PD-1)-receptor en blokkeert de interactie met de liganden PD-L1 en PD-L2. Ipilimumab blokkeert anti-cytotoxisch T-lymfocyt geassocieerd antigen 4 (CTLA-4). Hierdoor kunnen de immuuncellen van het afweersysteem de tumorcellen weer herkennen en opruimen. In een fase 2 studie werd een intracranieële tumorrespons bereikt bij 16 van de 35 patiënten. In een tweede fase 2 studie met 94 patiënten werd bij 57% een intracranieel klinisch behandelresultaat bereikt. In een cohort van patiënten

met gemetastaseerd melanoom zijn nivolumab concentraties aangetoond in de cerebrospinale vloeistof die in dezelfde range liggen als de concentratie waarbij 50% remming van het maximaal te bereiken effect optreedt (EC50) in vitro. Nivolumab en ipilimumab zijn immunoglobulinen behorend tot de IgG subklasse. Ze worden intraveneus toegediend en zijn relatief groot in vergelijking tot de moleculen die oraal toegediend kunnen worden. Over het algemeen wordt aangenomen dat grote moleculen de bloed-hersenbarrière niet kunnen passeren. Het therapeutisch effect van nivolumab en ipilimumab wordt toegeschreven aan een toename van het aantal geactiveerde T-lymfocyten. De T-lymfocyten kunnen systemisch geactiveerd worden en vervolgens de hersenmetastase infiltreren of de T-lymfocyten kunnen lokaal geactiveerd worden bij de hersentumor. Voor een lokale werking moet het antilichaam ook bij de hersenmetastase komen. Bepaalde subklassen van immunoglobulines kunnen ondanks hun hoge molecuulgewicht door cellen heen getransporteerd worden middels transcytose. Hiervoor dient het antilichaam te binden aan de neonatale Fc receptor. Van nivolumab is aangetoond dat het aan de neonatale Fc receptor bindt. De neonatale Fc receptor komt voor op macrofagen die zich ook in de choroid plexus bevinden. De choroid plexus produceert het grootste deel van de cerebrospinale vloeistof en de macrofagen in de choiroid plexus zouden dus kunnen zorgen voor nivolumab transport naar de cerebrospinale vloeistof.

In **Hoofdstuk 5** wordt een 'enzyme linked immunosorbent assay' (ELISA) beschreven waarmee de concentraties van nivolumab en pembrolizumab bepaald kunnen worden in serum en de cerebrospinale vloeistof. Met de beschreven methode kunnen de concentraties van nivolumab in serum en in de cerebrospinale vloeistof bepaald worden met een hoge sensitiviteit en specificiteit. De assay is gebaseerd op specifieke binding van nivolumab en pembrolizumab aan geïmmobiliseerd PD-1 gevolgd door enzymatische chemoluminescentie door anti-IgG4 gekoppeld aan paard radijs peroxidase (HRP). De ondergrens van de kwantificeringsrange in de cerebrospinale vloeistof is 2 ng/ml voor zowel nivolumab als pembrolizumab. De monsters waren voor langer dan een jaar stabiel bij -80 °C. De analysemethode is betrouwbaar en kan gebruikt worden voor het bepalen van de nivolumab en pembrolizumab spiegels bij patiënten.

**Hoofdstuk 6** beschrijft een analysemethode voor de kwantitatieve analyse van osimertinib, een covalent bindende EGFR tyrosine kinase remmer. Middels hoge prestatie vloeistof chromatografie gevolgd door tandem massa spectrometrie is de concentratie van osimertinib in plasma bepaald. De methodevalidatie is uitgevoerd over een concentratierange van 1 tot 1000 ng/ml met laagste concentratie corresponderend met de ondergrens van de kwantificeringsrange. Gradiënt elutie is

uitgevoerd op een 1.8  $\mu\text{m}$  trifunctionele bindende C18 kolom met 1% (v/v) mierenzuur in water en acetonitriël als mobiele fase. De analiet werd gedetecteerd in de geselecteerde reactie monitoringsmodus van de triple quadrupel massaspectrometer na positieve ionisatie met een verwarmd electrospray grensvlak. De precisie binnen één dag varieerde van 3.4 tot 10.3% en de dag tot dag precisie varieerde van 3.8 tot 10.4%. De juistheid bedroeg 95.5 tot 102.8%. Plasma voorbehandeling is gedaan door uitzouten en vloeistof-vloeistof extractie met behulp van acetonitriël en magnesiumsulfaat. Bovenstaande methode is vervolgens gebruikt voor het bepalen van osimertinib bloed plasmaspiegels bij patiënten met EGFR T790M gemuteerd gemetastaseerd niet-kleincellig longkanker.

In **Hoofdstuk 7** wordt een fase Ib/II studie beschreven waarin patiënten met Kirsten rat sarcoom viraal oncogen homolog wild-type (KRAS-WT) colorectaal kanker met een BRAFV600E mutatie en mutaties in de WNT celsignaleringsroute worden behandeld met doelgerichte therapie. Meer dan 90% van de colorectale tumoren hebben veranderingen in de WNT celsignaleringsroute. Acht tot tien procent van alle patiënten met gemetastaseerd KRAS-WT, BRAF gemuteerd colorectaal kanker reageren niet op een behandeling met de EGFR antilichamen cetuximab en panitumumab. In twee fase I studies met de combinatie van de BRAF remmer vemurafenib of encorafenib gegeven samen met cetuximab reageerde 35% en 19% van de patiënten. Toevoeging van een WNT remmer is een aantrekkelijke mogelijkheid om het slagingspercentage van de combinatietherapie verder te verhogen binnen deze patiëntenpopulatie. Deze strategie is onderzocht bij 20 patiënten met gemetastaseerd colorectaal kanker met KRAS-WT, BRAFV600E gemuteerd en veranderingen in de WNT celsignaleringsroute via R-spondin (RSPO) of E3 ubiquitine-proteïne ligase RING vinger 43 (RNF43) mutaties. De patiënten werden behandeld met de BRAF remmer encorafenib, de EGFR remmer cetuximab en de WNT remmer WNT974. Het primaire doel van de studie was het bepalen van de maximaal tolereerbare dosis van WNT974 in combinatie met encorafenib en cetuximab of het bepalen van een aanbevolen dosering voor fase II studies met deze combinatie. De combinatie van WNT974, encorafenib en cetuximab had antitumor activiteit. Bij tien procent van de patiënten werd de tumor meer dan 30% kleiner. Bij 85% van de patiënten zorgde de combinatie voor het stoppen van de tumorgroei en hield zo de ziekte onder controle. De triplet behandeling ging echter gepaard met een hoge incidentie van bottoxiciteit. Deze observaties hebben uiteindelijk geleid tot het beëindigen van deze studie.

In **Hoofdstuk 8** worden twee patiënten beschreven die ernstige bottoxiciteit hebben ontwikkeld in de studie met de combinatie van WNT974, encorafenib en cetuximab.



In **Hoofdstuk 9** worden de resultaten van een ‘first-in-man’ fase I studie van de DNA-proteïne kinase (DNA-PK) remmer M3814 beschreven. DNA-PK is een serine/threonine proteïne kinase die een essentiële rol speelt in de ‘DNA damage response’ en reguleert DNA dubbelstrengsbreuk reparatie via ‘non-homologous end joining (NHEJ)’. Het primaire doel van de studie was het bepalen van de maximaal tolereerbare dosis of het bepalen van een aanbevolen dosering voor fase II studies. In de fase I studie werden 31 patiënten geïncubeerd met gevorderde solide tumoren. Een standaard 3+3 design werd gebruikt voor de dosisescalatie. M3814 werd in een continue doseerschema oraal toegediend in cycli van 21 dagen. De startdosering was 100 mg één keer per dag (dd). De daaropvolgende cohorten kregen een dosering van 200 mg 1 dd, 150 mg 2 dd, 200 mg 2 dd, 300 mg 2 dd en 400 mg 2 dd. Bij één patiënt trad een dosis limiterende bijwerking op die bestond uit een combinatie van verschillende bijwerkingen. Misselijkheid (n=8), braken (n=6), vermoeidheid (n=6) en koorts (n=5) werden het vaakst gemeld als bijwerking gerelateerd aan M3814. M3814 werd snel geabsorbeerd en de mediane Tmax was 1.1-2.5 uur. Perifeer bloed-mononucleaire cellen (PBMC’s) werden gebruikt als een surrogaat voor weefsel om de farmacodynamische activiteit te kunnen aantonen. Een afname van de farmacodynamische biomarker (gefosforyleerd-DNA-PK / totaal DNA-PK) werd waargenomen. M3814 had een acceptabel veiligheidsprofiel. De maximaal tolereerbare dosis werd niet bereikt bij 400 mg 2 dd. De aanbevolen dosering als monotherapie voor fase II studies is 400 mg 2 dd.



## Dankwoord

Allereerst gaat mijn dank en waardering uit naar alle patiënten die ondanks de onzekerheid en kwetsbaarheid bereid waren om deel te nemen aan de verschillende studies. Dankzij hun deelname wordt de zorg en behandeling stap voor stap verbeterd. De techniek waarmee kankercellen opgespoord worden in het hersen- en ruggenvocht beschreven in hoofdstuk 2 wordt inmiddels uitgevoerd door het laboratorium voor de patiëntenzorg.

Graag wil ik een aantal mensen in het bijzonder bedanken voor hun hulp en begeleiding de afgelopen jaren. Jos, hartelijk dank voor de gedetailleerde feedback op mijn manuscripten en hulp bij de afronding van dit proefschrift. Top dat je ook nadat ik niet meer in het AvL werkte altijd bereikbaar voor me was waardoor ik alsnog snel mijn proefschrift heb kunnen afronden. Jan, dank voor het fundament van dit proefschrift en alles wat ik van je heb geleerd met betrekking tot de klinische farmacologie en fase 1 studies binnen de oncologie. Dieta, bedankt voor alles wat ik van je geleerd heb op het gebied van neuro-oncologie en diagnostiek.

Neeltje en Frans, dankzij de opleiding tot klinisch farmacoloog heb ik mijn blik kunnen verruimen buiten de oncologie tijdens mijn promotieonderzoek. Neeltje, dank voor jouw mentorschap en interesse in mijn onderzoeksprojecten. Frans, dank dat ik mijn opleiding onder jouw supervisie heb kunnen afronden.

Baukelien, ondanks dat wij aan één studie werkten, had je altijd een brede belangstelling voor mij en mijn andere onderzoeksprojecten. Ook jouw onvoorwaardelijke hulp, toen voor mij als OIO van de klinische farmacologie een onzekere tijd aanbrak, heb ik erg gewaardeerd. Heel veel dank hiervoor! Jolanda, heel veel dank voor je hulp in het begin van mijn promotieonderzoek. Marja, dank dat je altijd voor mij bent ingesprongen bij de CRO sponsorstudies. Dit heeft een belangrijke bijdrage geleverd aan een aantal hoofdstukken in dit proefschrift.

Dick, heel veel dank voor je deskundige hulp bij de biomarker en laboratorium studies. Daan en Dorothé, dank voor jullie adviezen, de ctDNA analyse en het implementeren van het CTC onderzoek op het AKL. Karolina en Harm, dank voor jullie hulp bij de statistische analyse van de CLM studie. Emilie Le Rhun, thank you for your contribution to the CMC studies. Brigitte en Patricia, bedankt voor jullie hulp bij het datamanagement van de CLM studies.

Nathalie, Natasha, Huib en Petur, heel veel dank voor jullie hulp en bijdrage aan hoofdstuk 8.

De oud medewerkers van het MC Slotervaart wil ik graag bedanken voor hun hulp en inzet bij de biomarker studies. Dankzij hen en de patiënten konden wij de controlegroepen opnemen in onze studies. De leden van de beoordelingscommissie wil ik bedanken voor het lezen en beoordelen van dit proefschrift. Tot slot wil ik mijn collega's in het Antoni van Leeuwenhoek bedanken voor hun hulp en ondersteuning bij het uitvoeren van de studies. In het bijzonder de verpleegkundigen, verpleegkundig specialisten en de artsen van de CRU, de medewerkers van alle ondersteunende afdelingen waaronder de laboratoria, het trialbureau, de apotheek, het triallab en de wetenschappelijke administratie.

Lieve Jill en Sanne, dank dat jullie mijn paranimfen zijn!

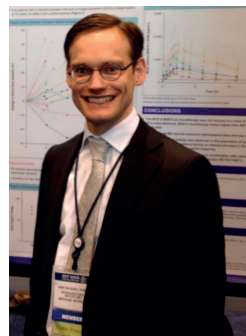
GE'ers, de repetities en mooie concerten de afgelopen jaren waren een welkome afleiding tijdens mijn promotieonderzoek. Collega onderzoekers, dank voor de gezellige vrijdagmiddagborrels, diners en legendarische OIO-weekenden! Lieve vrienden en familie, de weekenden met jullie in Amsterdam, Noord-Brabant, Limburg en Utrecht waren altijd erg gezellig. Heel veel dank hiervoor.

Bas en Frank, met de afronding van dit proefschrift is onze triplo compleet! Dank voor de discussies die ook mij enthousiast hebben gemaakt voor onderzoek en wetenschap. Ivette, dank je wel voor het geven van nieuwe invalshoeken bij mijn epidemiologische vraagstukken. Hanke, top dat je mij bijgespijkerd hebt over de radiologie. Lynn, Philou en Quinn, het gaat nog even duren voordat jullie het onderzoek beschreven in dit proefschrift kunnen lezen maar met de kافت van dit boekje hoop ik samen met metalen en glazen knikkers, een lampje en een magneet snel te laten zien wat wij op het lab allemaal kunnen.

Mam en pap, ik ben jullie erg dankbaar dat jullie mij gestimuleerd hebben en de kans hebben gegeven om mij te ontwikkelen en alle opleidingen te volgen die ik graag wilde doen en mij hierin onvoorwaardelijk te ondersteunen. Het resultaat hiervan staat beschreven in dit boek.

## Curriculum vitae

Mark Theodorus Johannes van Bussel was born on April 15<sup>th</sup>, 1987 in Helmond, the Netherlands. After graduating from 'VMBO, HAVO and VWO' at Varendonck College Astensomerem he went on to study Pharmacy at Utrecht University in 2007. He investigated the effects of beta-glucans and atorvastatin on atherosclerosis and inflammation in low density lipoprotein receptor deficient female mice in his bachelor research project. He moved to the United States of America for his master research internship at the Department of Medicine at The University of Alabama at Birmingham. There he investigated a novel generation pathway of the chemotactic peptide proline-glycine-proline inhibited by captopril. In 2013 Mark received his PharmD degree. Thereafter, he worked at the hospital pharmacy of VieCuri Medical Centre, Venlo. In 2015 he started with his PhD research under the supervision of prof. dr. Jan Schellens, dr. Dieta Brandsma and prof. dr. Jos Beijnen at the Netherlands Cancer Institute - Antoni van Leeuwenhoek. In addition to his PhD project, Mark also followed the clinical pharmacology training of the Dutch Society for Clinical Pharmacology and Biopharmacy.





## Overview of publications

### Publications and abstracts

Circulating epithelial tumor cell analysis in cerebrospinal fluid in patients with leptomeningeal metastases

**van Bussel MTJ**, Pluim D, Milojkovic Kerklaan B, Bol M, Linders TC, van den Broek D, Beijnen JH, Schellens JHM, Brandsma D.

*Accepted for publication in Neurology*

Intracranial antitumor responses of nivolumab and ipilimumab: a pharmacodynamic and pharmacokinetic perspective, a scoping systematic review.

**van Bussel MTJ**, Beijnen JH, Brandsma D.

*BMC Cancer. 2019;19(1):519.*

Enzyme linked immunosorbent assay for the quantification of nivolumab and pembrolizumab in human serum and cerebrospinal fluid.

Pluim D, Ros W, **van Bussel MTJ**, Brandsma D, Beijnen JH, Schellens JHM.

*Journal of Pharmaceutical and Biomedical Analysis 2019;164:128-134.*

EpCAM-based assays for epithelial tumor cell detection in cerebrospinal fluid.

**van Bussel MTJ**, Pluim D, Bol M, Beijnen JH, Schellens JHM, Brandsma D.

*Journal of Neuro-Oncology 2017;137(1):1-10.*

Liquid chromatography-tandem mass spectrometric assay for the T790M mutant EGFR inhibitor osimertinib (AZD9291) in human plasma.

Rood JJM, **van Bussel MTJ**, Schellens JHM, Beijnen JH, Sparidans RW.

*Journal of Chromatography B. 2016;1031:80-85.*

Safety, clinical activity and pharmacological biomarker evaluation of the DNA-dependent protein kinase (DNA-PK) inhibitor M3814: Results from two phase I trials.

Mau-Sorensen M, **van Bussel MTJ**, Kuipers M, Nielsen DL, Verheul HM, Aftimos P, de Jonge MJA, van Triest B, Falkenius J, Debus J, Troost E, Samuels M, Sarholz B, Budach V, Goel S, Locatelli G, Geertsens PF.

*Annals of Oncology 2018; 29 (Suppl\_8).*

A phase Ia/Ib trial of the DNA-PK inhibitor M3814 in combination with radiotherapy (RT) in patients (pts) with advanced solid tumors: Dose-escalation results.

van Triest B, Damstrup L, Falkenius J, Budach V, Troost E, Samuels M, Debus J, Mau-Sørensen M, Berghoff K, Strotman R, **van Bussel MTJ**, Goei S, Geertsen PF.

*Journal of Clinical Oncology* 2018; 36 (15\_Suppl): 2518.

Circulating tumor cells analysis in cerebrospinal fluid in patients with epithelial tumors with suspected leptomeningeal metastasis.

**van Bussel MTJ**, Pluim D, Milojkovic-Kerklaan B, Bol M, Beijnen JH, Schellens JHM, Brandsma D.

*NVKFB Scientific Spring Meeting 2018 Apr.*

Tumor cell detection by immunoflow cytometry and BRAF mutation analysis in cerebrospinal fluid of melanoma patients with suspected leptomeningeal metastases.

**van Bussel MTJ**, Pluim D, Milojkovic-Kerklaan B, van den Broek D, Beijnen JH, Boogerd W, Schellens JHM, Le Rhun E, Brandsma D.

*Neuro-Oncology* 2017; 19, (6\_suppl): vi41

Circulating tumor cells and circulating tumor DNA analysis in cerebrospinal fluid in melanoma patients with suspected leptomeningeal metastasis.

**van Bussel MTJ**, Pluim D, Milojkovic-Kerklaan B, van den Broek D, Beijnen JH, Boogerd W, Schellens JHM, Le Rhun E, Brandsma D.

*NVKFB Scientific Spring Meeting 2017 Apr.*

A multicenter phase I trial of the DNA-dependent protein kinase (DNA-PK) inhibitor M3814 in patients with solid tumors.

**van Bussel MTJ**, Mau-Soerensen M, Damstrup L, Nielsen D, Verheul HMW, Aftimos PG.

*Journal of Clinical Oncology* 2017; 35 (15\_Suppl): 2556.

### **Oral presentations**

Circulating tumor cells and driver mutation analysis in cerebrospinal fluid in patients with epithelial tumors with suspected leptomeningeal metastasis.

**van Bussel MTJ**, Pluim D, Milojkovic Kerklaan B, Bol M, Linders TC, van den Broek D, Beijnen JH, Schellens JHM, Brandsma D.

*FIGON Dutch Medicines Days 2018 Oct.*



Flow cytometry circulating tumor cell assays in CSF improve the diagnostic accuracy of leptomeningeal metastases of solid tumors.

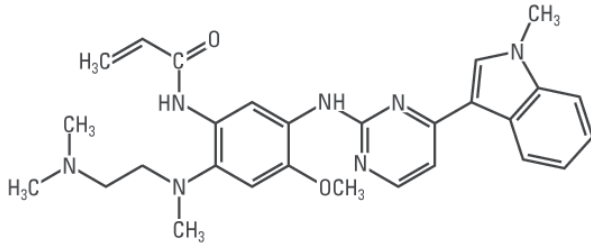
**van Bussel MTJ**, Milojkovic-Kerklaan B, Pluim D, Bol M, Hofland I, Westerga J, Tinteren H, Beijnen JH, Boogerd W, Schellens JHM, Brandsma D.

*LWNO scientific meeting 2015 Oct.*

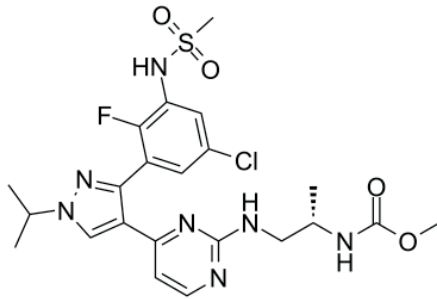


## Molecular structures

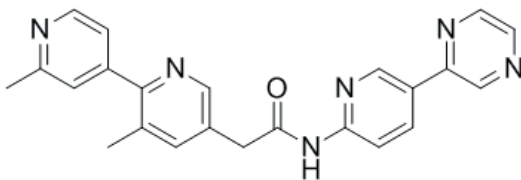
Osimertinib



Encorafenib



WNT974



M3814

